

UC Berkeley

UC Berkeley Electronic Theses and Dissertations

Title

Using integrable colored vertex models to study LLT polynomials, super ribbon functions, and domino tilings of the Aztec diamond

Permalink

<https://escholarship.org/uc/item/0br2j35m>

Author

Gitlin, Andrew

Publication Date

2022

Peer reviewed|Thesis/dissertation

Using integrable colored vertex models to study LLT polynomials, super ribbon
functions, and domino tilings of the Aztec diamond

by

Andrew Gitlin

A dissertation submitted in partial satisfaction of the

requirements for the degree of

Doctor of Philosophy

in

Mathematics

in the

Graduate Division

of the

University of California, Berkeley

Committee in charge:

Professor Sylvie Corteel, Chair

Professor Mark Haiman

Professor Nicolai Reshetikhin

Professor Igor Pak

Fall 2022

Using integrable colored vertex models to study LLT polynomials, super ribbon functions, and domino tilings of the Aztec diamond

Copyright 2022
by
Andrew Gitlin

Abstract

Using integrable colored vertex models to study LLT polynomials, super ribbon functions, and domino tilings of the Aztec diamond

by

Andrew Gitlin

Doctor of Philosophy in Mathematics

University of California, Berkeley

Professor Sylvie Corteel, Chair

The study of integrable systems - also known as vertex models, ice models, or multiline queues - is a classical subject, see e.g. [4, 48]. Recently they have enjoyed an advent into the world of (non)symmetric polynomials [12, 53, 9], and have been generalized to colored vertex models [8, 13, 14, 16, 21, 27] and polyqueue tableaux [21, 3]. In this thesis, we study three topics in algebraic combinatorics - LLT polynomials, super ribbon functions, and domino tilings of the Aztec diamond - using several Yang-Baxter integrable colored vertex models.

Employing the “white” vertices, we construct a certain class of partition functions that we show are equal to the LLT polynomials of Lascoux, Leclerc, and Thibon [39]. We then give alternate proofs of many properties of these polynomials, including symmetry and a Cauchy identity, using the vertex model formalism.

Employing the “white” and “purple” vertices, we construct a certain class of partition functions that we show are essentially equal to the super ribbon functions of Lam [38]. This construction generalizes our construction of partition functions equal to the LLT polynomials which employ just the “white” vertices. We then give proofs of many properties of these polynomials, namely a Cauchy identity and generalizations of known identities for supersymmetric Schur polynomials, using the vertex model formalism.

Finally, we study k -tilings (k -tuples of domino tilings) of the Aztec diamond. We describe two models - one based on the “purple” and “gray” vertices and one based on the “white” and “pink” vertices - for assigning a weight to each k -tiling, depending

on the number of dominos of certain types and the number of “interactions” between the tilings. We compute the generating polynomials of the k -tilings in both models, as well as the arctic curves of the k -tilings in certain limits of the interaction strength.

To mom, dad, and Emily,
whose love kept me going.

Contents

Contents	ii
List of Figures	iii
List of Tables	iv
1 Introduction	1
1.1 Partitions	1
1.2 Vertex models	4
1.3 The vertex models and (co-)interlacing partitions	8
1.4 Yang-Baxter integrability	9
2 LLT polynomials	15
2.1 Introduction	15
2.2 LLT polynomials	18
2.3 Vertex model	20
2.4 The symmetry of the LLT polynomials	24
2.5 Single rows	25
2.6 Cauchy identity	30
2.7 Examples	47
3 Super ribbon functions	49
3.1 Introduction	49
3.2 Ribbon tableaux and the Littlewood quotient map	51
3.3 Partition functions	56
3.4 Identities of supersymmetric LLT polynomials	57
3.5 Relating \mathcal{L}^S to \mathcal{G}	75
3.6 Cauchy identity	87
3.7 Example computations of \mathcal{L}^S and \mathcal{G}	100

4	Domino tilings of the Aztec diamond	103
4.1	Introduction	103
4.2	Domino tilings of the Aztec diamond	107
4.3	k -tilings and vertex models	112
4.4	Arctic curve computations	122
	Bibliography	135
A	Lozenge tilings of the hexagon	139
B	Equivalence of algebraic and graphical definitions for the L and M vertices	152
C	Proof of Lemma 3.2.13	155

List of Figures

4.1	The Aztec diamond of rank 3 (left) and an example of a domino tiling (right)	103
4.2	The 8 domino tilings of the Aztec diamond of rank 2	104
4.3	A typical tiling of the Aztec diamond of rank 1000	105
4.4	Two ways of slicing the Aztec diamond.	108
4.5	The empty tilings for the purple-gray model (left) and the white-pink model (right)	108
4.6	A domino tiling and the corresponding Maya diagrams in the purple-gray (left) and white-pink (right) models	110
4.7	An example of a 3-tiling of the rank 3 Aztec diamond	112
4.8	Domino tilings and vertex models	114
4.9	Purple-gray lattice configurations for the Aztec diamond of rank 2	115
4.10	An example of a 3-tiling of the rank 3 Aztec diamond (right), the corresponding sequence of 3-tuples of partitions (middle), and the corresponding purple-gray lattice configuration (left)	117
4.11	White-pink lattice configurations for the Aztec diamond of rank 2	120
4.12	Non-intersecting paths for the Aztec diamond of rank 2	123

4.13	Example of the bijection at $t = 0$ for $k = 2$: the 2-tuple of paths (left), the paths without the frozen steps (middle), and the 1-tuple of paths (right)	127
4.14	Example of the bijection at $t = 0$ for $k = 2$: the 2-tiling with the frozen dominos in black (left) and the corresponding 1-tiling (right)	127
4.15	Simulation and computed arctic curve for a 2-tiling of the Aztec diamond of rank 128 for $t = 0$	128
4.16	Simulation of a 2-tiling Aztec diamond of rank 128 for $t = 1000$	132
4.17	Top: Simulation of a rank 128 Aztec diamond for $t = 3$. Bottom: Simulation of a rank 128 Aztec diamond for $t = 1/3$.	134
4.18	Simulation of a 2-tiling of a rank 256 Aztec diamond for $t = 5$. Note the formation of a cusp along the South-East boundary of the Aztec diamond.	134
A.1	Example of the bijection between the 2-tilings of the $2 \times 3 \times 3$ hexagon at $t = 0$ and tilings of the $4 \times 3 \times 1$ hexagon. The top gives the bijection in terms of lattice path, while the bottom gives the lozenge tilings.	144
A.2	A simulation and computed arctic curve of a 1-tiling of an $100 \times 100 \times 100$ hexagon (left) and a simulation and computed arctic curve for 2-tiling a $50 \times 100 \times 150$ hexagon with $t = 0$ (right). The colors of the arctic curve show which pieces map to each other under the bijection.	145
A.3	A simulation and computed arctic curve for 2-tilings of the $100 \times 50 \times 100$ hexagon for large t ($t = 100$).	149

List of Tables

1.1	Algebraic definitions of the vertex weights	5
1.2	Graphical definitions of the vertex weights for $k = 1$	6
1.3	Graphical definitions of the vertex weights for general k	7
A.1	Generating functions of 2-tilings of the $a \times b \times c$ hexagon	151

Acknowledgments

I could not have completed this dissertation without the guidance of my advisor, Sylvie Corteel. Her insights and experience were crucial to the success of the research that eventually led to this dissertation. More than that, she has been a great mentor and role model over the last three years. Even when we were separated by thousands of miles and could only meet virtually (due to the COVID-19 pandemic and her relocation to Paris, France), she always went the extra mile to encourage me along my academic journey. She taught me the joys of algebraic combinatorics, connected me with other mathematicians with similar interests, and provided me opportunities that I would not have had otherwise - including the opportunity to conduct research and meet other mathematicians at Institut de recherche en informatique fondamentale (IRIF) in Paris.

I also could not have completed this dissertation without the valuable contributions of David Keating. From the Cauchy identity for supersymmetric LLT polynomials to the limit shapes of lozenge tilings of the hexagon, his brilliant insights and his hard work to turn intuitions into reality led to key results and opened up entire new avenues of investigation. I am grateful for our many collaborative discussions, as well as his guidance and mentorship.

I thank Jeremy Meza for collaborating with me (along with Sylvie Corteel and David Keating) to use vertex models to study LLT polynomials. His contributions, in particular his insights towards proving a Cauchy identity and his computer algorithms, were crucial to the success of the research. I also thank Frederick Huang for collaborating with me (along with Sylvie Corteel) to study the combinatorics of the stationary distribution of the multi-species asymmetric exclusion process.

I thank Andrés R. Vindas Meléndez, Christopher Ryba, Sylvie Corteel, Mitsuki Hanada, John Lentfer, and Melissa Sherman-Bennett for organizing the UC Berkeley Combinatorics Seminar over the past two years. The seminar helped build a community around combinatorics at the university. I learned a lot about many different active research areas throughout the combinatorics landscape, and I enjoyed giving a talk and sharing my own research at the seminar a couple of times.

I thank Sylvie Corteel, Mark Haiman, Nicolai Reshetikhin, and Igor Pak for serving on my dissertation committee.

Finally, I thank all my family and friends - in particular Xianglong Ni, Pranav Srinivasan, and Brendan Kelley-Bukovac - who, in one way or another, helped me along my academic journey and made me a better mathematician and person.

We say two partitions λ and μ **interlace** (and we write $\lambda \succeq \mu$) if

$$\lambda_1 \geq \mu_1 \geq \lambda_2 \geq \mu_2 \geq \dots$$

We say two partitions λ and μ **co-interlace** (and we write $\lambda \succeq' \mu$) if $\lambda' \succeq \mu'$. We say λ/μ is a **horizontal (vertical) strip** if λ and μ interlace (co-interlace).

The **content** of a cell $u = (i, j)$ in row i and column j of any Young diagram is $c(u) = j - i$. Notice that the c **content line** $y = x - c$ goes through the center of each cell with content c . The **Maya diagram** of λ is a doubly infinite sequence

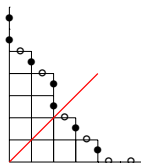
$$\dots, a_{-\frac{5}{2}}, a_{-\frac{3}{2}}, a_{-\frac{1}{2}}, a_{\frac{1}{2}}, a_{\frac{3}{2}}, a_{\frac{5}{2}}, \dots$$

of symbols in the alphabet $\{\circ = 0, \bullet = 1\}$, starting with infinitely many \bullet 's and ending with infinitely many \circ 's, where

$$a_{i+\frac{1}{2}} = \begin{cases} \bullet & \text{if } \lambda_j - j = i \text{ for some } j \\ \circ & \text{otherwise} \end{cases}.$$

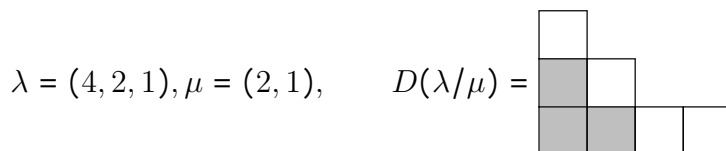
The Maya diagram of λ can be found by following the NE border of the Young diagram of λ from NW to SE, where each E step corresponds to a \circ and each S step corresponds to a \bullet , and moreover the steps corresponding to $a_{c-\frac{1}{2}}$ and $a_{c+\frac{1}{2}}$ lie on the left and right side of the c content line, respectively. It is easy to see that the 0 content line is the unique content line such that the number of \circ 's to its left equals the number of \bullet 's to its right.

Example 1.1.1. The Maya diagram of $(4, 3, 2, 2, 1)$ is $\dots \bullet \bullet \circ \circ \bullet \bullet \circ \bullet \circ \bullet \circ \bullet \circ \bullet \circ \bullet \circ \bullet \circ \dots$



In red, we have indicated the 0 content line; there are two \circ 's to its left and two \bullet 's to its right.

If λ and μ are partitions such that $D(\lambda) \supseteq D(\mu)$, then the **skew shape** λ/μ is the set of cells in $D(\lambda)$ not in $D(\mu)$. We draw $D(\lambda/\mu)$ by coloring the cells in $D(\mu)$ gray, such as below.



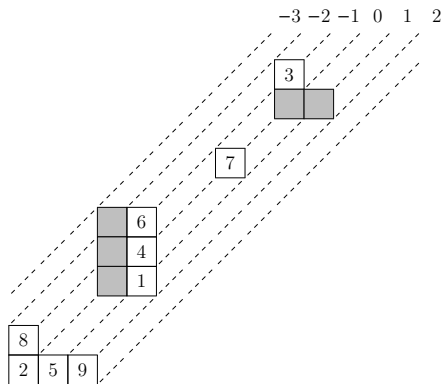
The size of λ/μ is $|\lambda/\mu| = |\lambda| - |\mu|$. A **semistandard Young tableau** of shape λ/μ is a filling of each cell of $D(\lambda/\mu)$ with a positive integer such that the rows are weakly increasing and the columns are strictly increasing. We call the set of all such fillings $\text{SSYT}(\lambda/\mu)$.

We can extend many of these definitions to k -tuples of (skew) partitions. Given a k -tuple of partitions $\lambda = (\lambda^{(1)}, \lambda^{(2)}, \dots, \lambda^{(k)})$, we define its conjugate to be $\lambda' = (\lambda^{(k)'}, \lambda^{(k-1)'}, \dots, \lambda^{(1)'})$ and its size to be $|\lambda| = |\lambda^{(1)}| + \dots + |\lambda^{(k)}|$. We define $\mathbf{0}$ to be the k -tuple (\emptyset^k) of empty partitions. Given a k -tuple of skew partitions $\lambda/\mu = (\lambda^{(1)}/\mu^{(1)}, \dots, \lambda^{(k)}/\mu^{(k)})$, we define a semistandard Young tableau of shape λ/μ to be a semistandard Young tableau on each $\lambda^{(j)}/\mu^{(j)}$, that is,

$$\text{SSYT}(\lambda/\mu) = \text{SSYT}(\lambda^{(1)}/\mu^{(1)}) \times \dots \times \text{SSYT}(\lambda^{(k)}/\mu^{(k)}).$$

We can picture this as placing the Young diagrams diagonally “on content lines” with the first shape in the South-West direction and the last shape in the North-East direction.

Example 1.1.2. Let $\lambda/\mu = ((3, 1), (2, 2, 2))/(1, 1, 1), (1), (2, 1)/(2)$. The top row labels the contents of each line.



We also extend the definition of interlacing to k -tuples of partitions; we write $\lambda \geq \mu$ if $\lambda^{(i)} \geq \mu^{(i)}$ for all $i \in [k]$. Similarly we extend the definitions of co-interlacing and horizontal/vertical strips to k -tuples of partitions. We define the Maya diagram of a k -tuple of partitions λ to be the k -tuple $(a^{(1)}, \dots, a^{(k)})$ where

$$a^{(i)} = \left(\dots, a_{-\frac{i}{2}}^{(i)}, a_{-\frac{i-1}{2}}^{(i)}, a_{-\frac{i-2}{2}}^{(i)}, a_{-\frac{i-3}{2}}^{(i)}, a_{-\frac{i-4}{2}}^{(i)}, a_{-\frac{i-5}{2}}^{(i)}, \dots \right)$$

is the Maya diagram of $\lambda^{(i)}$ for all $i \in [k]$. Finally, we define $P_p^{(k)}$ to be the set of k -tuples of partitions, each having p parts.

1.2 Vertex models

The vertex models we will use were originally studied in [22, 28, 20], although they can be realized as degenerations of vertex models introduced in [1] (see Lemma 1.4.1). We begin with some notation. For a vector $\mathbf{I} = (I_1, \dots, I_k) \in \mathbb{R}^k$, we define

$$|\mathbf{I}| = \sum_{m=1}^k I_m.$$

For vectors $\mathbf{I} = (I_1, \dots, I_k), \mathbf{J} = (J_1, \dots, J_k) \in \mathbb{R}^k$, we define

$$\varphi(\mathbf{I}, \mathbf{J}) = \sum_{1 \leq i < j \leq k} I_i J_j.$$

For variables x and t and an integer $n \geq 0$, we define the t -Pochhammer symbol

$$(x; t)_n = \prod_{m=0}^{n-1} (1 - xt^m).$$

We will also use the notation $\bar{x} = \frac{1}{xt^{k-1}}$ (when k is clear from context).

We will define our vertices both algebraically and graphically. There are two types of vertices: the L, L', M , and M' matrices are “box vertices” and the $R, R',$ and R'' matrices are “cross vertices.” Algebraically, a square vertex is a family of functions $(\{0, 1\}^k)^4 \rightarrow \mathbb{C}[x, t]$, one for each integer $k \geq 0$, whereas a cross vertex is a family of functions $(\{0, 1\}^k)^4 \rightarrow \mathbb{C}(x, y, t)$, one for each integer $k \geq 0$. In other words, a vertex associates a **weight** (either a polynomial in x, t for a box vertex or a rational function in x, y, t for a cross vertex) to every 4-tuple of vectors in $\{0, 1\}^k$ for each integer $k \geq 0$.

While the algebraic definitions give explicit formulae for the weights of the vertices, it is often more useful to think of a vertex graphically. We can draw a vertex as a face with four incident edges, each labelled by an element of $\{0, 1\}^k$. A face takes one of two forms:

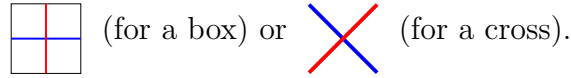
$$\begin{array}{c} \mathbf{K} \\ \square \\ \mathbf{J} \quad \mathbf{L} \\ \mathbf{I} \end{array} \text{ (a box) or } \begin{array}{c} \mathbf{J} \quad \mathbf{K} \\ \diagdown \quad \diagup \\ \mathbf{I} \quad \mathbf{L} \end{array} \text{ (a cross)}.$$

The edge labels describe colored paths moving through the face SW-to-NE (in a box) or left-to-right (in a cross). If an edge has the label $\mathbf{I} = (I_1, \dots, I_k) \in \{0, 1\}^k$, then for each $i \in [k]$, a path of color i is incident at the edge if and only if $I_i = 1$. For

Vertex	Algebraic definition
L	$L_x^{(k)}(\mathbf{I}, \mathbf{J}, \mathbf{K}, \mathbf{L}) = \mathbf{1}_{\mathbf{I}+\mathbf{J}=\mathbf{K}+\mathbf{L}} \prod_{i=1}^k \mathbf{1}_{I_i+J_i \neq 2} \cdot x^{ \mathbf{L} } t^{\varphi(\mathbf{L}, \mathbf{I}+\mathbf{J})}$
L'	$L_x^{\prime(k)}(\mathbf{I}, \mathbf{J}, \mathbf{K}, \mathbf{L}) = \mathbf{1}_{\mathbf{I}+\mathbf{J}=\mathbf{K}+\mathbf{L}} \prod_{i=1}^k \mathbf{1}_{K_i \geq J_i} \cdot x^{ \mathbf{L} } t^{\varphi(\mathbf{L}, \mathbf{K}-\mathbf{J})}$
M	$M_x^{(k)}(\mathbf{I}, \mathbf{J}, \mathbf{K}, \mathbf{L}) = x^k t^{\binom{k}{2}} L_x^{(k)}(\mathbf{I}, \mathbf{J}, \mathbf{K}, \mathbf{L})$
M'	$M_x^{\prime(k)}(\mathbf{I}, \mathbf{J}, \mathbf{K}, \mathbf{L}) = x^k L_x^{\prime(k)}(\mathbf{I}, \mathbf{J}, \mathbf{K}, \mathbf{L})$
R	$R_{y/x}^{(k)}(\mathbf{I}, \mathbf{J}, \mathbf{K}, \mathbf{L}) = \mathbf{1}_{\mathbf{I}+\mathbf{J}=\mathbf{K}+\mathbf{L}} \prod_{i=1}^k \mathbf{1}_{J_i \geq K_i} \cdot (-1)^{ \mathbf{J} - \mathbf{K} } (y/x)^{ \mathbf{J} } (x/y; t)_{ \mathbf{J} - \mathbf{K} } t^{\varphi(\mathbf{J}, \mathbf{K}-\mathbf{J})}$
R'	$R_{y/x}^{\prime(k)}(\mathbf{I}, \mathbf{J}, \mathbf{K}, \mathbf{L}) = \mathbf{1}_{\mathbf{I}+\mathbf{J}=\mathbf{K}+\mathbf{L}} \prod_{i=1}^k \mathbf{1}_{I_i+J_i \neq 2} \cdot (x/y)^{ \mathbf{L} } (-x/y; t)_{ \mathbf{K}+ \mathbf{L} }^{-1} t^{\varphi(\mathbf{L}, \mathbf{K}+\mathbf{L})}$
R''	$R_{x/y}^{\prime\prime(k)}(\mathbf{I}, \mathbf{J}, \mathbf{K}, \mathbf{L}) = \mathbf{1}_{\mathbf{I}+\mathbf{J}=\mathbf{K}+\mathbf{L}} \prod_{i=1}^k \mathbf{1}_{K_i \geq J_i} \cdot (x/y)^{ \mathbf{L} } (x/y; t)_{ \mathbf{K} - \mathbf{J} } t^{\varphi(\mathbf{L}, \mathbf{K}-\mathbf{J})}$

Table 1.1: Algebraic definitions of the vertex weights

example, with $k = 2$ (letting blue be color 1 and red be color 2), the path configuration associated to the edge labels $\mathbf{I} = (0, 1)$, $\mathbf{J} = (1, 0)$, $\mathbf{K} = (0, 1)$, $\mathbf{L} = (1, 0)$ is



The factor of $\mathbf{1}_{\mathbf{I}+\mathbf{J}=\mathbf{K}+\mathbf{L}}$ that appears in the algebraic definition of each vertex imposes a **path conservation** restriction: in order for a vertex to have a non-zero weight, the paths entering the vertex and the paths exiting the vertex must be the same.

To define the vertex weights graphically, we first define the weights in the case $k = 1$ in Table 1.2; the k -color weights are then defined in terms of the 1-color weights in Table 1.3.

For the white L and gray M weights, the equivalence of the algebraic and graphical definitions is shown in Appendix B. The equivalence for the other vertices can be shown similarly.

The box vertices will primarily be used to construct various lattices and their associated partition functions. A **lattice** is a rectangular grid of vertices, with the variables and the labels on the outer edges specified, but with the labels on the internal edges unspecified. A **lattice configuration** is a lattice with the labels on the internal edges specified, such that the weight of each vertex is non-zero. The weight of a lattice configuration is the product of the weights of the vertices.




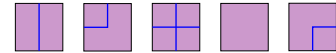



Vertex	One-color definition
L	$ \begin{array}{c} k \\ j \begin{array}{ c } \hline x \\ \hline \end{array} i \\ l \end{array} $  $L_x^{(1)}(i, j, k, l):$ 1 x x 1 1
L'	$ \begin{array}{c} k \\ j \begin{array}{ c } \hline x \\ \hline \end{array} i \\ l \end{array} $  $L_x^{(1)}(i, j, k, l):$ 1 1 x 1 x
M	$ \begin{array}{c} k \\ j \begin{array}{ c } \hline \bar{x} \\ \hline \end{array} i \\ l \end{array} $  $M_x^{(1)}(i, j, k, l):$ x 1 1 x x
M'	$ \begin{array}{c} k \\ j \begin{array}{ c } \hline x^{-1} \\ \hline \end{array} i \\ l \end{array} $  $M_x^{(1)}(i, j, k, l):$ x x 1 x 1
R	$ \begin{array}{c} x \ j \ \begin{array}{ c } \hline k \\ \hline \end{array} \\ y \ i \ \begin{array}{ c } \hline l \\ \hline \end{array} \end{array} $  $R_{y/x}^{(1)}(i, j, k, l):$ $1 - y/x$ y/x 1 y/x 1
R'	$ \begin{array}{c} x \ j \ \begin{array}{ c } \hline k \\ \hline \end{array} \\ y \ i \ \begin{array}{ c } \hline l \\ \hline \end{array} \end{array} $  $R_{y/x}^{(1)}(i, j, k, l):$ $\frac{1}{1+y/x}$ $\frac{y/x}{1+y/x}$ $\frac{1}{1+y/x}$ $\frac{y/x}{1+y/x}$ 1
R''	$ \begin{array}{c} x \ j \ \begin{array}{ c } \hline k \\ \hline \end{array} \\ y \ i \ \begin{array}{ c } \hline l \\ \hline \end{array} \end{array} $  $R_{x/y}^{(1)}(i, j, k, l):$ $1 - x/y$ 1 x/y x/y 1

Table 1.2: Graphical definitions of the vertex weights for $k = 1$


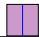


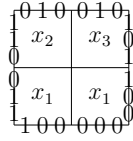
Vertex	k -color definition
L	$L_x^{(k)}(\mathbf{I}, \mathbf{J}, \mathbf{K}, \mathbf{L}) = \prod_{i=1}^k L_{xt^{\delta_i}}^{(1)}(I_i, J_i, K_i, L_i)$ where $\delta_i = \#$ colors greater than i that are present
L'	$L_x'^{(k)}(\mathbf{I}, \mathbf{J}, \mathbf{K}, \mathbf{L}) = \prod_{i=1}^k L_{xt^{\delta_i}'}^{(1)}(I_i, J_i, K_i, L_i)$ where $\delta_i' = \#$ colors greater than i of the form 
M	$M_x^{(k)}(\mathbf{I}, \mathbf{J}, \mathbf{K}, \mathbf{L}) = \prod_{i=1}^k t^{\beta_i} M_{xt^{\alpha_i-\beta_i}}^{(1)}(I_i, J_i, K_i, L_i)$ where $\alpha_i = \#$ colors greater than i that don't exit right $\beta_i = \#$ colors greater than i that exit top
M'	$M_x'^{(k)}(\mathbf{I}, \mathbf{J}, \mathbf{K}, \mathbf{L}) = \prod_{i=1}^k t^{\gamma_i} M_{xt^{-\gamma_i}}^{(1)}(I_i, J_i, K_i, L_i)$ where $\gamma_i = \#$ colors greater than i of the form 
R	$R_{y/x}^{(k)}(\mathbf{I}, \mathbf{J}, \mathbf{K}, \mathbf{L}) = \prod_{i=1}^k R_{y/(xt^{\epsilon_i})}^{(1)}(I_i, J_i, K_i, L_i)$ where $\epsilon_i = \#$ colors greater than i of the form 
R'	$R_{y/x}'^{(k)}(\mathbf{I}, \mathbf{J}, \mathbf{K}, \mathbf{L}) = \prod_{i=1}^k R_{y/(xt^{\epsilon_i}')}^{(1)}(I_i, J_i, K_i, L_i)$ where $\epsilon_i' = \#$ colors greater than i that are present
R''	$R_{x/y}''^{(k)}(\mathbf{I}, \mathbf{J}, \mathbf{K}, \mathbf{L}) = \prod_{i=1}^k R_{t^{\epsilon_i}x/y}''^{(1)}(I_i, J_i, K_i, L_i)$ where $\epsilon_i'' = \#$ colors greater than i of the form 

Table 1.3: Graphical definitions of the vertex weights for general k

Example 1.2.1. Consider the following lattice of white vertices with $k = 3$.



Then the weight of one possible lattice configuration is

(Here blue is color 1, red is color 2, and green is color 3.)

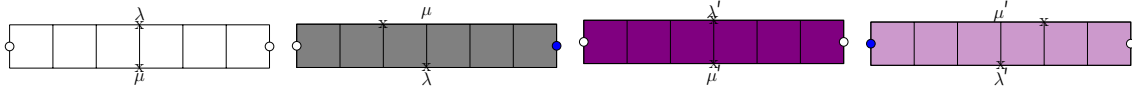
Given a lattice L , the associated **partition function** is

$$\sum_{C \in LC(L)} \text{weight}(C)$$

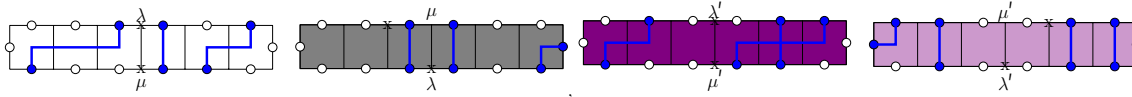
where $LC(L)$ is the set of valid lattice configurations on L . Often, when it is clear from context, we will abuse notation and let the drawing of the lattice be equal to the partition function of the vertex model on the lattice.

1.3 The vertex models and (co-)interlacing partitions

In the case $k = 1$, there is a very natural interpretation of single rows of our box vertices in terms of (co-)interlacing partitions. Given two partitions λ and μ such that $\lambda_1 + \ell(\lambda) \leq n$ and $\mu_1 + \ell(\mu) \leq n$, we can draw rows of n vertices with border conditions as follows.



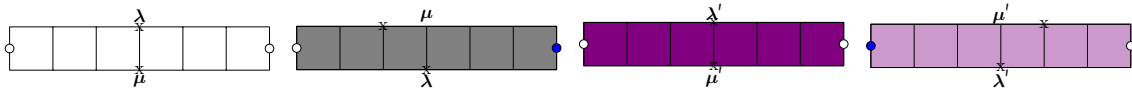
Here a partition on the boundary of the array means that the border condition is given by the corresponding Maya diagram, and we mark the position of the 0 content line with an x . For example, with $\lambda = (3, 2, 2)$ and $\mu = (2, 2, 0)$, we get the following configurations.



It is easy to see that each row has no valid configurations unless $\mu \leq \lambda$, in which case it has one valid configuration with weight $x^{|\lambda|-|\mu|}$. Thus the weight of each row is

$$\begin{cases} x^{|\lambda|-|\mu|} & \text{if } \mu \leq \lambda \\ 0 & \text{otherwise} \end{cases}$$

It is easy to generalize this interpretation of rows of vertices to general values of k in the case $t = 1$. Given two k -tuples of partitions $\boldsymbol{\mu}$ and $\boldsymbol{\lambda}$ such that $\lambda_1^{(i)} + \ell(\lambda^{(i)}) \leq n$ for all $i \in [k]$, we can draw rows of n vertices with border conditions as follows.



Here a k -tuple of partitions on the boundary of the array means that, for all $i \in [k]$, the i -th component of the border condition is given by the Maya diagram corresponding to the i -th partition. It is easy to see that each row has no valid configurations unless $\boldsymbol{\mu} \leq \boldsymbol{\lambda}$, in which case it has one valid configuration with weight $x^{|\boldsymbol{\lambda}|-|\boldsymbol{\mu}|}$ when $t = 1$. Thus the weight of each row is

$$\begin{cases} x^{|\boldsymbol{\lambda}|-|\boldsymbol{\mu}|} & \text{if } \boldsymbol{\mu} \leq \boldsymbol{\lambda} \\ 0 & \text{otherwise} \end{cases}$$

when $t = 1$.

1.4 Yang-Baxter integrability

One of the main technical tools we will need in the following chapters is the Yang-Baxter integrability of our vertex models (Propositions 1.4.6-1.4.9). The Yang-Baxter equation (YBE), which was first introduced in statistical mechanics as a bridge to quantum mechanics, can be thought of as a sort of commutation relation between the vertices. The Yang-Baxter integrability of our vertex models will follow from work done in [1]. Each of our vertex weights can be realized as a degeneration of the vertex weights $W_z(\mathbf{A}, \mathbf{B}; \mathbf{C}, \mathbf{D}|r, s)$ from [1, Definition 5.1.1].

Lemma 1.4.1 ([28, Lemma 3.1]). *We adopt the notation of [1], except we use t in place of q . In particular, we let $W_z(\mathbf{A}, \mathbf{B}; \mathbf{C}, \mathbf{D}|r, s)$ be the vertex weights from [1, Definition 5.1.1] with t in place of q . Then*

$$\begin{aligned}
 \begin{array}{c} \mathbf{C} \\ \square x \mathbf{D} \\ \mathbf{A} \end{array} &= \lim_{\alpha \rightarrow 0} (-\alpha)^d \lim_{\beta \rightarrow 0} \beta^{-2d} W_{x/\alpha}(\mathbf{A}, \mathbf{B}; \mathbf{C}, \mathbf{D}|(x/\alpha)^{1/2}, \beta), \\
 \begin{array}{c} \mathbf{C} \\ \blacksquare y \mathbf{D} \\ \mathbf{A} \end{array} &= \lim_{Y \rightarrow 0} Y^{-d} \lim_{S \rightarrow 0} W_1(\mathbf{A}, \mathbf{B}; \mathbf{C}, \mathbf{D}|Sy^{-1/2}, SY^{1/2}), \\
 \begin{array}{c} \mathbf{B} \quad \mathbf{C} \\ \diagdown \quad \diagup \\ \mathbf{A} \quad \mathbf{D} \end{array} &= \lim_{\alpha \rightarrow 0} W_{x/y}(\mathbf{A}, \mathbf{B}; \mathbf{C}, \mathbf{D}|(x/\alpha)^{1/2}, (y/\alpha)^{1/2}), \\
 \begin{array}{c} \mathbf{B} \quad \mathbf{C} \\ \color{yellow} \times \\ \mathbf{A} \quad \mathbf{D} \end{array} &= \lim_{\alpha \rightarrow 0} W_{x/\alpha}(\mathbf{A}, \mathbf{B}; \mathbf{C}, \mathbf{D}|(x/\alpha)^{1/2}, (-y/\alpha)^{-1/2}), \\
 \begin{array}{c} \mathbf{B} \quad \mathbf{C} \\ \color{orange} \times \\ \mathbf{A} \quad \mathbf{D} \end{array} &= \lim_{S \rightarrow 0} W_1(\mathbf{A}, \mathbf{B}; \mathbf{C}, \mathbf{D}|Sx^{-1/2}, Sy^{-1/2}).
 \end{aligned}$$

Proof. This follows from various corollaries in [1, Section 8.3] along with the algebraic definitions of the L (white box), L' (purple box), R (white cross), R' (yellow cross), and R'' (orange cross) matrices.

- For the L matrix, this follows from [1, Cor. 8.3.6].
- For the L' matrix, this follows from [1, Cor. 8.3.4].
- For the R matrix, this follows from [1, Cor. 8.3.1] (substituting $s = (y/\alpha)^{1/2}$).
- For the R' matrix, this follows from [1, Cor. 8.3.8] (substituting $s = (-y/\alpha)^{-1/2}$).
- For the R'' matrix, this follows from [1, Cor. 8.3.3].

□

Although the M and M' matrices are not mentioned in the previous lemma, they too can be realized as degenerations of the W_z weights; their algebraic definitions are

$$\begin{aligned} M_x^{(k)}(\mathbf{I}, \mathbf{J}, \mathbf{K}, \mathbf{L}) &= x^k t^{\binom{k}{2}} L_{\bar{x}}^{(k)}(\mathbf{I}, \mathbf{J}, \mathbf{K}, \mathbf{L}), \\ M_x'^{(k)}(\mathbf{I}, \mathbf{J}, \mathbf{K}, \mathbf{L}) &= x^k L_{x^{-1}}'^{(k)}(\mathbf{I}, \mathbf{J}, \mathbf{K}, \mathbf{L}) \end{aligned}$$

and the L and L' matrices can be realized as degenerations of the W_z weights by the lemma.

As shown in [1], the W_z weights satisfy the Yang-Baxter equation.

Theorem 1.4.2 ([1, Prop. 5.1.4]). *The W_z weights satisfy the YBE*

$$\begin{aligned} &\sum_{\mathbf{I}_2, \mathbf{J}_2, \mathbf{K}_2} W_{\chi/\gamma}(\mathbf{I}_1, \mathbf{J}_1; \mathbf{I}_2, \mathbf{J}_2 | r, s) W_{\chi/z}(\mathbf{K}_1, \mathbf{J}_2; \mathbf{K}_2, \mathbf{J}_3 | r, \tau) W_{\gamma/z}(\mathbf{K}_2, \mathbf{I}_2; \mathbf{K}_3, \mathbf{I}_3 | s, \tau) \\ &= \sum_{\mathbf{I}_2, \mathbf{J}_2, \mathbf{K}_2} W_{\gamma/z}(\mathbf{K}_1, \mathbf{I}_1; \mathbf{K}_2, \mathbf{I}_2 | s, \tau) W_{\chi/z}(\mathbf{K}_2, \mathbf{J}_1; \mathbf{K}_3, \mathbf{J}_2 | r, \tau) W_{\chi/\gamma}(\mathbf{I}_2, \mathbf{J}_2; \mathbf{I}_3, \mathbf{J}_3 | r, s) \end{aligned} \tag{1.1}$$

for all $\chi, \gamma, z, r, s, \tau \in \mathbb{C}$ and choice of boundary condition $\mathbf{I}_1, \mathbf{J}_1, \mathbf{K}_1, \mathbf{I}_3, \mathbf{J}_3, \mathbf{K}_3 \in \{0, 1\}^k$. Using the conventions of [1], we can draw this diagrammatically as

$$\sum_{\mathbf{I}_2, \mathbf{J}_2, \mathbf{K}_2} w \left(\begin{array}{c} \mathbf{K}_3 \\ (\chi; r) \mathbf{J}_1 \nearrow \mathbf{I}_2 \xrightarrow{\quad} \mathbf{I}_3 \\ (\gamma; s) \mathbf{I}_1 \nearrow \mathbf{J}_2 \xrightarrow{\quad} \mathbf{J}_3 \\ \mathbf{K}_1 \\ (z; \tau) \end{array} \right) = \sum_{\mathbf{I}_2, \mathbf{J}_2, \mathbf{K}_2} w \left(\begin{array}{c} \mathbf{K}_3 \\ (\chi; r) \mathbf{J}_1 \xrightarrow{\quad} \mathbf{J}_2 \nearrow \mathbf{I}_3 \\ (\gamma; s) \mathbf{I}_1 \xrightarrow{\quad} \mathbf{I}_2 \nearrow \mathbf{J}_3 \\ \mathbf{K}_1 \\ (z; \tau) \end{array} \right)$$

where solid arrows are fixed and dashed arrows are summed over.

Remark 1.4.3. *Let us say a quick word about where Theorem 1.4.2 comes from. Bazhanov and Shadrnikov [5] constructed the fundamental R -matrix for the quantum affine superalgebra $U_q(\widehat{\mathfrak{sl}}(m|n))$, and showed that it satisfied the Yang-Baxter equation. (Although this was not the method used in [5, Section 3], the fact that this matrix satisfies the Yang-Baxter equation can be verified via a direct computation using the explicit formulae for its entries.) Aggarwal, Borodin, and Wheeler [1] constructed the W_z weights by applying the fusion procedure originating in [37] to the fundamental R -matrix, specializing to $m = 1$, and applying analytic continuation. The Yang-Baxter equation for the W_z weights falls out from the Yang-Baxter equation for the fundamental R -matrix.*

As a consequence of Lemma 1.4.1 and Theorem 1.4.2, our vertices satisfy several YBEs, which we list below. We will derive Prop. 1.4.4, 1.4.6, and 1.4.7; the others can be derived via a suitable change of variables (to go from white to gray or from purple to pink). Prop. 1.4.4 is proven in a different (combinatorial) way in [22, Theorem 4.1].

Proposition 1.4.4 ([28, Prop. 3.2]). *The L and R matrices satisfy the YBE*

$$\sum_{\text{interior paths}} w \left(\begin{array}{c} \text{K}_3 \\ \begin{array}{c} y \\ x \end{array} \\ \text{K}_1 \end{array} \begin{array}{c} I_3 \\ J_3 \end{array} \right) = \sum_{\text{interior paths}} w \left(\begin{array}{c} \text{K}_3 \\ \begin{array}{c} x \\ y \end{array} \\ \text{K}_1 \end{array} \begin{array}{c} I_3 \\ J_3 \end{array} \right)$$

for any choice of boundary condition $\mathbf{I}_1, \mathbf{J}_1, \mathbf{K}_1, \mathbf{I}_3, \mathbf{J}_3, \mathbf{K}_3$.

Proposition 1.4.5 ([22, Prop. 6.2]). *The L , M , and R matrices satisfy the YBE*

$$\sum_{\text{interior paths}} w \left(\begin{array}{c} \text{K}_3 \\ \begin{array}{c} y \\ \bar{x} \end{array} \\ \text{K}_1 \end{array} \begin{array}{c} I_3 \\ J_3 \end{array} \right) = \sum_{\text{interior paths}} w \left(\begin{array}{c} \text{K}_3 \\ \begin{array}{c} \bar{x} \\ y \end{array} \\ \text{K}_1 \end{array} \begin{array}{c} I_3 \\ J_3 \end{array} \right)$$

for any choice of boundary condition $\mathbf{I}_1, \mathbf{J}_1, \mathbf{K}_1, \mathbf{I}_3, \mathbf{J}_3, \mathbf{K}_3$.

Proposition 1.4.6 ([28, Prop. 3.3]). *The L , L' , and R' matrices satisfy the YBE*

$$\sum_{\text{interior paths}} w \left(\begin{array}{c} \text{K}_3 \\ \begin{array}{c} y \\ x \end{array} \\ \text{K}_1 \end{array} \begin{array}{c} I_3 \\ J_3 \end{array} \right) = \sum_{\text{interior paths}} w \left(\begin{array}{c} \text{K}_3 \\ \begin{array}{c} x \\ y \end{array} \\ \text{K}_1 \end{array} \begin{array}{c} I_3 \\ J_3 \end{array} \right)$$

for any choice of boundary condition $\mathbf{I}_1, \mathbf{J}_1, \mathbf{K}_1, \mathbf{I}_3, \mathbf{J}_3, \mathbf{K}_3$.

Proposition 1.4.7 ([28, Prop. 3.4]). *The L' and R'' matrices satisfy the YBE*

$$\sum_{\text{interior paths}} w \left(\begin{array}{c} \text{K}_3 \\ \begin{array}{c} y \\ x \end{array} \\ \text{K}_1 \end{array} \begin{array}{c} I_3 \\ J_3 \end{array} \right) = \sum_{\text{interior paths}} w \left(\begin{array}{c} \text{K}_3 \\ \begin{array}{c} x \\ y \end{array} \\ \text{K}_1 \end{array} \begin{array}{c} I_3 \\ J_3 \end{array} \right)$$

for any choice of boundary condition $\mathbf{I}_1, \mathbf{J}_1, \mathbf{K}_1, \mathbf{I}_3, \mathbf{J}_3, \mathbf{K}_3$.

Proposition 1.4.8 ([20, Prop. 3.1]). *The L' , M , and R' matrices satisfy the YBE*

$$\sum_{\text{interior paths}} w \left(\begin{array}{c} \text{K}_3 \\ \begin{array}{c} y \\ \bar{x} \end{array} \\ \text{K}_1 \end{array} \begin{array}{c} I_3 \\ J_3 \end{array} \right) = \sum_{\text{interior paths}} w \left(\begin{array}{c} \text{K}_3 \\ \begin{array}{c} \bar{x} \\ y \end{array} \\ \text{K}_1 \end{array} \begin{array}{c} I_3 \\ J_3 \end{array} \right)$$

for any choice of boundary condition $\mathbf{I}_1, \mathbf{J}_1, \mathbf{K}_1, \mathbf{I}_3, \mathbf{J}_3, \mathbf{K}_3$.

Multiplying both sides by $(-\alpha)^{|\mathbf{J}_3|}(SY^{1/2})^{-2|\mathbf{J}_3|}Y^{-|\mathbf{I}_3|}$ gives

$$\begin{aligned}
& \sum_{\mathbf{I}_2, \mathbf{J}_2, \mathbf{K}_2} W_{x/\alpha}(\mathbf{I}_1, \mathbf{J}_1; \mathbf{I}_2, \mathbf{J}_2 | (x/\alpha)^{1/2}, Sy^{-1/2}) \\
& \quad \cdot (-\alpha)^{|\mathbf{J}_3|}(SY^{1/2})^{-2|\mathbf{J}_3|} W_{x/\alpha}(\mathbf{K}_1, \mathbf{J}_2; \mathbf{K}_2, \mathbf{J}_3 | (x/\alpha)^{1/2}, SY^{-1/2}) \\
& \quad \cdot Y^{-|\mathbf{I}_3|} W_1(\mathbf{K}_2, \mathbf{I}_2; \mathbf{K}_3, \mathbf{I}_3 | Sy^{-1/2}, SY^{1/2}) \\
= & \sum_{\mathbf{I}_2, \mathbf{J}_2, \mathbf{K}_2} Y^{-|\mathbf{I}_2|} W_1(\mathbf{K}_1, \mathbf{I}_1; \mathbf{K}_2, \mathbf{I}_2 | Sy^{-1/2}, SY^{1/2}) \\
& \quad \cdot (-\alpha)^{|\mathbf{J}_2|}(SY^{1/2})^{-2|\mathbf{J}_2|} W_{x/\alpha}(\mathbf{K}_2, \mathbf{J}_1; \mathbf{K}_3, \mathbf{J}_2 | (x/\alpha)^{1/2}, SY^{-1/2}) \\
& \quad \cdot (-\alpha)^{|\mathbf{J}_3|-|\mathbf{J}_2|} S^{-2|\mathbf{J}_3|+2|\mathbf{J}_2|} W_{x/\alpha}(\mathbf{I}_2, \mathbf{J}_2; \mathbf{I}_3, \mathbf{J}_3 | (x/\alpha)^{1/2}, Sy^{-1/2})
\end{aligned}$$

where we use $|\mathbf{I}_2| + |\mathbf{J}_2| = |\mathbf{I}_3| + |\mathbf{J}_3|$ by path conservation on the right-hand side. Substituting $\alpha = -S^2$ and $\beta = SY^{1/2}$ gives

$$\begin{aligned}
& \sum_{\mathbf{I}_2, \mathbf{J}_2, \mathbf{K}_2} W_{x/\alpha}(\mathbf{I}_1, \mathbf{J}_1; \mathbf{I}_2, \mathbf{J}_2 | (x/\alpha)^{1/2}, (-y/\alpha)^{-1/2}) \\
& \quad \cdot (-\alpha)^{|\mathbf{J}_3|} \beta^{-2|\mathbf{J}_3|} W_{x/\alpha}(\mathbf{K}_1, \mathbf{J}_2; \mathbf{K}_2, \mathbf{J}_3 | (x/\alpha)^{1/2}, \beta) \\
& \quad \cdot Y^{-|\mathbf{I}_3|} W_1(\mathbf{K}_2, \mathbf{I}_2; \mathbf{K}_3, \mathbf{I}_3 | Sy^{-1/2}, SY^{1/2}) \\
= & \sum_{\mathbf{I}_2, \mathbf{J}_2, \mathbf{K}_2} Y^{-|\mathbf{I}_2|} W_1(\mathbf{K}_1, \mathbf{I}_1; \mathbf{K}_2, \mathbf{I}_2 | Sy^{-1/2}, SY^{1/2}) \\
& \quad \cdot (-\alpha)^{|\mathbf{J}_2|} \beta^{-2|\mathbf{J}_2|} W_{x/\alpha}(\mathbf{K}_2, \mathbf{J}_1; \mathbf{K}_3, \mathbf{J}_2 | (x/\alpha)^{1/2}, \beta) \\
& \quad \cdot W_{x/\alpha}(\mathbf{I}_2, \mathbf{J}_2; \mathbf{I}_3, \mathbf{J}_3 | (x/\alpha)^{1/2}, (-y/\alpha)^{-1/2}).
\end{aligned}$$

Taking $S \rightarrow 0$ and $Y \rightarrow 0$ (hence also $\alpha = -S^2 \rightarrow 0$ and $\beta = SY^{1/2} \rightarrow 0$) and then applying Lemma 1.4.1 gives the desired YBE

$$\begin{aligned}
& \sum_{\mathbf{I}_2, \mathbf{J}_2, \mathbf{K}_2} R'_{y/x}(\mathbf{I}_1, \mathbf{J}_1; \mathbf{I}_2, \mathbf{J}_2) L_x(\mathbf{K}_1, \mathbf{J}_2; \mathbf{K}_2, \mathbf{J}_3) L'_y(\mathbf{K}_2, \mathbf{I}_2; \mathbf{K}_3, \mathbf{I}_3) \\
= & \sum_{\mathbf{I}_2, \mathbf{J}_2, \mathbf{K}_2} L'_y(\mathbf{K}_1, \mathbf{I}_1; \mathbf{K}_2, \mathbf{I}_2) L_x(\mathbf{K}_2, \mathbf{J}_1; \mathbf{K}_3, \mathbf{J}_2) R'_{y/x}(\mathbf{I}_2, \mathbf{J}_2; \mathbf{I}_3, \mathbf{J}_3).
\end{aligned}$$

□

Proof of Proposition 1.4.7. Fix $S, Y, x, y \in \mathbb{C}$ and let $\alpha = -S^2$ and $\beta = SY^{1/2}$. Substituting $\chi = 1$, $\gamma = 1$, $z = 1$, $r = Sx^{-1/2}$, $s = Sy^{-1/2}$, and $\tau = SY^{-1/2}$ into (1.1)

gives

$$\begin{aligned} & \sum_{\mathbf{I}_2, \mathbf{J}_2, \mathbf{K}_2} W_1(\mathbf{I}_1, \mathbf{J}_1; \mathbf{I}_2, \mathbf{J}_2 | Sx^{-1/2}, Sy^{-1/2}) W_1(\mathbf{K}_1, \mathbf{J}_2; \mathbf{K}_2, \mathbf{J}_3 | Sx^{-1/2}, SY^{-1/2}) W_1(\mathbf{K}_2, \mathbf{I}_2; \mathbf{K}_3, \mathbf{I}_3 | Sy^{-1/2}, SY^{1/2}) \\ &= \sum_{\mathbf{I}_2, \mathbf{J}_2, \mathbf{K}_2} W_1(\mathbf{K}_1, \mathbf{I}_1; \mathbf{K}_2, \mathbf{I}_2 | Sy^{-1/2}, SY^{1/2}) W_1(\mathbf{K}_2, \mathbf{J}_1; \mathbf{K}_3, \mathbf{J}_2 | Sx^{-1/2}, SY^{1/2}) W_1(\mathbf{I}_2, \mathbf{J}_2; \mathbf{I}_3, \mathbf{J}_3 | Sx^{-1/2}, Sy^{-1/2}). \end{aligned}$$

Multiplying both sides by $Y^{-|\mathbf{I}_3| - |\mathbf{J}_3|}$ gives

$$\begin{aligned} & \sum_{\mathbf{I}_2, \mathbf{J}_2, \mathbf{K}_2} W_1(\mathbf{I}_1, \mathbf{J}_1; \mathbf{I}_2, \mathbf{J}_2 | Sx^{-1/2}, Sy^{-1/2}) \\ & \quad \cdot Y^{-|\mathbf{J}_3|} W_1(\mathbf{K}_1, \mathbf{J}_2; \mathbf{K}_2, \mathbf{J}_3 | Sx^{-1/2}, SY^{-1/2}) \\ & \quad \cdot Y^{-|\mathbf{I}_3|} W_1(\mathbf{K}_2, \mathbf{I}_2; \mathbf{K}_3, \mathbf{I}_3 | Sy^{-1/2}, SY^{1/2}) \\ &= \sum_{\mathbf{I}_2, \mathbf{J}_2, \mathbf{K}_2} Y^{-|\mathbf{I}_2|} W_1(\mathbf{K}_1, \mathbf{I}_1; \mathbf{K}_2, \mathbf{I}_2 | Sy^{-1/2}, SY^{1/2}) \\ & \quad \cdot Y^{-|\mathbf{J}_2|} W_1(\mathbf{K}_2, \mathbf{J}_1; \mathbf{K}_3, \mathbf{J}_2 | Sx^{-1/2}, SY^{1/2}) \\ & \quad \cdot W_1(\mathbf{I}_2, \mathbf{J}_2; \mathbf{I}_3, \mathbf{J}_3 | Sx^{-1/2}, Sy^{-1/2}) \end{aligned}$$

where we use $|\mathbf{I}_2| + |\mathbf{J}_2| = |\mathbf{I}_3| + |\mathbf{J}_3|$ by path conservation on the right-hand side. Taking $S \rightarrow 0$ and $Y \rightarrow 0$ and then applying Lemma 1.4.1 gives the desired YBE

$$\begin{aligned} & \sum_{\mathbf{I}_2, \mathbf{J}_2, \mathbf{K}_2} R_{x/y}''(\mathbf{I}_1, \mathbf{J}_1; \mathbf{I}_2, \mathbf{J}_2) L_x'(\mathbf{K}_1, \mathbf{J}_2; \mathbf{K}_2, \mathbf{J}_3) L_y'(\mathbf{K}_2, \mathbf{I}_2; \mathbf{K}_3, \mathbf{I}_3) \\ &= \sum_{\mathbf{I}_2, \mathbf{J}_2, \mathbf{K}_2} L_y'(\mathbf{K}_1, \mathbf{I}_1; \mathbf{K}_2, \mathbf{I}_2) L_x'(\mathbf{K}_2, \mathbf{J}_1; \mathbf{K}_3, \mathbf{J}_2) R_{x/y}''(\mathbf{I}_2, \mathbf{J}_2; \mathbf{I}_3, \mathbf{J}_3). \end{aligned}$$

□

Chapter 2

LLT polynomials

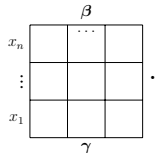
2.1 Introduction

LLT polynomials are a family of symmetric polynomials, which can be seen as a t -deformation of products of skew Schur functions. They were originally introduced by Lascoux, Leclerc and Thibon (for whom the polynomials are eponymously named) in [39] to study certain plethysm coefficients, and they were defined via a relationship with the Fock space representation of a quantum affine Lie algebra. The original definition expresses the LLT polynomials as a sum over k -ribbon tableaux, weighted with a spin statistic which arises naturally in this representation [39, 32]. Bylund and Haiman discovered an alternative way to model LLT polynomials, instead indexed by k -tuples of skew Young diagrams, weighted with an inversion statistic, as described in [30]. While not apparent from either definition, LLT polynomials possess many astonishing properties:

- I. they are symmetric in the variables $X_n = \{x_1, \dots, x_n\}$ [39];
- II. when their indexing tuple of partitions is a tuple of single rows, they are equal to the modified Hall-Littlewood polynomials $\widetilde{H}_\mu(X_n; t)$ [39];
- III. they satisfy a Cauchy-like identity [38];
- IV. they are Schur-positive, i.e. they expand as a $\mathbb{N}[t]$ -linear combination of Schur polynomials [40, 29].

Using the vertex models defined in Chapter 1, we prove several new results on LLT polynomials and give new (combinatorial) proofs of several of the known listed properties above. The main result can be summarized as follows.

Theorem 2.1.1 (Thm. 2.3.3). *Let β/γ be a tuple of skew partitions. There is an integrable vertex model whose partition function $\mathcal{Z}_{\beta/\gamma}(X_n; t)$ is precisely the coinversion LLT polynomial $\mathcal{L}_{\beta/\gamma}(X_n; t)$. Explicitly, $\mathcal{Z}_{\beta/\gamma}(X_n; t)$ is the partition function associated to the lattice*



Here we present a new formulation of LLT polynomials, which we call a *coinversion LLT polynomial*. They serve as a generating function for k -tuples of semistandard Young tableaux, weighted with a *coinversion* statistic. The definition is easily seen to be equivalent to the inversion definition after inverting t and multiplying by a suitable power of t . This new formulation was detailed to the fourth author in personal correspondence with M. Haiman, and can be reviewed in the first of a recent series of publications [7].

We take the time now to expound on the details of properties I-IV. and outline the organization of this chapter.

I. Symmetry. The definition of LLT polynomials as spin-generating functions arises naturally in the study of the representation theory of the Fock space for $\mathcal{U}_q(\widehat{\mathfrak{sl}}_n)$. In particular, there are natural vertex operators on this space whose action on basis elements is captured by the LLT polynomials. The symmetry of the LLT polynomials follows from the commutativity of these vertex operators. Later, a purely combinatorial proof was given using the inversion variant of LLT polynomials [31].

As innocuous as it is, the symmetry of the LLT polynomials has had several important uses in combinatorics. In [30], the authors conjectured a combinatorial formula for the Frobenius character of the ring of diagonal coinvariants (known later as the shuffle conjecture). This Frobenius character is inherently symmetric, owing to a natural S_n -module structure for the diagonal coinvariant ring. The combinatorial formula was shown to expand into LLT polynomials, thus witnessing their symmetry. A similar argument was used later in [31] to show that a proposed monomial expansion for Macdonald polynomials was indeed symmetric.

We use the integrability of our vertex model to provide another proof that LLT polynomials are symmetric. Our proof is combinatorial, modulo the underlying representation theory governing the Yang-Baxter equation.

II. Single Rows. From the definition of coinversion LLT polynomials (Definition 2.2.4 below), one can easily see that at $t = 1$, the definition devolves into a product of Schur functions

$$\mathcal{L}_{\beta/\gamma}(X; 1) = s_{\beta^{(1)}/\gamma^{(1)}}(X) \cdots s_{\beta^{(k)}/\gamma^{(k)}}(X).$$

Hence, the LLT polynomial $\mathcal{L}_\mu(X; t)$ indexed by the tuple of partitions $\boldsymbol{\mu} = (\mu^{(1)}, \dots, \mu^{(k)})$ gives a t -analog $c_{\mu^{(1)}, \dots, \mu^{(k)}}^\lambda(t)$ of the classical Littlewood-Richardson coefficients.

When each partition $\mu^{(j)}$ has only one part μ_j , $c_{\mu_1, \dots, \mu_k}^\lambda(t)$ coincides (up to a power of t) with the Kostka-Foulkes polynomial $K_{\lambda, \mu}(t)$. The Kostka-Foulkes polynomials have seemingly endless appearances in representation theory and combinatorics; in particular, they are the coefficients of a Schur function on the basis of transformed Hall-Littlewood polynomials $H_\mu(X; t)$. Hence, the identity

$$\mathcal{L}_\mu(X; t) = t^d H_\mu(X; t) \quad (2.1)$$

holds, for some integer d . The original proof of (2.1) relies on the geometry of an underlying flag variety. We apply our vertex model to provide an alternate (combinatorial) proof.

III. Cauchy identity. A Cauchy identity was given in [38] for the original spin-generating LLT polynomials. We prove the following Cauchy identity for coinversion LLT polynomials

$$\sum_{\lambda} \mathcal{L}_\lambda(X_n; t) \mathcal{L}_{\lambda^{\text{rot}}}(Y_n; t) = \prod_{i,j=1}^n \prod_{m=0}^{k-1} (1 - x_i y_j t^m)^{-1} \quad (2.2)$$

where λ^{rot} denotes the tuple of partitions gotten by rotating each partition 180 degrees and then reversing the order. As remarked in [38], the reader is warned that (2.2) does not imply that the LLT polynomials form an orthogonal basis under some inner product, as they are not linearly independent.

IV. Schur positivity. It was shown in [40] that when the LLT polynomials are indexed by tuples of partitions, then their coefficients in the Schur basis are certain affine Kazhdan-Lusztig polynomials. As it is known that these Kazhdan-Lusztig polynomials have non-negative coefficients, the result implies that LLT polynomials are Schur-positive. This argument was extended in [29] to arbitrary skew partitions, and moreover generalized to any complex reductive Lie group. Unfortunately, it is not clear how the vertex model formalism can be used to tackle the notion of positivity.

This chapter is organized as follows. In Section 2.2, we define the coinversion LLT polynomials and review the necessary combinatorial preliminaries. In Section 2.3, we use the white vertices defined in Chapter 1 to define a partition function, which we show equals the coinversion LLT polynomial. In Section 2.5 we show that LLT polynomials coincide with Hall-Littlewood polynomials, and in Section 2.6 we show that they satisfy the above Cauchy identity. Finally, in Section 2.7, we provide some examples of using Theorem 2.3.3 to compute coinversion LLT polynomials.

2.2 LLT polynomials

Let $T = (T^{(1)}, \dots, T^{(k)})$ be a semistandard Young tableau on a tuple of skew partitions $\beta/\gamma = (\beta^{(1)}/\gamma^{(1)}, \dots, \beta^{(k)}/\gamma^{(k)})$. We choose the reading order on cells by reading from the smallest to the largest content line, moving along a each content line from SW to NE. We say two cells **attack** each other if either (1) they are on the same content line or (2) they are on adjacent content lines, with the cell on the larger content line in an earlier shape. We define an **attacking inversion** of T to be a pair of attacking cells with different entries in which the larger entry precedes the smaller in reading order.

Definition 2.2.1. *Let β/γ be a tuple of skew partitions. The inversion LLT polynomial is the generating function*

$$\mathcal{G}_{\beta/\gamma}(X; t) = \sum_{T \in \text{SSYT}(\beta/\gamma)} t^{\text{inv}(T)} x^T$$

where $\text{inv}(T)$ is the number of attacking inversions of T .

Remark 2.2.2. *Definition 2.2.1 was first given in [30], but it is not evidently related to the original spin-generating functions $G_{\lambda/\mu}^{(k)}(X; q)$ defined in [39]. The connection materializes via the Littlewood k -quotient map (Definition 3.2.5), which is a weight-preserving bijection between semistandard ribbon tableaux and tuples of semistandard Young tableaux on the quotient shape. It was shown in [30] that there is some constant e depending only on the shape β/γ such that*

$$G_{\lambda/\mu}^{(k)}(X; t) = t^e \mathcal{G}_{\beta/\gamma}(X; t^{-2}). \tag{2.3}$$

where β/γ is the k -quotient of λ/μ .

As is the case for Macdonald polynomials, the number of attacking inversions can be reformulated as the number of inversion triples, which we now define. Given a tuple β/γ of skew partitions, we say that three cells $u, v, w \in \mathbb{Z} \times \mathbb{Z}$ form a **triple** of β/γ if

1. $v \in \lambda/\mu$;
2. they are situated as below

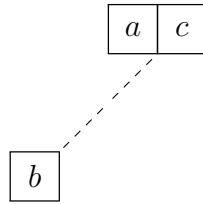


namely with v and w on the same content line and w in a later shape, and u on a content line one smaller, in the same row as w ; and

3. if u and w are in row r of $\lambda^{(j)}/\mu^{(j)}$, then u and w must be between the cells $(r, \mu_r^{(j)})$ and $(r, \lambda_r^{(j)} + 1)$, inclusive.

It is important to note that while v must be a cell in β/γ , we allow the cells u and w to not be in any of the skew shapes, in which case u must be at the end of some row in γ and w must be the cell directly to the right of the end of some row in β .

Definition 2.2.3. Let β/γ be a tuple of skew partitions and let $T \in \text{SSYT}(\beta/\gamma)$. Let a, b, c be the entries in the cells of a triple (u, v, w) , where we set $a = 0$ and $c = \infty$ if the respective cell is not in β/γ . We say the triple of entries



is a **coinversion triple** if $a \leq b \leq c$ and an **inversion triple** if $b < a \leq c$ or $a \leq c < b$.

There are 7 coinversion triples in Example 1.1.2 above: $(0, 2, 4)$, $(0, 2, 7)$, $(3, 4, \infty)$, $(0, 4, 7)$, $(4, 5, \infty)$, $(1, 9, \infty)$, and $(0, 9, \infty)$. However, we note that Definition 2.2.3, and that of a triple, depends not merely on the tuple of skew partitions β/γ , but on the individual tuples of partitions β, γ . Indeed, if in Example 1.1.2, we made the superficial change in the third skew shape from $(1)/(0)$ to $(2, 2)/(2, 1)$, then we would introduce another coinversion triple $(0, 9, \infty)$. Likewise, if we consider the third skew shape being instead $(1, 0)/(0, 0)$, then we introduce the coinversion triples $(0, 8, \infty)$ and $(0, 6, \infty)$. It's easily seen that any extra coinversion triples present are independent of the filling T .

Definition 2.2.4. Let β/γ be a tuple of skew partitions. The coinversion LLT polynomial is the generating function

$$\mathcal{L}_{\beta/\gamma}(X; t) = \sum_{T \in \text{SSYT}(\beta/\gamma)} t^{\text{coinv}(T)} x^T$$

where $\text{coinv}(T)$ is the number of coinversion triples of T .

In light of the preceding remarks, we note that if β/γ and β^*/γ^* are two representations of the same skew shapes, then their coinversion LLT polynomials differ by an overall power of t .

Note that in a semistandard filling T on some tuple of skew partitions, a pair of attacking entries forms an inversion if and only if they are in a (unique) inversion triple. Indeed, if $b < a \leq c$, then (a, b) is an attacking inversion, and likewise if $a \leq c < b$, then (b, c) is an attacking inversion. Hence, we have the identity

$$\mathcal{L}_{\beta/\gamma}(X; t) = t^m \mathcal{G}_{\beta/\gamma}(X; t^{-1}) \tag{2.5}$$

where m is the number of triples in β/γ . We give explicit formulae for m in Section 2.5.

Remark 2.2.5. *A simplified version of Definition 2.2.4, in which each shape in β/γ consists of a single row, can be found in [7]. There, the coinversion LLT polynomials are first defined, via the action of a Hecke algebra, as a polynomial truncation of a certain formal power series. It is then shown that this algebraic definition results in the combinatorial definition above.*

The formal power series in question consists of terms that are GL_n characters. This is the reason why our polynomials depend on the individual tuples of partitions β, γ . Indeed, the reader is welcome to view β and γ not as partitions, but really as dominant weights of GL_n , i.e. non-increasing lists of integers. In fact, this “LLT series” can be defined for any complex reductive Lie group (see [29]).

2.3 Vertex model

In this section we use the white L vertices defined in Chapter 1 to construct a partition function which we show equals the coinversion LLT polynomial defined above (with the appropriate choice of boundary conditions).

Recall the algebraic definition of the L matrix

$$L_x^{(k)}(\mathbf{I}, \mathbf{J}, \mathbf{K}, \mathbf{L}) = \mathbf{1}_{\mathbf{I}+\mathbf{J}=\mathbf{K}+\mathbf{L}} \prod_{i=1}^k \mathbf{1}_{I_i+J_i \neq 2} \cdot x^{|\mathbf{L}|} t^{\varphi(\mathbf{L}, \mathbf{I}+\mathbf{J})}.$$

Graphically, the constraint $\mathbf{I} + \mathbf{J} = \mathbf{K} + \mathbf{L}$ is a conservation property, meaning that the paths entering and the paths exiting must be the same. The constraint that there be no indices $i \in [k]$ such that $I_i + J_i = 2$ means that there can be at most one path of any given color. If these two constraints are satisfied, then the weight

can be expressed as

$$L_x^{(k)}(\mathbf{I}, \mathbf{J}; \mathbf{K}, \mathbf{L}) = x^{\substack{\# \text{ colors exiting the} \\ \text{vertex to the right}}} \prod_{\substack{\text{colors } i \text{ exiting the} \\ \text{vertex to the right}}} \frac{\# \text{ colors larger than } i \text{ that} \\ \text{appear in the vertex}}{t}. \quad (2.6)$$

When $k = 1$, this is the non-intersecting path model (also known as the five vertex model), as illustrated in [51, Thm. 7.16.1].

Given a k -tuple of partitions $\boldsymbol{\lambda} = (\lambda^{(1)}, \dots, \lambda^{(k)})$ and an integer i , we define

$$\boldsymbol{\lambda}(i) = (a_{i-\frac{1}{2}}^{(1)}, \dots, a_{i-\frac{1}{2}}^{(k)}) \in \{0, 1\}^k$$

where $a = (a^{(1)}, \dots, a^{(k)})$ is the Maya diagram of $\boldsymbol{\lambda}$. Let

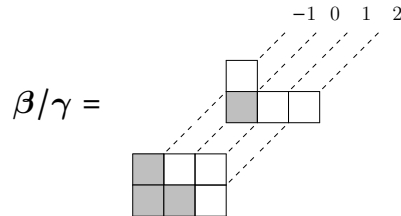
$$\begin{aligned} r = r(\boldsymbol{\beta}/\boldsymbol{\gamma}) &= \min\{i \in \mathbb{Z} : \boldsymbol{\gamma}(i) \neq \mathbf{1}\}, \\ s = s(\boldsymbol{\beta}/\boldsymbol{\gamma}) &= \max\{i \in \mathbb{Z} : \boldsymbol{\beta}(i) \neq \mathbf{0}\} + 1. \end{aligned}$$

With this notation, we introduce a lattice that will be of particular interest to us:

$$W_n(\boldsymbol{\beta}/\boldsymbol{\gamma}) := \begin{array}{ccccc} & \boldsymbol{\beta}(r) & \dots & \boldsymbol{\beta}(s) & \\ \mathbf{0} & \begin{array}{|c|c|c|} \hline x_n & \cdots & x_n \\ \hline \end{array} & & & \mathbf{0} \\ & \vdots & & \vdots & \vdots \\ \mathbf{0} & \begin{array}{|c|c|c|} \hline x_1 & \cdots & x_1 \\ \hline \end{array} & & & \mathbf{0} \\ & \boldsymbol{\gamma}(r) & \dots & \boldsymbol{\gamma}(s) & \end{array} \quad (2.7)$$

Following [45], we define the **bandwidth** $\text{band}(\boldsymbol{\beta}/\boldsymbol{\gamma}) := s(\boldsymbol{\beta}/\boldsymbol{\gamma}) - r(\boldsymbol{\beta}/\boldsymbol{\gamma})$ to be one less than the number of columns in this lattice. To simplify notation, we will often replace $\boldsymbol{\beta}(r) \dots \boldsymbol{\beta}(s)$ with $\boldsymbol{\beta}$ and $\boldsymbol{\gamma}(r) \dots \boldsymbol{\gamma}(s)$ with $\boldsymbol{\gamma}$ to indicate the top and bottom boundary conditions.

Example 2.3.1. Let $\boldsymbol{\beta}/\boldsymbol{\gamma} = ((3, 3)/(2, 1), (3, 1)/(1, 0))$ and $n = 2$.



We compute $r = -1$ and $s = 3$, and

$$L_{\beta/\gamma} = \begin{array}{cccccc} & & -1 & 0 & 1 & 2 & 3 & & \\ & & (0,0) & (0,1) & (0,0) & (1,0) & (1,1) & & \\ (0,0) & & \boxed{x_2} & \boxed{x_2} & \boxed{x_2} & \boxed{x_2} & \boxed{x_2} & & (0,0) \\ & (0,0) & \boxed{x_1} & \boxed{x_1} & \boxed{x_1} & \boxed{x_1} & \boxed{x_1} & & (0,0) \\ & & (0,1) & (1,0) & (0,1) & (1,0) & (0,0) & & \end{array}$$

where we have included the column indices (in addition to the variables and the outer edge labels).

We let $\mathcal{Z}_{\beta/\gamma}(X_n; t)$ denote the partition function of $W_n(\beta/\gamma)$, that is,

$$\mathcal{Z}_{\beta/\gamma}(X_n; t) = \sum_{L \in LC(W_n(\beta/\gamma))} \text{weight}(L).$$

Remark 2.3.2. *It is easy to see that the partition function does not change if we expand the lattice to go from column $r' \leq r$ to column $s' \geq s$. Indeed, for all $r' < r$, we have $\gamma(r') = \beta(r') = \mathbf{1}$ so each color is forced to travel vertically through column r' , contributing a factor of 1 to the weight of each lattice configuration. Similarly, for all $s' > s$, we have $\gamma(s') = \beta(s') = \mathbf{0}$ so column s' is empty, contributing a factor of 1 to the weight of each lattice configuration.*

Having set up the necessary notation, we can state the main theorem of this chapter.

Theorem 2.3.3 ([22, Thm. 3.4]). *Let β/γ be a tuple of skew partitions. Then*

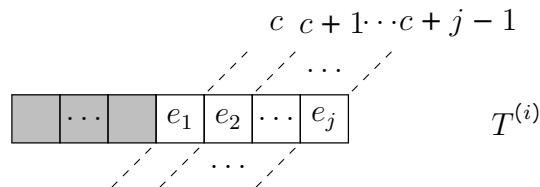
$$\mathcal{Z}_{\beta/\gamma}(X_n; t) = \mathcal{L}_{\beta/\gamma}(X_n; t).$$

Some examples of using this theorem to compute LLT polynomials are given in Section 2.7.

This theorem will follow from a weight-preserving bijection

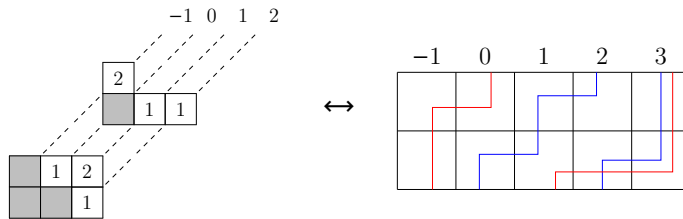
$$\varphi : \text{SSYT}(\beta/\gamma) \rightarrow LC(W_n(\beta/\gamma)).$$

Given $T \in \text{SSYT}(\beta/\gamma)$, the corresponding lattice configuration $L = \varphi(T)$ is constructed as follows. Each row in T corresponds to a colored path in L . Fix a row



in T . The corresponding path in L has color i , enters via the bottom of column c and exits via the top of column $c + j$, and crosses from column $c + m - 1$ to column $c + m$ at row e_m for each index $m \in [j]$.

Example 2.3.4. Let $\beta/\gamma = ((3, 3)/(2, 1), (3, 1)/(1, 0))$ and $n = 2$. Then



where in the lattice configuration blue is color 1, red is color 2, and we have omitted the variables and the edge labels (as we will do often).

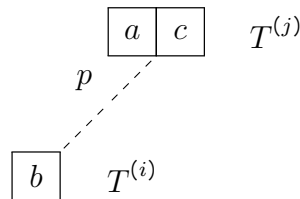
The invertibility of φ is straightforward; indeed this is a well-known fact for one color [51, Thm. 7.16.1] and the proof for k colors follows from applying the proof for one color to each of the k colors independently. The following proposition then completes the proof of Theorem 2.3.3.

Proposition 2.3.5 ([22, Prop. 3.6]). Let $T \in \text{SSYT}(\beta/\gamma)$ and let $\varphi(T)$ be the corresponding lattice configuration, as defined above. Then

$$\text{coinv}(T) = \sum_{\text{vertices } V \text{ in } \varphi(T)} \sum_{\text{colors } i \text{ exiting } V \text{ to the right}} (\# \text{ colors larger than } i \text{ that appear in } V).$$

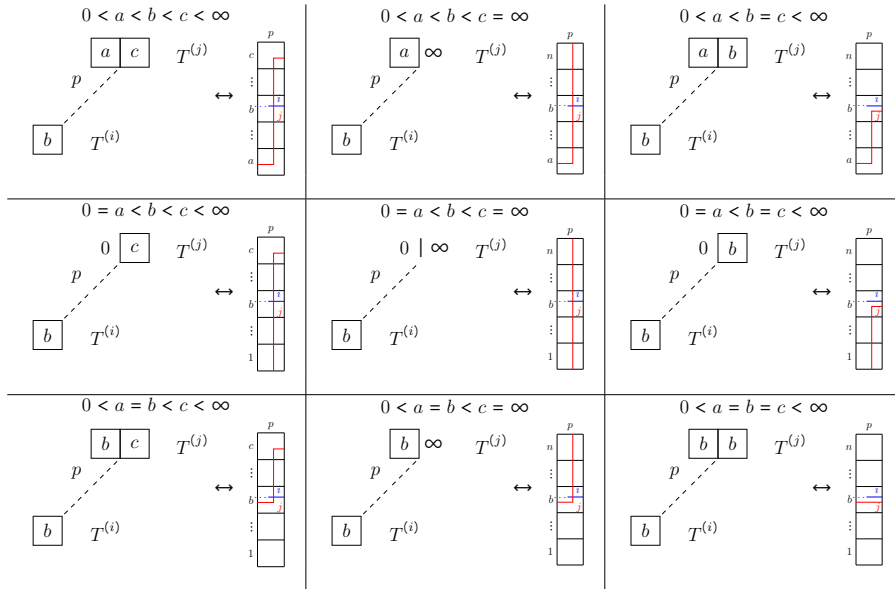
In particular, the weight of the lattice configuration $\varphi(T)$ is $x^T t^{\text{coinv}(T)}$.

Proof. The left-hand side counts the number of coinversion triples in T ; that is, the number of triples of boxes in T



with p denoting the content line, $i < j$, and $a \leq b \leq c$, where we set $a = 0$ and $c = \infty$ if the respective box is empty. One can observe that the coinversion triple can be recovered just from i, j, b, p , so we will identify each coinversion triple with the corresponding quadruple (i, j, b, p) . The right-hand side counts the number of

quadruples (i, j, b, p) where V is the vertex in $\varphi(T)$ at row b and column p , i is a color exiting V to the right, and j is a color larger than i that appears in V . The proposition follows from the fact that the left-hand side quadruples correspond to the right-hand side quadruples via φ . To verify this correspondence, we split into cases based on the form of the coinversion triple.



□

2.4 The symmetry of the LLT polynomials

The Yang-Baxter equation (Prop. 1.4.4) can be used to give an alternate proof that the coinversion LLT polynomials $\mathcal{L}_{\beta/\gamma}(X; t)$ are symmetric in the X variables. This was originally shown in [39], and later proven purely combinatorially in [31].

Theorem 2.4.1 ([22, Thm. 4.2]). *The coinversion LLT polynomial $\mathcal{L}_{\beta/\gamma}(X; t)$ is symmetric in the X variables.*

Proof. It is enough to show that swapping x_i and x_j leaves the partition function $\mathcal{Z}_{\beta/\gamma}(X; t)$ unchanged, for any $i < j$. Consider two rows

$$\begin{array}{ccccc} \mathbf{0} & x_j & \cdots & x_j & \mathbf{0} \\ \mathbf{0} & x_i & \cdots & x_i & \mathbf{0} \end{array}$$

in $W_n(\beta/\gamma)$. We insert an R matrix at the left end and repeatedly apply the YBE to get

$$\begin{array}{c} \mathbf{0} \\ \mathbf{0} \end{array} \begin{array}{|c|c|c|} \hline x_j & \dots & x_j \\ \hline x_i & \dots & x_i \\ \hline \end{array} \begin{array}{c} \mathbf{0} \\ \mathbf{0} \end{array} = \begin{array}{c} \mathbf{0} \\ \mathbf{0} \end{array} \begin{array}{|c|c|c|} \hline x_i & \dots & x_i \\ \hline x_j & \dots & x_j \\ \hline \end{array} \begin{array}{c} \mathbf{0} \\ \mathbf{0} \end{array} .$$

To get a non-zero entry of the R matrix, we have $\mathbf{I} = \mathbf{J} = \mathbf{0}$ if and only if $\mathbf{K} = \mathbf{L} = \mathbf{0}$, in which case $R_{x_j/x_i}(\mathbf{0}, \mathbf{0}, \mathbf{0}, \mathbf{0}) = 1$. Therefore the above equality becomes

$$\begin{array}{c} \mathbf{0} \\ \mathbf{0} \end{array} \begin{array}{|c|c|c|} \hline x_j & \dots & x_j \\ \hline x_i & \dots & x_i \\ \hline \end{array} \begin{array}{c} \mathbf{0} \\ \mathbf{0} \end{array} = \begin{array}{c} \mathbf{0} \\ \mathbf{0} \end{array} \begin{array}{|c|c|c|} \hline x_i & \dots & x_i \\ \hline x_j & \dots & x_j \\ \hline \end{array} \begin{array}{c} \mathbf{0} \\ \mathbf{0} \end{array} .$$

□

The technique used to swap two white rows in the previous proof is sometimes called the “train argument.” We will use this technique many times throughout this thesis.

2.5 Single rows

In this section, we consider the case when $\gamma = \emptyset$ and each partition in β has a single part i.e. β is a k -tuple of single rows. In this case, we can view β as a (weak) composition β , and we will abuse notation by writing $\mathcal{L}_\beta(X; t)$ to mean the polynomial $\mathcal{L}_\beta(X; t)$. Using the results of the previous section, we give another proof that the LLT polynomial indexed by β coincides with a certain Hall-Littlewood polynomial. The exact statement is as follows.

Let $K_{\lambda, \mu}(t) \in \mathbb{Z}[t]$ denote the Kostka-Foulkes polynomial. Let $H_\mu(X; t)$ denote the transformed Hall-Littlewood polynomials, given by their Schur expansion

$$H_\mu(X; t) = \sum_{\lambda \geq \mu} K_{\lambda, \mu}(t) s_\lambda(X) \tag{2.8}$$

where the sum is over partitions λ that dominate μ (i.e. $|\lambda| = |\mu|$ and $\sum_{i=1}^j \lambda_i \geq \sum_{i=1}^j \mu_i$ for all j). We define the modified Hall-Littlewood polynomials $\tilde{H}_\mu(X; t)$ by

$$\tilde{H}_\mu(X; t) = t^{n(\mu)} H_\mu(X; t^{-1}) \tag{2.9}$$

where $n(\mu) = \sum_i (i-1)\mu_i$. Similarly, we define the modified Kostka-Foulkes polynomials $\widetilde{K}_{\lambda,\mu}(t) := t^{n(\mu)} K_{\lambda,\mu}(t^{-1})$, so that

$$\widetilde{H}_\mu(X; t) = \sum_{\lambda \geq \mu} \widetilde{K}_{\lambda,\mu}(t) s_\lambda(X). \quad (2.10)$$

The following is due to [39], albeit in a different form than stated below.

Proposition 2.5.1 ([22, Prop. 5.1]). *Let μ be a partition, viewed also as a tuple of rows. Then*

$$\mathcal{G}_\mu(X; t) = \widetilde{H}_\mu(X; t). \quad (2.11)$$

where we recall that $\mathcal{G}_\mu(X; t)$ denotes the inversion LLT polynomials.

The polynomials $\widetilde{K}_{\lambda,\mu}(t)$ have many geometric interpretations. It is a well known fact [42] that when $t = q$ is the cardinality of a finite field \mathbb{F}_q , $GL_n(\mathbb{F}_q)$ acts on the set of \mathbb{F}_q -rational points of a flag variety, and $\widetilde{K}_{\lambda,\mu}(q)$ equals the value of an irreducible character χ_λ in this representation on a unipotent element u with Jordan form specified by μ . Prop. 2.5.1 is proven in [39] by showing that there is a cell decomposition of a similar flag variety whose cells are indexed by k -tuples of tableaux and whose dimensions are precisely the inversion statistic defined in Section 2.2.

As far as the author is aware, the only known proofs of Prop. 2.5.1 rely on the geometry of an underlying flag variety. We present a new proof using our vertex model formulation of coinversion LLT polynomials. Using (2.9) and (2.5), (2.11) becomes

$$\mathcal{L}_\mu(X; t) = t^{m(\mu)-n(\mu)} H_\mu(X; t) \quad (2.12)$$

where we recall that $m(\mu)$ is the number of triples in μ . We derive the following explicit formula for m which holds for all tuples of partitions β , not just those consisting of single rows.

Proposition 2.5.2 ([22, Prop. 5.2]). *Let β be a tuple of partitions. Then,*

$$m(\beta) = \#\{a < b, i, j \mid 0 \leq \beta_j^{(b)} - j + i < \beta_i^{(a)}\} + \sum_{\substack{a < b \\ i, j}} \max(\min(\beta_i^{(a)} - i, \beta_j^{(b)} - j) + \min(i, j), 0) \quad (2.13)$$

Proof. We count triples by the cell labelled v in (2.4), as this cell must always be in the shape β . Fix a cell $v = (i, \ell) \in \beta^{(a)}$. If (u, v, w) is a triple, then u, w must lie in (or adjacent to) some $\beta_j^{(b)}$ for $b > a$. For each row $\beta_j^{(b)}$, let w be the unique cell in this row on the same content line as v and let u be the cell directly to the left of w . Then (u, v, w) is a triple if

1. u, w are both in $\beta_j^{(b)}$;
2. u is the cell $(j, 0)$ just before the beginning of the row; or
3. u is the cell $(j, \beta_j^{(b)})$ at the end of the row.

In other words, v forms a triple with two cells in row $\beta_j^{(b)}$ exactly when $\beta_j^{(b)}$ has a cell of content $c(v)$ or $c(v) - 1$. As the set of contents of cells in the row $\beta_j^{(b)}$ is precisely the interval $[1 - j, \beta_j^{(b)} - j]$, we have

$$(u, v, w) \text{ is a triple} \iff 1 - j \leq c(v) \leq \beta_j^{(b)} - j + 1 \iff i - j \leq \ell - 1 \leq \beta_j^{(b)} + i - j.$$

As $\ell - 1$ ranges over the interval $[0, \beta_i^{(a)} - 1]$, after summing over ℓ, i, j and $a < b$, we find that the number of triples (u, v, w) is

$$\begin{aligned} m(\beta) &= \sum_{\substack{a < b \\ i, j}} \# \left([0, \beta_i^{(a)} - 1] \cap [i - j, \beta_j^{(b)} + i - j] \right) \\ &= \sum_{\substack{a < b \\ i, j}} \# \left([-i, \beta_i^{(a)} - i - 1] \cap [-j, \beta_j^{(b)} - j] \right) \\ &= \sum_{\substack{a < b \\ i, j}} \max(\min(\beta_i^{(a)} - i - 1, \beta_j^{(b)} - j) - \max(-i, -j) + 1, 0) \\ &= \sum_{\substack{a < b \\ i, j}} \max(\min(\beta_i^{(a)} - i, \beta_j^{(b)} - j) + \min(i, j), 0) + \begin{cases} 1 & : -\min(i, j) \leq \beta_j^{(b)} - j \leq \beta_i^{(a)} - i - 1 \\ 0 & : \text{else} \end{cases} \\ &= \sum_{\substack{a < b \\ i, j}} \max(\min(\beta_i^{(a)} - i, \beta_j^{(b)} - j) + \min(i, j), 0) + \begin{cases} 1 & : i - \min(i, j) \leq \beta_j^{(b)} - j + i < \beta_i^{(a)} \\ 0 & : \text{else} \end{cases}. \end{aligned}$$

The condition $i - \min(i, j) \leq \beta_j^{(b)} - j + i$ is seen to be equivalent to $0 \leq \beta_j^{(b)} - j + i$ in either case $i \leq j$ or $j \leq i$. \square

Given a composition β , we define $\text{Inv}(\beta) = \#\{i < j \mid \beta_i > \beta_j\}$.

Lemma 2.5.3 ([22, Cor. 5.3]). *Let μ be a partition and let β be a rearrangement of the parts of μ . Then*

$$m(\beta) = n(\mu) + \text{Inv}(\beta)$$

where $n(\mu) = \sum_i (i - 1)\mu_i$.

Proof. As β is k -tuple of single rows, the only terms that contribute to the right-hand side of (2.13) are when $i = j = 1$. Thus,

$$\begin{aligned} m(\beta) &= \#\{a < b \mid 0 \leq \beta^{(b)} < \beta^{(a)}\} + \sum_{a < b} \max(\min(\beta^{(a)} - 1, \beta^{(b)} - 1) + 1, 0) \\ &= \text{inv}(\beta) + \sum_{a < b} \min(\beta^{(a)}, \beta^{(b)}). \end{aligned}$$

The result follows from the identity $n(\mu) = \sum_{a < b} \min(\beta^{(a)}, \beta^{(b)})$. □

With Lemma 2.5.3, (2.12) becomes

$$\mathcal{L}_\mu(X; t) = t^{\text{Inv}(\mu)} H_\mu(X; t). \tag{2.14}$$

We establish the following statement, giving another proof of (2.14).

Proposition 2.5.4 ([22, Prop. 5.5]). *Let μ be a partition and let β be a rearrangement of the parts of μ . Then*

$$\mathcal{L}_\beta(X; t) = t^{\text{Inv}(\beta)} H_\mu(X; t).$$

In particular, if $\mu^{\text{rev}} = (\mu_n, \dots, \mu_1)$ is μ in reverse order, then

$$\mathcal{L}_{\mu^{\text{rev}}}(X; t) = H_\mu(X; t).$$

Proof. Using Prop. 2.5.5 below, it suffices to prove the particular case with μ^{rev} . Viewing μ^{rev} as a composition rather than as a tuple of rows, we recast the definition of $\mathcal{L}_{\mu^{\text{rev}}}(X; t)$ as a sum over fillings of the diagram $D(\mu^{\text{rev}})$:

$$\mathcal{L}_{\mu^{\text{rev}}}(X; t) = \sum_{\substack{\sigma: \mu^{\text{rev}} \rightarrow \mathbb{Z}_+ \\ \text{rows} \leq}} t^{\text{coinv}(\sigma)} x^\sigma \tag{2.15}$$

where the sum is over fillings of μ^{rev} with weakly increasing rows, and $\text{coinv}(\sigma)$ counts triples of the form

$$\begin{array}{|c|c|} \hline a & c \\ \hline \end{array} \tag{2.16}$$

$$\begin{array}{|c|} \hline b \\ \hline \end{array}$$

with $a \leq b \leq c$ (we set $a = 0$ if it is not in μ^{rev}).

We recall the combinatorial definition of $H_\mu(X; t)$, given in [31], by exchanging q and t in the combinatorial formula for Macdonald polynomials and setting $q = 0$:

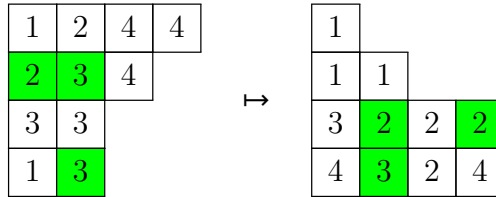
$$H_\mu(X; t) = \sum_{\substack{\sigma: \mu' \rightarrow \mathbb{Z}_+ \\ \text{cols} \searrow}} t^{\text{coinv}'(\sigma)} x^\sigma. \tag{2.17}$$

Here, the sum is over fillings σ of the conjugate Young diagram $D(\mu')$ with weakly decreasing columns, and $\text{coinv}'(\sigma)$ counts triples of the form

$$\begin{array}{|c|} \hline x \\ \hline y \\ \hline \end{array} \quad \begin{array}{|c|} \hline z \\ \hline \end{array} \tag{2.18}$$

with $x \leq z \leq y$ (we set $y = 0$ if it is not in μ').

Define Φ to be the map from fillings of μ^{rev} to fillings of μ' which rotates 90 degrees counterclockwise and swaps entries i and $n - i + 1$. For example:



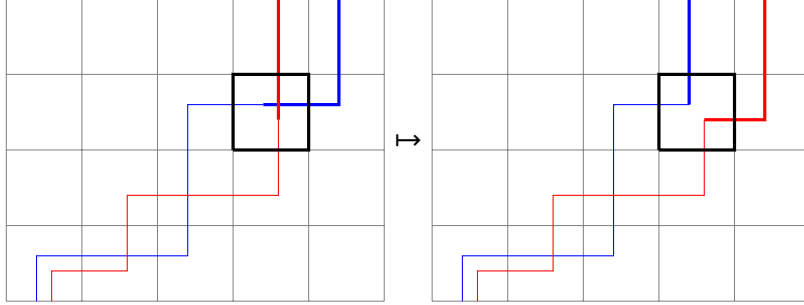
It is clear that Φ is a bijection and (after setting $a = y$, $b = z$, and $c = x$) maps coinversion triples as in (2.16) precisely to triples as in (2.18). In other words, Φ is a weight-preserving bijection from terms in (2.15) to terms in (2.17). \square

Proposition 2.5.5 ([22, Prop. 5.4]). *Let μ be a partition and let β be a rearrangement of the parts of μ . Then*

$$\mathcal{L}_\mu(X; t) = t^{\text{Inv}(\mu) - \text{Inv}(\beta)} \mathcal{L}_\beta(X; t).$$

Proof. It suffices to prove this statement in the case when β is obtained from μ by a single swap of consecutive rows, and in fact we only need to consider the case when $\mu = (\mu_1, \mu_2)$ and $\beta = (\mu_2, \mu_1)$. We take blue to be color 1 and red to be color 2. As the case $\mu_1 = \mu_2$ is trivial, we assume $\mu_1 > \mu_2$. In this case, in any path configuration of $W_n(\mu)$, the blue path will end to the right of the red path. Since the paths start at the same face, there exists a last face of the form $\begin{array}{|c|} \hline \color{blue}{\square} \color{red}{\square} \\ \hline \end{array}$. Taking a path configuration of $W_n(\mu)$ and swapping the colors of the paths after this face gives a bijection with

path configurations of $W_n(\beta)$. For example,



It's clear that the number of coinversions decreases by one after swapping, so that

$$\mathcal{L}_\mu(X; t) = t \mathcal{L}_\beta(X; t).$$

□

2.6 Cauchy identity

In this section, we give another proof of a Cauchy identity for LLT polynomials. A Cauchy identity was given in [38] for the original spin-generating LLT polynomials, whereas our Cauchy identity is for coinversion LLT polynomials; however the reader can readily use (2.3) to rederive the identity in [38].

Theorem 2.6.1 ([22, Thm. 6.1]). *[Cauchy Identity] Fix $n, k \geq 1$. Then*

$$\sum_{\lambda} t^{d(\lambda)} \mathcal{L}_\lambda(X_n; t) \mathcal{L}_\lambda(Y_n; t) = \prod_{i,j=1}^n \prod_{m=0}^{k-1} (1 - x_i y_j t^m)^{-1} \quad (2.19)$$

where the sum is over k -tuples λ of partitions with n non-negative parts and $d(\lambda)$ is given in Lemma 2.6.7.

To prove Theorem 2.6.1, we will use a method of using vertex models to prove Cauchy-type identities given in [53].

Row-to-row transfer matrices

We introduce two types of semi-infinite **row-to-row transfer matrices**. The first is obtained by concatenating infinitely many L matrices, and the second is

obtained by concatenating infinitely many M matrices. Graphically, we represent these matrices as follows:

$$T(x) = x \begin{array}{|c|c|c|c|c|} \hline & & & & \dots \\ \hline \end{array}$$

$$T^*(x) = \bar{x} \begin{array}{|c|c|c|c|c|} \hline & & & & \dots \\ \hline \end{array}$$

For $T(x)$ we write the parameter x to the left of the row to indicate that every face has weights given by L_x , and similarly for $T^*(x)$. An entry of the matrix is given by fixing the incoming (left and bottom) and outgoing (top and right) paths on the boundary and summing over the weight of all configurations respecting these boundary conditions.

Note that the matrix entries are well-defined only if we assume $|x| < 1$, which means that any matrix entry with unbounded degree in x is equal to 0, hence

$$x \begin{array}{|c|c|c|c|c|} \hline & & & & \dots \\ \hline \end{array} \bullet = 0 = \bar{x} \begin{array}{|c|c|c|c|c|} \hline & & & & \dots \\ \hline \end{array} \circ$$

We are interested in certain submatrices given by

$$T_+(x) := x \begin{array}{|c|c|c|c|c|} \hline & & & & \dots \\ \hline \end{array} \circ$$

$$T_+^*(x) := \bar{x} \begin{array}{|c|c|c|c|c|} \hline & & & & \dots \\ \hline \end{array} \bullet$$

where to simplify notation we use a black circle to indicate the vector $\mathbf{1}$ and a white circle to indicate the vector $\mathbf{0}$. Graphically, fixing how the paths enter and exit the row from the top and bottom, the corresponding entry $T_+(x)$ is the sum over the weight all possible infinite row configurations of white boxes such that the leftmost edge is unoccupied and only empty boxes appear sufficiently far to the right, respecting the top and bottom boundary conditions. The corresponding entry of $T_+^*(x)$ is the sum over the weight all possible infinite row configurations of gray boxes such that the leftmost edge is unoccupied and only boxes with all paths horizontal appear sufficiently far to the right respecting the top and bottom boundary conditions.

Repeated application of the Yang-Baxter equation (1.4.5) yields the following:

Proposition 2.6.2 ([22, Prop. 6.3]). *The matrices $T_+(y)$ and $T_+^*(x)$ satisfy*

$$(2.20)$$

Proof of Theorem 2.6.1

The proof comes in several steps. We begin with the equation

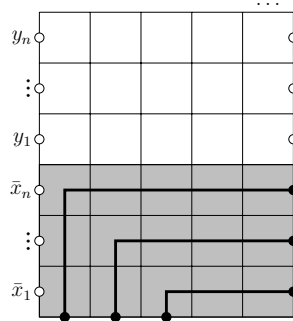
$$(2.21)$$

which follows from repeated applications of Prop. 2.6.2. Here the gray rows are generated by T_+^* and the white rows are generated by T_+ .

We first simplify the left-hand side of (2.21). As no paths enter from the left, we can factorize the left-hand side as follows:

The first factor equals 1, since there are no paths. To evaluate the second factor, we

observe that the only non-zero contribution occurs for the following configuration:

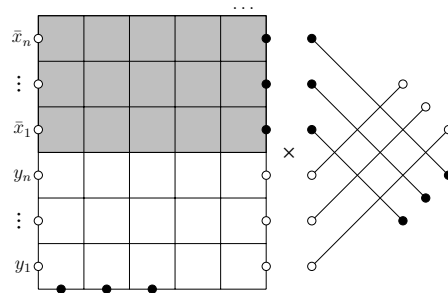


in which the bold paths indicate that paths of every color follow the trajectory. This has weight

$$\left(x_1^k t^{\binom{k}{2}}\right)^{n-1} \left(x_2^k t^{\binom{k}{2}}\right)^{n-2} \cdots \left(x_{n-1}^k t^{\binom{k}{2}}\right)^1 = (x^{\rho_n})^k t^{\binom{n}{2}\binom{k}{2}}. \quad (2.22)$$

where we recall $\rho_n = (n-1, \dots, 0)$ and x^{ρ_n} denotes the monomial $x_1^{n-1} \cdots x_n^0$.

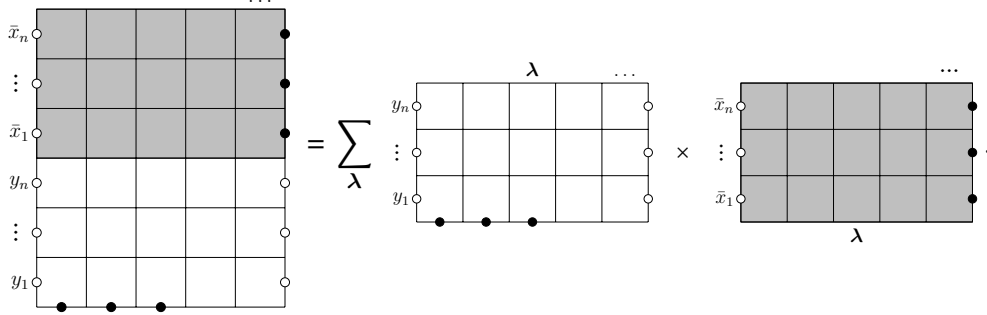
We now simplify the right-hand side of (2.21). The right edge of the lattice is situated at infinity, hence a non-zero contribution is possible only if the lowest n edges are unoccupied and the highest n edges are occupied. Therefore we can factorize the right-hand side as follows:



The only non-zero contribution to the second factor is

$$= \prod_{i,j=1}^n \prod_{m=0}^{k-1} (1 - x_i y_j t^m). \quad (2.23)$$

The first factor can be expressed as



We know from Theorem 2.3.3 that the first factor in the sum is $\mathcal{L}_{\lambda}(y_1, \dots, y_n; t)$. In the next subsection, we will prove that the second factor in the sum is

$$\mathcal{L}_{\lambda}^*(x_1, \dots, x_n; t) := \begin{array}{c} \dots \\ \bar{x}_n \\ \vdots \\ \bar{x}_1 \\ \lambda \end{array} = (x^{\rho_n})^k t^{\binom{n}{2} \binom{k}{2}} t^{d(\lambda)} \mathcal{L}_{\lambda}(X_n; t) \quad (2.24)$$

where $d(\lambda)$ is given in Lemma 2.6.7. In light of (2.22), (2.23), and (2.24), we see that (2.21) becomes

$$(x^{\rho_n})^k t^{\binom{n}{2} \binom{k}{2}} = \prod_{i,j=1}^n \prod_{m=0}^{k-1} (1 - x_i y_j t^m) \sum_{\lambda} (x^{\rho_n})^k t^{\binom{n}{2} \binom{k}{2}} t^{d(\lambda)} \mathcal{L}_{\lambda}(X_n; t) \mathcal{L}_{\lambda}(Y_n; t).$$

Rearranging gives Theorem 2.6.1.

Calculation of \mathcal{L}_{λ}^*

Definition 2.6.3. Let N, n, k be non-negative integers. Given a partition λ with n non-negative parts, each of which is $\leq N$, we define its **complement** in an $N \times n$ box to be the partition

$$\lambda^c = (N - \lambda_n, \dots, N - \lambda_1).$$

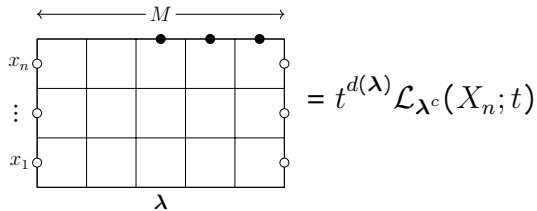
Given $\lambda \in P_n^k$, we define its complement in an $N \times n$ box to be the k -tuple of partitions $\lambda^c = ((\lambda^c)^{(1)}, \dots, (\lambda^c)^{(k)})$ where

$$(\lambda^c)^{(i)} = (\lambda^{(k-i)})^c.$$

(We will use this notation in Chapter 2. In Chapter 3, we will actually define the above to be the complement in an $n \times N$ box, as necessitated by the use of purple/pink vertices.)

To derive (2.24), we need the following two identities of LLT polynomials.

Proposition 2.6.4 ([22, Prop. 6.4]). *Let $\lambda = (\lambda^{(1)}, \dots, \lambda^{(k)})$ be a k -tuple of partitions, each having n non-negative parts. Fix the number of columns M such that $\text{band}(\lambda) < M$ and let $N = M - n$. Let λ^c be the complement of λ in an $N \times n$ box. We have*



where $d(\lambda)$ is given below in Lemma 2.6.7. In other words, if $\mathbf{B} = ((N^n)^k)$ (the k -tuple of partitions, each of which has all n of its parts equal to N), then

$$\mathcal{L}_{\mathbf{B}/\lambda}(X_n; t) = t^{d(\lambda)} \mathcal{L}_{\lambda^c}(X_n; t). \tag{2.25}$$

Proposition 2.6.5 ([22, Prop. 6.5]). *Let λ and N be as in Prop. 2.6.4. Then*

$$\mathcal{L}_\lambda(X_n; t) = (x_1 \cdots x_n)^{kN} t^{\tilde{d}(\lambda)} \mathcal{L}_{\lambda^c}(X_n^{-1}; t) \tag{2.26}$$

where

$$\tilde{d}(\lambda) = (k - 1)|\lambda| - nN \binom{k}{2}. \tag{2.27}$$

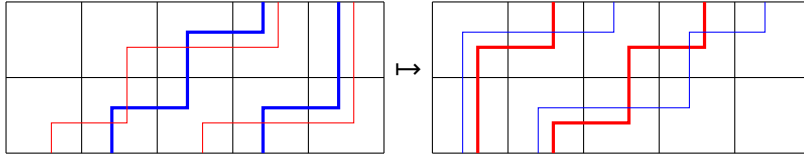
Remark 2.6.6. *Prop. 2.6.5 has a representation-theoretic meaning. At $q = 1$, (2.26) is simply a statement of contragredient duality for (tensor products of) irreducible representations of GL_n . One can use this same duality, together with the machinery of affine Hecke algebras, to conclude the statement for arbitrary q .*

A similar result was proven in [50, Prop. 10] for the class of generalized Hall-Littlewood polynomials defined therein. These polynomials coincide, up to a power of t , with coinversion LLT polynomials when the indexing tuple consists of rectangles.

For the proof of Prop. 2.6.4, we construct a bijection $LC(W_n(\mathbf{B}/\lambda)) \rightarrow LC(W_n(\lambda^c/\mathbf{0}))$, which we show is weight-preserving (up to an overall power of t and rearranging the X variables) using a “corner flipping argument.” The proof of Prop. 2.6.5 is similar, but we use a bijection $LC(W_n(\lambda/\mathbf{0})) \rightarrow LC(W_n(\lambda^c/\mathbf{0}))$.

Proof of Prop. 2.6.4. There is a bijection $\Phi : LC(W_n(\mathbf{B}/\lambda)) \rightarrow LC(W_n(\lambda^c/\mathbf{0}))$ given by rotating 180 degrees and reversing the colors. For example, with two colors

we have



Note that horizontal steps in row i become horizontal steps in row $n - i + 1$ under this bijection, so the X weight remains unchanged up to switching x_i and x_{n-i+1} . By Lemma 2.6.7 below, the bijection decreases the t weight by $d(\boldsymbol{\lambda})$. Thus

$$\mathcal{L}_{\mathbf{B}/\boldsymbol{\lambda}}(X_n; t) = t^{d(\boldsymbol{\lambda})} \mathcal{L}_{\boldsymbol{\lambda}^c}(x_n, \dots, x_1; t) = \mathcal{L}_{\boldsymbol{\lambda}^c}(X_n; t)$$

where the last equality uses Theorem 2.4.1. □

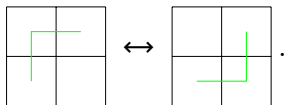
Lemma 2.6.7 ([22, Lemma 6.6]). *Let $\boldsymbol{\lambda}$ and Φ be as in the proof of Prop. 2.6.4. Then*

$$d(\boldsymbol{\lambda}) := \text{coinv } T - \text{coinv } \Phi(T)$$

is independent of T . In particular,

$$d(\boldsymbol{\lambda}) = \binom{n}{2} \binom{k}{2} - \#\{i, j, a < b \mid \lambda_i^{(b)} - i < \lambda_j^{(a)} - j\}. \quad (2.28)$$

Proof. For any k -tuple of skew partitions $\boldsymbol{\beta}/\boldsymbol{\gamma}$, $LC(W_n(\boldsymbol{\beta}/\boldsymbol{\gamma}))$ is connected under corner flips



It thus suffices to show that if $T \in LC(W_n(\boldsymbol{\lambda}/\mathbf{0}))$ and $f(T) \in LC(W_n(\boldsymbol{\lambda}/\mathbf{0}))$ results from flipping a single corner of T , then

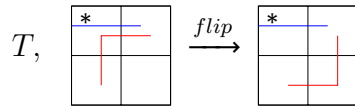
$$\text{coinv } T - \text{coinv } f(T) = \text{coinv } \Phi(T) - \text{coinv } \Phi(f(T)). \quad (2.29)$$

As coinversions are counted pairwise between colors and Φ interchanges down-flippable corners with up-flippable corners, without loss of generality it suffices to prove (2.29) in the case when $\boldsymbol{\lambda} = (\lambda^{(1)}, \lambda^{(2)})$ and $f(T)$ results from T by flipping a corner down. The table below shows the 10 possible local configurations of paths where a corner of T might be down-flippable, along with the corresponding corner in $\Phi(T)$. (Here blue is color 1 and red is color 2.)

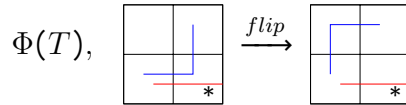
Case	1 (R)	2 (B)	3 (B)	4 (B)	5 (B)	6 (R)	7 (R)	8 (B)	9 (R)	10 (R)
T										
$\Phi(T)$										

We will do case 1 in detail. The rest can be done similarly.

In case 1 the original local configuration of T contributes a power of t as the blue path exits right and a red path is present. Suppose that flipping the red corner down causes T to lose a power of t . Marking the original face with a $*$, we must be in the situation

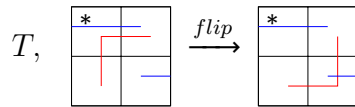


where no blue path is present in the bottom-right face (since a blue path exiting right would contribute a power of t , and the presence of a blue path in the top-right face prevents a blue path from exiting up). In $\Phi(T)$ this corresponds to the situation

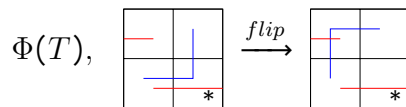


where no red path is present in the top-left face. Here the bottom-left face originally contributed a power of t , which is lost after the flip. Thus we lose a power of t in both T and $\Phi(T)$.

Now suppose there was no change in the power of t after flipping the corner in T . Then we must be in the situation

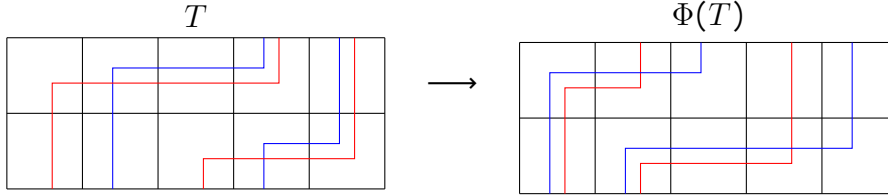


where a blue path exits right in the bottom-right face contributing a power of t to make up for the one lost from the top-left face. In $\Phi(T)$ this corresponds to



where now the top-left face contributes a power of t to make up for the one lost from the bottom-left face. Thus there is no net change in the power of t for either T or $\Phi(T)$.

From this we see that $\text{coinv } T - \text{coinv } \Phi(T)$ is independent of T . It is left to compute this quantity for some T . We choose T such that all the paths stay as high as possible (no up-flips available). For this choice of configuration T , in $\Phi(T)$ the paths are as low as possible (no down-flips available). For example:



For two colors, one can check that the powers of t in T and $\Phi(T)$ are given by

$$\begin{aligned} \text{coinv } T &= \sum_{i=1}^n \min(N - \lambda_i^{(1)}, N - \lambda_i^{(2)}) + \sum_{i=1}^n \#\{j < i \mid \lambda_i^{(2)} - i \geq \lambda_j^{(1)} - j\}, \\ \text{coinv } \Phi(T) &= \sum_{i=1}^n \min((\lambda^c)_i^{(2)}, (\lambda^c)_i^{(1)}) + \sum_{i=1}^n \#\{j \geq i \mid (\lambda^c)_j^{(1)} - j > (\lambda^c)_i^{(2)} - i\} \\ &= \sum_{i=1}^n \min(N - \lambda_i^{(1)}, N - \lambda_i^{(2)}) + \sum_{i=1}^n \#\{j \geq i \mid \lambda_i^{(2)} - i < \lambda_j^{(1)} - j\} \end{aligned}$$

where in each expression, the first sum counts powers of t coming from \square_{-} and the second sum counts powers of t coming from \square_{+} . We have

$$\begin{aligned} d(\boldsymbol{\lambda}) &= \text{coinv } T - \text{coinv } \Phi(T) \\ &= \sum_{i=1}^n \#\{j < i \mid \lambda_i^{(2)} - i \geq \lambda_j^{(1)} - j\} - \sum_{i=1}^n \#\{j \geq i \mid \lambda_i^{(2)} - i < \lambda_j^{(1)} - j\} \\ &= \binom{n}{2} - \#\{i, j \mid \lambda_i^{(2)} - i < \lambda_j^{(1)} - j\}. \end{aligned}$$

To extend this to k colors, we sum over all pairs of colors $a < b$ and get

$$d(\boldsymbol{\lambda}) = \binom{n}{2} \binom{k}{2} - \sum_{a < b} \#\{i, j \mid \lambda_i^{(b)} - i < \lambda_j^{(a)} - j\}.$$

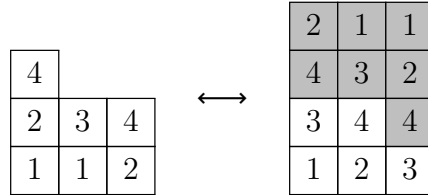
□

Proof of Prop. 2.6.5. Upon specialization at $t = 1$ and $k = 1$ of (2.26), we arrive at a well-known identity of Schur functions [51, Ex. 7.41]

$$s_\lambda(X_n) = (x_1 \cdots x_n)^N s_{\lambda^c}(X_n^{-1})$$

which is proven combinatorially using a bijection $\text{SSYT}(\lambda) \rightarrow \text{SSYT}(\lambda^c)$. We recall that bijection here.

Fix a partition λ with $n \geq \ell(\lambda)$ and $N \geq \lambda_1$. Fix $T \in \text{SSYT}(\lambda)$ and let ν^1, \dots, ν^N denote the (possibly empty) columns of T , left to right. Let $\tilde{\nu}^i$ be the column whose entries are $[n] \setminus \{j \mid j \in \nu^i\}$, arranged in increasing order. Define $\Phi(T)$ to be the tableau with columns $\tilde{\nu}^N, \dots, \tilde{\nu}^1$, left to right. An example is given below with $n = 4$ and $N = 3$.



Now if $T = (T^{(1)}, \dots, T^{(k)}) \in \text{SSYT}(\boldsymbol{\lambda})$, then we abuse notation and write

$$\Phi(T) = (\Phi(T^{(k)}), \dots, \Phi(T^{(1)})) \in \text{SSYT}(\boldsymbol{\lambda}^c)$$

to be the reversal of applying the bijection Φ individually to each tableau. We further abuse notation and write $\Phi(T) \in LC(W_n(\boldsymbol{\lambda}^c/\mathbf{0}))$ to be the corresponding lattice configuration, when $T \in LC(W_n(\boldsymbol{\lambda}/\mathbf{0}))$ is a lattice configuration. Note that if T has weight x^T in the X variables, then $\Phi(T)$ will have weight $(x^{-1})^T (x_1 \cdots x_n)^{kN}$ in the X variables. The proposition then follows from Lemma 2.6.8 below. \square

Lemma 2.6.8 ([22, Lemma 6.7]). *Let $\boldsymbol{\lambda}$, N , and Φ be as in the proof of Proposition 2.6.5. Then*

$$\tilde{d}(\boldsymbol{\lambda}) := \text{coinv } T - \text{coinv } \Phi(T)$$

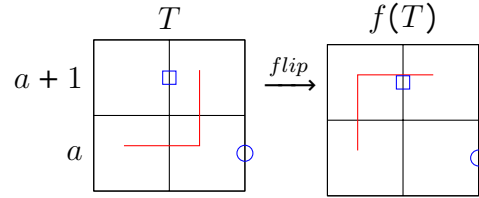
is independent of T . In particular,

$$\tilde{d}(\boldsymbol{\lambda}) = (k - 1)|\boldsymbol{\lambda}| - nN \binom{k}{2}. \tag{2.30}$$

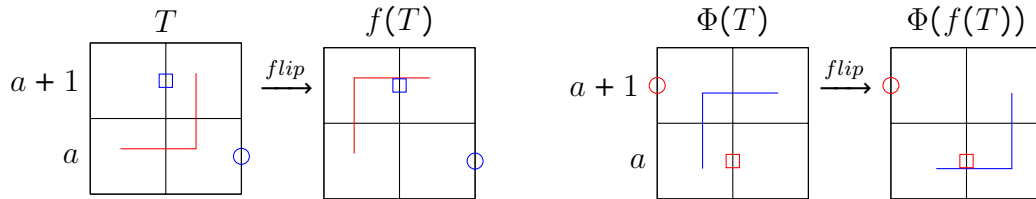
Proof. Similarly as in the proof of Lemma 2.6.7 (noting that once again Φ interchanges down-flippable corners with up-flippable corners), it suffices to prove

$$\text{coinv } T - \text{coinv } f(T) = \text{coinv } \Phi(T) - \text{coinv } \Phi(f(T)) \tag{2.31}$$

in the case when $\lambda = (\lambda^{(1)}, \lambda^{(2)})$ and $f(T)$ results from T by flipping a corner up. Letting blue be color 1 and red be color 2, we consider the case



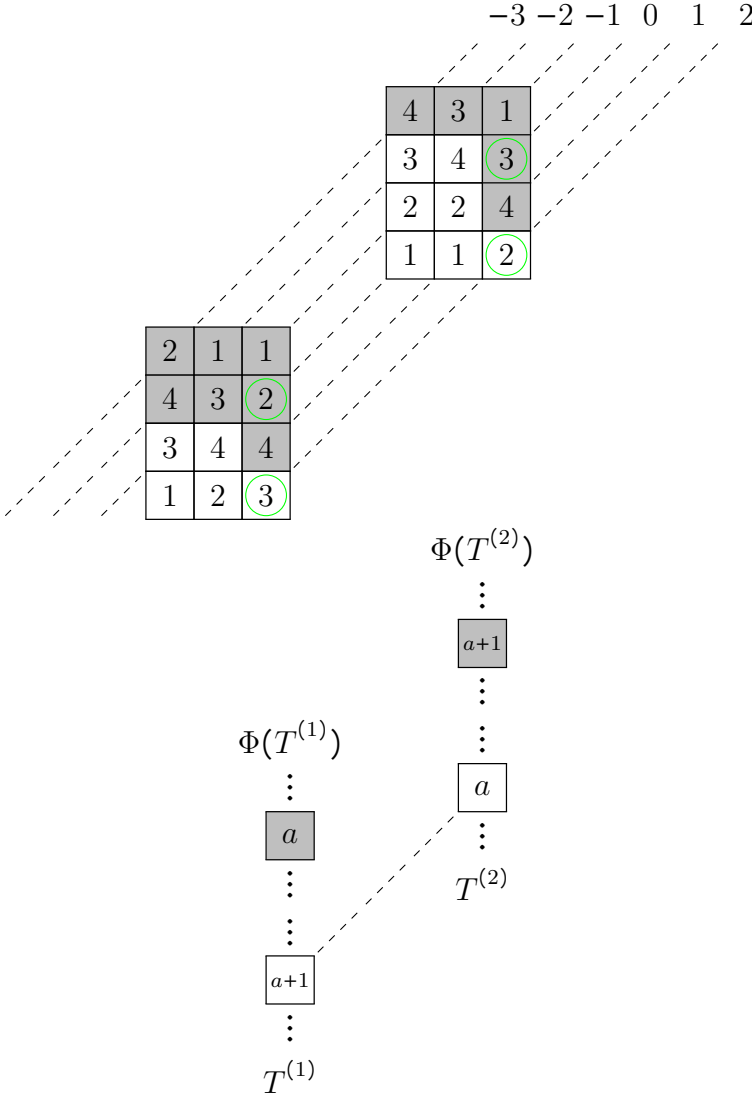
where a blue path goes through the square but not the circle in T . (The other cases can be shown similarly.) Since the configuration $f(T)$ is obtained from T by flipping a red corner up from row a to row $a + 1$, the tableaux $f(T)$ is obtained from T by swapping an entry $a \in T^{(2)}$ with $a + 1 \in f(T^{(2)})$. Therefore the tableaux $\Phi(f(T))$ is obtained from $\Phi(T)$ by swapping an entry $a + 1 \in \Phi(T^{(2)})$ with $a \in \Phi(f(T^{(2)}))$, hence the configuration $\Phi(f(T))$ is obtained from $\Phi(T)$ by flipping a blue corner down from row $a + 1$ to row a .



We claim that a red path goes through the square but not the circle in $\Phi(T)$, hence

$$\text{coinv } \Phi(T) - \text{coinv } \Phi(f(T)) = -1 = \text{coinv } T - \text{coinv } f(T).$$

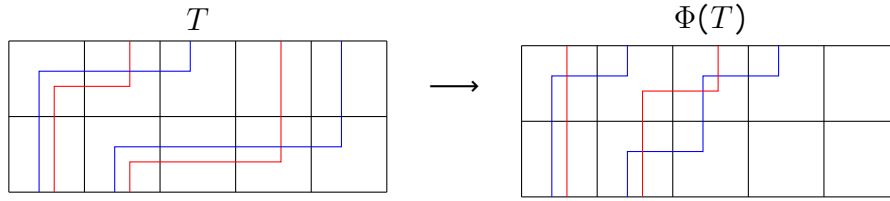
A blue path goes through the square in T , so there is an entry $a + 1 \in T^{(1)}$ on the same content line as the entry $a \in T^{(2)}$. A blue path does not go through the circle in T , so the cell directly below this $a + 1$ (if it is in T at all) cannot contain an a . Thus $\Phi(T^{(1)})$ contains an a but not an $a + 1$ in the corresponding column. The case is pictured below, with a concrete example on the left and the general case on the right; gray cells denote cells in the complement shape, and a is the circled green 2 in the left picture.



Let c_1 denote the column containing $\boxed{a+1} \in T^{(1)}$ and $\boxed{a} \in \Phi(T^{(1)})$ and let c_2 denote the column containing $\boxed{a} \in T^{(2)}$ and $\boxed{a+1} \in \Phi(T^{(2)})$. Due to column strictness, in both c_1 and c_2 the set of numbers between the a and the $a + 1$ is exactly the interval $[a + 2, n]$. Thus the number of cells between the a and the $a + 1$ is the same, and since we know $\boxed{a+1} \in T^{(1)}$ and $\boxed{a} \in T^{(2)}$ are on the same content line, then so too must $\boxed{a} \in \Phi(T^{(1)})$ and $\boxed{a+1} \in \Phi(T^{(2)})$. Therefore the cell $\boxed{a} \in \Phi(T^{(1)})$ corresponds to a red path going through the square in $\Phi(T)$. We can also conclude that $\Phi(T^{(1)})$ does not contain an $a + 1$ on the content line immediately above the content line

containing this a ; by semistandardness, the only place this $a + 1$ could go on this content line is the cell directly above the a , but we know $\Phi(T^{(1)})$ does not contain an $a + 1$ in the same column as the a . Therefore a red path does not go through the circle in $\Phi(T)$.

We now explicitly calculate $\tilde{d}(\boldsymbol{\lambda}) = \text{coinv } T - \text{coinv } \Phi(T)$ for some T . We choose the configuration in which the paths are as low as possible (no down-flips available). On the tuple of tableaux, this corresponds to the superstandard filling, i.e. the filling in which the i -th row is filled with only i 's. Hence $\Phi(T)$ is the configuration in which the paths are as high as possible (no up-flips available).



As in the proof of Lemma 2.6.7, one can check that the powers of t in T and $\Phi(T)$ are given by

$$\begin{aligned} \text{coinv } T &= \sum_{i=1}^n \min(\lambda_i^{(1)}, \lambda_i^{(2)}) + \sum_{i=1}^n \#\{j \geq i \mid \lambda_j^{(1)} - j > \lambda_i^{(2)} - i\}, \\ \text{coinv } \Phi(T) &= \sum_{i=1}^n \min(\lambda_i^{(1),c}, \lambda_i^{(2),c}) + \sum_{i=1}^n \#\{j \leq i \mid \lambda_i^{(1),c} - i < \lambda_j^{(2),c} - j\} \\ &= \sum_{i=1}^n \min(N - \lambda_{N-i}^{(1)}, N - \lambda_{N-i}^{(2)}) + \sum_{i=1}^n \#\{j \leq i \mid -\lambda_{N-i}^{(1)} - i < -\lambda_{N-j}^{(2),c} - j\} \\ &= Nn - \sum_{i=1}^n \max(\lambda_i^{(1)}, \lambda_i^{(2)}) + \sum_{i=1}^n \#\{j \leq i \mid \lambda_{N-i}^{(1)} + i > \lambda_{N-j}^{(2)} + j\} \\ &= Nn - \sum_{i=1}^n \max(\lambda_i^{(1)}, \lambda_i^{(2)}) + \sum_{i=1}^n \#\{j \geq i \mid \lambda_i^{(1)} - i > \lambda_j^{(2)} - j\}. \end{aligned}$$

Hence

$$\begin{aligned} \tilde{d}(\boldsymbol{\lambda}) &= \text{coinv } T - \text{coinv } \Phi(T) \\ &= \sum_{i=1}^n \min(\lambda_i^{(1)}, \lambda_i^{(2)}) - Nn + \sum_{i=1}^n \max(\lambda_i^{(1)}, \lambda_i^{(2)}) \\ &= |\lambda^{(1)}| + |\lambda^{(2)}| - Nn. \end{aligned}$$

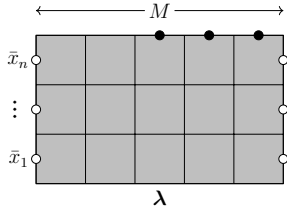
To extend this to k colors, we sum over all pairs of colors $a < b$ and get

$$\tilde{d}(\boldsymbol{\lambda}) = (k-1)|\boldsymbol{\lambda}| - nN\binom{k}{2}.$$

□

Continuing with our calculation of $\mathcal{L}_{\boldsymbol{\lambda}}^*$, we switch from the L weights to the M weights in Prop. 2.6.4.

Corollary 2.6.9 ([22, Cor. 6.9]). *Fix $\boldsymbol{\lambda}$ and M as in Prop. 2.6.4. We have*



$$= (x_1 \cdots x_n)^{kM} t^{n^2 \binom{k}{2}} t^{\tilde{d}(\boldsymbol{\lambda}) + d(\boldsymbol{\lambda})} \mathcal{L}_{\boldsymbol{\lambda}^c}(X_n^{-1}; t).$$

Proof. Recall the algebraic definition of the M weights

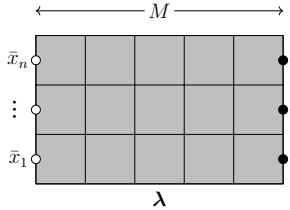
$$M_x^{(k)}(\mathbf{I}, \mathbf{J}, \mathbf{K} \mathbf{L}) = x^k t^{\binom{k}{2}} L_{\bar{x}}^{(k)}(\mathbf{I}, \mathbf{J}, \mathbf{K} \mathbf{L})$$

where $\bar{x} = \frac{1}{x_i t^{k-1}}$. Thus, to switch to M weights in Prop. 2.6.4, we first take $x_i \mapsto \bar{x}_i = \frac{1}{x_i t^{k-1}}$ and then multiply each face in row i by $x_i^k t^{\binom{k}{2}}$. This gives

$$\begin{aligned} & (x_1 \cdots x_n)^{kM} t^{nM \binom{k}{2}} t^{d(\boldsymbol{\lambda})} \mathcal{L}_{\boldsymbol{\lambda}^c}(x_1^{-1} t^{-k+1}, \dots, x_n^{-1} t^{-k+1}; t) \\ &= (x_1 \cdots x_n)^{kM} t^{nM \binom{k}{2}} t^{d(\boldsymbol{\lambda})} t^{-(k-1)|\boldsymbol{\lambda}^c|} \mathcal{L}_{\boldsymbol{\lambda}^c}(x_1^{-1}, \dots, x_n^{-1}; t) \\ &= (x_1 \cdots x_n)^{kM} t^{nM \binom{k}{2}} t^{d(\boldsymbol{\lambda})} t^{(k-1)|\boldsymbol{\lambda}| - k(k-1)n(M-n)} \mathcal{L}_{\boldsymbol{\lambda}^c}(X_n^{-1}; t) \\ &= (x_1 \cdots x_n)^{kM} t^{n^2 \binom{k}{2}} t^{-n(M-n) \binom{k}{2}} t^{(k-1)|\boldsymbol{\lambda}|} t^{d(\boldsymbol{\lambda})} \mathcal{L}_{\boldsymbol{\lambda}^c}(X_n^{-1}; t) \\ &= (x_1 \cdots x_n)^{kM} t^{n^2 \binom{k}{2}} t^{\tilde{d}(\boldsymbol{\lambda}) + d(\boldsymbol{\lambda})} \mathcal{L}_{\boldsymbol{\lambda}^c}(X_n^{-1}; t). \end{aligned}$$

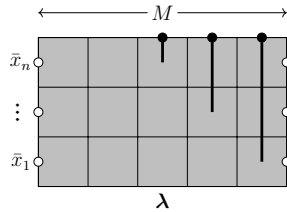
□

Corollary 2.6.10 ([22, Cor. 6.10]). *Fix $\boldsymbol{\lambda}$ and M as in Prop. 2.6.4. We have*

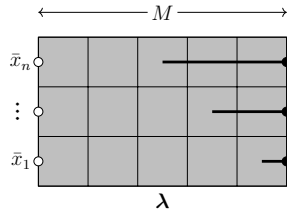


$$= (x^{\rho_n})^k (x_1 \cdots x_n)^{k(M-n)} t^{\binom{n}{2} \binom{k}{2}} t^{\tilde{d}(\boldsymbol{\lambda}) + d(\boldsymbol{\lambda})} \mathcal{L}_{\boldsymbol{\lambda}^c}(X_n^{-1}; t)$$

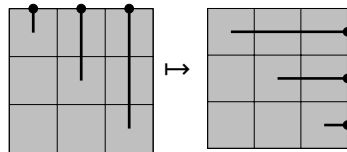
Proof. By the nature of the M weights, in order for a configuration of the lattice in Cor. 2.6.9 to have a non-zero weight, the configuration must have the form



i.e. the i -th path of each color must end with $n - i + 1$ vertical steps. Similarly the configurations of the lattice in this corollary must have the form



i.e. the i -th path of each color must end with i horizontal steps. There is a weight-preserving bijection from configurations in Cor. 2.6.9 to configurations in this corollary by taking



(while fixing the beginnings of the paths) and multiplying by $(x_1 \cdots x_n)^{-nk} (x^{\rho_n})^k t^{-\binom{n+1}{2} \binom{k}{2}}$. □

Proposition 2.6.11 ([22, Prop. 6.11]). *Let $\lambda = (\lambda^{(1)}, \dots, \lambda^{(k)})$ be a k -tuple of partitions, each with n non-negative parts. Then,*

$$\mathcal{L}_\lambda^*(X_n; t) = (x^{\rho_n})^k t^{\binom{n}{2} \binom{k}{2}} t^{d(\lambda)} \mathcal{L}_\lambda(X_n; t)$$

Proof. Fix the number of columns M as usual. Combining Prop. 2.6.5 and Cor. 2.6.10 yields

$$= (x^{\rho_n})^k t^{\binom{n}{2} \binom{k}{2}} t^{d(\lambda)} \mathcal{L}_\lambda(X_n; t).$$

Note that this is independent of M . Taking $M \rightarrow \infty$ gives the proposition. \square

We are finally ready to prove the Cauchy identity.

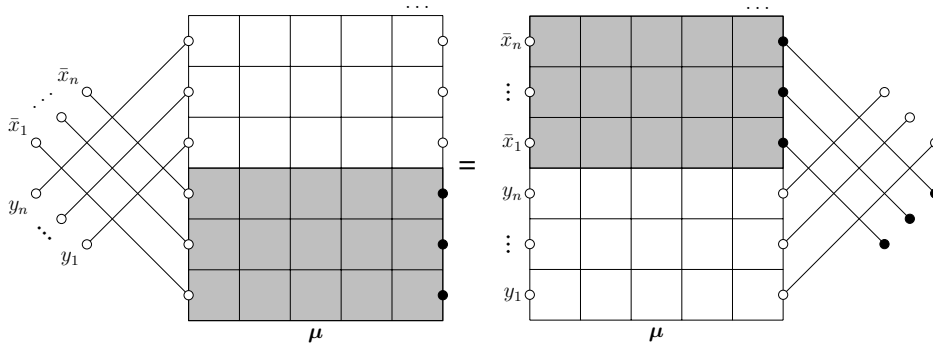
Proof of Theorem 2.6.1. Combining (2.22), (2.23), and Prop. 2.6.11, we see that (2.21) becomes

$$(x^{\rho_n})^k t^{\binom{n}{2}\binom{k}{2}} = \prod_{i,j=1}^n \prod_{m=0}^{k-1} (1 - x_i y_j t^m) \sum_{\lambda} (x^{\rho_n})^k t^{\binom{n}{2}\binom{k}{2}} t^{d(\lambda)} \mathcal{L}_{\lambda}(X_n; t) \mathcal{L}_{\lambda}(Y_n; t).$$

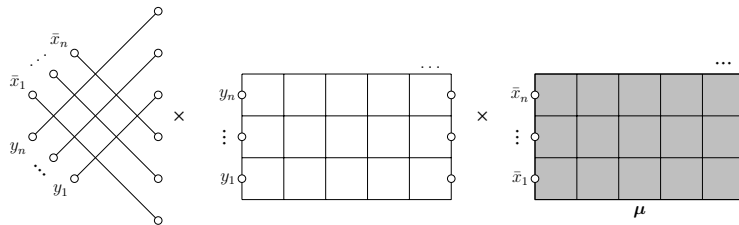
Cancelling $(x^{\rho_n})^k t^{\binom{n}{2}\binom{k}{2}}$ from both sides gives the desired identity. \square

Reformulations of the Cauchy identity

A similar argument holds when we let the paths enter the bottom at positions indexed by a tuple of partitions μ :



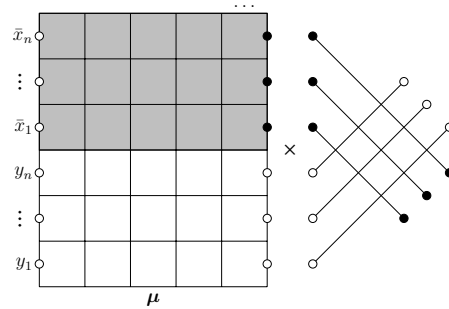
On the left-hand side, we get



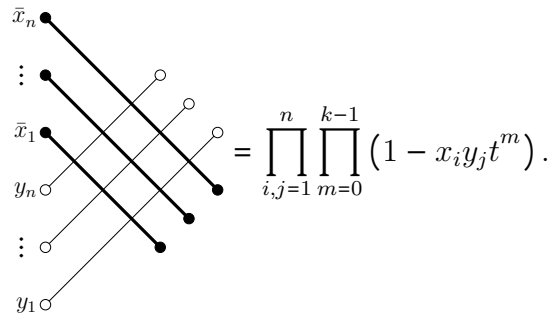
The first factor is 1, the second factor is 1, and the third factor is

$$\mathcal{L}_{\mu}^*(X_n; t) = (x^{\rho_n})^k t^{\binom{n}{2}\binom{k}{2}} t^{d(\mu)} \mathcal{L}_{\mu}(X_n; t).$$

We can factorize the right-hand side as follows:



The second factor is



The first factor is

$$\begin{aligned} & \sum_{\lambda} \begin{array}{c} \lambda \quad \dots \\ y_n \circ \quad \square \quad \square \quad \square \quad \square \quad \circ \\ \vdots \quad \square \quad \square \quad \square \quad \square \quad \circ \\ y_1 \circ \quad \square \quad \square \quad \square \quad \square \quad \circ \\ \mu \end{array} \times \begin{array}{c} \dots \\ \bar{x}_n \bullet \quad \square \quad \square \quad \square \quad \square \quad \bullet \\ \vdots \quad \square \quad \square \quad \square \quad \square \quad \bullet \\ \bar{x}_1 \bullet \quad \square \quad \square \quad \square \quad \square \quad \bullet \\ \lambda \end{array} \\ &= \mathcal{L}_{\lambda/\mu}(X_n; t) \mathcal{L}_{\lambda}(X_n; t) \\ &= \mathcal{L}_{\lambda/\mu}(X_n; t) (x^{\rho_n})^k t^{\binom{n}{2} \binom{k}{2}} t^{d(\lambda)} \mathcal{L}_{\lambda}(X_n; t). \end{aligned}$$

Rearranging, we get the following reformulation of the Cauchy identity:

Proposition 2.6.12 ([22, Prop. 6.12]).

$$\sum_{\lambda} t^{d(\lambda)} \mathcal{L}_{\lambda}(X_n; t) \mathcal{L}_{\lambda/\mu}(Y_n; t) = t^{d(\mu)} \mathcal{L}_{\mu}(X_n; t) \prod_{i,j=1}^n \prod_{m=0}^{k-1} (1 - x_i y_j t^m)^{-1}$$

Take \mathbf{B} to be the smallest box containing λ and let λ^c be the complement taken in this box. Define $\lambda^{\text{rot}} := \mathbf{B}/\lambda^c$, which we can think of as $(\lambda^{(k),\text{rot}}, \dots, \lambda^{(1),\text{rot}})$ where λ^{rot} is λ rotated 180 degrees. Plugging in λ^c into (2.25) for this choice of \mathbf{B} , we see that

$$\mathcal{L}_{\lambda^{\text{rot}}}(X_n; t) = t^{d(\lambda^c)} \mathcal{L}_{\lambda}(X_n; t).$$

Using this to replace one of the \mathcal{L}_{λ} in the sum in Theorem 2.6.1, and noting that $d(\lambda^c) = d(\lambda)$, we can reformulate the Cauchy identity as follows:

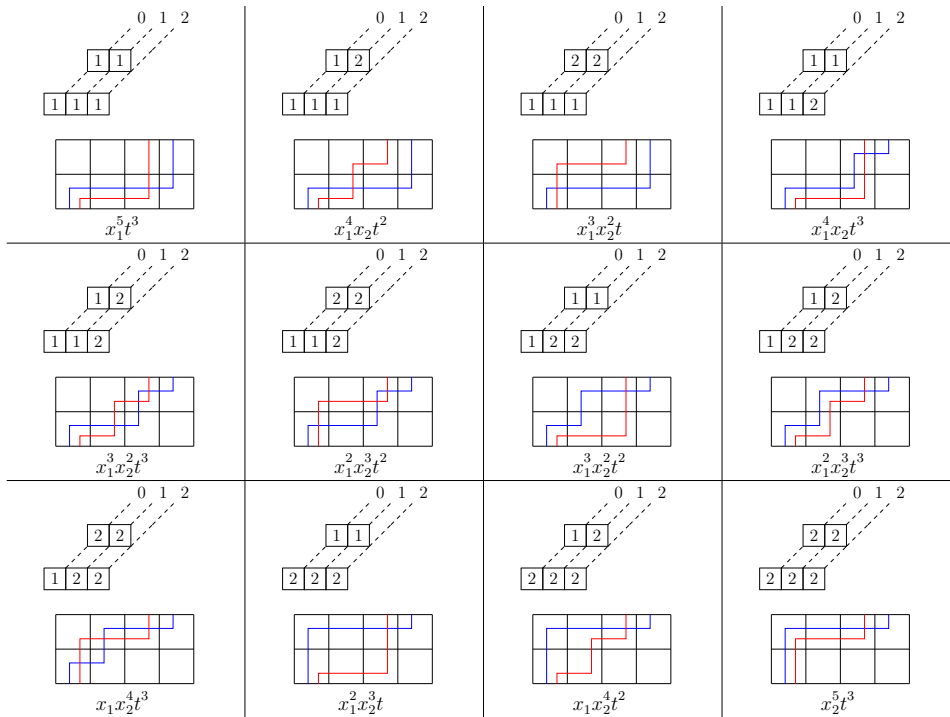
Corollary 2.6.13 ([22, Cor. 6.13]).

$$\sum_{\lambda} \mathcal{L}_{\lambda}(X_n; t) \mathcal{L}_{\lambda^{\text{rot}}}(Y_n; t) = \prod_{i,j=1}^n \prod_{m=0}^{k-1} (1 - x_i y_j t^m)^{-1}$$

2.7 Examples

Throughout this section, blue is color 1 and red is color 2. We use Theorem 2.3.3 to compute two coinversion LLT polynomials.

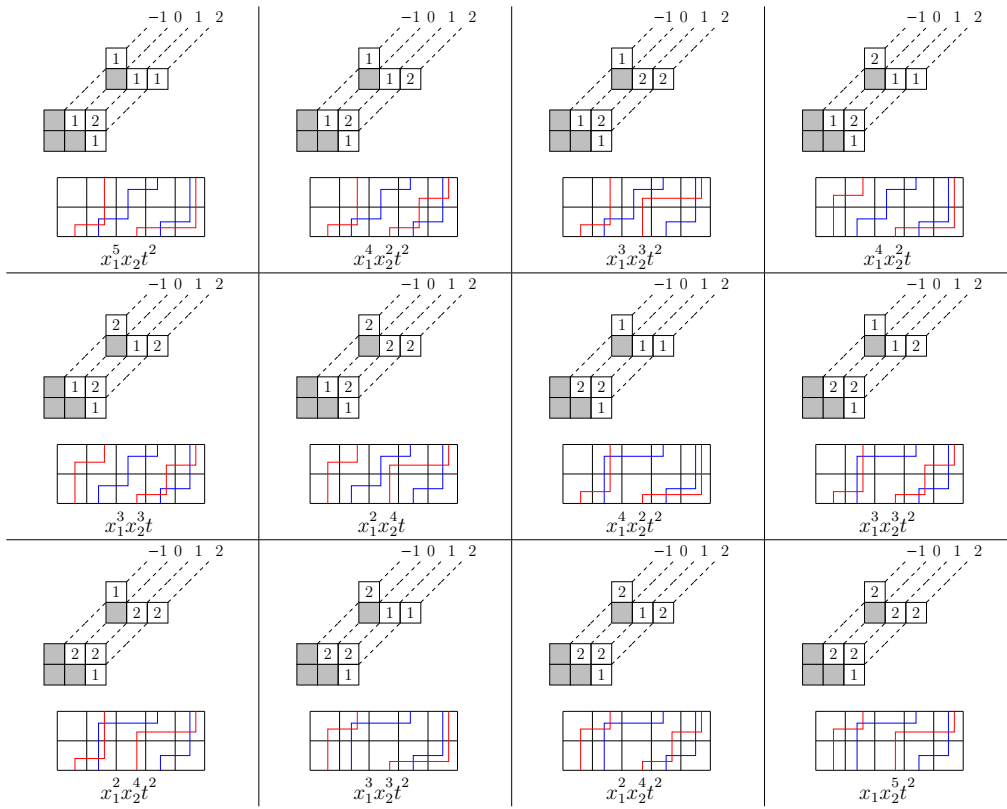
First we compute $\mathcal{L}_{\beta/\gamma}(x_1, \dots, x_n; t)$ where $\beta/\gamma = ((3)/(0), (2)/(0))$ and $n = 2$. There are 12 semistandard Young tableaux of shape β/γ with entries in $\{1, 2\}$, which are shown below along with the corresponding lattices and polynomials.



Therefore the coinversion LLT polynomial is

$$\begin{aligned} \mathcal{L}_{((3)/(0),(2)/(0))}(x_1, x_2; t) &= t(x_1^2 x_2^3 + x_1^3 x_2^2) \\ &\quad + t^2(x_1 x_2^4 + x_1^2 x_2^3 + x_1^3 x_2^2 + x_1^4 x_2) \\ &\quad + t^3(x_2^5 + x_1 x_2^4 + x_1^2 x_2^3 + x_1^3 x_2^2 + x_1^4 x_2 + x_1^5). \end{aligned}$$

Next, we compute $\mathcal{L}_{\beta/\gamma}(x_1, \dots, x_n; t)$ where $\beta/\gamma = ((3, 3)/(2, 1), (3, 1)/(1, 0))$ and $n = 2$. Again there are 12 semistandard Young tableaux, shown below along with the corresponding lattices and polynomials.



Therefore the coinversion LLT polynomial is

$$\begin{aligned} \mathcal{L}_{((3,3)/(2,1),(3,1)/(1,0))}(x_1, x_2; t) &= t(x_1^2 x_2^4 + x_1^3 x_2^3 + x_1^4 x_2^2) \\ &\quad + t^2(x_1 x_2^5 + 2x_1^2 x_2^4 + 3x_1^3 x_2^3 + 2x_1^4 x_2^2 + x_1^5 x_2). \end{aligned}$$

Chapter 3

Super ribbon functions

3.1 Introduction

Supersymmetric LLT polynomials $\mathcal{G}_{\lambda/\mu}^{(k)}(X_n; Y_m; t)$ were introduced in [38] (in which they are called super ribbon functions). As the name suggests, these polynomials are supersymmetric in the X and Y variables (see Definition 3.4.6) and specialize to LLT polynomials when $m = 0$ (see [28, Remark B.3]). The supersymmetric LLT polynomials have several other interesting specializations in addition to the LLT polynomials, including the metaplectic symmetric functions, where were introduced in [15], and the supersymmetric Schur polynomials, which can be realized as characters of certain simple modules of the Lie superalgebra $\mathfrak{gl}(n|m)$ [6].

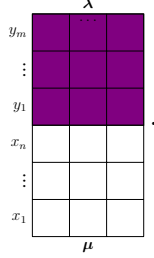
In this chapter, we will study supersymmetric LLT polynomials from the perspective of integrable vertex models. As was shown in the previous chapter, as well as in [1, 22, 23], the LLT polynomials can be realized as a certain class of partition functions constructed from an integrable vertex model. In [15], the authors constructed a vertex model whose partition functions are the metaplectic symmetric functions. In this paper, we generalize these results by showing the that there is an integrable vertex model whose partition functions are the supersymmetric LLT polynomials. The main result of this chapter can be summarized as follows.

Theorem 3.1.1 (Prop. 3.5.9). *Suppose the k -tuple of skew shapes λ/μ is the k -quotient of the skew shape λ/μ . There is a Yang-Baxter integrable vertex model whose partition function $\mathcal{L}_{\lambda/\mu}^S(X_n; Y_m; t)$ is equal to*

$$\mathcal{L}_{\lambda/\mu}^S(X_n; Y_m; t) = t^{\square} \mathcal{G}_{\lambda/\mu}^{(k)}(X_n; Y_m; t^{1/2})$$

for some half-integer $\square \in \frac{1}{2}\mathbb{Z}$, where $\mathcal{G}_{\lambda/\mu}^{(k)}(X_n; Y_m; t)$ is the super ribbon function.

Explicitly, $\mathcal{L}_{\lambda/\mu}^S(X_n; Y_m; t)$ is the partition function associated to the lattice



This chapter is organized as follows. In Section 3.2, we describe how to relate tuples of semistandard Young tableaux to semistandard ribbon tableaux through the Littlewood quotient map, and we extend this map to the case of super tableaux. In Section 3.3, we define the relevant partition functions that give rise to the supersymmetric LLT polynomials $\mathcal{L}_{\lambda/\mu}^S$. In Section 3.4, we prove a variety of properties of the $\mathcal{L}_{\lambda/\mu}^S$. The main result of this section is

Theorem 3.1.2. *The polynomials $\mathcal{L}_{\lambda/\mu}^S(X_n; Y_m; t)$ satisfy the following properties.*

1. (Symmetry, Lemma 3.4.4) *The polynomials $\mathcal{L}_{\lambda/\mu}^S(X_n; Y_m; t)$ are symmetric in the X and Y variables.*
2. (Cancellation, Lemma 3.4.5) $\mathcal{L}_{\lambda/\mu}^S(X_{n-1}, r; Y_{m-1}, -r; t) = \mathcal{L}_{\lambda/\mu}^S(X_{n-1}; Y_{m-1}; t)$
3. (Homogeneity, Lem. 3.4.9) *The polynomial $\mathcal{L}_{\lambda/\mu}^S(X_n; Y_m; t)$ is homogeneous in the X and Y variables of degree $|\lambda/\mu| = |\lambda| - |\mu|$.*
4. (Restriction, Lemma 3.4.8)

$$\begin{aligned} \mathcal{L}_{\lambda/\mu}^S(X_{n-1}, 0; Y_m; t) &= \mathcal{L}_{\lambda/\mu}^S(X_{n-1}; Y_m; t), \\ \mathcal{L}_{\lambda/\mu}^S(X_n; Y_{m-1}, 0; t) &= \mathcal{L}_{\lambda/\mu}^S(X_n; Y_{m-1}; t) \end{aligned}$$

5. (Factorization, Lemma 3.4.10) *If there exist τ and η such that*

$$\lambda^{(i)} = (m + \tau_1^{(i)}, \dots, m + \tau_n^{(i)}, \eta_1^{(i)}, \dots, \eta_s^{(i)})$$

for all i , then

$$\mathcal{L}_{\lambda}^S(X_n; Y_m; t) = \mathcal{L}_{\tau}(X_n; t) \cdot t^{g(\eta)} \mathcal{L}_{\eta'}(Y_m; t^{-1}) \cdot \prod_{l=0}^{k-1} \prod_{i=1}^n \prod_{j=1}^m (t^l x_i + y_j).$$

The first two properties together imply the supersymmetry of the $\mathcal{L}_{\lambda/\mu}^S(X_n; Y_m; t)$. In the case where $\lambda = (\lambda)$ is a 1-tuple of partitions, one can show that the supersymmetric LLT polynomial $\mathcal{L}_{\lambda}^S(X_n; Y_m; t)$ is exactly the supersymmetric Schur polynomial $s_{\lambda}(X_n; Y_m)$. In fact, taking $\mu = \mathbf{0}$ and $k = 1$ in Theorem 3.1.2, these properties uniquely characterize the supersymmetric Schur polynomials (see [46, Section 2.1.2] and [43, Example I.3.23]). However, we suspect (but do not prove) that the properties in Theorem 3.1.2 do not uniquely characterize the supersymmetric LLT polynomials, even in the case $\mu = \mathbf{0}$.

In Section 3.5, we relate the supersymmetric LLT polynomials to the super ribbon functions introduced in [38], by proving Theorem 3.1.1. Finally, in Section 3.6, we show the supersymmetric LLT polynomials satisfy a Cauchy identity. The main result of this section is

Theorem 3.1.3 (Thm. 3.6.13). *Let μ and ν be tuples of partitions each with infinitely many parts only finitely many of which are non-zero. Fix positive integers n, m, p, q . Then*

$$\begin{aligned} & \sum_{\lambda} t^{d(\mu, \lambda)} \mathcal{L}_{\nu/\lambda}^S(X_n, Y_m; t) \mathcal{L}_{\mu/\lambda}^S(W_p, Z_q; t) \\ &= \Omega(X_n, Y_m, W_p, Z_q; t) \sum_{\lambda} t^{d(\lambda, \nu)} \mathcal{L}_{\lambda/\mu}^S(X_n, Y_m; t) \mathcal{L}_{\lambda/\nu}^S(W_p, Z_q; t) \end{aligned} \tag{3.1}$$

where

$$\Omega(X_n, Y_m, W_p, Z_q; t) = \prod_{l=0}^{k-1} \prod_{i, i'=1}^n \prod_{j, j'=1}^m \prod_{\alpha, \alpha'=1}^p \prod_{\beta, \beta'=1}^q \frac{(1 - x_i w_{\alpha} t^l)(1 - y_{j'} z_{\beta'} t^l)}{(1 + y_j w_{\alpha'} t^l)(1 + x_{i'} z_{\beta} t^l)}.$$

3.2 Ribbon tableaux and the Littlewood quotient map

This section provides necessary background information and establishes some notation for the rest of this chapter. In Chapters 1 and 2, we ventured into the world of tableaux on tuples of skew shapes and defined coinversion LLT polynomials. In Section 3.2, we venture into the world of ribbon tableaux and connect the two worlds via the Littlewood quotient map. In Section 3.2, we define super ribbon functions and extend the Littlewood quotient map to a bijection between super ribbon tableaux (Definition 3.2.7) and semistandard super Young tableaux (Definition 3.2.10). This bijection plays a pivotal role in the rest of this chapter, because it allows us to relate our partition functions (Definition 3.3.2) to the super ribbon functions in Prop. 3.5.9.

Ribbon tableaux and the Littlewood quotient map

First we discuss semistandard ribbon tableaux. We define a bijection, called the Littlewood quotient map, relating them and tuples of semistandard Young tableaux.

Fix a positive integer k . A k -**ribbon** is a skew shape of size k that is connected and does not contain any 2×2 square. The head (tail) of a k -ribbon is the SE-most (NW-most) cell in its Young diagram. A **horizontal (vertical) k -ribbon strip** of shape λ/μ is a tiling of λ/μ by k -ribbons such that the head (tail) of each ribbon is adjacent to the southern (western) boundary of the shape. We let $\text{HRS}_k(\lambda/\mu)$ ($\text{VRS}_k(\lambda/\mu)$) denote the set of horizontal (vertical) k -ribbon strips of shape λ/μ .

Throughout this chapter, we will omit k when it is clear from context. For example, we will use “ribbon” and “ k -ribbon” interchangeably.

Definition 3.2.1. A *semistandard k -ribbon tableau* of shape λ/μ is a tiling of λ/μ by k -ribbons and a labelling of the k -ribbons by positive integers such that, for all i ,

1. removing all ribbons labelled j for $j > i$ gives a valid skew shape $\lambda_{\leq i}/\mu$, and
2. the subtableau of ribbons labelled i form a horizontal k -ribbon strip of shape $\lambda_{\leq i}/\lambda_{\leq i-1}$.

We let $\text{SSRT}_k(\lambda/\mu)$ denote the set of semistandard k -ribbon tableau of shape λ/μ .

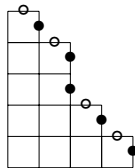
Following the exposition of [47, Section 3], we now define the Littlewood k -quotient map. This map was introduced in [41]; another (perhaps clearer) formulation, as well as a proof that the map is a bijection, is given in [52].

We first define the k -**quotient map**, which is a function

$$\{\text{skew partitions } \lambda/\mu\} \rightarrow \{k\text{-tuples } \boldsymbol{\lambda}/\boldsymbol{\mu} = (\lambda^{(0)}/\mu^{(0)}, \dots, \lambda^{(k-1)}/\mu^{(k-1)}) \text{ of skew partitions}\}.$$

This function can be defined graphically as follows. Given a partition λ , we truncate its Maya diagram to a finite sequence (a_0, \dots, a_{r-1}) of East = \circ and South = \bullet steps by following the North-East boundary of λ from North-West to South-East.

Example 3.2.2 (cf. Ex. 1.1.1). *The Maya diagram of $(4,3,2,2,1)$ is $\circ \bullet \circ \bullet \circ \bullet \circ \bullet \circ \bullet$.*



Remark 3.2.3. Observe that postpending finitely many \circ 's to a Maya diagram does not change the corresponding partition. Thus we can take the length r of the Maya diagram (a_0, \dots, a_{r-1}) to be a multiple of k .

Let λ be a partition with Maya diagram (a_0, \dots, a_{r-1}) . By the preceding remark, we may assume $s = r/k$ is an integer. We define the k -**quotient** of λ to be the k -tuple of partitions

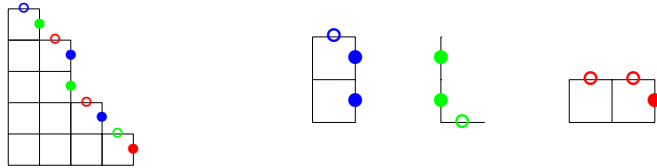
$$\boldsymbol{\lambda} = (\lambda^{(0)}, \dots, \lambda^{(k-1)})$$

where, for each i , $\lambda^{(i)}$ is the partition corresponding to the Maya diagram

$$(a_i, a_{k+i}, \dots, a_{(s-1)k+i}).$$

We define the k -quotient of a skew partition λ/μ to be the k -tuple $\boldsymbol{\lambda}/\boldsymbol{\mu}$ of skew partitions, where $\boldsymbol{\lambda}$ and $\boldsymbol{\mu}$ are the k -quotients of λ and μ respectively. Here we require λ and μ to have the same number of parts, postpending parts equalling 0 to μ if necessary.

Example 3.2.4. The 3-quotient of $(4, 3, 2, 2, 1)$ is $((1, 1), (0, 0), (2))$.



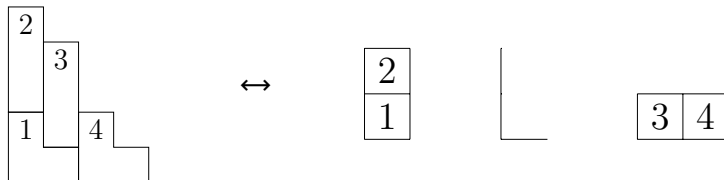
We are now ready to define the Littlewood k -quotient map.

Definition 3.2.5. Let $\boldsymbol{\lambda}/\boldsymbol{\mu}$ be the k -quotient of λ/μ . The **Littlewood k -quotient map** is a bijection

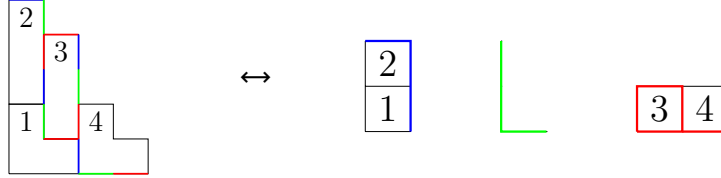
$$\text{SSRT}_k(\lambda/\mu) \rightarrow \text{SSYT}(\boldsymbol{\lambda}/\boldsymbol{\mu})$$

defined as follows. Fix $T \in \text{SSRT}_k(\lambda/\mu)$. For each i , we put an i into each cell of the k -quotient of $\lambda_{\leq i}/\lambda_{\leq i-1}$ (which lies inside $\boldsymbol{\lambda}/\boldsymbol{\mu}$). In this fashion, we place positive integers into the cells of $\boldsymbol{\lambda}/\boldsymbol{\mu}$, resulting in $\mathbf{T} = (T^{(0)}, \dots, T^{(k-1)}) \in \text{SSYT}(\boldsymbol{\lambda}/\boldsymbol{\mu})$.

Example 3.2.6. In Example 3.2.4, we found that the 3-quotient of $\lambda = (4, 3, 2, 2, 1)$ was $\boldsymbol{\lambda} = ((1, 1), (0, 0), (2))$. One can compute that



via the Littlewood 3-quotient map. For example, when $i = 3$, one can compute the k -quotient of $\lambda_{\leq i}/\lambda_{\leq i-1}$ as follows.



Here we have drawn the Maya diagrams of both $\lambda_{\leq 3}$ and $\lambda_{\leq 2}$. From this, we see that that a cell at coordinates $(1, 1)$ is added in $T^{(2)}$, and we fill it with a 3.

Extending the Littlewood quotient map to super tableaux

Throughout this subsection, let $\mathcal{A} = \{1 < 2 < \dots\}$ and $\mathcal{A}' = \{1' < 2' < \dots\}$. Also fix a total order on $\mathcal{A} \cup \mathcal{A}'$ that is compatible with the natural orders on \mathcal{A} and \mathcal{A}' .

Definition 3.2.7. A *super k -ribbon tableau* of shape λ/μ is a tiling of λ/μ by k -ribbons and a labelling of the k -ribbons by the alphabet $\mathcal{A} \cup \mathcal{A}'$ such that

1. for $i \in \mathcal{A} \cup \mathcal{A}'$, the ribbons with label $\leq i$ form a valid skew shape $\lambda_{\leq i}/\mu$;
2. for $i \in \mathcal{A}$, the subtableau of ribbons labelled i form a horizontal k -ribbon strip;
and
3. for $i' \in \mathcal{A}'$, the subtableau of ribbons labelled i' form a vertical k -ribbon strip.

We let $\text{SRT}_k(\lambda/\mu)$ denote the set of super k -ribbon tableau of shape λ/μ .

Note that a SRT in the alphabet \mathcal{A} of shape λ/μ is the same as a SSRT of shape λ/μ . Moreover, there is a bijection between SRT in the alphabet \mathcal{A}' of shape λ/μ and SSRT of shape λ'/μ' , given by conjugation (and unpriming the labels).

The height $h(R)$ of a ribbon R is the number of rows it contains. The **spin** of a super ribbon tableau T is

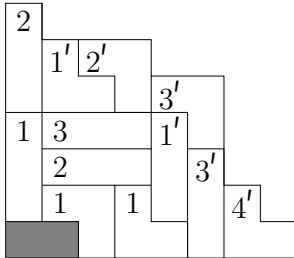
$$\text{spin}(T) = \sum_R (h(R) - 1)$$

where the sum is taken over all ribbons R in T .

Definition 3.2.8. [38, Definition 44] The *super k -ribbon function* associated to a skew partition λ/μ is the generating function

$$\mathcal{G}_{\lambda/\mu}^{(k)}(X; Y; t) = \sum_{T \in \text{SRT}_k(\lambda/\mu)} t^{\text{spin}(T)} x^{\text{weight}(T)} y^{\text{weight}'(T)}.$$

Example 3.2.9. We use the ordering $1 < 2 < \dots < 1' < 2' < \dots$ on $\mathcal{A} \cup \mathcal{A}'$. Let $k = 3$ and $\lambda/\mu = (8, 7, 6, 6, 6, 4, 1)/(2)$. The super ribbon tableau



has spin $1\bar{4}$ and contributes

$$t^{14} x_1^3 x_2^2 x_3^1 y_1^2 y_2^1 y_3^2 y_4^1$$

to $\mathcal{G}_{\lambda/\mu}^{(k)}(X; Y; t)$.

Definition 3.2.10. A **semistandard super Young tableau** of shape λ/μ is a filling of each cell of $D(\lambda)$ with an element of $\mathcal{A} \cup \mathcal{A}'$ such that

1. the rows and the columns are weakly increasing,
2. the entries in \mathcal{A} are strictly increasing along columns, and
3. the entries in \mathcal{A}' are strictly increasing along rows.

We let $\text{SSSYT}(\lambda/\mu)$ denote the set of semistandard super Young tableaux of shape λ/μ . Given a tuple $\boldsymbol{\lambda}/\boldsymbol{\mu} = (\lambda^{(1)}/\mu^{(1)}, \dots, \lambda^{(k)}/\mu^{(k)})$ of skew partitions, a semistandard super Young tableau of shape $\boldsymbol{\lambda}/\boldsymbol{\mu}$ is a semistandard super Young tableau on each $\lambda^{(j)}/\mu^{(j)}$, that is,

$$\text{SSSYT}(\boldsymbol{\lambda}/\boldsymbol{\mu}) = \text{SSSYT}(\lambda^{(1)}/\mu^{(1)}) \times \dots \times \text{SSSYT}(\lambda^{(k)}/\mu^{(k)}).$$

Note that a SSSYT in the alphabet \mathcal{A} of shape λ/μ is the same as a SSYT of shape λ/μ . Moreover, there is a bijection between SSSYT in the alphabet \mathcal{A}' of shape λ/μ and SSYT of shape λ'/μ' , given by conjugation (and unpriming the labels).

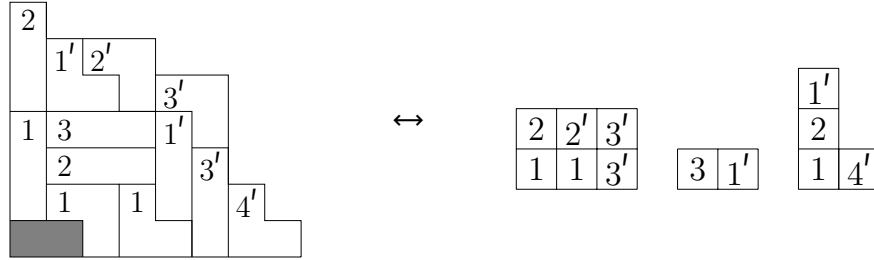
We are now ready to extend the Littlewood k -quotient map.

Definition 3.2.11. The (**extended**) **Littlewood k -quotient map** is a bijection

$$\text{SRT}_k(\lambda/\mu) \rightarrow \text{SSSYT}(\boldsymbol{\lambda}/\boldsymbol{\mu})$$

where $\boldsymbol{\lambda}/\boldsymbol{\mu}$ is the k -quotient of λ/μ . We simply take Definition 3.2.5 and extend the set of labels: for each $i \in \mathcal{A} \cup \mathcal{A}'$, we put an i into each cell of the k -quotient of $\lambda_{\leq i}/\lambda_{\leq i-1}$.

Example 3.2.12.



The following facts, which we prove in Appendix C, can be useful in computing the (extended) Littlewood k -quotient map in examples.

Lemma 3.2.13 ([28, Lemma 2.16]). *Suppose $T \leftrightarrow \mathbf{T}$ via the (extended) Littlewood k -quotient map.*

1. *A ribbon in T labelled i corresponds to a cell labelled i in \mathbf{T} , so the number of ribbons in T labelled i equals the number of cells labelled i in \mathbf{T} .*
2. *Two ribbons R, R' in T whose tails u, u' have the same content modulo k correspond to two cells v, v' in the same shape in \mathbf{T} . Moreover, in this case,*

$$\frac{c(u) - c(u')}{k} = c(v) - c(v').$$

3.3 Partition functions

In the following definitions, let λ/μ be a k -tuple of skew partitions, each having p parts. Recall from Theorem 2.3.3 that the coinversion LLT polynomial $\mathcal{L}_{\lambda/\mu}(X_n; t)$ is the partition function associated to the lattice

$$W_n(\lambda/\mu) = \begin{array}{c} \lambda \\ \begin{array}{|c|c|c|} \hline & \cdots & \\ \hline & & \\ \hline & & \\ \hline & & \\ \hline \end{array} \\ \mu \end{array}.$$

Definition 3.3.1. *We define $\mathcal{L}_{\lambda/\mu}^P(X_n; t)$ to be the partition function associated to the lattice*

$$P_n(\lambda/\mu) := \begin{array}{c} \lambda \\ \begin{array}{|c|c|c|} \hline & \cdots & \\ \hline & & \\ \hline & & \\ \hline & & \\ \hline \end{array} \\ \mu \end{array}.$$

Definition 3.3.2. We define the **supersymmetric LLT polynomial** $\mathcal{L}_{\lambda/\mu}^S(X_n; Y_m; t)$ to be the partition function associated to the lattice

$$S_{n,m}(\lambda/\mu) := \begin{array}{c} \lambda \\ \begin{array}{|c|c|c|} \hline & & \\ \hline y_m & & \\ \hline \vdots & & \\ \hline y_1 & & \\ \hline x_n & & \\ \hline \vdots & & \\ \hline x_1 & & \\ \hline \mu \end{array} \end{array}.$$

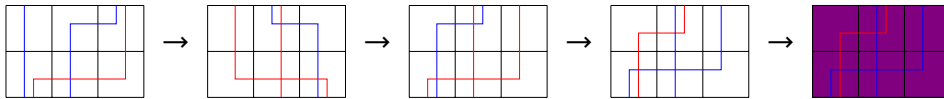
3.4 Identities of supersymmetric LLT polynomials

In this section, we establish various properties of the partition functions $\mathcal{L}_{\lambda/\mu}^S$ of Definition 3.3.2. These include four properties (summarized in Theorem 3.1.2) which generalize four properties that uniquely characterize the supersymmetric Schur polynomials.

Let $P_p^{(k)}$ be the set of k -tuples of partitions, each having p parts. Given a non-negative integer n and $\lambda, \mu \in P_p^{(k)}$, there is a bijection

$$\psi : LC(W_n(\lambda/\mu)) \rightarrow LC(P_n(\lambda'/\mu')).$$

Explicitly, $\psi(C)$ is obtained from C by inverting the vertical parts of the paths, reflecting the lattice over its left edge, changing each color i to color $k - i$, and making the vertices purple. For example,



where we have done each step in order (and where blue is color 1 and red is color 2).

Fix $\lambda, \mu \in P_p^{(k)}$. Also fix a sufficiently large number of columns; specifically, the number of columns must be larger than each $\text{band}(\lambda/\mu)$. If λ/μ is a horizontal strip, then there is a unique configuration $C_{\lambda/\mu}$ on a single white row with top boundary λ , bottom boundary μ , and empty left/right boundaries. Similarly, if λ/μ is a vertical strip, then there is a unique configuration on a single purple row with top boundary λ , bottom boundary μ , and empty left/right boundaries.

Lemma 3.4.1 ([28, Lemma 4.1]). *There exists a function $g : P_p^{(k)} \rightarrow \mathbb{Z}_{\geq 0}$ so that*

$$\mathcal{L}_{\lambda/\mu}(x; t) = t^{g(\lambda) - g(\mu)} \mathcal{L}_{\lambda'/\mu'}^P(x; t^{-1})$$

for all $\lambda, \mu \in P_p^{(k)}$ such that λ/μ is a horizontal strip.

Proof. Fix $\lambda, \mu \in P_p^{(k)}$ such that λ/μ is a horizontal strip. Let $C = C_{\lambda/\mu}$. Note that C is the unique configuration on a single white row with top boundary λ , bottom boundary μ , and empty left/right boundaries. Moreover, $\psi(C)$ is the unique configuration on a single purple row with top boundary λ' , bottom boundary μ' , and empty left/right boundaries. Thus

$$\begin{aligned} \mathcal{L}_{\lambda/\mu}(x; t) &= \text{weight}(C) = x^\alpha t^\beta, \\ \mathcal{L}_{\lambda'/\mu'}^P(x; t) &= \text{weight}(\psi(C)) = x^\gamma t^\delta \end{aligned}$$

for some non-negative integers $\alpha, \beta, \gamma, \delta$. Note

$$\begin{aligned} \alpha &= \#\{(i, j) \mid \text{the } i\text{-th smallest color exits right in the } b\text{-th leftmost box in } C\} \\ &= \#\{(i, j) \mid \text{the } i\text{-th largest color exits right in the } b\text{-th rightmost box in } \psi(C)\} = \gamma. \end{aligned}$$

Therefore

$$\mathcal{L}_{\lambda/\mu}(x; t) = x^\alpha t^\beta = t^{\beta + \delta} x^\gamma t^{-\delta} = t^{\beta + \delta} \mathcal{L}_{\lambda'/\mu'}^P(x; t^{-1}).$$

Also note

$$\begin{aligned} \beta + \delta &= \#\{(i, j, b) \mid i < j, \text{ in box } b \text{ of } C \text{ color } i \text{ exits right and color } j \text{ is present}\} \\ &\quad + \#\{(i', j', b') \mid i' > j', \text{ in box } b' \text{ of } \psi(C) \text{ color } i' \text{ is vertical and color } j' \text{ exits right}\} \\ &= \#\{(i, j, b) \mid i < j, \text{ in box } b \text{ of } C \text{ color } i \text{ exits right and color } j \text{ is present}\} \\ &\quad + \#\{(i, j, b) \mid i < j, \text{ in box } b \text{ of } C \text{ color } i \text{ is absent and color } j \text{ enters left}\} \\ &= \sum_b \sum_{i < j} \mathbf{1}_{b \text{ is "good" for } i \text{ and } j} \end{aligned}$$

where we say a box b is “good” for the colors $i < j$ if either color i exits right and color j is present, or color i is absent and color j enters left. Therefore

$$\mathcal{L}_{\lambda/\mu}(x; t) = t^{\tilde{g}(\lambda/\mu)} \mathcal{L}_{\lambda'/\mu'}^P(x; t^{-1})$$

where we have defined

$$\tilde{g}(\lambda/\mu) := \sum_{\substack{\text{boxes } b \\ \text{of } C_{\lambda/\mu}}} \sum_{\substack{\text{colors} \\ i < j}} \mathbf{1}_{b \text{ is "good" for } i \text{ and } j}.$$

We can recursively define the desired function g by the rule

$$g(\lambda) = \begin{cases} g(\mu) + \tilde{g}(\lambda/\mu) & \text{if there exists } \mu \in P_p^{(k)} - \{\lambda\} \text{ such that } \lambda/\mu \text{ is a horizontal strip} \\ 0 & \text{otherwise (i.e. if } \lambda = \mathbf{0}) \end{cases}.$$

Provided that $g(\lambda)$ is well-defined (i.e. $g(\mu) + \tilde{g}(\lambda/\mu)$ is independent of μ) for all $\lambda \in P_p^{(k)}$,

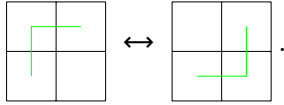
$$\mathcal{L}_{\lambda/\mu}(x; t) = t^{\tilde{g}(\lambda/\mu)} \mathcal{L}_{\lambda'/\mu'}^P(x; t^{-1}) = t^{g(\lambda) - g(\mu)} \mathcal{L}_{\lambda'/\mu'}^P(x; t^{-1})$$

for all $\lambda, \mu \in P_p^{(k)}$ such that λ/μ is a horizontal strip. To show g is well-defined, we induct on the number of cells in λ . Clearly $g(\mathbf{0}) = 0$ is well-defined. Fix $\lambda \in P_p^{(k)} - \{\mathbf{0}\}$ and assume g is well-defined on elements of $P_p^{(k)}$ with strictly fewer boxes than λ . Fix $\alpha, \mu \in P_p^{(k)} - \{\lambda\}$ such that λ/α and λ/μ are horizontal strips. There exist (not necessarily distinct)

$$\begin{aligned} \beta^0 = \mathbf{0}, \dots, \beta^{r-1} = \alpha, \beta^r = \lambda \in P_p^{(k)}, \\ \nu^0 = \mathbf{0}, \dots, \nu^{r-1} = \mu, \nu^r = \lambda \in P_p^{(k)} \end{aligned}$$

such that β^i/β^{i-1} and ν^i/ν^{i-1} are horizontal strips for all i . Note that each sequence completely determines a configuration of paths on an $r \times M$ lattice with top boundary λ and bottom boundary $\mathbf{0}$, since they determine the state of the paths at every row.

Since the two configurations have the same top and bottom boundary, it is possible to get from one configuration to the other via corner flips



A straightforward corner flipping argument shows that the quantity

$$\sum_b \sum_{i < j} \mathbf{1}_{b \text{ is "good" for } i \text{ and } j}$$

is the same for both configurations. Therefore

$$\tilde{g}(\beta^r/\beta^{r-1}) + \tilde{g}(\beta^{r-1}/\beta^{r-2}) + \dots + \tilde{g}(\beta^1/\beta^0) = \tilde{g}(\nu^r/\nu^{r-1}) + \tilde{g}(\nu^{r-1}/\nu^{r-2}) + \dots + \tilde{g}(\nu^1/\nu^0).$$

Applying the inductive hypothesis, we have

$$\begin{aligned} \tilde{g}(\beta^r/\beta^{r-1}) + g(\beta^{r-1}) - g(\beta^{r-2}) + \dots + g(\beta^1) - g(\beta^0) \\ = \tilde{g}(\nu^r/\nu^{r-1}) + g(\nu^{r-1}) - g(\nu^{r-2}) + \dots + g(\nu^1) - g(\nu^0). \end{aligned}$$

The sums telescope to give

$$\tilde{g}(\boldsymbol{\beta}^r / \boldsymbol{\beta}^{r-1}) + g(\boldsymbol{\beta}^{r-1}) - g(\boldsymbol{\beta}^0) = \tilde{g}(\boldsymbol{\nu}^r / \boldsymbol{\nu}^{r-1}) + g(\boldsymbol{\nu}^{r-1}) - g(\boldsymbol{\nu}^0)$$

which we can rewrite as

$$\tilde{g}(\boldsymbol{\lambda} / \boldsymbol{\alpha}) + g(\boldsymbol{\alpha}) - g(\mathbf{0}) = \tilde{g}(\boldsymbol{\lambda} / \boldsymbol{\mu}) + g(\boldsymbol{\mu}) - g(\mathbf{0}).$$

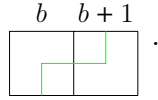
Therefore $g(\boldsymbol{\alpha}) + \tilde{g}(\boldsymbol{\lambda} / \boldsymbol{\alpha}) = g(\boldsymbol{\mu}) + \tilde{g}(\boldsymbol{\lambda} / \boldsymbol{\mu})$. □

Corollary 3.4.2 ([28, Cor. 4.2]). $g(\boldsymbol{\lambda}) = g(\boldsymbol{\lambda}')$

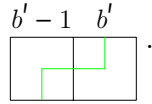
Proof. We induct on the number of cells in $\boldsymbol{\lambda}$. Note that $g(\mathbf{0}) = 0 = g(\mathbf{0}')$. Fix $\boldsymbol{\lambda} \in P_p^{(k)} - \{\mathbf{0}\}$ and assume $g(\boldsymbol{\mu}) = g(\boldsymbol{\mu}')$ for all $\boldsymbol{\mu} \in P_p^{(k)}$ with strictly fewer cells than $\boldsymbol{\lambda}$. Since $\boldsymbol{\lambda} \neq \mathbf{0}$, there exists $\boldsymbol{\mu} \in P_p^{(k)}$ that can be obtained by removing a single cell u from $\boldsymbol{\lambda}$. We want to show $g(\boldsymbol{\lambda}) = g(\boldsymbol{\lambda}')$. It is enough to show $\tilde{g}(\boldsymbol{\lambda} / \boldsymbol{\mu}) = \tilde{g}(\boldsymbol{\lambda}' / \boldsymbol{\mu}')$, since then

$$g(\boldsymbol{\lambda}) = g(\boldsymbol{\mu}) + \tilde{g}(\boldsymbol{\lambda} / \boldsymbol{\mu}) = g(\boldsymbol{\mu}') + \tilde{g}(\boldsymbol{\lambda}' / \boldsymbol{\mu}') = g(\boldsymbol{\lambda}').$$

Let $\lambda^{(i)}$ be the partition to which u belongs. Since $\boldsymbol{\lambda} / \boldsymbol{\mu}$ consists of the single cell u in $\lambda^{(i)} / \mu^{(i)}$, every color in every box in $C_{\boldsymbol{\lambda} / \boldsymbol{\mu}}$ is either vertical or absent, with the exception of the color i in two adjacent boxes, which has the form



Note that $C_{\boldsymbol{\lambda}' / \boldsymbol{\mu}'}$ is exactly the configuration $\psi(C_{\boldsymbol{\lambda} / \boldsymbol{\mu}})$ with white in place of purple. Therefore every color in every box in $C_{\boldsymbol{\lambda}' / \boldsymbol{\mu}'}$ is either vertical or absent, with the exception of the color $i' = k - i$ in two adjacent boxes, which has the form



We have

$$\begin{aligned} \tilde{g}(\boldsymbol{\lambda} / \boldsymbol{\mu}) &= \#\{j > i : j \text{ is vertical in box } b \text{ of } C_{\boldsymbol{\lambda} / \boldsymbol{\mu}}\} + \#\{h < i : h \text{ is absent in box } b + 1 \text{ of } C_{\boldsymbol{\lambda} / \boldsymbol{\mu}}\} \\ &= \#\{j' < i' : j' \text{ is absent in box } b' \text{ of } C_{\boldsymbol{\lambda}' / \boldsymbol{\mu}'}\} + \#\{h' > i' : h' \text{ is vertical in box } b' - 1 \text{ of } C_{\boldsymbol{\lambda}' / \boldsymbol{\mu}'}\} \\ &= \tilde{g}(\boldsymbol{\lambda}' / \boldsymbol{\mu}'). \end{aligned}$$

□

Theorem 3.4.3 ([28, Thm. 4.3]).

$$\mathcal{L}_{\lambda/\mu}^S(X_n; Y_m; t) = t^{g(\lambda)-g(\mu)} \mathcal{L}_{\lambda'/\mu'}^S(Y_m; X_n; t^{-1})$$

Proof. If λ/μ is a horizontal strip, then by Lemma 3.4.1, we have

$$\mathcal{L}_{\lambda/\mu}(x; t) = t^{g(\lambda)-g(\mu)} \mathcal{L}_{\lambda'/\mu'}^P(x; t^{-1}). \quad (3.2)$$

If λ/μ is a vertical strip, then by Lemma 3.4.1 (with t^{-1} in place of t and with λ'/μ' in place of λ/μ) and Cor. 3.4.2, we have

$$\mathcal{L}_{\lambda/\mu}^P(x; t) = t^{g(\lambda)-g(\mu)} \mathcal{L}_{\lambda'/\mu'}^P(x; t^{-1}). \quad (3.3)$$

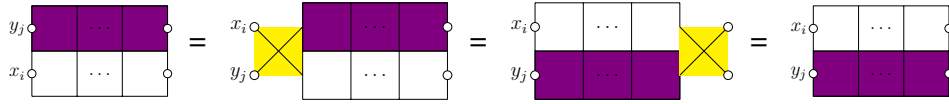
Using (3.2) or (3.3) at each row of our lattice, we have

$$\begin{aligned} \mathcal{L}_{\lambda/\mu}^S(X_n; Y_m; t) &= \begin{array}{c} \lambda \\ \begin{array}{|c|c|c|} \hline y_m & & \\ \hline \vdots & & \\ \hline y_1 & & \\ \hline x_n & & \\ \hline \vdots & & \\ \hline x_1 & & \\ \hline \mu \end{array} \end{array} \\ &= \sum \mathcal{L}_{\lambda/\alpha^{m+n-1}}^P(y_m; t) \dots \mathcal{L}_{\alpha^{n+1}/\alpha^n}^P(y_1; t) \mathcal{L}_{\alpha^n/\alpha^{n-1}}^P(x_n; t) \dots \mathcal{L}_{\alpha^1/\mu}^P(x_1; t) \\ &= \sum t^{g(\lambda)-g(\mu)} \mathcal{L}_{\lambda'/\alpha^{m+n-1}'}^P(y_m; t^{-1}) \dots \mathcal{L}_{\alpha^{n+1}'/\alpha^{n-1}'}^P(y_1; t^{-1}) \mathcal{L}_{\alpha^{n-1}'/\alpha^{n-1}'}^P(x_n; t^{-1}) \dots \mathcal{L}_{\alpha^1'/\mu'}^P(x_1; t^{-1}) \\ &= t^{g(\lambda)-g(\mu)} \sum \mathcal{L}_{\lambda'/\beta^{m+n-1}'}^P(y_m; t^{-1}) \dots \mathcal{L}_{\beta^{n+1}'/\beta^n}^P(y_1; t^{-1}) \mathcal{L}_{\beta^n/\beta^{n-1}}^P(x_n; t^{-1}) \dots \mathcal{L}_{\beta^1/\mu'}^P(x_1; t^{-1}) \\ &= t^{g(\lambda)-g(\mu)} \begin{array}{c} \lambda' \\ \begin{array}{|c|c|c|} \hline y_m & & \\ \hline \vdots & & \\ \hline y_1 & & \\ \hline x_n & & \\ \hline \vdots & & \\ \hline x_1 & & \\ \hline \mu' \end{array} \end{array} = t^{g(\lambda)-g(\mu)} \begin{array}{c} \lambda' \\ \begin{array}{|c|c|c|} \hline x_n & & \\ \hline \vdots & & \\ \hline x_1 & & \\ \hline y_m & & \\ \hline \vdots & & \\ \hline y_1 & & \\ \hline \mu' \end{array} \end{array} = \mathcal{L}_{\lambda'/\mu'}^S(Y_m; X_n; t^{-1}) \end{aligned}$$

where

- the sums in the second and third lines are over all $\alpha^0 = \mu, \dots, \alpha^{m+n} = \lambda$ such that α^i/α^{i-1} is a horizontal strip for all $i \leq n$ and a vertical strip for all $i > n$,
- the sum in the fourth line is over all $\beta^0 = \mu', \dots, \beta^{m+n} = \lambda'$ such that β^i/β^{i-1} is a vertical strip for all $i \leq n$ and a horizontal strip for all $i > n$, and

- the second-to-last equality uses repeated applications of Prop. 1.4.6:



□

The technique used to swap a white row and a purple row at the end of the previous proof is sometimes called the “train argument” (cf. the proof of Theorem 2.4.1). This technique is used again to prove the following lemma.

Lemma 3.4.4 ([28, Lemma 4.4]). *The partition function associated to any lattice that can be obtained from the lattice $S_{n,m}(\lambda/\mu)$ (Definition 3.3.2) by permuting the rows is equal to $\mathcal{L}_{\lambda/\mu}^S(X_n; Y_m; t)$. In particular, $\mathcal{L}_{\lambda/\mu}^S(X_n; Y_m; t)$ is symmetric in the X and Y variables separately.*

Proof. Two rows can be swapped using the train argument along with Prop. 1.4.4 (to swap two white rows), Prop. 1.4.6 (to swap a white row and a purple row), or Prop. 1.4.7 (to swap two purple rows). □

Next we prove a certain cancellation property for the polynomials $\mathcal{L}_{\lambda/\mu}^S(X_n; Y_m; t)$.

Lemma 3.4.5 (Cancellation). *[[28, Lemma 4.5]] For $n, m \geq 1$, we have*

$$\mathcal{L}_{\lambda/\mu}^S(X_{n-1}, r; Y_{m-1}, -r; t) = \mathcal{L}_{\lambda/\mu}^S(X_{n-1}; Y_{m-1}; t).$$

Proof. Using Lemma 3.4.4, we can write

$$\mathcal{L}_{\lambda/\mu}^S(X_{n-1}, r; Y_{m-1}, -r; t) = \sum_{\alpha} \begin{array}{c} \lambda \\ \begin{array}{|c|c|c|} \hline -r & & \\ \hline r & & \\ \hline y_{m-1} & & \\ \hline \vdots & & \\ \hline y_1 & & \\ \hline x_{n-1} & & \\ \hline \vdots & & \\ \hline x_1 & & \\ \hline \end{array} \\ \mu \end{array} = \sum_{\alpha} \begin{array}{c} \lambda \\ \begin{array}{|c|c|c|} \hline -r & & \\ \hline r & & \\ \hline \end{array} \\ \alpha \end{array} \cdot \begin{array}{c} \alpha \\ \begin{array}{|c|c|c|} \hline y_{m-1} & & \\ \hline \vdots & & \\ \hline y_1 & & \\ \hline x_{n-1} & & \\ \hline \vdots & & \\ \hline x_1 & & \\ \hline \end{array} \\ \mu \end{array}.$$

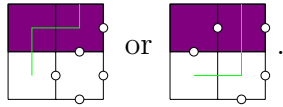
We will show that, for all $\alpha \neq \lambda$, there is an involution φ_{α} on the set of configurations of the lattice

$$L_{\lambda/\alpha} = \begin{array}{c} \lambda \\ \begin{array}{|c|c|c|} \hline -r & & \\ \hline r & & \\ \hline \end{array} \\ \alpha \end{array}$$

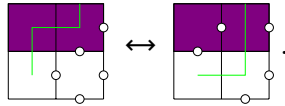
such that $\text{weight}(\varphi_\alpha(C)) = -\text{weight}(C)$ for all C . Therefore

$$\mathcal{L}_{\lambda/\mu}^S(X_{n-1}, r; Y_{m-1}, -r; t) = \begin{array}{c} \lambda \\ \begin{array}{|c|c|} \hline \text{purple} & \text{purple} \\ \hline \end{array} \\ \begin{array}{|c|c|} \hline \text{white} & \text{white} \\ \hline \end{array} \\ \lambda \end{array} = \begin{array}{c} \lambda \\ \begin{array}{|c|c|} \hline \text{purple} & \text{purple} \\ \hline \end{array} \\ \begin{array}{|c|c|} \hline \text{white} & \text{white} \\ \hline \end{array} \\ \mu \end{array} = \begin{array}{c} \lambda \\ \begin{array}{|c|c|} \hline \text{purple} & \text{purple} \\ \hline \end{array} \\ \begin{array}{|c|c|} \hline \text{white} & \text{white} \\ \hline \end{array} \\ \mu \end{array} = \mathcal{L}_{\lambda/\mu}^S(X_{n-1}; Y_{m-1}; t).$$

Fix $\alpha \neq \lambda$ and a configuration C on $L_{\lambda/\alpha}$. Since $\alpha \neq \lambda$, there exist two consecutive columns c and $c + 1$ of C and a color i such that, in columns c and $c + 1$ of C , color i has the form



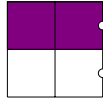
Let c be the rightmost column for which there exists a color of this form in columns c and $c + 1$, and let i be the largest color of this form in columns c and $c + 1$. We define $\varphi_\alpha(C)$ to be the result of flipping color i in columns c and $c + 1$



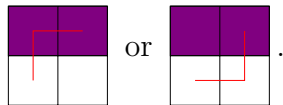
Clearly φ_α is an involution. To show $\text{weight}(\varphi_\alpha(C)) = -\text{weight}(C)$, we must show

$$\text{weight} \left(\begin{array}{c} -r \\ \begin{array}{|c|c|} \hline \text{purple} & \text{purple} \\ \hline \end{array} \\ \begin{array}{|c|c|} \hline \text{white} & \text{white} \\ \hline \end{array} \\ r \end{array} \right) = -\text{weight} \left(\begin{array}{c} -r \\ \begin{array}{|c|c|} \hline \text{purple} & \text{purple} \\ \hline \end{array} \\ \begin{array}{|c|c|} \hline \text{white} & \text{white} \\ \hline \end{array} \\ r \end{array} \right) \quad (3.4)$$

regardless of the paths taken by the other colors. However, by the maximality of c and i , we know that every color not equal to i must have the form



and every color greater than i must not have the form



With these constraints, some straightforward computations show (3.4) holds. \square

Combining Lemmas 3.4.4 and 3.4.5, we can now conclude that the polynomials $\mathcal{L}_{\lambda/\mu}^S(X; Y; t)$ are supersymmetric in the X and Y variables.

Definition 3.4.6. A family of polynomials $\{p(X_n; Y_m) : n, m \in \mathbb{Z}_{\geq 0}\}$ is *supersymmetric* if

- $p(\sigma(X_n); Y_m) = p(X_n; Y_m; t)$ for any permutation $\sigma \in S_n$ (i.e. $p(X_n; Y_m)$ is symmetric in the X variables),
- $p(X_n; \tau(Y_m)) = p(X_n; Y_m; t)$ for any permutation $\tau \in S_m$ (i.e. $p(X_n; Y_m)$ is symmetric in the Y variables), and
- $p(X_{n-1}, r; Y_{m-1}, -r) = p(X_{n-1}; Y_{m-1})$ when $n, m \geq 1$.

Theorem 3.4.7 ([28, Thm. 4.7]). The polynomials $\mathcal{L}_{\lambda/\mu}^S(X_n; Y_m; t)$ are supersymmetric in the X and Y variables.

We proceed by proving a certain restriction property for the $\mathcal{L}_{\lambda/\mu}^S(X_n; Y_m; t)$.

Lemma 3.4.8 (Restriction). [28, Lemma 4.8] We have

$$\begin{aligned} \mathcal{L}_{\lambda/\mu}^S(X_{n-1}, 0; Y_m; t) &= \mathcal{L}_{\lambda/\mu}^S(X_{n-1}; Y_m; t), \\ \mathcal{L}_{\lambda/\mu}^S(X_n; Y_{m-1}, 0; t) &= \mathcal{L}_{\lambda/\mu}^S(X_n; Y_{m-1}; t). \end{aligned}$$

Proof. Using Lemma 3.4.4, we can write

$$\mathcal{L}_{\lambda/\mu}^S(X_{n-1}, 0; Y_m; t) = \sum_{\alpha} \begin{array}{c} \lambda \\ \begin{array}{|c|c|c|} \hline 0 & \cdots & \\ \hline \end{array} \\ \alpha \\ \begin{array}{|c|c|c|} \hline 0 & \cdots & \\ \hline \end{array} \end{array} \begin{array}{c} \alpha \\ \begin{array}{|c|c|c|} \hline y_m & & \\ \hline \vdots & & \\ \hline y_1 & & \\ \hline \end{array} \\ \mu \\ \begin{array}{|c|c|c|} \hline x_{n-1} & & \\ \hline \vdots & & \\ \hline x_1 & & \\ \hline \end{array} \end{array}$$

It is easy to see that

$$\begin{array}{c} \lambda \\ \begin{array}{|c|c|c|} \hline 0 & \cdots & \\ \hline \end{array} \\ \alpha \end{array} = 1_{\lambda=\alpha}.$$

Therefore

$$\mathcal{L}_{\lambda/\mu}^S(X_{n-1}, 0; Y_m; t) = \begin{array}{c} \lambda \\ \begin{array}{|c|c|c|} \hline y_m & & \\ \hline \vdots & & \\ \hline y_1 & & \\ \hline \end{array} \\ \mu \\ \begin{array}{|c|c|c|} \hline x_{n-1} & & \\ \hline \vdots & & \\ \hline x_1 & & \\ \hline \end{array} \end{array} = \mathcal{L}_{\lambda/\mu}^S(X_{n-1}; Y_m; t) \quad (3.5)$$

A similar argument shows that

$$\mathcal{L}_{\lambda/\mu}^S(X_n; Y_{m-1}, 0; t) = \mathcal{L}_{\lambda/\mu}^S(X_n; Y_{m-1}; t).$$

Alternatively, we can deduce

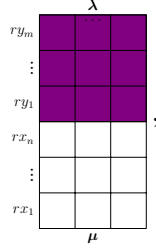
$$\begin{aligned} \mathcal{L}_{\lambda/\mu}^S(X_n; Y_{m-1}, 0; t) &= t^{g(\lambda)-g(\mu)} \mathcal{L}_{\lambda'/\mu'}^S(Y_{m-1}, 0; X_n; t^{-1}) && \text{(by Theorem 3.4.3)} \\ &= t^{g(\lambda)-g(\mu)} \mathcal{L}_{\lambda'/\mu'}^S(Y_{m-1}; X_n; t^{-1}) && \text{(by (3.5))} \\ &= t^{g(\lambda)-g(\mu)} (t^{-1})^{g(\lambda')-g(\mu')} \mathcal{L}_{\lambda/\mu}^S(X_n; Y_{m-1}; t) && \text{(by Theorem 3.4.3)} \\ &= \mathcal{L}_{\lambda/\mu}^S(X_n; Y_{m-1}; t). && \text{(by Cor. 3.4.2)} \end{aligned}$$

□

Lemma 3.4.9 ([28, Lemma 4.9]). *The polynomial $\mathcal{L}_{\lambda/\mu}^S(X_n; Y_m; t)$ is homogeneous in the X and Y variables of degree $|\lambda/\mu| = |\lambda| - |\mu|$ i.e.*

$$\mathcal{L}_{\lambda/\mu}^S(rX_n; rY_m; t) = r^{|\lambda/\mu|} \mathcal{L}_{\lambda/\mu}^S(X_n; Y_m; t).$$

Proof. This follows from the fact that, in any configuration of the lattice



the total number of right steps taken by the paths is $|\lambda/\mu|$. □

The factorization property

The goal of this subsection is to prove the following lemma.

Lemma 3.4.10 (Factorization). *[[28, Lemma 4.10]] Fix $\lambda \in P_p^{(k)}$. Suppose there exist τ and η such that*

$$\lambda^{(i)} = (m + \tau_1^{(i)}, \dots, m + \tau_n^{(i)}, \eta_1^{(i)}, \dots, \eta_s^{(i)})$$

for all i , where $s = p - n$. Then

$$\mathcal{L}_{\lambda}^S(X_n; Y_m; t) = \mathcal{L}_{\tau}^S(X_n; t) \cdot t^{g(\eta)} \mathcal{L}_{\eta'}^S(Y_m; t^{-1}) \cdot \prod_{l=0}^{k-1} \prod_{i=1}^n \prod_{j=1}^m (t^l x_i + y_j).$$

Throughout this subsection, let λ , τ , and η be as in the above lemma. Moreover, it is easy to see that the above lemma holds if $n = 0$ or $m = 0$, so we will assume $n, m \geq 1$ throughout the rest of this subsection. To prove the above lemma, we need two smaller lemmas.

Lemma 3.4.11 ([28, Lemma 4.11]). *Let λ , τ , and η be as in Lemma 3.4.10. Then the polynomial*

$$t^{g(\eta)} \mathcal{L}_{\eta'}(Y_m; t^{-1}) = \mathcal{L}_{\eta}^P(Y_m; t)$$

is a factor of the polynomial $\mathcal{L}_{\lambda}^S(X_n; Y_m; t)$. In fact,

$$\mathcal{L}_{\lambda}^S(X_n; Y_m; t) = \mathcal{L}_{\eta}^P(Y_m; t) \cdot \mathcal{L}_{m+\tau}^S(X_n; Y_m; t)$$

where $(m + \tau)_j^{(i)} = m + \tau_j^{(i)}$ for all i and j .

Lemma 3.4.12 ([28, Lemma 4.12]). *Let λ , τ , and η be as in Lemma 3.4.10. Then*

$$\mathcal{L}_{\lambda}^S(X_{n-1}, r; Y_{m-1}, -t^l r; t) = 0$$

for all $l \in \{0, \dots, k-1\}$.

Given these two lemmas, let us prove Lemma 3.4.10.

Proof of Lemma 3.4.10. Fix $l \in \{0, \dots, k-1\}$. Since

$$\mathcal{L}_{\lambda}^S(X_{n-1}, r; Y_{m-1}, -t^l r; t) = 0$$

by Lemma 3.4.12, we know $t^l x_n + y_m$ is a factor of $\mathcal{L}_{\lambda}^S(X_n; Y_m; t)$. Thus, since $\mathcal{L}_{\lambda}^S(X_n; Y_m; t)$ is symmetric in the X and Y variables separately by Lemma 3.4.4,

$$\prod_{i=1}^n \prod_{j=1}^m (t^l x_i + y_j)$$

is a factor of $\mathcal{L}_{\lambda}^S(X_n; Y_m; t)$. Since this holds for all $l \in \{0, \dots, k-1\}$,

$$\prod_{l=0}^{k-1} \prod_{i=1}^n \prod_{j=1}^m (t^l x_i + y_j)$$

is a factor of $\mathcal{L}_{\lambda}^S(X_n; Y_m; t)$. Moreover, since $t^{g(\eta)} \mathcal{L}_{\eta'}(Y_m; t^{-1})$ is a factor of $\mathcal{L}_{\lambda}^S(X_n; Y_m; t)$ by Lemma 3.4.11, we know

$$t^{g(\eta)} \mathcal{L}_{\eta'}(Y_m; t^{-1}) \cdot \prod_{l=0}^{k-1} \prod_{i=1}^n \prod_{j=1}^m (t^l x_i + y_j)$$

is a factor of $\mathcal{L}_\lambda^S(X_n; Y_m; t)$. Thus there is a polynomial $f(X_n; Y_m; t)$ such that

$$\mathcal{L}_\lambda^S(X_n; Y_m; t) = f(X_n; Y_m; t) \cdot t^{g(\eta)} \mathcal{L}_{\eta'}(Y_m; t^{-1}) \cdot \prod_{l=0}^{k-1} \prod_{i=1}^n \prod_{j=1}^m (t^l x_i + y_j). \quad (3.6)$$

It remains to show $f(X_n; Y_m; t) = \mathcal{L}_\tau(X_n; t)$.

Combining (3.6) with Lemma 3.4.11, we get

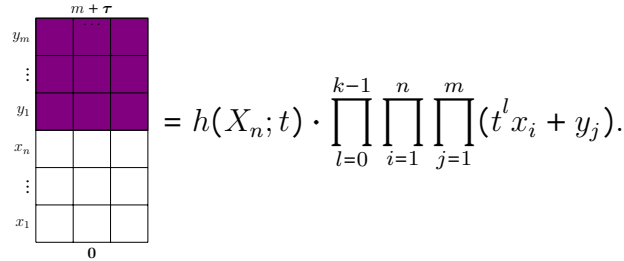
$$\mathcal{L}_{m+\tau}^S(X_n; Y_m; t) = f(X_n; Y_m; t) \cdot \prod_{l=0}^{k-1} \prod_{i=1}^n \prod_{j=1}^m (t^l x_i + y_j). \quad (3.7)$$

Given a polynomial $p(X_n; Y_m; t)$, let $\deg_Y(p(X_n; Y_m; t))$ be its total degree in the Y variables. Recall $\mathcal{L}_{m+\tau}^S(X_n; Y_m; t)$ is the partition function associated to the lattice $S_{n,m}(m+\tau)$ (Definition 3.3.2). In any configuration of this lattice, a given path can take at most one step right in a purple row. Thus, since there are m purple rows and since there are n paths of each of the k colors, we have

$$\deg_Y(\mathcal{L}_{m+\tau}^S(X_n; Y_m; t)) \leq mnk = \deg_Y\left(\prod_{l=0}^{k-1} \prod_{i=1}^n \prod_{j=1}^m (t^l x_i + y_j)\right).$$

This inequality along with (3.7) implies $f(X_n; Y_m; t) = h(X_n; t)$ for some polynomial $h(X_n; t)$. It remains to show $h(X_n; t) = \mathcal{L}_\tau(X_n; t)$.

We can rewrite (3.7) as



$$= h(X_n; t) \cdot \prod_{l=0}^{k-1} \prod_{i=1}^n \prod_{j=1}^m (t^l x_i + y_j).$$

We interpret both sides of the above equation as polynomials in the Y variables. On the right-hand side, the coefficient of $y_1^{nk} \dots y_m^{nk}$ is $h(X_n; t)$. A configuration of the lattice on the left-hand side has a weight of the form $p(X_n; t) \cdot y_1^{nk} \dots y_m^{nk}$ for some polynomial $p(X_n; t)$ if and only if each path of each color takes one right step in each

purple row. Thus the $y_1^{nk} \dots y_m^{nk}$ term on the left-hand side is exactly

$$\begin{aligned}
 & \begin{array}{c} m + \tau \\ \begin{array}{|c|c|c|c|c|c|c|} \hline y_m & & & & & & \\ \hline \vdots & & & & & & \\ \hline y_1 & & & & & & \\ \hline x_n & & & & & & \\ \hline \vdots & & & & & & \\ \hline x_1 & & & & & & \\ \hline \end{array} \\ \hline \mathbf{0} \end{array} = \begin{array}{c} \tau \\ \begin{array}{|c|c|c|c|} \hline x_n & \dots & & \\ \hline \vdots & & & \\ \hline x_1 & & & \\ \hline \end{array} \\ \hline \mathbf{0} \end{array} \cdot \begin{array}{c} m + \tau \\ \begin{array}{|c|c|c|c|c|c|c|} \hline y_m & & & & & & \\ \hline \vdots & & & & & & \\ \hline y_1 & & & & & & \\ \hline \end{array} \\ \hline \tau \end{array} \\
 & = \mathcal{L}_\tau(X_n; t) \cdot y_1^{nk} \dots y_m^{nk}.
 \end{aligned}$$

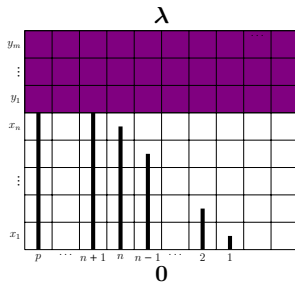
(Here, each path takes one right step in each purple row.) Thus $h(X_n; t) = \mathcal{L}_\tau(X_n; t)$. \square

We are left to prove Lemmas 3.4.11 and 3.4.12.

Proof of Lemma 3.4.11. Using Theorem 3.4.3 and the fact that $g(\mathbf{0}) = 0$, we have

$$\mathcal{L}_\eta^P(Y_m; t) = \mathcal{L}_\eta^S(; Y_m; t) = t^{g(\eta)} \mathcal{L}_{\eta'}^S(Y_m; ; t^{-1}) = t^{g(\eta)} \mathcal{L}_{\eta'}(Y_m; t^{-1}).$$

Recall $\mathcal{L}_\lambda^S(X_n; Y_m; t)$ is the partition function associated to the lattice $S_{n,m}(\lambda/\mu)$. Any configuration of this lattice must have the form



where we have labelled the columns for convenience. Consider the behavior of the paths starting in columns n and $n + 1$ in the j -th purple row for some $j \in [m]$. Note that a path can take at most one step right in a given purple row.

- Since $\lambda_n^{(i)} = m + \tau_n^{(i)} \geq m$ for all i , the paths starting in column n must exit the m -th purple row weakly right of column $n - m$, so they must exit the j -th purple row weakly right of column $n - j$.
- Since the paths starting in column $n + 1$ enter the first purple row in column $n + 1$, they must exit the j -th purple row weakly left of column $n + 1 - j$.

This argument shows that the remainder of the paths starting in columns $n + 1, \dots, p$ and the remainder of the paths starting in columns $1, \dots, n$ can be chosen independently of each other, and that the weight of the overall configuration is the weight of the configuration consisting of the paths starting in columns $n + 1, \dots, p$ times the weight of the configuration consisting of the paths starting in columns $1, \dots, n$. It follows that

$$\mathcal{L}_\lambda^S(X_n; Y_m; t) = \begin{array}{c} \lambda_{\{n+1, \dots, p\}} \\ \begin{array}{c} y_m \\ \vdots \\ y_1 \\ x_n \\ \vdots \\ x_1 \\ p \quad \dots \quad n+1 \quad n \quad n-1 \quad \dots \quad 2 \quad 1 \\ \mathbf{0} \end{array} \end{array} \cdot \begin{array}{c} \lambda_{\{1, \dots, n\}} \\ \begin{array}{c} y_m \\ \vdots \\ y_1 \\ x_n \\ \vdots \\ x_1 \\ p \quad \dots \quad n+1 \quad n \quad n-1 \quad \dots \quad 2 \quad 1 \\ \mathbf{0} \end{array} \end{array}$$

where, for a set $S = \{s_1 < \dots < s_j\} \subseteq \{1, \dots, p\}$, we define

$$\lambda_S = (\lambda_S^{(1)}, \dots, \lambda_S^{(k)}) \text{ with } \lambda_S^{(i)} = (\lambda_{s_1}^{(i)}, \dots, \lambda_{s_j}^{(i)}).$$

Since $\lambda_{\{n+1, \dots, p\}} = \eta$, the first factor is exactly

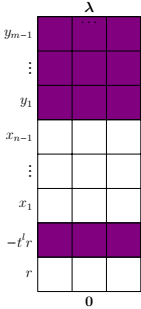
$$\begin{array}{c} \eta \\ \begin{array}{c} y_m \\ \vdots \\ y_1 \\ x_n \\ \vdots \\ x_1 \\ p \quad \dots \quad n+1 \quad n \quad n-1 \quad \dots \quad 2 \quad 1 \\ \mathbf{0} \end{array} \end{array} = \begin{array}{c} \eta \\ \begin{array}{c} y_m \\ \vdots \\ y_1 \\ \mathbf{0} \end{array} \end{array} = \mathcal{L}_\eta^P(Y_m; t).$$

Since $\lambda_{\{1, \dots, n\}} = m + \tau$, the second factor is exactly

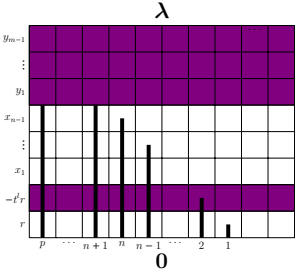
$$\begin{array}{c} m + \tau \\ \begin{array}{c} y_m \\ \vdots \\ y_1 \\ x_n \\ \vdots \\ x_1 \\ p \quad \dots \quad n+1 \quad n \quad n-1 \quad \dots \quad 2 \quad 1 \\ \mathbf{0} \end{array} \end{array} = \begin{array}{c} m + \tau \\ \begin{array}{c} y_m \\ \vdots \\ y_1 \\ x_n \\ \vdots \\ x_1 \\ \mathbf{0} \end{array} \end{array} = \mathcal{L}_{m+\tau}^S(X_n; Y_m; t).$$

□

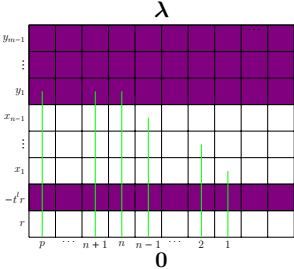
Proof of Lemma 3.4.12. By Lemma 3.4.4, $\mathcal{L}_\lambda^S(X_{n-1}, r; Y_{m-1}, -t^l r; t)$ is the partition function associated to the lattice



Any configuration of this lattice must have the form



where we have labelled the columns for convenience. In a configuration, if there exists a color i such that the path of color i starting in column 1 goes vertically in the bottom two rows, then color i must have the form



A path can take at most one step right in a given purple row, so the path of color i starting in column n can make at most $m - 1$ total steps right in the lattice. However, since $\lambda_n^{(i)} = m + \tau_n^{(i)} \geq m$, the path of color i starting in column n must make at least m total steps right in the lattice. This is a contradiction, which means that in any configuration, every path starting in column 1 must make at least one step right

somewhere in the bottom two rows. Therefore

$$\mathcal{L}_{\lambda/\mu}^S(X_{n-1}, r; Y_{m-1}, -t^l r; t) = \sum_{\alpha} -t^l r \begin{array}{c} \alpha \\ \begin{array}{|c|c|c|} \hline \color{purple} & \color{purple} & \color{purple} \\ \hline \color{white} & \color{white} & \color{white} \\ \hline \color{white} & \color{white} & \color{white} \\ \hline \color{white} & \color{white} & \color{white} \\ \hline \color{white} & \color{white} & \color{white} \\ \hline \color{white} & \color{white} & \color{white} \\ \hline \end{array} \\ 0 \end{array} \begin{array}{c} \lambda \\ \begin{array}{|c|c|c|} \hline \color{purple} & \color{purple} & \color{purple} \\ \hline \color{purple} & \color{purple} & \color{purple} \\ \hline \color{purple} & \color{purple} & \color{purple} \\ \hline \color{white} & \color{white} & \color{white} \\ \hline \color{white} & \color{white} & \color{white} \\ \hline \color{white} & \color{white} & \color{white} \\ \hline \color{white} & \color{white} & \color{white} \\ \hline \color{white} & \color{white} & \color{white} \\ \hline \end{array} \\ \alpha \end{array}$$

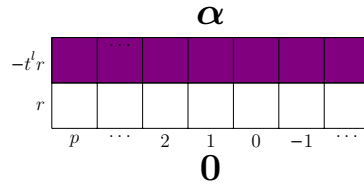
where the sum is over all α such that $\alpha_1^{(i)} > 0$ for all i . We will show that, for all such α , there is an involution φ_{α} on the set of configurations of the lattice

$$L_{\alpha} = \begin{array}{c} \alpha \\ \begin{array}{|c|c|c|} \hline \color{purple} & \color{purple} & \color{purple} \\ \hline \color{white} & \color{white} & \color{white} \\ \hline \color{white} & \color{white} & \color{white} \\ \hline \color{white} & \color{white} & \color{white} \\ \hline \color{white} & \color{white} & \color{white} \\ \hline \color{white} & \color{white} & \color{white} \\ \hline \end{array} \\ 0 \end{array}$$

such that $\text{weight}(\varphi_{\alpha}(C)) = -\text{weight}(C)$ for all C . Therefore

$$\mathcal{L}_{\lambda/\mu}^S(X_{n-1}, r; Y_{m-1}, -r; t) = 0.$$

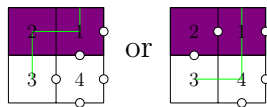
Fix α with $\alpha_1^{(i)} > 0$ for all i and fix a configuration C on the lattice L_{α} . We again label the columns for convenience as follows.



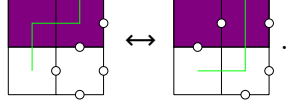
Given a color i , let c_i be the column in which the path of color i starting in column 1 exits the lattice through the top. Since every path starting in column 1 must make at least one step right, $c_i \leq 0$ for all i . We define an ordering $<$ on the colors by

$$i < j \Leftrightarrow c_i > c_j \text{ OR } c_i = c_j \text{ and } i < j.$$

Let i be the $(l + 1)$ -th largest color in this ordering (so that $l = \#\{j : i < j\}$). In columns $c_i + 1$ and c_i of C , color i has the form



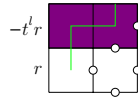
where we have labelled the boxes for convenience. We define $\varphi_\alpha(C)$ to be the result of flipping color i in columns $c_i + 1$ and c_i



Clearly φ_α is an involution. To show $\text{weight}(\varphi_\alpha(C)) = -\text{weight}(C)$, we must show

$$\text{weight} \left(\begin{array}{c} -t^l \\ \text{Diagram} \\ r \end{array} \right) = -\text{weight} \left(\begin{array}{c} -t^l \\ \text{Diagram} \\ r \end{array} \right) \quad (3.8)$$

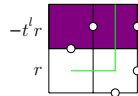
regardless of the paths taken by the other colors. Compared to the configuration with color i absent, the presence of color i in the form



contributes $-t^l r \cdot t^a$ to the overall weight, where

$$a = \#\{j > i : j \text{ is vertical in box 2}\} + \#\{j < i : j \text{ exits right in box 3}\}.$$

Compared to the configuration with color i in the form



contributes $r \cdot t^b$ to the overall weight, where

$$b = \#\{j > i : j \text{ appears in box 3}\} + \#\{j < i : j \text{ exits right in box 1}\} \\ + \#\{j < i : j \text{ exits right in box 3}\} + \#\{j < i : j \text{ exits right in box 4}\}.$$

It is easy to see that

$$b - a = \#\{j > i : j \text{ appears in box 3}\} - \#\{j > i : j \text{ is vertical in box 2}\} \\ + \#\{j < i : j \text{ exits right in box 1}\} + \#\{j < i : j \text{ exits right in box 4}\} \\ = \#\{j > i : c_i \geq c_j\} + \#\{j < i : c_i > c_j\} \\ = \#\{j : j > i\} \\ = l.$$

Therefore

$$\frac{\text{weight} \left(\begin{array}{c} \text{Diagram 1} \\ -t^l r \\ r \end{array} \right)}{\text{weight} \left(\begin{array}{c} \text{Diagram 2} \\ -t^l r \\ r \end{array} \right)} = \frac{-t^l r \cdot t^a}{r \cdot t^b} = -t^{l+a-b} = -1.$$

Thus (3.8) holds. \square

Swapping single rows

In this subsection, we prove an identity of the supersymmetric LLT polynomials in the case $\mu = \mathbf{0}$ and $p = 1$. As in Section 2.5, we can view λ as a (weak) composition λ , and for any composition $\nu = (\nu_1, \dots, \nu_k)$, we define

$$\text{Inv}(\nu) = \#\{a < b : \nu_a > \nu_b\}.$$

Taking $m = 0$ in the following proposition, we recover Prop. 2.5.5; in fact, these two propositions are proven in nearly identical ways.

Proposition 3.4.13 ([28, Prop. 4.13]). *Let $\lambda \in P_1^{(k)}$. If $\nu \in P_1^{(k)}$ is a rearrangement of λ , then*

$$\mathcal{L}_\lambda^S(X_n; Y_m; t) = t^{\text{Inv}(\lambda) - \text{Inv}(\nu)} \mathcal{L}_\nu^S(X_n; Y_m; t).$$

Proof. It is enough to show that, given $i \in [k-1]$,

$$\mathcal{L}_\lambda^S(X_n; Y_m; t) = t \cdot \mathcal{L}_\nu^S(X_n; Y_m; t)$$

where $\lambda_1 \geq \dots \geq \lambda_i > \lambda_{i+1} \geq \dots \geq \lambda_k$ and

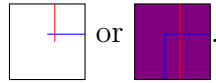
$$\nu_j = \begin{cases} \lambda_j & j \neq i, i+1 \\ \lambda_{i+1} & j = i \\ \lambda_i & j = i+1 \end{cases}.$$

We will let blue be color i and red be color $i+1$. We will now define a bijection

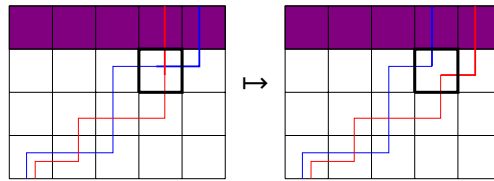
$$\rho : LC(S_{n,m}(\lambda)) \rightarrow LC(S_{n,m}(\nu)).$$

Fix a configuration $C \in S_{n,m}(\lambda)$. Since $\lambda_i > \lambda_{i+1}$, the column in which color i exits the lattice is strictly right of the column in which color $i+1$ exits the lattice. Therefore, since color i and color $i+1$ enter the lattice in the same column, C must

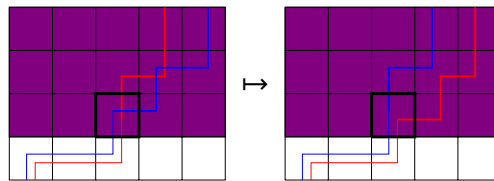
have a row in which color i enters weakly left and exits strictly right of color $i + 1$. Thus C must have a vertex of the form



Consider the NE-most vertex V of this form. Swap color i and color $i + 1$ in every vertex NE of V . For example:

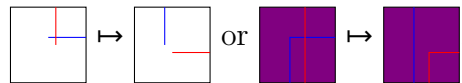


and



The result is a configuration $\rho(C) \in LC(S_{n,m}(\nu))$. It's clear that ρ is a bijection. We will now compare $\text{weight}(C)$ with $\text{weight}(\rho(C))$. There are four types of vertices to consider.

1. For the vertex V itself, the effect of applying ρ is



In either case, it is easy to see that the weight before applying ρ is t times the weight after applying ρ .

2. For any vertex not NE of V , ρ does not change the configuration, so the weight is not changed.
3. For any vertex NE of V in which either color i or color $i + 1$ is absent, ρ swaps color i and color $i + 1$, but the weight is not changed.
4. For any vertex NE of V in which both color i and color $i + 1$ are present, this vertex must have the form



Applying ρ swaps color i and color $i + 1$, resulting in



It is easy to see that the weight is not changed.

Therefore

$$\text{weight}(C) = t \cdot \text{weight}(\rho(C))$$

and the proposition follows. □

3.5 Relating \mathcal{L}^S to \mathcal{G}

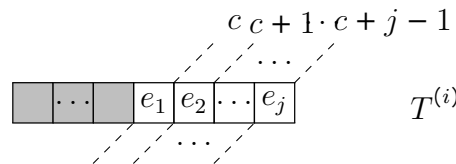
The goal of this section is to relate the partition function $\mathcal{L}_{\lambda/\mu}^S$ of Definition 3.3.2 to the super ribbon function $\mathcal{G}_{\lambda/\mu}^{(k)}$ of Definition 3.2.8. In [23] the authors construct a lattice model whose partition function is equal to the spin LLT polynomials. Lemma 3.5.6 below, which relates our vertex model to the spin LLT polynomial, can also be interpreted as a mapping between our vertex model and the one in [23] (see Remark 3.5.7).

Fix a positive integer k . Let λ/μ be the k -quotient of λ/μ . Let $\mathcal{A} = \{1 < 2 < \dots < n\}$ and $\mathcal{A}' = \{1' < 2' < \dots < m'\}$. We use the ordering $1 < 2 < \dots < n < 1' < 2' < \dots < m'$ on $\mathcal{A} \cup \mathcal{A}'$.

We begin by constructing a bijection

$$\text{SSSYT}(\lambda/\mu) \rightarrow LC(S_{n,m}(\lambda/\mu)).$$

We do this in the usual way in which each row of i -th tableaux maps to a path of color i . Precisely, given $\mathbf{T} = (T^{(1)}, \dots, T^{(k)}) \in \text{SSSYT}(\lambda/\mu)$, the corresponding $C \in LC(S_{n,m}(\lambda/\mu))$ is constructed as follows. Fix a row



in T . (Here we have labelled the diagonal content lines going through the row.) The corresponding path in C has color i , enters the lattice via the bottom of column c , exits the lattice via the top of column $c + j$, and crosses from column $c + l - 1$ to column $c + l$ at

$$\begin{cases} \text{the } a\text{-th white row} & \text{if } e_l = a \in \mathcal{A} \\ \text{the } a\text{-th purple row} & \text{if } e_l = a' \in \mathcal{A}' \end{cases}$$

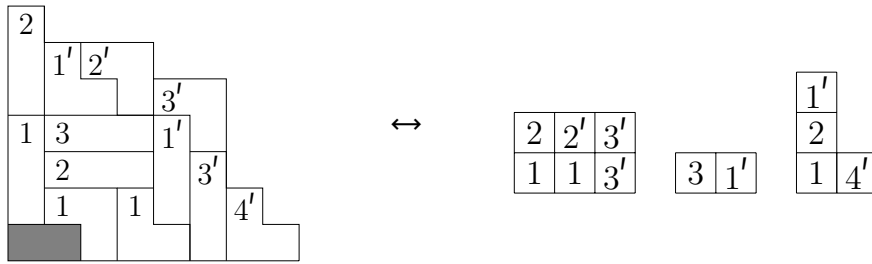
for each index $l \in [j]$. Recall that the Littlewood k -quotient map is a bijection

$$\text{SRT}_k(\lambda/\mu) \rightarrow \text{SSSYT}(\lambda/\mu).$$

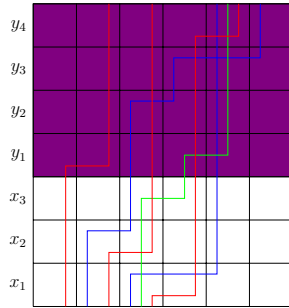
The composition of these two bijections gives a bijection

$$\theta : \text{SRT}_k(\lambda/\mu) \rightarrow LC(S_{n,m}(\lambda/\mu)).$$

Example 3.5.1. Let $n = 3$, $m = 4$, and $k = 3$. Recall Example 3.2.12.



The corresponding configuration is



where blue is color 1, green is color 2, and red is color 3.

Remark 3.5.2. The bijection $\text{SSSYT}(\lambda/\mu) \rightarrow LC(S_{n,m}(\lambda/\mu))$ becomes a bijection

$$\text{SSYT}(\lambda/\mu) \rightarrow LC(W_n(\lambda/\mu)).$$

when $m = 0$. This bijection was used in Chapter 2 to prove Theorem 2.3.3.

Remark 3.5.3. The bijection θ restricts to bijections

$$\text{HRS}_k(\lambda/\mu) \rightarrow LC(W_1(\lambda/\mu)), \quad \text{VRS}_k(\lambda/\mu) \rightarrow LC(P_1(\lambda/\mu))$$

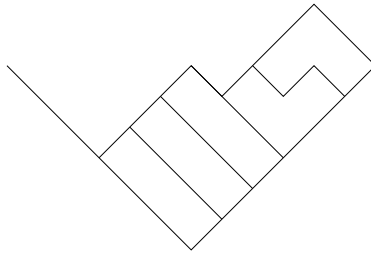
by labelling each ribbon in a horizontal (vertical) k -ribbon strip with a 1 (1^l).

For the rest of this section, we switch to drawing our Young diagrams in Russian convention, so rows are oriented SW-to-NE and columns are oriented SE-to-NW. The reason for this switch is to allow for an elegant graphical interpretation of θ . Let $T \in \text{SRT}_k(\lambda/\mu)$ and let $C = \theta(T) \in LC(S_{n,m}(\boldsymbol{\lambda}/\boldsymbol{\mu}))$. By the construction of θ , we note that

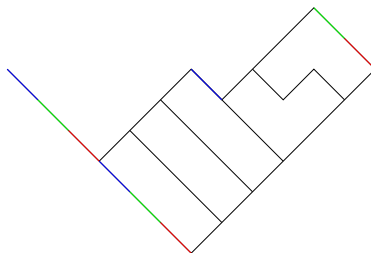
1. for each $i \in \mathcal{A}$, the horizontal ribbon strip $\lambda_{\leq i}/\lambda_{\leq i-1}$ of ribbons labelled i in T corresponds to the i -th white row in C ; and
2. for each $i' \in \mathcal{A}'$, the vertical ribbon strip $\lambda_{\leq i'}/\lambda_{\leq i'-1}$ of ribbons labelled i' in T corresponds to the i' -th purple row in C .

Given a horizontal (vertical) ribbon strip inside T , we “drop down” the Maya diagrams of the top and bottom boundaries to obtain the top and bottom boundaries of the corresponding white (purple) row in C . Moreover, the top and bottom boundaries of the row uniquely determine the path configuration of the row.

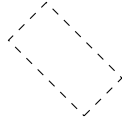
Example 3.5.4. Take $k = 3$. Let blue be color 1, green be color 2, and red be color 3. Consider the following horizontal 3-ribbon strip of shape $(6, 6, 3, 0, 0, 0)/(0, 0, 0, 0, 0, 0)$.



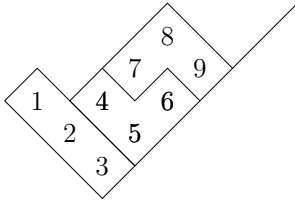
We now color the steps on the top and bottom boundaries, from left to right. A South-East step in position $i \pmod k$ gets color i . North-East steps are not colored.



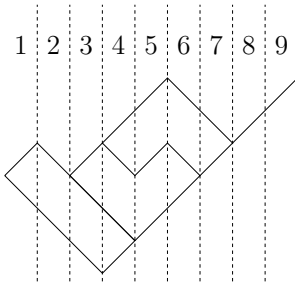
We now “drop down” the steps on the top and bottom boundaries of the horizontal 3-ribbon strip to obtain the top and bottom boundaries of the corresponding white row. The steps in positions $(j - 1)k + 1, \dots, (j - 1)k + k$ correspond to the j -th



(two cells in the same column and ribbon) can be placed in T . For example, if T is

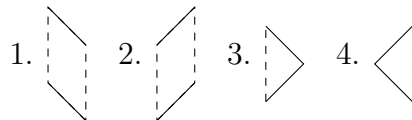


there are 4 such positions - cells 1 and 2, cells 2 and 3, cells 4 and 5, and cells 8 and 9 - and indeed the spin is 4. We can count these positions according to the “slice” containing the middle of each tile. In our example, the slices are given by



so slices 2, 3, 4, and 6 each contribute 1 to the spin and the other slices do not contribute to the spin. In each slice, there are only four shapes that can appear.

1. a column parallelogram (two adjacent halves of cells in the same column and ribbon)
2. a row parallelogram (two adjacent halves of cells in the same row and ribbon)
3. a head triangle (half of the head of a ribbon)
4. a tail triangle (half of the tail of a ribbon)



(Of course, a slice could also consist of a single SE step or a single NE step.) Any other shapes cannot appear in a slice, because if it did, the ribbon containing the shape would either contain a 2×2 square or not be a valid skew shape. It is clear that the contribution of a slice to the spin equals the number of column parallelograms in the slice.

In the following two lemmas, we use the above discussion to characterize the spin in terms of $\theta(T)$, when T is a horizontal/vertical ribbon strip.

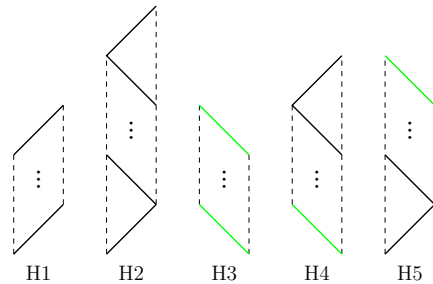
Lemma 3.5.6 ([28, Lemma 5.6]). *Let T be a horizontal k -ribbon strip. In the corresponding white row $\theta(T)$,*

$$\text{spin}(T) = \sum_{a < b} \left(\# \begin{array}{|c|} \hline \color{blue}{\rule{1cm}{0.4pt}} \\ \color{red}{\rule{1cm}{0.4pt}} \\ \hline \end{array} + \# \begin{array}{|c|} \hline \color{blue}{\rule{1cm}{0.4pt}} \\ \color{red}{\rule{1cm}{0.4pt}} \\ \hline \end{array} + \# \begin{array}{|c|} \hline \color{red}{\rule{1cm}{0.4pt}} \\ \color{blue}{\rule{1cm}{0.4pt}} \\ \hline \end{array} + \# \begin{array}{|c|} \hline \color{red}{\rule{1cm}{0.4pt}} \\ \color{blue}{\rule{1cm}{0.4pt}} \\ \hline \end{array} \right).$$

Proof. The fact that T is a horizontal ribbon strip restricts the possible forms of the slices.

1. If a head triangle appears, it must be at the bottom of the slice. This is because the head of a ribbon must touch the SE boundary.
2. If a tail triangle appears, it must be at the top of the slice. Suppose the tail triangle of ribbon R appears below a shape in ribbon S in slice i . Then, in all slices in which both R and S appear, S is above R . As every ribbon has length k , R appears in slices $i, \dots, i + k$ and S appears in slices $i - j, \dots, i - j + k$ for some $j \in \{0, \dots, k\}$. In particular, in slice $i - j + k$, the head triangle of S appears above R , which contradicts the first restriction.

With these restrictions in mind, one can show that each slice must have one of the following five forms:



Here \vdots indicates arbitrarily many (possibly 0) copies of the shape, and South-East steps on the top/bottom boundaries are colored as in our graphical interpretation of θ (see Example 3.5.4).

Remark 3.5.7. *The five types of slices we draw here are in bijection with the five types of allowed vertices given in [23, Figure 14]. To see this, suppose we are looking at a slice whose top and bottom boundaries correspond to color a . Then we can map it to a vertex of the form given in [23] by assigning arrows to the edges of the vertex according to the following rules:*

1. *If the top boundary of the slice is a NE (SE) step then the top edge of the vertex gets a down (up) arrow. Similarly for the bottom boundary of the slice.*
2. *If the slice contains a head triangle, assign a left arrow to the k -th eastern horizontal edge. If the slice contains a tail triangle, assign a left arrow to the 1st western horizontal edge.*
3. *If a ribbon whose head is in a slice of color b passes through the slice, then assign left arrows to the $(b + k - a \pmod k)$ -th eastern horizontal edge and the $((b + k - a \pmod k) + 1)$ -th western horizontal edge.*
4. *Otherwise assign right arrows to the horizontal edges.*

Assigning each slice a weight of $x^{\#\text{head triangles}}_t \# \text{col. parallelograms}$ makes this a weight-preserving bijection. Through the bijection θ defined above, the rest of this proof can be seen as giving a weight-preserving bijection between our vertex model and that of [23].

We claim that there is a one-to-one correspondence between the five possible forms of a slice in T and the five possible path configurations of the corresponding color in the corresponding white vertex in $\theta(T)$.



The correspondence is obvious for H3, H4, and H5 from the top/bottom boundary conditions. Moreover, from the top/bottom boundary conditions, slices of the form H1 or H2 correspond to path configurations of the form W1 or W2. To show the correspondence for H1 and H2, we will show that a slice of the form H2 always gives a configuration of the form W2 and vice versa.

- Suppose slice i has the form H2. It contains the head triangle of a ribbon, so slice $i - k$ will contain the tail triangle of this ribbon. This slice then must have the form H2 or H4. If slice $i - k$ has the form H2, then we can repeat this argument to show that slice $i - 2k$ has the form H2 or H4. Since there are finitely many ribbons, eventually we find that slice $i - jk$ has the form H4, for some positive integer j , and slices $i - (j - 1)k, \dots, i - k, i$ have the form

H2. Since slice $i - jk$ has the form H4, the corresponding path configuration has the form W4, in which the path exits right. Thus the path configuration corresponding to slice $i - (j - 1)k$ must have the path entering left, so it must have the form W2, in which the path exits right. Repeating, we conclude the path configuration corresponding to slice i has the form W2.

- Suppose slice i corresponds to a path configuration of the form W2. We know a path enters the slice from the left, so slice $i - k$ must correspond to a path configuration in which the path exits right. This path configuration then must have the form W2 or W4. If slice $i - k$ corresponds to a path configuration of the form W2, then we can repeat this argument to show that slice $i - 2k$ corresponds to a path configuration of the form W2 or W4. Since there are finitely many vertices, eventually we find that slice $i - jk$ corresponds to a path configuration of the form W4 and slices $i - (j - 1)k, \dots, i - k, i$ correspond to path configurations of the form W2, for some positive integer j . Since slice $i - jk$ corresponds to a path configuration of the form W4, it must have the form H4, so it contains the tail triangle of a ribbon. We see that slice $i - (j - 1)k$ contains the head triangle of this ribbon, so this slice has the form H2. It follows that slice $i - (j - 1)k$ also contains the tail triangle of a ribbon. Repeating, we conclude slice i has the form H2.

Recall that slice $i = (j - 1)k + a$ in T corresponds to color a in the j -th leftmost vertex V in $\theta(T)$. The contribution of this slice to $\text{spin}(T)$ equals the number of column parallelograms in the slice. Looking at the five possible forms of a slice, we see that this equals zero if slice i has the form H1, which is equivalent to color a being absent in V . Otherwise, it equals the number of ribbons R that appear in slice i but whose head/tail triangles do not.

Let R be such a ribbon, and let slice s be the slice that contains the tail triangle of R . Since slice i contains a column parallelogram of R but not the head/tail triangle of R , we have $s < i < s + k$. Let $b \in [k]$ be such that $b \equiv s \pmod{k}$, and note that $b \neq a$. If $b < a$, then the tail triangle of R appears in slice $(j - 1)k + b$, so slice $(j - 1)k + b$ has the form H2 or H4, so the path configuration of color b in V has the form W2 or W4, so color b exits V to the right. If $b > a$, then the head triangle of R appears in slice $(j - 1)k + b$, so slice $(j - 1)k + b$ has the form H2 or H5, so the path configuration of color b in V has the form W2 or W5, so color b enters V from the left.

We can now conclude

$$\begin{aligned} \text{spin}(T) &= \sum_V \sum_a \mathbf{1}_{a \text{ appears in } V} \cdot \left(\sum_{b < a} \mathbf{1}_{b \text{ exits } V \text{ to the right}} + \sum_{b > a} \mathbf{1}_{b \text{ enters } V \text{ from the left}} \right) \\ &= \sum_{a < b} \left(\# \begin{array}{|c|} \hline \text{---} \\ \hline \end{array} + \# \begin{array}{|c|} \hline \text{---} \\ \hline \end{array} \right) + \sum_{a < b} \left(\# \begin{array}{|c|} \hline \text{---} \\ \hline \end{array} + \# \begin{array}{|c|} \hline \text{---} \\ \hline \end{array} \right) \\ &= \sum_{a < b} \left(\# \begin{array}{|c|} \hline \text{---} \\ \hline \end{array} + \# \begin{array}{|c|} \hline \text{---} \\ \hline \end{array} + \# \begin{array}{|c|} \hline \text{---} \\ \hline \end{array} + \# \begin{array}{|c|} \hline \text{---} \\ \hline \end{array} \right). \end{aligned}$$

□

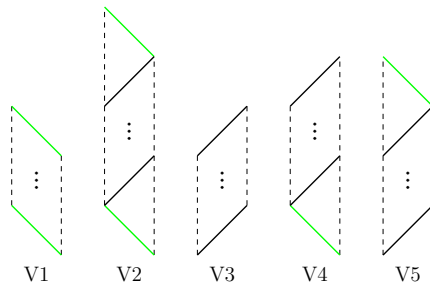
Lemma 3.5.8 ([28, Lemma 5.8]). *Let T be a vertical k -ribbon strip. In the corresponding purple row $\theta(T)$,*

$$\text{spin}(T) = \sum_{a < b} \left(\# \begin{array}{|c|} \hline \text{---} \\ \hline \end{array} + \# \begin{array}{|c|} \hline \text{---} \\ \hline \end{array} + \# \begin{array}{|c|} \hline \text{---} \\ \hline \end{array} + \# \begin{array}{|c|} \hline \text{---} \\ \hline \end{array} \right).$$

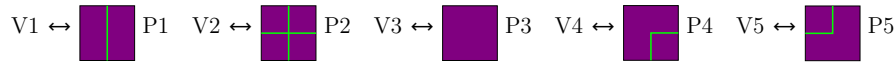
Proof. We follow the same ideas as in the proof of the previous lemma. The fact that T is a vertical ribbon strip restricts the possible forms of the slices.

1. If a tail triangle appears, it must be at the bottom of the slice. This is because the tail of a ribbon must touch the SW boundary.
2. If a head triangle appears, it must be at the top of the slice. Suppose the head triangle of ribbon R appears below a shape in ribbon S in slice i . Then, in all slices in which both R and S appear, S is above R . As every ribbon has length k , R appears in slices $i - k, \dots, i$ and S appears in slices $i - j, \dots, i - j + k$ for some $j \in \{0, \dots, k\}$. In particular, in slice $i - j$, the tail triangle of S appears above R , which contradicts the first restriction.

With these restrictions in mind, we see that each slice must have one of the following five forms:



We claim that there is a one-to-one correspondence between the five possible forms of a slice in T and the five possible path configurations of the corresponding color in the corresponding purple vertex in $\theta(T)$.



The correspondence is obvious for V3, V4, and V5 from the top/bottom boundary conditions. Moreover, from the top/bottom boundary conditions, slices of the form V1 or V2 correspond to path configurations of the form P1 or P2. To show the correspondence for V1 and V2, we will show that a slice of the form V2 always gives a configuration of the form P2 and vice versa.

- Suppose slice i has the form V2. It contains the tail triangle of a ribbon, so slice $i + k$ will contain the head triangle of this ribbon. This slice then must have the form V2 or V5. If slice $i + k$ has the form V2, then we can repeat this argument to show that slice $i + 2k$ has the form V2 or V5. Since there are finitely many ribbons, eventually we find that slice $i + jk$ has the form V5, for some positive integer j , and slices $i, i + k, \dots, i + (j - 1)k$ have the form V2. Since slice $i + jk$ has the form V5, the corresponding path configuration has the form P5, in which the path enters left. Thus the path configuration corresponding to slice $i + (j - 1)k$ must have the path exiting right, so it must have the form P2, in which the path exits right. Repeating, we conclude the path configuration corresponding to slice i has the form P2.
- Suppose slice i corresponds to a path configuration of the form P2. We know a path exits the slice to the right, so slice $i + k$ must correspond to a path configuration in which the path enters left. This path configuration then must have the form P2 or P5. If slice $i + k$ corresponds to a path configuration of the form P2, then we can repeat this argument to show that slice $i + 2k$ corresponds to a path configuration of the form P2 or P5. Since there are finitely many vertices, eventually we find that slice $i + jk$ corresponds to a path configuration of the form P5 and slices $i, i + k, \dots, i + (j - 1)k$ correspond to path configurations of the form P2, for some positive integer j . Since slice $i + jk$ corresponds to a path configuration of the form P5, it must have the form V5, so it contains the head triangle of a ribbon. We see that slice $i + (j - 1)k$ contains the tail triangle of this ribbon, so this slice has the form V2. It follows that slice $i + (j - 1)k$ also contains the head triangle of a ribbon. Repeating, we conclude slice i has the form V2.

Recall that slice $i = (j - 1)k + a$ in T corresponds to color a in the j -th leftmost vertex V in $\theta(T)$. The contribution of this slice to $\text{spin}(T)$ equals the number of column parallelograms in the slice. Looking at the five possible forms of a slice, we see that this equals zero unless slice i has the form V1, which is equivalent to the path configuration of color a having form P1 in V , that is, color a being vertical in V . In that case, the contribution to the spin equals the number of ribbons R that appear in slice i but whose head/tail triangles do not.

Let R be such a ribbon, and let slice s be the slice that contains the head triangle of R . Since slice i contains a column parallelogram of R but not the head/tail triangle of R , we have $s - k < i < s$. Let $b \in [k]$ be such that $b \equiv s \pmod k$, and note that $b \neq a$. If $b < a$, then the tail triangle of R appears in slice $(j - 1)k + b$, so slice $(j - 1)k + b$ has the form V2 or V4, so the path configuration of color b in V has the form P2 or P4, so color b exits V to the right. If $b > a$, then the head triangle of R appears in slice $(j - 1)k + b$, so slice $(j - 1)k + b$ has the form V2 or V5, so the path configuration of color b in V has the form P2 or P5, so color b enters V from the left.

From this we conclude

$$\begin{aligned} \text{spin}(T) &= \sum_V \sum_a \mathbf{1}_{a \text{ is vertical in } V} \cdot \left(\sum_{b < a} \mathbf{1}_{b \text{ exits } V \text{ to the right}} + \sum_{b > a} \mathbf{1}_{b \text{ enters } V \text{ from the left}} \right) \\ &= \sum_{a < b} \left(\# \begin{array}{|c|c|} \hline \color{red}{\downarrow} & \color{red}{\downarrow} \\ \hline \color{blue}{\leftarrow} & \color{blue}{\leftarrow} \\ \hline \end{array} + \# \begin{array}{|c|c|} \hline \color{red}{\downarrow} & \color{red}{\downarrow} \\ \hline \color{blue}{\leftarrow} & \color{blue}{\leftarrow} \\ \hline \end{array} \right) + \sum_{a < b} \left(\# \begin{array}{|c|c|} \hline \color{red}{\downarrow} & \color{red}{\downarrow} \\ \hline \color{blue}{\leftarrow} & \color{blue}{\leftarrow} \\ \hline \end{array} + \# \begin{array}{|c|c|} \hline \color{red}{\downarrow} & \color{red}{\downarrow} \\ \hline \color{blue}{\leftarrow} & \color{blue}{\leftarrow} \\ \hline \end{array} \right) \\ &= \sum_{a < b} \left(\# \begin{array}{|c|c|} \hline \color{red}{\downarrow} & \color{red}{\downarrow} \\ \hline \color{blue}{\leftarrow} & \color{blue}{\leftarrow} \\ \hline \end{array} + \# \begin{array}{|c|c|} \hline \color{red}{\downarrow} & \color{red}{\downarrow} \\ \hline \color{blue}{\leftarrow} & \color{blue}{\leftarrow} \\ \hline \end{array} + \# \begin{array}{|c|c|} \hline \color{red}{\downarrow} & \color{red}{\downarrow} \\ \hline \color{blue}{\leftarrow} & \color{blue}{\leftarrow} \\ \hline \end{array} + \# \begin{array}{|c|c|} \hline \color{red}{\downarrow} & \color{red}{\downarrow} \\ \hline \color{blue}{\leftarrow} & \color{blue}{\leftarrow} \\ \hline \end{array} \right). \end{aligned}$$

where V varies over the vertices in $\theta(T)$ and a and b vary over the colors. □

Using the previous two lemmas, we are now ready to relate $\mathcal{L}_{\lambda/\mu}^S$ to $\mathcal{G}_{\lambda/\mu}^{(k)}$.

Proposition 3.5.9 ([28, Prop. 5.9]). *Let λ/μ be the k -quotient of λ/μ . Then*

$$\mathcal{L}_{\lambda/\mu}^S(X_n; Y_m; t) = t^\square \mathcal{G}_{\lambda/\mu}^{(k)}(X_n; Y_m; t^{1/2})$$

for some half-integer $\square \in \frac{1}{2}\mathbb{Z}$. In fact, in any configuration of the lattice $S_{n,m}(\lambda/\mu)$,

$$\square = \frac{1}{2} \sum_{a < b} \left(\# \begin{array}{|c|c|} \hline \color{red}{\downarrow} & \color{red}{\downarrow} \\ \hline \color{blue}{\leftarrow} & \color{blue}{\leftarrow} \\ \hline \end{array} + \# \begin{array}{|c|c|} \hline \color{red}{\downarrow} & \color{red}{\downarrow} \\ \hline \color{blue}{\leftarrow} & \color{blue}{\leftarrow} \\ \hline \end{array} - \# \begin{array}{|c|c|} \hline \color{red}{\downarrow} & \color{red}{\downarrow} \\ \hline \color{blue}{\leftarrow} & \color{blue}{\leftarrow} \\ \hline \end{array} - \# \begin{array}{|c|c|} \hline \color{red}{\downarrow} & \color{red}{\downarrow} \\ \hline \color{blue}{\leftarrow} & \color{blue}{\leftarrow} \\ \hline \end{array} \right) + \frac{1}{2} \sum_{a < b} \left(\# \begin{array}{|c|c|} \hline \color{red}{\downarrow} & \color{red}{\downarrow} \\ \hline \color{blue}{\leftarrow} & \color{blue}{\leftarrow} \\ \hline \end{array} - \# \begin{array}{|c|c|} \hline \color{red}{\downarrow} & \color{red}{\downarrow} \\ \hline \color{blue}{\leftarrow} & \color{blue}{\leftarrow} \\ \hline \end{array} \right). \tag{3.9}$$

Proof. Recall the bijection $\theta : \text{SRT}_k(\lambda/\mu) \rightarrow LC(S_{n,m}(\boldsymbol{\lambda}/\boldsymbol{\mu}))$. It is enough to show

$$\text{weight}(\theta(T)) = t^\square t^{\frac{1}{2} \text{spin}(T)} x^{\text{weight}(T)} y^{\text{weight}'(T)}$$

for all $T \in \text{SRT}_k(\lambda/\mu)$, for some half-integer \square that does not depend on T . Fix a super ribbon tableau $T \in \text{SRT}_k(\lambda/\mu)$ and let $C = \theta(T) \in LC(S_{n,m}(\boldsymbol{\lambda}/\boldsymbol{\mu}))$ be the corresponding path configuration. It is clear that the X weights (Y weights) match, since each ribbon labelled $a \in \mathcal{A}$ ($a' \in \mathcal{A}'$) in T corresponds to a path taking a step right in the a -th white (purple) row of C . We are left to consider the powers of t . From the previous two lemmas, we see that

$$\begin{aligned} \text{spin}(T) &= \sum_{a < b} \left(\# \begin{array}{|c|} \hline \text{---} \\ \hline \text{---} \\ \hline \end{array} + \# \begin{array}{|c|} \hline \text{---} \\ \hline \text{---} \\ \hline \end{array} + \# \begin{array}{|c|} \hline \text{---} \\ \hline \text{---} \\ \hline \end{array} + \# \begin{array}{|c|} \hline \text{---} \\ \hline \text{---} \\ \hline \end{array} \right) \\ &+ \sum_{a < b} \left(\# \begin{array}{|c|} \hline \text{---} \\ \hline \text{---} \\ \hline \end{array} + \# \begin{array}{|c|} \hline \text{---} \\ \hline \text{---} \\ \hline \end{array} + \# \begin{array}{|c|} \hline \text{---} \\ \hline \text{---} \\ \hline \end{array} + \# \begin{array}{|c|} \hline \text{---} \\ \hline \text{---} \\ \hline \end{array} \right) \\ &= \sum_{a < b} \left(2 \cdot \# \begin{array}{|c|} \hline \text{---} \\ \hline \text{---} \\ \hline \end{array} + \# \begin{array}{|c|} \hline \text{---} \\ \hline \text{---} \\ \hline \end{array} + \# \begin{array}{|c|} \hline \text{---} \\ \hline \text{---} \\ \hline \end{array} \right) \\ &+ \sum_{a < b} \left(\# \begin{array}{|c|} \hline \text{---} \\ \hline \text{---} \\ \hline \end{array} + \# \begin{array}{|c|} \hline \text{---} \\ \hline \text{---} \\ \hline \end{array} + \# \begin{array}{|c|} \hline \text{---} \\ \hline \text{---} \\ \hline \end{array} + \# \begin{array}{|c|} \hline \text{---} \\ \hline \text{---} \\ \hline \end{array} \right) \\ &= 2 \text{coinv}(C) - \sum_{a < b} \left(\# \begin{array}{|c|} \hline \text{---} \\ \hline \text{---} \\ \hline \end{array} - \# \begin{array}{|c|} \hline \text{---} \\ \hline \text{---} \\ \hline \end{array} \right) \\ &+ 2 \text{coinv}'(C) - \sum_{a < b} \left(\# \begin{array}{|c|} \hline \text{---} \\ \hline \text{---} \\ \hline \end{array} + \# \begin{array}{|c|} \hline \text{---} \\ \hline \text{---} \\ \hline \end{array} - \# \begin{array}{|c|} \hline \text{---} \\ \hline \text{---} \\ \hline \end{array} - \# \begin{array}{|c|} \hline \text{---} \\ \hline \text{---} \\ \hline \end{array} \right) \end{aligned}$$

where

$$\text{coinv}(C) = \sum_{a < b} \left(\# \begin{array}{|c|} \hline \text{---} \\ \hline \text{---} \\ \hline \end{array} + \# \begin{array}{|c|} \hline \text{---} \\ \hline \text{---} \\ \hline \end{array} \right) \text{ and } \text{coinv}'(C) = \sum_{a < b} \left(\# \begin{array}{|c|} \hline \text{---} \\ \hline \text{---} \\ \hline \end{array} + \# \begin{array}{|c|} \hline \text{---} \\ \hline \text{---} \\ \hline \end{array} \right)$$

are the powers of t coming from the white and purple vertices in C , respectively. Thus

$$\frac{1}{2} \text{spin}(T) + \square = \text{coinv}(C) + \text{coinv}'(C)$$

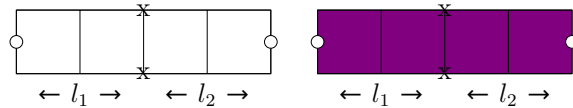
where \square is the quantity (3.9). A corner flipping argument shows that \square is independent of the configuration C , and the result follows. \square

3.6 Cauchy identity

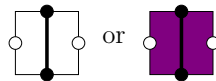
As was shown in Theorem 2.6.1, as well as in [1, 38, 22], the LLT polynomials satisfy a Cauchy identity. We would like to prove a similar theorem for the super-symmetric LLT polynomials. Just as we did to prove Theorem 2.6.1, we will proceed in the style of [53]. It will be useful to define $P_{l_1, l_2}^{(k)}$, for $0 \leq l_1, l_2 \leq \infty$, to be the set of k -tuples of partitions with l_1 parts whose largest part is less than or equal to l_2 .

Single rows

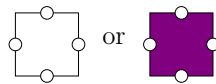
In order to construct our Cauchy identity, we will employ infinitely long rows of vertices. For the white and purple vertices, it is relatively easy to define a row of infinite length. We start by defining the following finite length rows, where the allowed states on the top and bottom boundaries are indexed by partitions $P_{l_1, l_2}^{(k)}$. Pictorially these are given by



Each row has length $l_1 + l_2$ and we explicitly mark the zero content line. We can increase l_1 by extending the partitions indexing the boundary states with zero parts; similarly we can increase l_2 by adding empty faces to the right. Note that increasing l_1 adds faces of the form



on the left, while increasing l_2 adds faces of the form

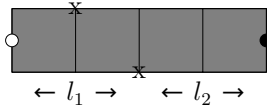


on the right; since these vertices have weight 1, increasing l_1 and l_2 does not change the weight of the row. In fact, we may take $l_1, l_2 \rightarrow \infty$ and allow the boundary states to be indexed by partitions with infinitely many parts as long as only finitely many parts are non-zero.

For the gray and pink vertices, we must be slightly more careful. Note that

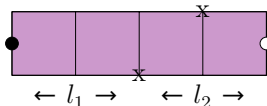
$$\begin{array}{c} \blacksquare \end{array} = x^k t^{\binom{k}{2}}, \quad \begin{array}{c} \blacksquare \\ \hline \blacksquare \end{array} = 1, \quad \begin{array}{c} \blacksquare \\ \hline \blacksquare \\ \hline \blacksquare \end{array} = 1, \quad \begin{array}{c} \blacksquare \\ \hline \blacksquare \\ \hline \blacksquare \\ \hline \blacksquare \end{array} = x^k.$$

For the gray faces, we consider a row of finite length, such that the allowed states on the bottom are indexed by partitions in $P_{l_1, l_2}^{(k)}$, and the allowed states on the top are indexed by partitions in $P_{l_1-1, l_2}^{(k)}$. We draw this as



The boundary condition on the right allows us to increase l_2 by adding faces where every path is horizontal without changing the weight of the row. However, increasing l_1 by adding zero parts to the partitions does affect the weight since faces where all the paths are vertical have a non-trivial contribution due to the change of variable.

For the pink faces, we consider a row of finite length, such that the allowed states on the bottom are indexed by partitions in $P_{l_1, l_2}^{(k)}$, and the allowed states on the top are indexed by partitions in $P_{l_1+1, l_2-1}^{(k)}$. We draw this as



In this case, we can increase l_1 by adding zero parts to the partitions without changing the weight of the row, as this amounts to adding faces on the left where every color is a cross. However, increasing l_2 by adding empty faces on the right does affect the weight. We will see later that the contribution to the weight coming from increasing l_1 in the case of the gray faces, and the contribution to the weight coming from increasing l_2 in the case of the pink faces, cancels out in the Cauchy identity, allowing us to circumvent this issue.

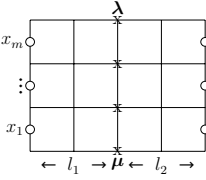
Remark 3.6.1. *Suppose the bottom boundary of a row is indexed by μ while the top boundary is indexed by λ . Recall from Section 1.3 that, for the white faces, in order for the row to have a non-zero weight, λ must be obtained from μ by adding a horizontal strip. Similarly, for the purple faces, λ must be obtained from μ by adding a vertical strip. For the gray faces, λ must be obtained from μ by removing a horizontal strip. For the pink faces, λ must be obtained from μ by removing a vertical strip.*

Some partition functions

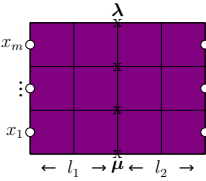
Here we will construct certain lattice models, using the single rows above, whose partition functions will be used in our Cauchy identities. In what follows, we will

always consider our partitions λ and μ to be k -tuples of partitions, each with a infinitely many parts, only finitely many of which are non-zero. We will truncate the partitions, removing only zero parts, to limit the number of parts as needed.

Given λ and μ , choose positive integers l_1, l_2 such that each partition has at most l_1 non-zero parts and largest part at most l_2 . Truncate λ and μ so that they are in $P_{l_1, l_2}^{(k)}$. Recall from Section 3.3 that for the white faces we have

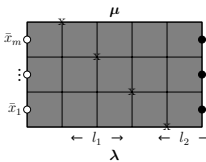
$$\mathcal{L}_{\lambda/\mu}(X_m; t) =$$


and for the purple faces we have

$$\mathcal{L}_{\lambda/\mu}^P(X_m; t) =$$


where both are independent of the choice of l_1 and l_2 . In particular, the limit as $l_1, l_2 \rightarrow \infty$ of these partition functions is well-defined.

For the gray faces, fix the number of variables m . This time, given λ and μ , choose positive integers l_1, l_2 such that each partition of λ has $\leq l_1$ non-zero parts, each partition of μ has $\leq l_1 - m$ non-zero parts, and each partition of both tuples has largest part $\leq l_2$. Truncate the partitions so that $\lambda \in P_{l_1, l_2}^{(k)}$ and $\mu \in P_{l_1 - m, l_2}^{(k)}$. Define

$$\mathcal{L}_{\lambda/\mu}^*(X_m; t) :=$$


We have the following proposition.

Proposition 3.6.2 ([28, Prop. 6.2]). *We have*

$$\mathcal{L}_{\lambda/\mu}^*(X_m; t) = (x_1 \dots x_m)^{(l_1 - m)k} (x^{\rho_m})^k t^{m(2l_1 - m - 1)} \binom{k}{2} t^{d(\lambda, \mu)} \mathcal{L}_{\lambda/\mu}(X_m; t)$$

where $d(\lambda, \mu)$ and $\mathcal{L}_{\lambda/\mu}$ are independent of l_1, l_2 . Furthermore, $d(\lambda, \mu)$ is given by

$$d(\lambda, \mu) = \sum_{a < b} \#\{i, j \mid \mu_j^{(a)} - j > \mu_i^{(b)} - i\} - \sum_{a < b} \#\{i, j \mid \lambda_j^{(a)} - j > \lambda_i^{(b)} - i\}.$$

The proof is essentially identical to that of Prop. 2.6.11, for which this is a slight generalization. (We can recover Prop. 2.6.11 by taking $\mu = \mathbf{0}$ and $l_1 = m = n$.) Note that \mathcal{L}^* is independent of l_2 and we may take $l_2 \rightarrow \infty$.

For the pink faces, again fix the number of variables m . Given λ and μ , choose positive integers l_1, l_2 such that the number of non-zero parts of each partition of both tuples is $\leq l_1$, the largest part of every partition in λ is $\leq l_2$, and the largest part of every partition in μ is $\leq l_2 - m$. Truncate the partitions so that $\lambda \in P_{l_1, l_2}^{(k)}$, and $\mu \in P_{l_1+m, l_2-m}^{(k)}$. Define

$$(\mathcal{L}^P)_{\lambda/\mu}^*(X_m; t) :=$$

We would like to be able to write $(\mathcal{L}^P)^*$ in terms of \mathcal{L}^P . In order to do so we will prove a series of lemmas. Recall the definition of the complement of a k -tuple of partitions from Definition 2.6.3 (and note the slight change in notation).

Lemma 3.6.3 ([28, Lemma 6.3]). *Fix $\lambda \in P_{l_1, l_2}^{(k)}$ and $\mu \in P_{l_1, l_2-m}^{(k)}$. Let $\tilde{\mu} \in P_{l_1, l_2}^{(k)}$ be the tuple of partitions one gets by adding m to every part of every partition in μ . Then*

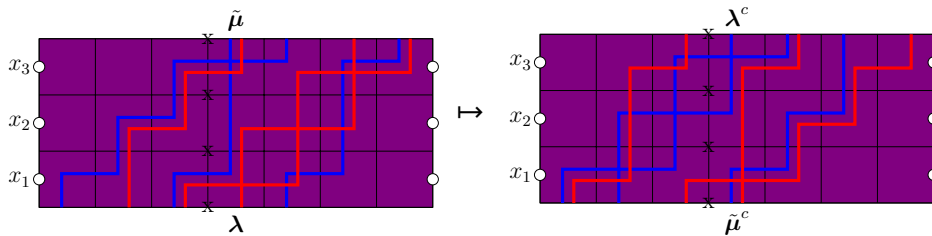
$$\mathcal{L}_{\tilde{\mu}/\lambda}^P(X_m; t) = t^{d_P(\lambda, \mu)} \mathcal{L}_{\lambda^c/\tilde{\mu}^c}^P(X_m; t)$$

where complements are taken in an $l_1 \times l_2$ box and $d_P(\lambda, \mu) = d(\lambda, \mu)$ is independent of l_1, l_2 .

Proof. There is a bijection between configurations with bottom boundary λ and top boundary $\tilde{\mu}$ and configurations with bottom boundary $\tilde{\mu}^c$ and top boundary λ^c , given by rotating 180 degrees and reversing the order of the colors. For example, with

$$\lambda = ((2, 1, 0), (1, 1, 1)), \mu = ((1, 0, 0), (1, 1, 0)), l_1 = m = 3, l_2 = 4$$

we have $\lambda^c = ((3, 3, 3), (4, 3, 2))$, $\tilde{\mu} = ((4, 3, 3), (4, 4, 3))$, $\tilde{\mu}^c = ((1, 0, 0), (1, 1, 0))$. For a particular configuration we would map



It is easy to show that under this bijection the x weight does not change, up to switching x_i and x_{m-i+1} , as horizontal steps in row i become horizontal steps in row $m - i + 1$. A corner flipping argument shows that the difference in the power of t before and after the mapping does not depend on the configuration (see for example the proof of Lemma 2.6.7). This shows that

$$\mathcal{L}_{\tilde{\mu}/\lambda}^P(X_m; t) = t^{d_P(\lambda, \mu)} \mathcal{L}_{\lambda^c/\tilde{\mu}^c}^P(x_m, \dots, x_1; t) = t^{d_P(\lambda, \mu)} \mathcal{L}_{\lambda^c/\tilde{\mu}^c}^P(X_m; t)$$

where the last equality uses the symmetry of \mathcal{L}^P . Note that increasing l_1 by adding zero parts to λ and parts of size m to $\tilde{\mu}$ does not change the power of t on either side of the bijection as this only adds paths that staircase (i.e. take one step right in each row). Similarly increasing l_2 by adding empty columns does not effect the power of t on either side. Thus $d_P(\lambda, \mu)$ is independent of l_1 and l_2 . As shown in the next lemma, $d_P(\lambda, \mu) = d(\lambda, \mu)$. \square

Lemma 3.6.4 ([28, Lemma 6.4]). *Let λ, μ be as in the previous lemma. Then*

$$d_P(\lambda, \mu) = \sum_{a < b} \#\{i, j | \mu_j^{(a)} - j > \mu_i^{(b)} - i\} - \sum_{a < b} \#\{i, j | \lambda_j^{(a)} - j > \lambda_i^{(b)} - i\}.$$

Proof. First let's assume that $\mu = \mathbf{0}$ and $k = 2$. In this case, every part in $\tilde{\mu}$ equals m . We can calculate $d_P(\lambda, \mu)$ using any choice of configuration. We will pick the configuration T of $\tilde{\mu}/\lambda$ such all the paths are as low as possible. In this case, each path will begin as a staircase going right until it reaches the column in which it ends, and will then travel vertically to its endpoint. Consider a single path of the first color (blue) corresponding to the j -th row of the skew shape. For it to contribute a power of t a path of the second color (red) must travel vertically in a face in which the blue path exits right. Suppose we have such a red path, corresponding to the i -th row. As a path travels vertically only in the column in which it ends, the blue path must end to the right of the red path, i.e. $j < i$. Further, in order for the red path to cross the blue path while traveling vertically its staircase must be weakly below the blue staircase, so the blue path must start weakly left of the red path, i.e. $\lambda_j^{(1)} - j \leq \lambda_i^{(2)} - i$. We see that

$$\text{coinv}'(T) = \#\{j < i | \lambda_j^{(1)} - j \leq \lambda_i^{(2)} - i\}$$

where $\text{coinv}'(T)$ is the power of t in the configuration T .

Using our mapping, the configuration T gets mapped to a configuration T' of $\lambda^c/\tilde{\mu}^c$ in which all the paths are as high as possible. In this case, the paths all begin travelling vertically and then staircase to their endpoint. Similar reasoning shows

that for the j -th blue path to exit right while the i -th red path is vertical, the blue path must begin weakly left of the red path, and the blue path must end to the right of red path. This gives

$$\begin{aligned} \text{coinv}'(T') &= \#\{j \geq i | (\lambda^c)_j^{(1)} - j > (\lambda^c)_i^{(2)} - i\} \\ &= \#\{j \geq i | \lambda_j^{(1)} - j > \lambda_i^{(2)} - i\}. \end{aligned}$$

From this we find

$$\begin{aligned} d_P(\boldsymbol{\lambda}, \mathbf{0}) &= \#\{j < i | \lambda_j^{(1)} - j \leq \lambda_i^{(2)} - i\} - \#\{j \geq i | \lambda_j^{(1)} - j > \lambda_i^{(2)} - i\} \\ &= \#\{j < i | \lambda_j^{(1)} - j \leq \lambda_i^{(2)} - i\} + \#\{j < i | \lambda_j^{(1)} - j > \lambda_i^{(2)} - i\} \\ &\quad - \#\{j < i | \lambda_j^{(1)} - j > \lambda_i^{(2)} - i\} - \#\{j \geq i | \lambda_j^{(1)} - j > \lambda_i^{(2)} - i\} \\ &= \#\{j < i\} - \#\{i, j | \lambda_j^{(1)} - j > \lambda_i^{(2)} - i\}. \end{aligned}$$

Noting that $\#\{i, j | \mu_j^{(1)} - j > \mu_i^{(2)} - i\} = \#\{j < i\}$ when $\boldsymbol{\mu} = \mathbf{0}$, we get the result in the case $\boldsymbol{\mu} = \mathbf{0}$ and $k = 2$. Summing over all pairs of colors $a < b$ gives the result in the case $\boldsymbol{\mu} = \mathbf{0}$ and k general.

To prove the general case, let $\boldsymbol{\lambda}$ and $\boldsymbol{\mu}$ be as in the statement of the lemma. Consider a lattice with $n + m$ rows. Let $\boldsymbol{\nu} = \mathbf{0}$, so that every part of $\tilde{\boldsymbol{\nu}}$ equals $n + m$. From the above calculation we know that

$$d_P(\boldsymbol{\lambda}, \mathbf{0}) = \sum_{a < b} \#\{j < i\} - \sum_{a < b} \#\{i, j | \lambda_j^{(a)} - j > \lambda_i^{(b)} - i\}.$$

This can be calculated using any configuration of $\boldsymbol{\lambda}/\tilde{\boldsymbol{\nu}}$. Let us choose a configuration such that the top boundary of the m -th row is given by $\tilde{\boldsymbol{\mu}}$. Then the contribution to the change in power of t from the rows above the m -th row is given by

$$d_P(\tilde{\boldsymbol{\mu}}, \mathbf{0}) = \sum_{a < b} \#\{j < i\} - \sum_{a < b} \#\{i, j | \tilde{\mu}_j^{(a)} - j > \tilde{\mu}_i^{(b)} - i\}$$

while the contribution from the m -th row and below is given by $d_P(\boldsymbol{\lambda}, \boldsymbol{\mu})$. Since the contribution from the two pieces must equal the overall change in power of t , we see that

$$\begin{aligned} d_P(\boldsymbol{\lambda}, \boldsymbol{\mu}) &= d_P(\boldsymbol{\lambda}, \mathbf{0}) - d_P(\tilde{\boldsymbol{\mu}}, \mathbf{0}) \\ &= \sum_{a < b} \#\{i, j | \tilde{\mu}_j^{(a)} - j > \tilde{\mu}_i^{(b)} - i\} - \sum_{a < b} \#\{i, j | \lambda_j^{(a)} - j > \lambda_i^{(b)} - i\} \\ &= \sum_{a < b} \#\{i, j | \mu_j^{(a)} - j > \mu_i^{(b)} - i\} - \sum_{a < b} \#\{i, j | \lambda_j^{(a)} - j > \lambda_i^{(b)} - i\} \end{aligned}$$

as desired. \square

Lemma 3.6.5 ([28, Lemma 6.5]). *Let $\lambda, \mu, m, l_1, l_2$ be as in the Lemma 3.6.3. Then*

$$= (x_1 \dots x_m)^{k(l_1+l_2)} t^{d_P(\lambda, \mu)} \mathcal{L}_{\lambda^c / \tilde{\mu}^c}^P(X_m^{-1}; t).$$

Proof. We start with Lemma 3.6.3. To change from purple faces to pink faces, for each $i \in [m]$, we take $x_i \mapsto \frac{1}{x_i}$ and multiply every face in the i -th row by x_i^k . This gives the desired equation. \square

Lemma 3.6.6 ([28, Lemma 6.6]). *Let $\lambda, \mu, m, l_1, l_2$ be as in the previous lemma, except now consider μ as an element of $P_{l_1+m, l_2}^{(k)}$ (i.e. add m more parts equal to 0). Then*

$$= (x_1 \dots x_m)^{k(l_1+l_2+1)} t^{d_P(\lambda, \mu)} \mathcal{L}_{\lambda^c / \tilde{\mu}^c}^P(X_m^{-1}; t).$$

Proof. Starting with the lattice in the previous lemma, we add a path of each color on the left edge of each row. The paths entering from the left must end packed to the left at the top. This, along with the shift right by m of the zero content line, means that the top boundary is now given by μ . Adding the paths entering from the left changes the weight by the factor $(x_1 \dots x_m)^k$. \square

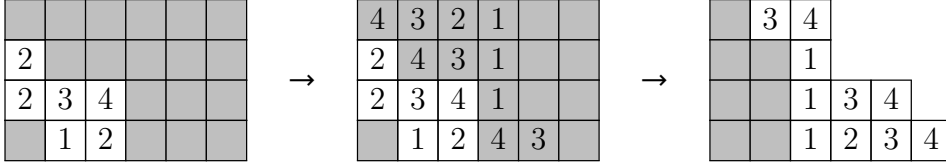
Finally we must relate the LLT polynomial of a skew partition with that of its complement.

Lemma 3.6.7 ([28, Lemma 6.7]). *Let $\lambda \in P_{l_1, l_2}^{(k)}$ and $\mu \in P_{l_1, l_2-m}^{(k)}$. Let $\tilde{\mu} \in P_{l_1, l_2}^{(k)}$ be the tuple of partitions one gets by adding m to every part of every partition in μ . We have*

$$\mathcal{L}_{\lambda/\mu}^P(X_m; t) = (x_1 \dots x_m)^{kl_1} \mathcal{L}_{\lambda^c / \tilde{\mu}^c}^P(X_m^{-1}; t).$$

Proof. We construct a bijection $\text{SSYT}(\lambda/\mu) \rightarrow \text{SSYT}(\lambda^c / \tilde{\mu}^c)$ as follows. For each skew partition in λ/μ , draw it inside an $l_1 \times l_2$ box. Given any SSYT of the skew shape, go from left to right, row-by-row, and fill the cells of the box with the largest available integer not already used in that row. After rotating 180 degrees the newly filled cells of the box are a SSYT of the corresponding skew partition in $\lambda^c / \tilde{\mu}^c$.

For example, let $\lambda = (3, 3, 1, 0)$, $\mu = (1, 0, 0, 0)$, $l_1 = m = 4$, $l_2 = 6$. Then we have $\lambda^c = (6, 5, 3, 3)$ and $\tilde{\mu}^c = (2, 2, 2, 1)$. Consider the filling below.



Note that under this map the x weights transform as $x^T \mapsto (x_1 \dots x_m)^{kl_1} (x^T)^{-1}$. We are left to determine what happens to the powers of t . It is easy to check that, in terms of lattice paths, flipping a corner of color a up (down) on one side of the bijection corresponds to flipping a corner of color $k - a + 1$ down (up) on the other side. As the space of configurations on both sides is connected under corner flips, a corner flipping argument (see Lemma 2.6.8) shows the difference in the powers of t does not depend on the configuration. Thus there is some overall power of t difference, call it $\tilde{d}_P(\boldsymbol{\lambda}, \boldsymbol{\mu})$, so that

$$\mathcal{L}_{\boldsymbol{\lambda}/\boldsymbol{\mu}}^P(X_m; t) = (x_1 \dots x_m)^{kl_1} t^{\tilde{d}_P(\boldsymbol{\lambda}, \boldsymbol{\mu})} \mathcal{L}_{\boldsymbol{\lambda}^c/\tilde{\boldsymbol{\mu}}^c}^P(X_m^{-1}; t).$$

We need only to compute the difference in the power of t for a specific choice of configurations to compute $\tilde{d}_P(\boldsymbol{\lambda}, \boldsymbol{\mu})$. A similar argument to the one used in the proof of Lemma 3.6.4 shows $\tilde{d}_P(\boldsymbol{\lambda}, \boldsymbol{\mu}) = 0$. \square

Combining all the above lemmas gives the following proposition.

Proposition 3.6.8 ([28, Prop. 6.8]). *We have*

$$(\mathcal{L}_{\boldsymbol{\lambda}/\boldsymbol{\mu}}^P)^*(X_m; t) = (x_1 \dots x_m)^{k(l_2+1)} t^{d_P(\boldsymbol{\lambda}, \boldsymbol{\mu})} \mathcal{L}_{\boldsymbol{\lambda}/\boldsymbol{\mu}}^P(X_m; t)$$

where the whole thing is independent of l_1 , and $d_P(\boldsymbol{\lambda}, \boldsymbol{\mu})$ and $\mathcal{L}_{\boldsymbol{\lambda}/\boldsymbol{\mu}}^P$ are also independent of l_2 .

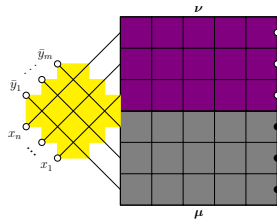
Cauchy identities

Using the above we will now prove several Cauchy identities for the \mathcal{L} and \mathcal{L}^P .

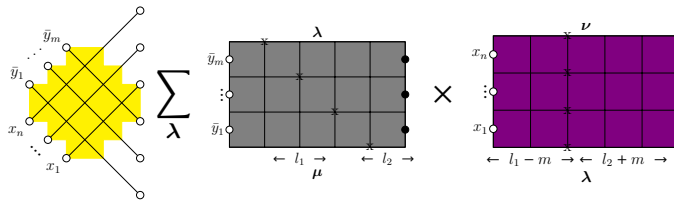
Proposition 3.6.9 ([28, Prop. 6.9]). *Let $\boldsymbol{\mu}$ and $\boldsymbol{\nu}$ be tuples of partitions each with infinitely many parts only finitely many of which are non-zero. Then*

$$\sum_{\boldsymbol{\lambda}} t^{d(\boldsymbol{\mu}, \boldsymbol{\lambda})} \mathcal{L}_{\boldsymbol{\mu}/\boldsymbol{\lambda}}(Y_m; t) \mathcal{L}_{\boldsymbol{\nu}/\boldsymbol{\lambda}}^P(X_n; t) = \left(\prod_{i,j} \prod_{l=0}^{k-1} (1 + x_i y_j t^l)^{-1} \right) \sum_{\boldsymbol{\lambda}} t^{d(\boldsymbol{\lambda}, \boldsymbol{\nu})} \mathcal{L}_{\boldsymbol{\lambda}/\boldsymbol{\mu}}^P(X_n; t) \mathcal{L}_{\boldsymbol{\lambda}/\boldsymbol{\nu}}(Y_m; t)$$

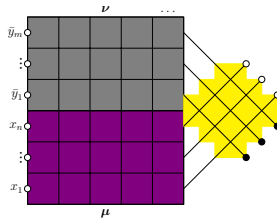
Proof. Given μ and ν , choose positive integer l_1 and l_2 such that maximum number of non-zero parts of a partition in ν is less than $l_1 - m$ and the largest part of any partition in ν is less than $l_2 + m$. Note this ensures that l_1 is greater than the maximum number of non-zero parts of a partition in μ and that l_2 is greater than the largest part of any partition in μ . Truncate the partitions so that $\mu \in P_{l_1, l_2}^{(k)}$ and $\nu \in P_{l_1 - m, l_2 + m}^{(k)}$. Consider the following partition function.



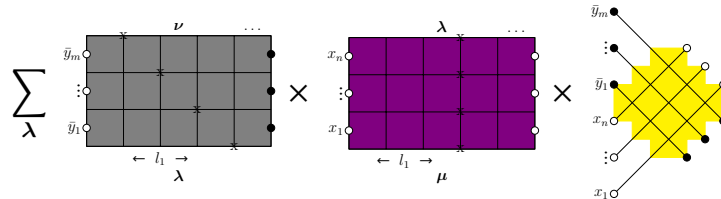
This can be split into three pieces as follows.



From the previous subsection, in particular Prop. 3.6.2, every piece is independent of l_2 , so we may take $l_2 \rightarrow \infty$. Here the crosses have weight one. Using the YBE to move the crosses to the other side gives



Since we have taken $l_2 \rightarrow \infty$ and paths cannot travel horizontally across a purple face, we know that the paths originating from the bottom boundary must exit from the gray faces at the right boundary. Splitting this into parts, we get



Equating the two sums gives

$$\sum_{\lambda} \mathcal{L}_{\mu/\lambda}^*(Y_m; t) \mathcal{L}_{\nu/\lambda}^P(X_n; t) = \left(\prod_{i,j} \prod_{l=0}^{k-1} (1 + x_i y_j t^l)^{-1} \right) \sum_{\lambda} \mathcal{L}_{\lambda/\mu}^P(X_n; t) \mathcal{L}_{\lambda/\nu}^*(Y_m; t).$$

where the prefactor on the RHS comes from the crosses. Using Prop. 3.6.2, we get

$$\begin{aligned} & \sum_{\lambda} (y)^{(l_1-m)k} (y^{\rho_m})^k t^{(ml_1 - \binom{m+1}{2}) \binom{k}{2}} t^{d(\mu, \lambda)} \mathcal{L}_{\mu/\lambda}(Y_m; t) \mathcal{L}_{\nu/\lambda}^P(X_n; t) \\ &= \left(\prod_{i,j} \prod_{l=0}^{k-1} (1 + x_i y_j t^l)^{-1} \right) \sum_{\lambda} (y)^{(l_1-m)k} (y^{\rho_m})^k t^{(ml_1 - \binom{m+1}{2}) \binom{k}{2}} t^{d(\lambda, \nu)} \mathcal{L}_{\lambda/\mu}^P(X_n; t) \mathcal{L}_{\lambda/\nu}(Y_m; t). \end{aligned}$$

Many terms (in particular all the terms involving l_1) cancel, and we can then take $l_1 \rightarrow \infty$, giving the proposition. \square

An analogous proof, using white boxes in place of purple boxes and white crosses in place of yellow crosses, gives the following proposition.

Proposition 3.6.10 ([28, Prop. 6.10]). *Let μ and ν be tuples of partitions each with infinitely many parts only finitely many of which are non-zero. Then*

$$\sum_{\lambda} t^{d(\mu, \lambda)} \mathcal{L}_{\nu/\lambda}(X_n; t) \mathcal{L}_{\mu/\lambda}(Y_m; t) = \prod_{i,j} \prod_{l=0}^{k-1} (1 - x_i y_j t^l) \sum_{\lambda} t^{d(\lambda, \nu)} \mathcal{L}_{\lambda/\mu}(X_n; t) \mathcal{L}_{\lambda/\nu}(Y_m; t).$$

This is a slight generalization of Prop. 2.6.12 (which we can recover by taking $\nu = \mathbf{0}$, setting $m = n$, and swapping X and Y).

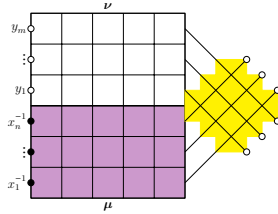
Using the white faces and the pink faces, we have the following.

Proposition 3.6.11 ([28, Prop. 6.11]). *Let μ and ν be tuples of partitions each with infinitely many parts only finitely many of which are non-zero. Then*

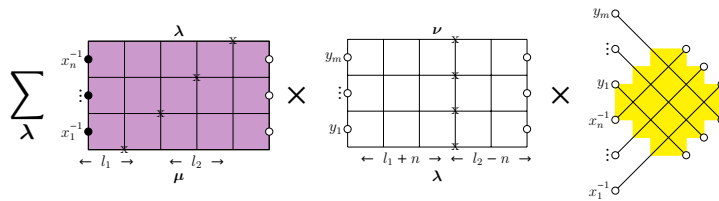
$$\left(\prod_{i,j} \prod_{l=0}^{k-1} (1 + x_i y_j t^l)^{-1} \right) \sum_{\lambda} t^{d_P(\lambda, \nu)} \mathcal{L}_{\lambda/\mu}(Y_m; t) \mathcal{L}_{\lambda/\nu}^P(X_n; t) = \sum_{\lambda} t^{d_P(\mu, \lambda)} \mathcal{L}_{\mu/\lambda}^P(X_n; t) \mathcal{L}_{\nu/\lambda}(Y_m; t).$$

Proof. Given μ and ν , choose positive integers l_1, l_2 such that l_1 is greater than or equal to the number of non-zero parts in μ and ν , l_2 is greater than or equal to the largest part in μ , and $l_2 - n$ is greater than or equal to the largest part in ν .

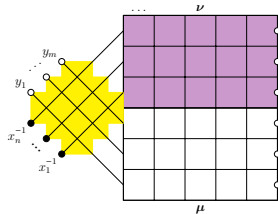
Consider the following partition function.



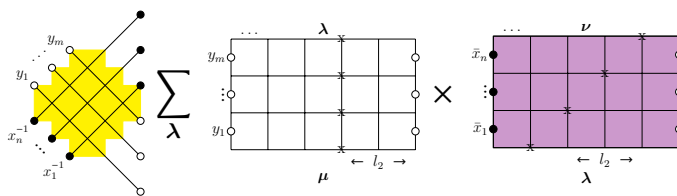
This can be split as



From the previous subsection, in particular Prop. 3.6.8, every piece is independent of l_1 , so we may take $l_1 \rightarrow \infty$. We can use the YBE to move the crosses to the other side to get



which we split into



(Sufficiently far to the left in the white faces every column is dense with vertical paths, so the paths from the cross must enter in the pink faces.) Setting this equal to the other sum gives

$$\left(\prod_{i,j} \prod_{l=0}^{k-1} (1 + x_i y_j t^l)^{-1} \right) \sum_{\lambda} \mathcal{L}_{\lambda/\mu}(Y_m; t) (\mathcal{L}^P)_{\lambda/\nu}^*(X_n; t) = \sum_{\lambda} (\mathcal{L}^P)_{\mu/\lambda}^*(X_n; t) \mathcal{L}_{\nu/\lambda}(Y_m; t)$$

where the prefactor on the LHS comes from the crosses. Using Prop. 3.6.8 we have

$$\begin{aligned} & \left(\prod_{i,j} \prod_{l=0}^{k-1} (1 + x_i y_j t^l)^{-1} \right) \sum_{\lambda} (x_1 \dots x_n)^{k(l_2+1)} t^{d_P(\lambda, \nu)} \mathcal{L}_{\lambda/\mu}(Y_m; t) \mathcal{L}_{\lambda/\nu}^P(X_n; t) \\ & = \sum_{\lambda} (x_1 \dots x_n)^{k(l_2+1)} t^{d_P(\mu, \lambda)} \mathcal{L}_{\mu/\lambda}^P(X_n; t) \mathcal{L}_{\nu/\lambda}(Y_m; t). \end{aligned}$$

Canceling the terms involving l_2 gives the proposition. \square

Changing the white faces to purple faces, a similar computation to the above gives

Proposition 3.6.12 ([28, Lemma 6.12]). *Let μ and ν be tuples of partitions each with infinitely many parts only finitely many of which are non-zero. Then*

$$\left(\prod_{i,j} \prod_{l=0}^{k-1} (1 - x_i y_j t^l) \right) \sum_{\lambda} t^{d_P(\lambda, \nu)} \mathcal{L}_{\lambda/\mu}^P(Y_m; t) \mathcal{L}_{\lambda/\nu}^P(X_n; t) = \sum_{\lambda} t^{d_P(\mu, \lambda)} \mathcal{L}_{\mu/\lambda}^P(X_n; t) \mathcal{L}_{\nu/\lambda}^P(Y_m; t).$$

(One must be careful to only consider terms with finite degree in y ; this forces the paths to only travel from the SW to the SE on the cross.)

Combining these identities, we now come to the main result of this section: a Cauchy identity for the supersymmetric LLT polynomials.

Theorem 3.6.13 ([28, Thm. 6.13]). *Let μ and ν be tuples of partitions each with infinitely many parts only finitely many of which are non-zero. Fix positive integers n, m, p, q . Then*

$$\begin{aligned} & \sum_{\lambda} t^{d(\mu, \lambda)} \mathcal{L}_{\nu/\lambda}^S(X_n, Y_m; t) \mathcal{L}_{\mu/\lambda}^S(W_p, Z_q; t) \\ & = \prod_{l=0}^{k-1} \prod_{i,i'=1}^n \prod_{j,j'=1}^m \prod_{\alpha, \alpha'=1}^p \prod_{\beta, \beta'=1}^q \frac{(1 - x_i w_{\alpha} t^l)(1 - y_{j'} z_{\beta'} t^l)}{(1 + y_j w_{\alpha'} t^l)(1 + x_{i'} z_{\beta} t^l)} \sum_{\lambda} t^{d(\lambda, \nu)} \mathcal{L}_{\lambda/\mu}^S(X_n, Y_m; t) \mathcal{L}_{\lambda/\nu}^S(W_p, Z_q; t) \end{aligned} \tag{3.10}$$

Proof. We can rewrite the LHS as

$$LHS = \sum_{\lambda, \sigma, \rho} \mathcal{L}_{\nu/\rho}^P(Y_m; t) \mathcal{L}_{\rho/\lambda}(X_n; t) t^{d_P(\mu, \sigma)} \mathcal{L}_{\mu/\sigma}^P(Z_q; t) t^{d(\sigma, \lambda)} \mathcal{L}_{\sigma/\lambda}(W_p; t)$$

where we use the fact that

$$d(\mu, \lambda) = d_P(\mu, \sigma) + d(\sigma, \lambda).$$

Applying Prop. 3.6.10 on the sum over λ with the second and fourth LLTs gives

$$\begin{aligned} LHS &= \prod_{l=0}^{k-1} \prod_{i=1}^n \prod_{\alpha=1}^p (1 - x_i w_\alpha t^l) \\ &\quad \times \sum_{\lambda, \sigma, \rho} \mathcal{L}_{\nu/\rho}^P(Y_m; t) \mathcal{L}_{\lambda/\sigma}(X_n; t) t^{d_P(\mu, \sigma)} \mathcal{L}_{\mu/\sigma}^P(Z_q; t) t^{d(\lambda, \rho)} \mathcal{L}_{\lambda/\rho}(W_p; t). \end{aligned}$$

Applying Prop. 3.6.9 on the sum over ρ with the first and fourth LLTs gives

$$\begin{aligned} LHS &= \prod_{l=0}^{k-1} \prod_{i=1}^n \prod_{j=1}^m \prod_{\alpha, \alpha'=1}^p \frac{1 - x_i w_\alpha t^l}{1 + y_j w_{\alpha'} t^l} \\ &\quad \times \sum_{\lambda, \sigma, \rho} \mathcal{L}_{\rho/\lambda}^P(Y_m; t) \mathcal{L}_{\lambda/\sigma}(X_n; t) t^{d_P(\mu, \sigma)} \mathcal{L}_{\mu/\sigma}^P(Z_q; t) t^{d(\rho, \nu)} \mathcal{L}_{\rho/\nu}(W_p; t). \end{aligned}$$

Applying Prop. 3.6.11 on the sum over σ with the second and third LLTs gives

$$\begin{aligned} LHS &= \prod_{l=0}^{k-1} \prod_{i, i'=1}^n \prod_{j=1}^m \prod_{\alpha, \alpha'=1}^p \prod_{\beta=1}^q \frac{1 - x_i w_\alpha t^l}{(1 + y_j w_{\alpha'} t^l)(1 + x_{i'} z_\beta t^l)} \\ &\quad \times \sum_{\lambda, \sigma, \rho} \mathcal{L}_{\rho/\lambda}^P(Y_m; t) \mathcal{L}_{\sigma/\mu}(X_n; t) t^{d_P(\sigma, \lambda)} \mathcal{L}_{\sigma/\lambda}^P(Z_q; t) t^{d(\rho, \nu)} \mathcal{L}_{\rho/\nu}(W_p; t). \end{aligned}$$

Finally, applying Prop. 3.6.12 on the sum over λ with the first and third LLTs gives

$$\begin{aligned} LHS &= \prod_{l=0}^{k-1} \prod_{i, i'=1}^n \prod_{j, j'=1}^m \prod_{\alpha, \alpha'=1}^p \prod_{\beta, \beta'=1}^q \frac{(1 - x_i w_\alpha t^l)(1 - y_{j'} z_{\beta'} t^l)}{(1 + y_j w_{\alpha'} t^l)(1 + x_{i'} z_\beta t^l)} \\ &\quad \times \sum_{\lambda, \sigma, \rho} \mathcal{L}_{\lambda/\sigma}^P(Y_m; t) \mathcal{L}_{\sigma/\mu}(X_n; t) t^{d_P(\lambda, \rho)} \mathcal{L}_{\lambda/\rho}^P(Z_q; t) t^{d(\rho, \nu)} \mathcal{L}_{\rho/\nu}(W_p; t) \end{aligned}$$

which can be combined into

$$\begin{aligned} &LHS \\ &= \prod_{l=0}^{k-1} \prod_{i, i'=1}^n \prod_{j, j'=1}^m \prod_{\alpha, \alpha'=1}^p \prod_{\beta, \beta'=1}^q \frac{(1 - x_i w_\alpha t^l)(1 - y_{j'} z_{\beta'} t^l)}{(1 + y_j w_{\alpha'} t^l)(1 + x_{i'} z_\beta t^l)} \sum_{\lambda} t^{d(\lambda, \nu)} \mathcal{L}_{\lambda/\mu}^S(X_n, Y_m; t) \mathcal{L}_{\lambda/\nu}^S(W_p, Z_q; t) \\ &= RHS \end{aligned}$$

where we again use the fact that

$$d(\lambda, \nu) = d_P(\lambda, \rho) + d(\rho, \nu).$$

□

3.7 Example computations of \mathcal{L}^S and \mathcal{G}

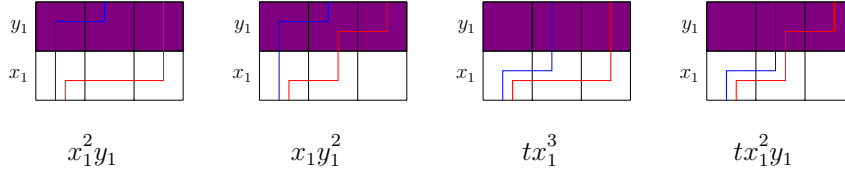
Example 3.7.1. The 2-quotient of $\lambda = (4, 2)$ is $\lambda = ((1), (2))$.



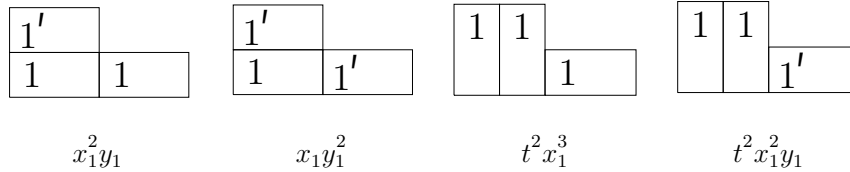
Therefore, by Prop. 3.5.9, we must have

$$\mathcal{L}_\lambda^S(x_1; y_1; t) = t^\square \mathcal{G}_\lambda^{(2)}(x_1; y_1; t^{1/2})$$

for some half-integer $\square \in \frac{1}{2}\mathbb{Z}$. To compute $\mathcal{L}_\lambda^S(x_1; y_1; t)$, we note that there are 4 configurations of the lattice $S_{1,1}(\lambda)$.



Therefore $\mathcal{L}_\lambda^S(x_1; y_1; t) = x_1^2 y_1 + x_1 y_1^2 + t x_1^3 + t x_1^2 y_1$. To compute $\mathcal{G}_\lambda^{(2)}(x_1; y_1; t^{1/2})$, we note that there are 4 super 2-ribbon tableaux of shape λ in the alphabet $\{1 < 1'\}$.



Therefore $\mathcal{G}_\lambda^{(2)}(x_1; y_1; t^{1/2}) = x_1^2 y_1 + x_1 y_1^2 + t^2 x_1^3 + t^2 x_1^2 y_1$. (The way we've ordered the lattice configurations and the super ribbon tableaux agrees with the bijection θ from Section 3.5, so that the i -th lattice configuration corresponds to the i -th super ribbon tableaux via θ .) We see

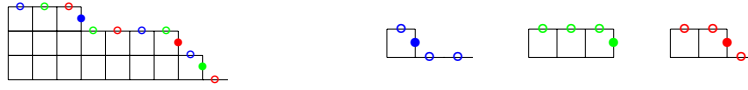
$$\mathcal{L}_\lambda^S(x_1; y_1; t) = \mathcal{G}_\lambda^{(2)}(x_1; y_1; t^{1/2}),$$

so in fact $\square = 0$ in this case. This agrees with the fact that the quantity

$$\square = \frac{1}{2} \sum_{a < b} \left(\# \begin{array}{|c|c|} \hline \color{red}{\square} & \color{blue}{\square} \\ \hline \color{blue}{\square} & \color{red}{\square} \\ \hline \end{array} + \# \begin{array}{|c|c|} \hline \color{blue}{\square} & \color{red}{\square} \\ \hline \color{red}{\square} & \color{blue}{\square} \\ \hline \end{array} - \# \begin{array}{|c|c|} \hline \color{red}{\square} & \color{red}{\square} \\ \hline \color{blue}{\square} & \color{blue}{\square} \\ \hline \end{array} - \# \begin{array}{|c|c|} \hline \color{blue}{\square} & \color{blue}{\square} \\ \hline \color{red}{\square} & \color{red}{\square} \\ \hline \end{array} \right) + \frac{1}{2} \sum_{a < b} \left(\# \begin{array}{|c|c|} \hline \color{red}{\square} & \color{red}{\square} \\ \hline \color{red}{\square} & \color{red}{\square} \\ \hline \end{array} - \# \begin{array}{|c|c|} \hline \color{blue}{\square} & \color{blue}{\square} \\ \hline \color{blue}{\square} & \color{blue}{\square} \\ \hline \end{array} \right)$$

is equal to 0 in each of these 4 configurations.

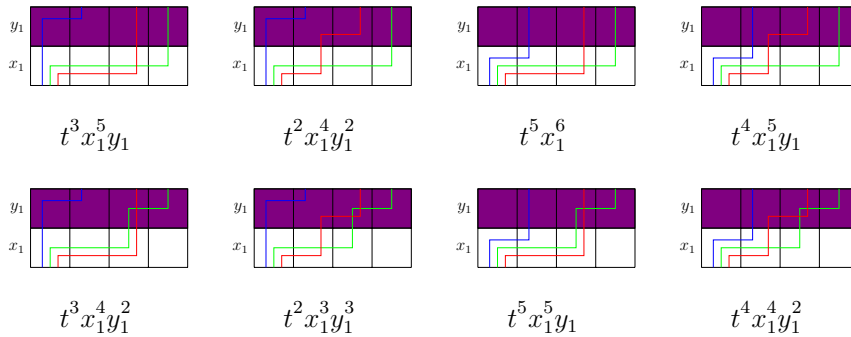
Example 3.7.2. The 3-quotient of $\lambda = (8, 7, 3)$ is $\boldsymbol{\lambda} = ((1), (3), (2))$.



Therefore, by Prop. 3.5.9, we must have

$$\mathcal{L}_{\boldsymbol{\lambda}}^S(x_1; y_1; t) = t^{\square} \mathcal{G}_{\boldsymbol{\lambda}}^{(3)}(x_1; y_1; t^{1/2})$$

for some half-integer $\square \in \frac{1}{2}\mathbb{Z}$. We can thus compute $\mathcal{G}_{\boldsymbol{\lambda}}^{(3)}(x_1; y_1; t^{1/2})$ by computing $\mathcal{L}_{\boldsymbol{\lambda}}^S(x_1; y_1; t)$ and \square . To compute $\mathcal{L}_{\boldsymbol{\lambda}}^S(x_1; y_1; t)$, we note that there are 8 configurations of the lattice $S_{1,1}(\boldsymbol{\lambda})$.



Therefore

$$\mathcal{L}_{\boldsymbol{\lambda}}^S(x_1; y_1; t) = t^3 x_1^5 y_1 + t^2 x_1^4 y_1^2 + t^5 x_1^6 + t^4 x_1^5 y_1 + t^3 x_1^4 y_1^2 + t^2 x_1^3 y_1^3 + t^5 x_1^5 y_1 + t^4 x_1^4 y_1^2.$$

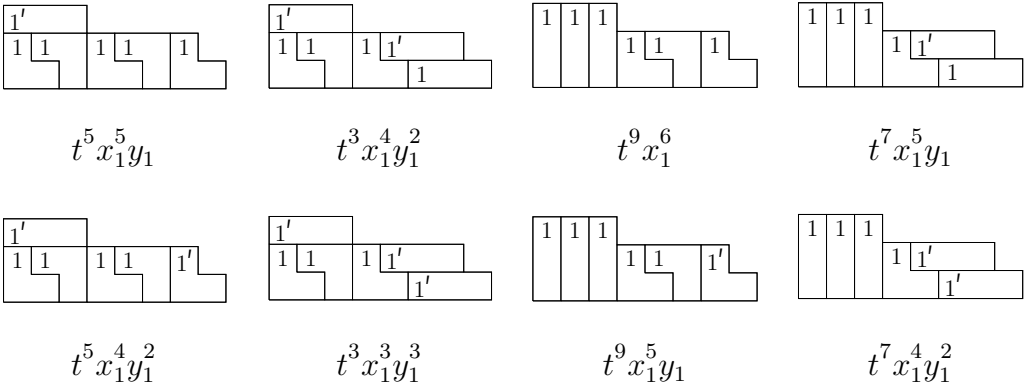
We can also observe that the quantity

$$\square = \frac{1}{2} \sum_{a < b} \left(\# \begin{array}{|c|c|} \hline \color{blue}{\rule{0.5ex}{0.5ex}} & \color{blue}{\rule{0.5ex}{0.5ex}} \\ \hline \color{red}{\rule{0.5ex}{0.5ex}} & \color{red}{\rule{0.5ex}{0.5ex}} \\ \hline \end{array} + \# \begin{array}{|c|c|} \hline \color{red}{\rule{0.5ex}{0.5ex}} & \color{red}{\rule{0.5ex}{0.5ex}} \\ \hline \color{blue}{\rule{0.5ex}{0.5ex}} & \color{blue}{\rule{0.5ex}{0.5ex}} \\ \hline \end{array} - \# \begin{array}{|c|c|} \hline \color{blue}{\rule{0.5ex}{0.5ex}} & \color{red}{\rule{0.5ex}{0.5ex}} \\ \hline \color{red}{\rule{0.5ex}{0.5ex}} & \color{blue}{\rule{0.5ex}{0.5ex}} \\ \hline \end{array} - \# \begin{array}{|c|c|} \hline \color{red}{\rule{0.5ex}{0.5ex}} & \color{blue}{\rule{0.5ex}{0.5ex}} \\ \hline \color{blue}{\rule{0.5ex}{0.5ex}} & \color{red}{\rule{0.5ex}{0.5ex}} \\ \hline \end{array} \right) + \frac{1}{2} \sum_{a < b} \left(\# \begin{array}{|c|c|} \hline \color{blue}{\rule{0.5ex}{0.5ex}} & \color{red}{\rule{0.5ex}{0.5ex}} \\ \hline \color{red}{\rule{0.5ex}{0.5ex}} & \color{blue}{\rule{0.5ex}{0.5ex}} \\ \hline \end{array} - \# \begin{array}{|c|c|} \hline \color{red}{\rule{0.5ex}{0.5ex}} & \color{blue}{\rule{0.5ex}{0.5ex}} \\ \hline \color{blue}{\rule{0.5ex}{0.5ex}} & \color{red}{\rule{0.5ex}{0.5ex}} \\ \hline \end{array} \right)$$

is equal to $\frac{1}{2}$ in each of these 8 configurations, so $\square = \frac{1}{2}$. We can now compute

$$\begin{aligned} \mathcal{G}_{\boldsymbol{\lambda}}^{(3)}(x_1; y_1; t) &= t^{-2\square} \mathcal{L}_{\boldsymbol{\lambda}}^S(x_1; y_1; t^2) \\ &= t^5 x_1^5 y_1 + t^3 x_1^4 y_1^2 + t^9 x_1^6 + t^7 x_1^5 y_1 + t^5 x_1^4 y_1^2 + t^3 x_1^3 y_1^3 + t^9 x_1^5 y_1 + t^7 x_1^4 y_1^2. \end{aligned}$$

We see this agrees with the result obtained from explicitly computing all the super 3-ribbon tableaux of shape λ in the alphabet $\{1 < 1'\}$.



(Again, the way we've ordered the lattice configurations and the super ribbon tableaux agrees with the bijection θ from Section 3.5.)

Chapter 4

Domino tilings of the Aztec diamond

4.1 Introduction

Domino tilings of the Aztec diamond were first studied in 1992 in [24, 25]. The Aztec diamond of rank m is the set of lattice squares inside the diamond-shaped region

$$AD_m = \{(x, y) \in \mathbb{R}^2 : |x| + |y| \leq m + 1\}.$$

The Aztec diamond of rank 3 is drawn on the left of Figure 4.1. A domino is a pair of orthogonally adjacent lattice squares, and a domino tiling of a region is a partitioning of the region into non-overlapping dominos. For example, a domino tiling of the rank 3 Aztec diamond is drawn on the right of Figure 4.1, and the domino tilings of the Aztec diamond of rank 2 are displayed in Figure 4.2.

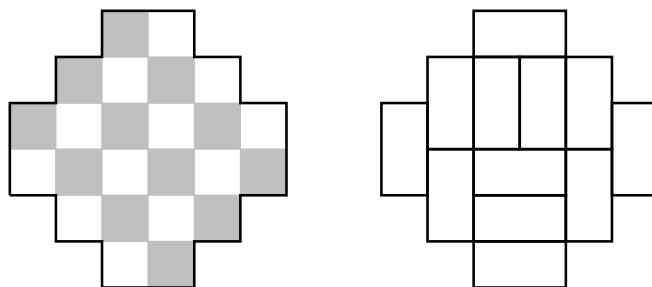


Figure 4.1: The Aztec diamond of rank 3 (left) and an example of a domino tiling (right)

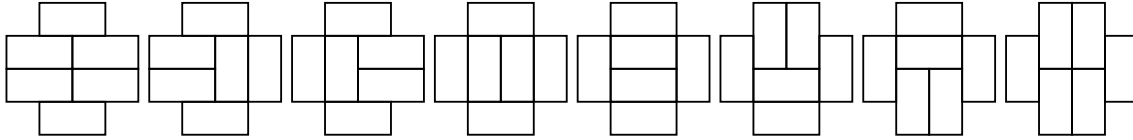


Figure 4.2: The 8 domino tilings of the Aztec diamond of rank 2

One surprising enumerative result is the following:

Theorem 4.1.1. *The number of domino tilings of the Aztec diamond of rank m is exactly $2^{\binom{m+1}{2}}$.*

There are numerous proofs of this theorem using many interesting combinatorial techniques, including random generation algorithms [24, 25], non-intersecting paths [26], and sequences of interlacing partitions [11, 10]. Thanks to these techniques, we know a lot about the asymptotic behavior of domino tilings of the Aztec diamond of rank m when $m \rightarrow \infty$. An important result is the arctic circle theorem of Jockusch, Propp, and Shor [33], which roughly states that a uniformly random tiling behaves in a brickwork pattern in four regions (called frozen regions or polar regions), one adjacent to each corner of the Aztec diamond, whose union is the complement of the largest circle (called the arctic circle) that can be inscribed within the Aztec diamond. A beautiful picture for $m = 1000$ can be found in Figure 4.3, which was taken from <https://sites.uclouvain.be/aztecdiamond/examples/>. More precisely:

Theorem 4.1.2 ([33, 49]). *For each m , consider a uniformly random domino tiling of the Aztec diamond of rank m scaled by a factor of $\frac{1}{m}$ in each axis to fit into the limiting diamond*

$$AD_\infty = \{|x| + |y| \leq 1\}$$

and let P_m be the image of the polar regions of the random tiling under this scaling transformation. Then, for all $\epsilon > 0$, as $m \rightarrow \infty$,

$$\left\{ (x, y) \in AD_\infty : x^2 + y^2 > \frac{1}{2} + \epsilon \right\} \cap \left(\frac{1}{m} AD_m \right) \subset P_m \subset \left\{ (x, y) \in AD_\infty : x^2 + y^2 > \frac{1}{2} - \epsilon \right\}$$

holds with probability tending to 1.

In the rest of this chapter, we say that the arctic curve for domino tilings of the Aztec diamond is the circle

$$x^2 + y^2 = \frac{1}{2}.$$

Cohn, Elkies, and Propp [17] later proved some results about the behavior of the tiling inside the arctic circle, specifically regarding the probability of observing a given domino in a given position and regarding the “height function” of the tiling. Many more papers have been written on domino tilings of the Aztec diamond, for example [49, 36, 34].

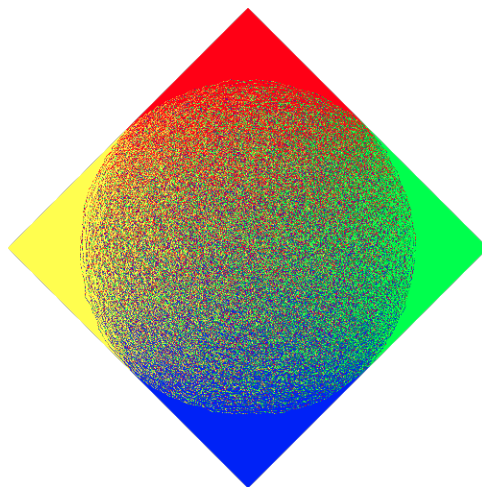


Figure 4.3: A typical tiling of the Aztec diamond of rank 1000

The goal of this chapter is to study superpositions of domino tilings of the Aztec diamond, using the colored vertex models defined in Chapter 1. For $k \geq 1$, we define a k -tiling of the Aztec diamond of rank m to be the superposition of k tilings, colored from 1 to k . These tilings are not independent; we define an interaction between the tilings of colors $i < j$ to be a pair of dominos, one of color i and one of color j , of a certain form. By relating these tilings to our colored vertex models, we prove the following theorem.

Theorem 4.1.3 (Thm. 4.3.3 and Thm. 4.3.6). *The generating function of the k -tilings of the rank m Aztec diamond is*

$$\prod_{\ell=0}^{k-1} \prod_{1 \leq i \leq j \leq m} (1 + t^{\ell} x_i y_j). \quad (4.1)$$

Here t follows the number of interactions, and x_i and y_j follow the numbers of dominos of certain types as defined in Section 4.2.

When $k = 1$, we recover known results for domino tilings of the Aztec diamond (Prop. 4.2.1). We also construct a bijection between k -tilings when $t = 0$ (i.e. no interactions) and 1-tilings, which allows us to compute the arctic curves for $t = 0$.

Theorem 4.1.4 (Thm. 4.4.6). *The arctic curve for k -tilings of the Aztec diamond when $t = 0$ is given by*

$$\begin{cases} x^2 + y^2 = \frac{1}{2}, & x \in [-\frac{1}{2}, \frac{1}{2}], y > \frac{1}{2} \\ (x + (k-1)y)^2 + (ky)^2 = \frac{1}{2}, & x \in [-\frac{1}{2k}, 1 - \frac{1}{2k}], y < -\frac{1}{2k} \\ \left(\frac{2x+(k-1)(x+y-1)}{2}\right)^2 + \left(\frac{2y+(k-1)(x+y-1)}{2}\right)^2 = \frac{1}{2}, & y \in [-\frac{1}{2k}, \frac{1}{2}], x > -\frac{k-1}{k+1}y + \frac{k}{k+1} \\ \left(\frac{2x+(k-1)(x+y-1)}{2k}\right)^2 + \left(\frac{2y+(k-1)(3y-x-1)}{2k}\right)^2 = \frac{1}{2}, & y \in [-\frac{1}{2k}, \frac{1}{2}], x < -\frac{k-1}{k+1}y - \frac{1}{k+1} \end{cases} \quad (4.2)$$

for each color.

Finally, we construct a bijection between k -tilings when $t = 0$ (i.e. no interactions) and k -tilings when $t \rightarrow \infty$ (i.e. maximum possible number of interactions), which allows us to compute the arctic curves for $t \rightarrow \infty$.

Corollary 4.1.5. *The arctic curve for k -tilings of the Aztec diamond when $t \rightarrow \infty$ is given by reflecting (4.2) over the line $y = x$.*

The chapter is organized as follows.

- In Section 4.2, we introduce domino tilings of the Aztec diamond, and we define two different models (purple-gray and white-pink) for relating a k -tiling to a sequence of k -tuples of partitions and for assigning a weight to a k -tiling.
- In Section 4.3, we relate the vertex models to the purple-gray and white-pink models, and we use the vertex models to compute the generating functions of the k -tilings.
- In Section 4.4, we relate domino tilings to collections of non-intersecting paths, which allows us to compute the arctic curve of the tilings for $t = 0$. We then relate the $t = 0$ and $t \rightarrow \infty$ cases, which allows us to compute the arctic curve of the tilings for $t \rightarrow \infty$.

We also present some lozenge k -tilings of the hexagon and compute their arctic curves for $t = 0$ in Appendix A.

4.2 Domino tilings of the Aztec diamond

The Aztec diamond

A lattice square is a 1×1 square $[a, a + 1] \times [b, b + 1]$ in \mathbb{R}^2 for some $a, b \in \mathbb{Z}$. A horizontal (vertical) domino is a 2×1 (1×2) rectangle consisting of two lattice squares, as shown below on the left (right).

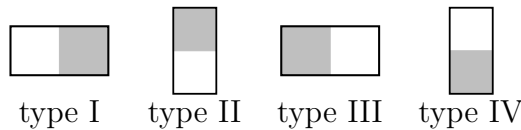


Given a region $R \subseteq \mathbb{R}^2$ consisting of lattice squares, a domino tiling of R is a partitioning of R into non-overlapping horizontal and vertical dominos. A k -tiling $\mathbf{T} = (T_1, \dots, T_k)$ is a k -tuple of domino tilings; we say the dominos in the i -th tiling T_i are colored i .

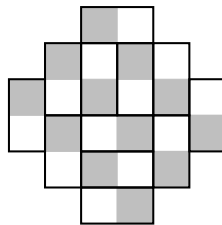
The **Aztec diamond** of rank m is the region in \mathbb{R}^2 which consists of all lattice squares lying completely inside the diamond-shaped region

$$\{(x, y) : |x| + |y| \leq m + 1\}.$$

We will be interested in domino tilings of the Aztec diamond. As we can draw \mathbb{R}^2 as a checkerboard, where the lattice square $[a, a + 1] \times [b, b + 1]$ is shaded white if $a + b + m$ is odd and gray if $a + b + m$ is even, we have four types of dominos with which to tile:



For example, here is one possible domino tiling of the Aztec diamond of rank $m = 3$.



Sequences of partitions and tilings of the Aztec diamond

We will actually use two different constructions to go from a sequence of interlacing partitions to a tiling of the Aztec diamond. In addition, for each construction, we will define the weight of a tiling as a polynomial in the variables $x_1, \dots, x_m, y_1, \dots, y_m$.

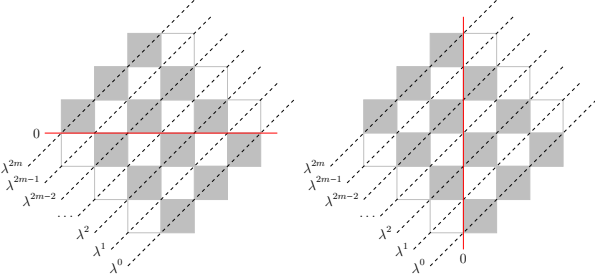


Figure 4.4: Two ways of slicing the Aztec diamond.

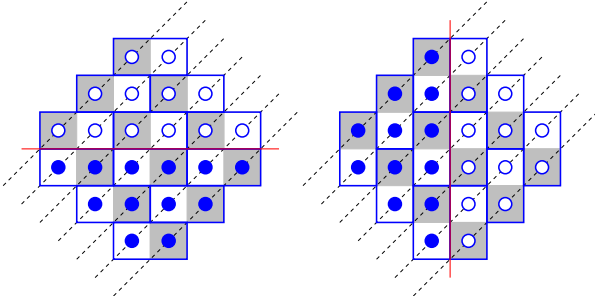
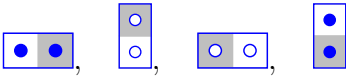


Figure 4.5: The empty tilings for the purple-gray model (left) and the white-pink model (right)



The first construction, which we will call the **purple-gray model**, is as follows. Specifying a domino tiling of the rank m Aztec diamond is equivalent to specifying $2m + 1$ Maya diagrams on the slices going from SW to NE (drawn as dashed lines), as in the left of Figure 4.4, where the 0 content line for the diagrams is drawn in red. We impose the condition that

$$\emptyset = \lambda^0 \leq' \lambda^1 \geq \dots \leq' \lambda^{2m-1} \geq \lambda^{2m} = \emptyset$$

and $\lambda_1^i + \ell(\lambda^i) \leq m$ for all i . (The Maya diagrams of these partitions are truncated to fit inside the Aztec diamond, with the 0 content line positioned as specified in the left of Figure 4.4. To recover the untruncated Maya diagram from the truncated one, we can pre-pend infinitely many \bullet 's and post-pend infinitely many \circ 's.) From these Maya diagrams, we can draw dominos according to the following rules.



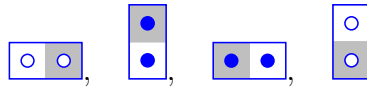
(There is a unique way to do this.) For example, if each $\lambda^\ell = \emptyset$, then the corresponding Maya diagrams and domino tiling are given on the left of Figure 4.5. We define the weight of a domino tiling of the Aztec diamond to be the product of the weights of the dominos, where we assign weights to the dominos according to the following rules.

- A domino of the form  whose top square is on slice $2i - 1$ gets weight x_i .
- A domino of the form  whose bottom square is on slice $2i - 1$ gets weight y_i .
- All other dominos get a weight of 1.



The second construction, which we will call the **white-pink model**, is as follows. Specifying a domino tiling of the Aztec diamond of rank m is equivalent to specifying $2m + 1$ Maya diagrams on the slices going from SW to NE (drawn as dashed lines), as in the right of Figure 4.4, where the 0 content line for the diagrams is drawn in red. We impose the condition that

$$\emptyset = \lambda^0 \leq \lambda^1 \geq' \dots \leq \lambda^{2m-1} \geq' \lambda^{2m} = \emptyset$$

and $\lambda_1^i + \ell(\lambda^i) \leq m$ for all i . (Similarly as in the purple-gray model, we truncate the Maya diagrams to fit inside the Aztec diamond.) From these Maya diagrams, we can draw dominos according to the following rules.



(There is a unique way to do this.) For example, if each $\lambda^\ell = \emptyset$, then the corresponding Maya diagrams and domino tiling are given on the right of Figure 4.5. We define the weight of a domino tiling of the Aztec diamond to be the product of the weights of the dominos, where we assign weights to the dominos according to the following rules.

- A domino of the form  whose left square is on slice $2i - 1$ gets weight x_i .
- A domino of the form  whose right square is on slice $2i - 1$ gets weight y_i .
- All other dominos get a weight of 1.

For example, consider the domino tiling in Figure 4.6. In the purple-gray model, this tiling gives the sequence of partitions

$$\emptyset \leq' (1, 1) \geq (1, 1) \leq' (2, 1) \geq (1) \leq' (2) \geq \emptyset$$

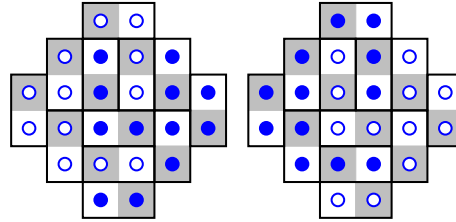


Figure 4.6: A domino tiling and the corresponding Maya diagrams in the purple-gray (left) and white-pink (right) models

and has weight $x_1^2 x_2 x_3 y_2 y_3^2$. In the white-pink model, this tiling gives the sequence of partitions

$$\emptyset \leq (1) \geq' \emptyset \leq (1) \geq' (1) \leq (1) \geq' \emptyset$$

and has weight $x_1 x_2 y_1 y_3$.

We define the generating function of each model to be

$$Z_{AD,model}^{(1)}(X_m; Y_m) := \sum_T w(T)$$

where the sum is over domino tilings T of the rank m Aztec diamond and the weight function w is determined by the *model* (which is either *purple-gray* or *white-pink*). Both models were studied previously in [11]; surprisingly, the generating functions are the same:

Proposition 4.2.1 ([11, Remark 2]). *For both the purple-gray model and the white-pink model, the generating function is*

$$Z_{AD}^{(1)}(X_m; Y_m) := \prod_{1 \leq i \leq j \leq m} (1 + x_i y_j).$$

We will generalize these two models to k -tilings, and recover this result in the case $k = 1$.

Extending the models to k -tilings

The two models in the previous section can be extended to k -tilings. For the purple-gray model, specifying a k -tiling of the Aztec diamond of rank m is equivalent to specifying a sequence of $2m + 1$ k -tuples of partitions satisfying

$$\mathbf{0} = \lambda^0 \leq' \lambda^1 \geq \dots \leq' \lambda^{2m-1} \geq \lambda^{2m} = \mathbf{0}.$$

For the white-pink model, specifying a k -tiling of the Aztec diamond of rank m is equivalent to specifying a sequence of $2m + 1$ k -tuples of partitions satisfying

$$\mathbf{0} = \boldsymbol{\lambda}^0 \leq \boldsymbol{\lambda}^1 \geq' \dots \leq \boldsymbol{\lambda}^{2m-1} \geq' \boldsymbol{\lambda}^{2m} = \mathbf{0}.$$

For both models, letting the k -tiling be $\mathbf{T} = (T_1, \dots, T_k)$ and letting the j -th k -tuple of partitions be $\boldsymbol{\lambda}^j = (\lambda^{(j,1)}, \dots, \lambda^{(j,k)})$ for all j , the i -th tiling T_i corresponds to the sequence of partitions $(\lambda^{(0,i)}, \dots, \lambda^{(2m,i)})$ for all i .

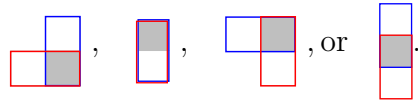
We define the weight of a k -tiling \mathbf{T} as a polynomial in the variables

$$x_1, \dots, x_m, y_1, \dots, y_m, t$$

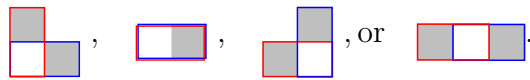
by the equation

$$w(\mathbf{T}) = w(T_1, \dots, T_k) = t^{\#\text{interactions in } \mathbf{T}} \prod_{i=1}^k w(T_i).$$

In other words, the weight of a k -tiling is the product of the weights of the individual tilings, times an additional factor of t for every **interaction** between two of the tilings. In the purple-gray model, an interaction is a pair of dominos of the form



In the white-pink model, an interaction is a pair of dominos of the form



Here blue is a smaller color than red.

For example, consider the 3-tiling of the rank 3 Aztec diamond in Figure 4.7. In the purple-gray model, the first tiling has weight $x_1^2 x_2 y_2^2 x_3 y_3^2$, the second has weight $x_1^3 y_1 y_2 y_3$, the third has weight $x_1 y_1 x_2 y_2$, and there are 11 interactions - 4 between blue and red, 3 between blue and green, and 4 between red and green. Thus the weight of this 3-tiling is

$$t^{11} x_1^6 y_1^2 x_2^2 y_2^4 x_3^3 y_3^3.$$

We define the generating function of each model to be

$$Z_{AD,model}^{(k)}(X_m; Y_m; t) := \sum_{\mathbf{T}} w(\mathbf{T})$$

where the sum is over k -tilings \mathbf{T} of the rank m Aztec diamond and the weight function w is determined by the *model* (which is either *purple-gray* or *white-pink*).

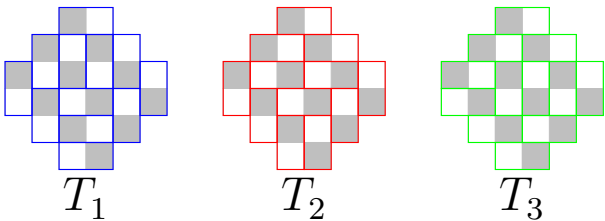
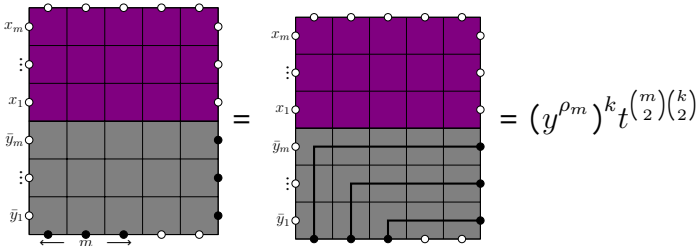


Figure 4.7: An example of a 3-tiling of the rank 3 Aztec diamond

4.3 k -tilings and vertex models

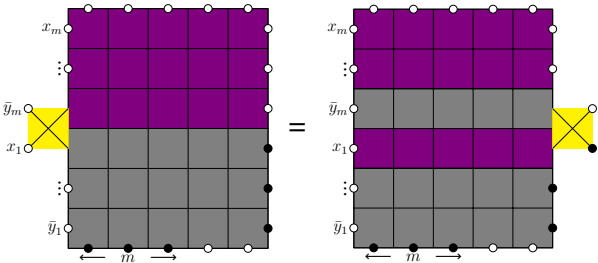
The purple-gray partition function

Consider the following lattice and its associated partition function.



Here $y^{\rho_m} = y_1^{m-1} y_2^{m-2} \dots y_m^{m-m}$, a white dot indicates the absence of all colors, and a black dot indicates the presence of all colors.

By inserting a yellow cross on the left we can use the YBE (Prop. 1.4.8) to get



from which we see that

$$= \prod_{l=0}^{k-1} (1 + x_1 y_m t^l)^{-1}.$$

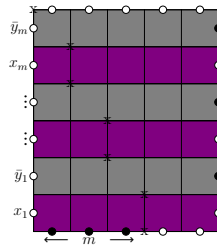
We can repeat this to get

$$\times \prod_{l=0}^{k-1} \prod_{1 \leq i \leq j \leq m} (1 + x_i y_j t^l)^{-1}$$

from which we see that

$$= (y^{\rho_m})^k t^{\binom{m}{2} \binom{k}{2}} \prod_{l=0}^{k-1} \prod_{1 \leq i \leq j \leq m} (1 + x_i y_j t^l).$$

Given a configuration of the lattice



and looking at the labels on the horizontal edges row by row from bottom to top, we get a sequence of $2m + 1$ k -tuples of Maya diagrams, where we mark the 0 content line with x's on the lattice. The corresponding $2m + 1$ k -tuples of partitions satisfy

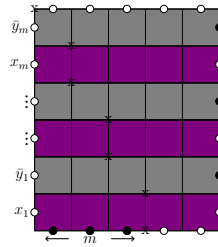
$$0 = \lambda^0 \leq' \lambda^1 \geq \dots \leq' \lambda^{2m-1} \geq \lambda^{2m} = 0.$$

Relating lattice configurations and k -tilings in the purple-gray model

Given a sequence of k -tuples of partitions

$$0 = \lambda^0 \leq' \lambda^1 \geq \dots \leq' \lambda^{2m-1} \geq \lambda^{2m} = 0,$$

we get both a configuration of the lattice



and a k -tiling of the Aztec diamond of rank m . For example, in Figure 4.8, the tiling on the left corresponds to the configuration on the right, and in Figure 4.9, we give the 8 configurations corresponding to the tilings of the rank 2 Aztec diamond, which were listed in Figure 4.2. As it turns out, the weight of the lattice configuration and the weight of the k -tiling are related.

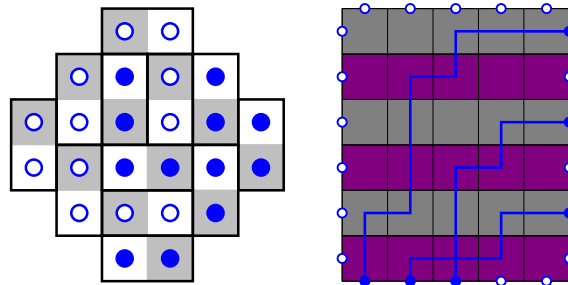


Figure 4.8: Domino tilings and vertex models

For the purple faces, one gets a t whenever you have a face of the form



where blue is a smaller color than red. It is easy to see that this equals the number of domino configurations of the form



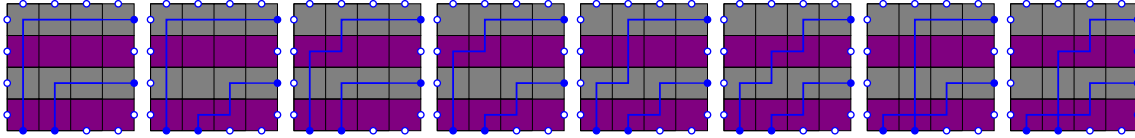


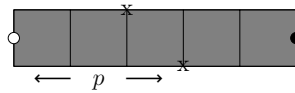
Figure 4.9: Purple-gray lattice configurations for the Aztec diamond of rank 2

which is one of the configurations that give a t . One gets an x_i whenever a path exits right in the i -th purple row. It is easy to see that this equals the number of dominos of the form



whose top square is on slice $2i - 1$, which equals the x_i power we give the dominos.

We are left to consider the gray faces. Let's look at the $(m - p + 1)$ -th gray row



for some $p \in [m]$. Let $y = y_{m-p+1}$. For a single color $a \in [k]$, we can write the contribution of the paths of color a to the power of y in the weight of the row as

$$\# \begin{array}{|c|} \hline \blacksquare \\ \hline \end{array} + \# \begin{array}{|c|} \hline \begin{array}{|c|} \hline \blacksquare \\ \hline \end{array} \\ \hline \end{array} + \# \begin{array}{|c|} \hline \begin{array}{|c|} \hline \blacksquare \\ \hline \end{array} \\ \hline \end{array}.$$

Lemma 4.3.1. *In the $(m - p + 1)$ -th gray row, for each color,*

$$\# \begin{array}{|c|} \hline \begin{array}{|c|} \hline \blacksquare \\ \hline \end{array} \\ \hline \end{array} + \# \begin{array}{|c|} \hline \blacksquare \\ \hline \end{array} = p - 1.$$

Proof. The left-hand side counts the number of paths exiting the row through the top. There are p paths entering the row through the bottom, 0 paths entering the row from the left, and 1 path exiting the row through the right. By path conservation, this means that there are $p + 0 - 1 = p - 1$ paths exiting the row through the top. \square

The number of vertices in which color a is absent equals the number of cells that get removed from the a -th partition, i.e.

$$\# \begin{array}{|c|} \hline \blacksquare \\ \hline \end{array} = |\lambda_{2(m-p+1)}^{(a)}| - |\lambda_{2(m-p+1)-1}^{(a)}|.$$

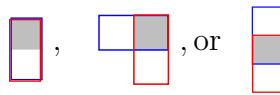
It is easy to see that this equals the number the number of dominos of the form



whose bottom square is on slice $2(m - p + 1) - 1$, which equals the y power we give the dominos. Therefore if we pull out a factor of y^{p-1} from the weight of the row, then the y -weights agree. For the t -weight of the row, we can write the t power as

$$\begin{aligned} & \sum_{1 \leq a < b \leq k} \#\{\text{faces} | a \text{ right, } b \text{ top}\} + \#\{\text{faces} | a \text{ not right, } b \text{ not right}\} \\ &= \sum_{1 \leq a < b \leq k} \#\{\text{faces} | a \text{ right, } b \text{ top}\} + \#\{\text{faces} | a \text{ not right, } b \text{ top}\} + \#\{\text{faces} | a \text{ not right, } b \text{ absent}\} \\ &= \sum_{1 \leq a < b \leq k} \#\{\text{faces} | b \text{ top}\} + \#\{\text{faces} | a \text{ not right, } b \text{ absent}\} \\ &= \sum_{1 \leq a < b \leq k} (p - 1) + \#\{\text{faces} | a \text{ not right, } b \text{ absent}\} \\ &= \binom{k}{2} (p - 1) + \sum_{1 \leq a < b \leq k} \#\{\text{faces} | a \text{ not right, } b \text{ absent}\} \end{aligned}$$

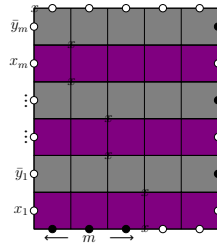
where we have used the fact that $\#\{\text{faces} : b \text{ exits top}\} = p - 1$ by the previous lemma. It is easy to see that $\#\{\text{faces} : a \text{ not right, } b \text{ absent}\}$ equals the number of domino configurations of the form



where blue is color a and red is color b , which are three of the configurations that give a t . Therefore if we pull out a factor of $t^{\binom{k}{2}(p-1)}$ from the row, then the t -weights agree.

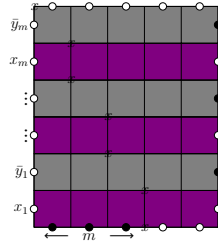
Putting it all together, we arrive at the following results.

Lemma 4.3.2 ([20, Lemma 4.2]). *There is a weight-preserving bijection between configurations of the purple-gray lattice*



and k -tilings of the Aztec diamond of rank m . By weight-preserving, we mean that the weight of the configuration is $(y^{\rho_m})^k t^{\binom{m}{2} \binom{k}{2}}$ times the weight of the k -tiling.

Theorem 4.3.3 ([20, Thm. 4.3]). *The partition function of*



with k colors is equal to $(y^{\rho_m})^k t^{\binom{m}{2}} \binom{k}{2}$ times the generating function of k -tilings of the Aztec diamond of rank m in the purple-gray model. We have

$$Z_{AD, \text{purple-gray}}^{(k)}(X_m; Y_m; t) = \prod_{l=0}^{k-1} \prod_{1 \leq i \leq j \leq m} (1 + x_i y_j t^l).$$

In Figure 4.10, we exhibit an example of the bijection for $k, m = 3$.

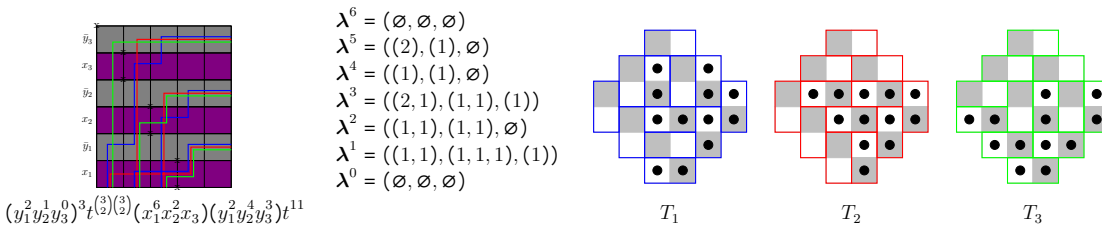
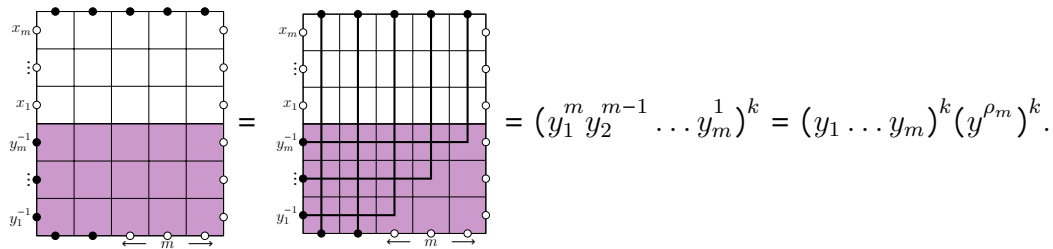


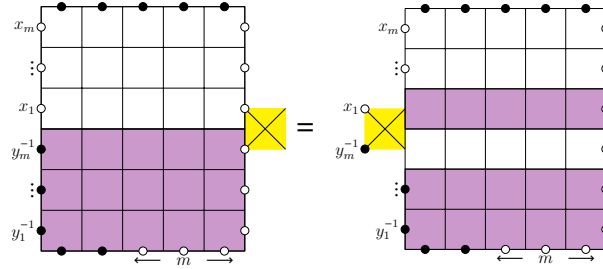
Figure 4.10: An example of a 3-tiling of the rank 3 Aztec diamond (right), the corresponding sequence of 3-tuples of partitions (middle), and the corresponding purple-gray lattice configuration (left)

The white-pink partition function

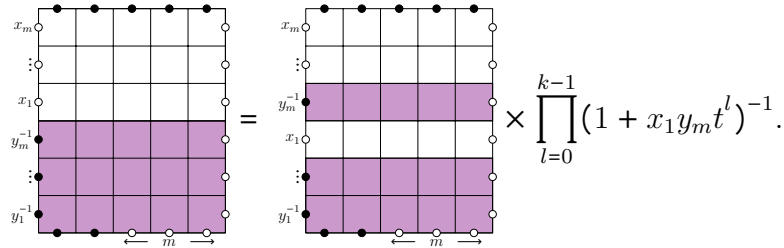
We can apply similar techniques to analyze the white-pink model. Consider the following lattice and its associated partition function.



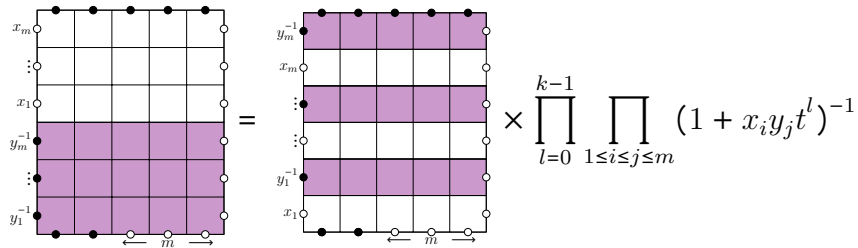
By inserting a yellow cross on the right we can use the YBE (Prop. 1.4.9)



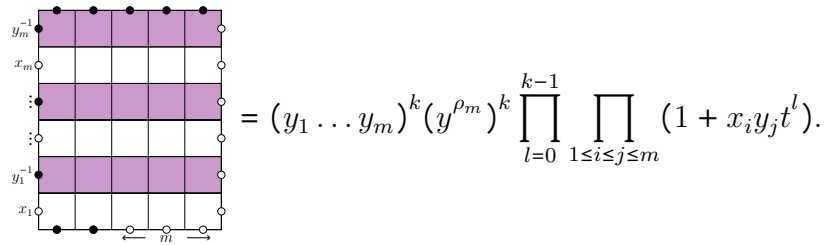
from which we see that



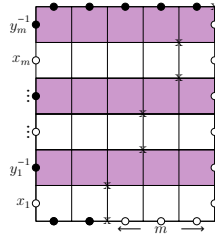
We can repeat this to get



from which we see that



Given a configuration of the lattice



and looking at the labels on the horizontal edges row by row from bottom to top, we get a sequence of $2m + 1$ k -tuples of Maya diagrams, where we mark the 0 content line with x 's on the lattice. The corresponding $2m + 1$ k -tuples of partitions satisfy

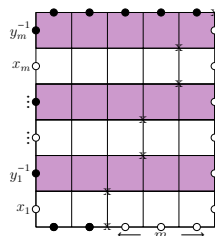
$$0 = \lambda^0 \leq \lambda^1 \geq' \dots \leq \lambda^{2m-1} \geq' \lambda^{2m} = 0.$$

Relating lattice configurations and k -tilings in the white-pink model

Given a sequence of k -tuples of partitions

$$0 = \lambda^0 \leq \lambda^1 \geq' \dots \leq \lambda^{2m-1} \geq' \lambda^{2m} = 0,$$

we get both a configuration of the lattice



and a k -tiling of the Aztec diamond of rank m . For example, in Figures 4.11, we give the 8 configurations corresponding to the 1-tilings of the rank 2 Aztec diamond, which were listed in Figure 4.2. As it turns out, the weight of the lattice configuration and the weight of the k -tiling are related.

Lemma 4.3.4. *In the l -th pink row, for each color,*

$$\# \begin{array}{|c|} \hline \square \\ \hline \square \\ \hline \end{array} + \# \begin{array}{|c|} \hline \square \\ \hline \square \\ \hline \end{array} = m - l + 1.$$

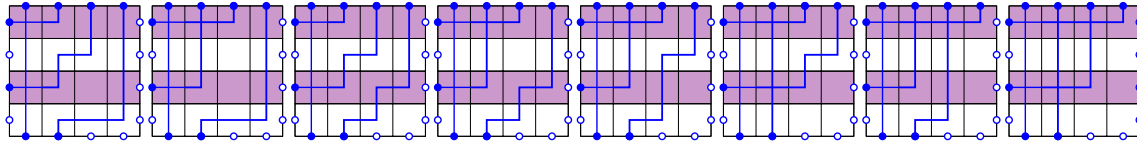


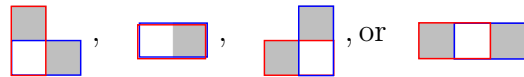
Figure 4.11: White-pink lattice configurations for the Aztec diamond of rank 2

Proof. In the l -th pink row, there are $l + 1$ particles entering from the bottom and $m + 2$ vertices. This means there are $(m + 2) - (l + 1) = m - l + 1$ vertices in which a particle does not enter from the bottom. \square

If we pull out a factor of y_l^{m-l+1} for the l -th pink row for each $l \in [m]$, then we get an overall factor of $(y_1 \dots y_m)^k (y^{\rho_m})^k$ on the left-hand side, which cancels with the same factor on the right-hand side. After removing this factor, the l -th pink row now contributes a y_l whenever there is a vertical path, which corresponds to a domino of the form



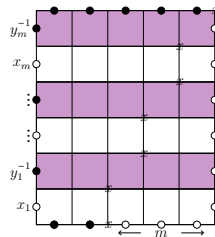
whose right square is on slice $2l - 1$. We get a t whenever a smaller color exits right and a larger color is vertical in a pink row, and whenever a smaller color exits right and a larger color is present in a white row. This corresponds to a pair of dominos of the form



where blue is a smaller color than red.

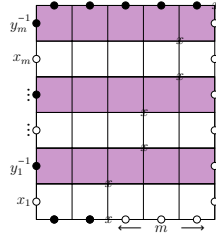
Putting it all together, we arrive at the following results.

Lemma 4.3.5 ([20, Lemma 4.5]). *There is a weight-preserving bijection between configurations of the white-pink lattice*



and k -tilings of the Aztec diamond of rank m . By weight-preserving, we mean that the weight of the configuration is $(y_1 \dots y_m)^k (y^{\rho_m})^k$ times the weight of the k -tiling.

Theorem 4.3.6 ([20, Thm. 4.6]). *The partition function of*



with k colors is equal to $(y_1 \dots y_m)^k (y^{\rho_m})^k$ times the generating function of k -tilings of the Aztec diamond in the white-pink model. We have

$$Z_{AD, \text{white-pink}}^{(k)}(X_m; Y_m; t) = \prod_{l=0}^{k-1} \prod_{1 \leq i \leq j \leq m} (1 + x_i y_j t^l).$$

Combining the two models

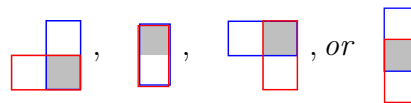
Since the generating functions of the two models are equal, we will write

$$Z_{AD}^{(k)}(X_m; Y_m; t) = \prod_{l=0}^{k-1} \prod_{1 \leq i \leq j \leq m} (1 + x_i y_j t^l).$$

Moreover, we get a surprising combinatorial statement.

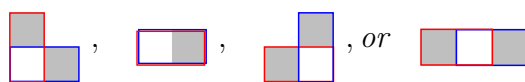
Proposition 4.3.7 ([20, Prop. 4.7]). *Fix integers $k, m, l, r_1, \dots, r_m, s_1, \dots, s_m \geq 0$. There is a bijection between:*



- k -tilings of the Aztec diamond of rank m with ℓ pairs of dominos of the form



where where blue is a smaller color than red, r_i dominos of the form whose top square is on slice $2i - 1$ for each $i \in [m]$, and s_i dominos of the form whose bottom square is on slice $2i - 1$ for each $i \in [m]$; and

- k -tilings of the Aztec diamond of rank m with ℓ pairs of dominos of the form



where where blue is a smaller color than red, r_i dominos of the form  whose left square is on slice $2i - 1$ for each $i \in [m]$, and s_i dominos of the form  whose right square is on slice $2i - 1$ for each $i \in [m]$.

We leave it as an open problem to find a combinatorial proof of the proposition.

4.4 Arctic curve computations

In this section, we consider arctic curves for k -tilings with fixed values of $t = t_0$ (or $t \rightarrow \infty$), defined as follows.

Definition 4.4.1. Fix $t_0 \geq 0$. Fix a positive integer m . Given a k -tiling $\mathbf{T} = (T_1, \dots, T_k)$ of the rank m Aztec diamond AD_m , define

$$w(\mathbf{T}; t) := t^{\# \text{ interactions in } \mathbf{T}}$$

(the weight of \mathbf{T} where we set all $x_i = 1$ and all $y_j = 1$). We generate a random k -tiling \mathbf{T} of AD_m with probability

$$p(\mathbf{T}; t_0) := \frac{w(\mathbf{T}; t_0)}{\sum_{\mathbf{S}} w(\mathbf{S}; t_0)},$$

where the sum is over all k -tilings \mathbf{S} of AD_m . Then we say that the curve described by the equation $f(x, y) = 0$ is the **arctic curve** for k -tilings of the Aztec diamond when $t = t_0$ for color $i \in [k]$ if, for all $\epsilon > 0$, the probability that

$$\{(x, y) \in AD_\infty : f(x, y) > \epsilon\} \cap \left(\frac{1}{m}AD_m\right) \subset P_m(T_i) \subset \{(x, y) \in AD_\infty : f(x, y) > -\epsilon\}$$

holds tends to 1 as $m \rightarrow \infty$. Here $\frac{1}{m}AD_m$ is AD_m scaled by $\frac{1}{m}$ in each axis to fit into the limiting diamond

$$AD_\infty = \{|x| + |y| \leq 1\}$$

and $P_m(T_i)$ is the image of the polar regions of T_i under this scaling transformation. The case $t \rightarrow \infty$ is defined similarly, where the probability of generating \mathbf{T} is now

$$\lim_{t \rightarrow \infty} p(\mathbf{T}; t) = \lim_{t \rightarrow \infty} \frac{w(\mathbf{T}; t)}{\sum_{\mathbf{S}} w(\mathbf{S}; t)}.$$

Remark 4.4.2. It is not obvious from Definition 4.4.1 that the arctic curves for different colors should be the same. In fact, the asymmetric definition of interactions would suggest otherwise. However, we will see that this is the case for $t = 0, 1$ and $t \rightarrow \infty$, and computer simulations suggest it is also the case for other values of t .

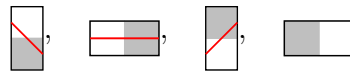
In the case $t = 1$, we have

$$p(\mathbf{T}; 1) = \frac{1}{\# \text{ } k\text{-tilings of } AD_m}.$$

Thus, by Theorem 4.1.2, the arctic curve for k -tilings of the Aztec diamond when $t = 1$ for all k colors is the circle $x^2 + y^2 = \frac{1}{2}$.

Schröder paths

To compute the arctic curves for $t = 0$ and $t \rightarrow \infty$, we need to consider Schröder paths. A Schröder path is a lattice path using NE (1,1), SE (1,-1), and E (2,0) steps starting at (x_0, y_0) and ending at $(x_0 + n, y_0)$ which does not go below the line $y = y_0$. We can assign paths to the dominos according to the following rules.



This gives a well-known [2, 26, 35] bijection between:

- domino tilings of the Aztec diamond of rank m and
- m -tuples of non-intersecting Schröder paths such that, for each $i \in [m]$, path i starts at $(-m - 1 + i, -i + \frac{1}{2})$ and ends at $(m + 1 - i, -i + \frac{1}{2})$.

Figure 4.12 illustrates this bijection in the case $m = 2$.

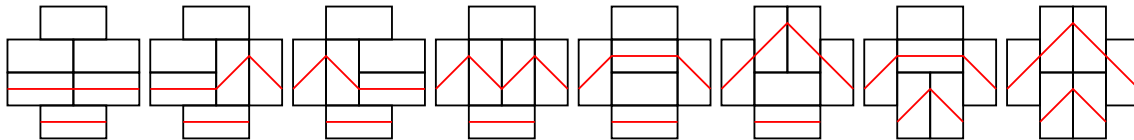
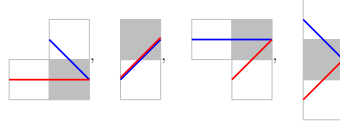


Figure 4.12: Non-intersecting paths for the Aztec diamond of rank 2

The weight of a domino tiling can be expressed in terms of Schröder paths. We will only consider the purple-gray model (but the white-pink model can be described similarly).

- The power of x_i is the number of down-right steps starting on slice $2i - 1$
- The power of y_i is the number of up-right steps starting on slice $2i - 1$.

- The power of t is the number of configurations of the form



where blue is a smaller color than red. In other words, we get a factor of t when a blue path meets a red path from above, or a blue and a red path take an up-right step together.

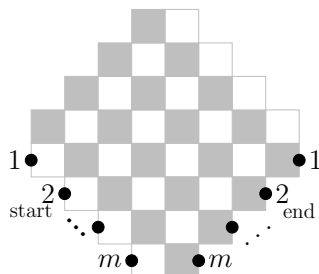
This follows easily from the definition of the weight of a k -tiling (Sections 4.2 and 4.2) in the purple-gray model.

The case $t = 0$

When $t = 0$, we have

$$Z_{AD}^{(k)}(X_m; Y_m; 0) = \prod_{l=0}^{k-1} \prod_{1 \leq i \leq j \leq m} (1 + x_i y_j 0^l) = \prod_{1 \leq i \leq j \leq m} (1 + x_i y_j) = Z_{AD}^{(1)}(X_m; Y_m).$$

In this section, we will prove $Z_{AD}^{(k)}(X_m; Y_m; 0) = Z_{AD}^{(1)}(X_m; Y_m)$ combinatorially, by constructing a weight-preserving bijection between k -tilings of the Aztec diamond with $t = 0$ and domino tilings of the Aztec diamond. This bijection can be expressed nicely in terms of Schröder paths. Label the starting and ending points of the paths as follows.



Note that starting point i and ending point i can be connected via $m - i + 1$ horizontal steps.

Before constructing the bijection, we need a better understanding of the behavior of the Schröder paths when $t = 0$. We begin with the case $k = 2$. We let blue be color 1 and red be color 2.

Proposition 4.4.3 ([20, Prop. 5.1]). *When $t = 0$, for any 2-tiling of the rank m Aztec diamond with non-zero weight:*

1. If $i < \frac{m+1}{2}$, then the i -th blue path is forced to have its first i steps be horizontal while the i -th red path is forced to have its first $i - 1$ steps be horizontal.
2. If $i = \lfloor \frac{m}{2} + 1 \rfloor$, then the i -th blue path is forced to have all its steps be horizontal while the i -th red path is forced to have its first $i - 1$ steps horizontal.
3. If $i \geq \lceil \frac{m}{2} + 1 \rceil$, then the i -th blue path is forced to have all its steps be horizontal and the i -th red path is forced to have all its steps horizontal.

In other words, the i -th blue path starts with $\min(i, m - i + 1)$ horizontal steps, and the i -th red path starts with $\min(i - 1, m - i + 1)$ horizontal steps.

Proof. We begin with three important observations.

1. The i -th and j -th paths of the same color may not intersect for $i \neq j$. This implies (using a simple induction argument from the m -th path to the 1st path) that the i -th path of each color may not go below the horizontal line connecting starting point i and ending point i .
2. The i -th blue path and the j -th red path may not intersect for $i < j$ when $t = 0$. The i -th blue path starts above the j -th red path, so if they did intersect, then at the first point of intersection, the blue path would meet the red path from above, which gives a t .
3. Suppose a blue path and a red path meet at two points A and Z , with A left of Z . Consider the behavior of the two paths at A . If both paths go up-right, then we get a t . If the blue path goes up-right and the red path goes horizontal or down-right, then the blue path is above the red path, but the two paths both reach Z later, so eventually the blue path will meet the red path from above, which gives a t . Thus, when $t = 0$, the blue path must not go up-right at A .

The 1st blue path and the 1st red path start at the same point and end at the same point. Therefore, by observation 3, the 1st blue path must start with a horizontal step.

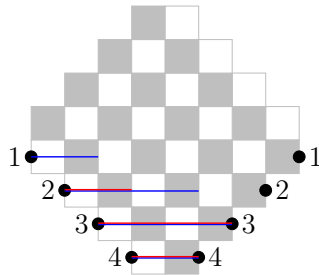
Now assume the proposition holds for the first $i - 1$ paths of both colors. We will show the proposition holds for the i -th paths. Suppose $i < m - i + 1$. We know the $(i - 1)$ -th blue path begins with $i - 1$ horizontal steps, so the i -th blue path must begin with $i - 1$ horizontal steps by observation 1, and moreover the i -th red path must begin with $i - 1$ horizontal steps by observation 2. Since the i -th blue path and the i -th red path begin by taking $i - 1$ horizontal steps together, the i -th blue path must take another horizontal step. (It can't go up-right by observation 3,

and it can't go down-right by observation 1.) Thus the i -th blue path begins with i horizontal steps. If we suppose instead that $i \geq m - i + 1$, then the same argument works, except the paths are forced to take all their steps horizontally. \square

Corollary 4.4.4 ([20, Cor. 5.2]). *When $t = 0$, for any 2-tiling of the rank m Aztec diamond with non-zero weight, the i -th blue path is weakly below the i -th red path and strictly above the $(i + 1)$ -th red path.*

Proof. The fact that the i -th blue path is strictly above the $(i + 1)$ -th red path follows from observation 2 (and the fact that the i -th blue path starts above the $(i + 1)$ -th red path). If the i -th blue path were ever strictly above the i -th red path, then since these paths end at the same point, there must be a point where the i -th blue path meets the i -th red path from above, giving a \square .

We will refer to the forced steps described in Prop. 4.4.3 as the frozen parts of the paths. For example, when $k = 2$ and $m = 4$, the frozen paths are as follows.



We are now ready to construct the bijection in the case $k = 2$.

Proposition 4.4.5 ([20, Prop. 5.3]). *There is a weight-preserving bijection between 2-tilings of the rank m Aztec diamond at $t = 0$ and domino tilings of the rank m Aztec diamond, given by shifting the i -th blue path down i steps and left i steps, and shifting the i -th red path down $i - 1$ steps and left $i - 1$ steps.*

Proof. By Prop. 4.4.3, it is easy to see that after shifting the paths, the frozen part of each path is shifted completely outside the Aztec diamond and the non-frozen part of each path remains inside the Aztec diamond. Since the i -th blue path is weakly below the i -th red path and strictly above the $(i + 1)$ -th red path before the shift by Cor. 4.4.4, after the shift it is strictly below the i -th red path and strictly above the $(i + 1)$ -th red path. That is, now the paths are non-intersecting. Non-intersecting Schröder paths are in bijection with domino tilings of the Aztec diamond. Since a horizontal step has a weight of 1, it follows that the bijection is weight-preserving. \square

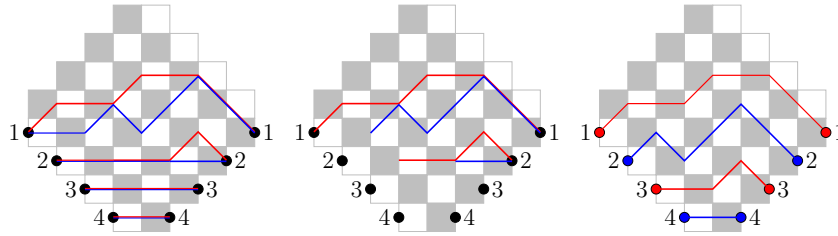


Figure 4.13: Example of the bijection at $t = 0$ for $k = 2$: the 2-tuple of paths (left), the paths without the frozen steps (middle), and the 1-tuple of paths (right)

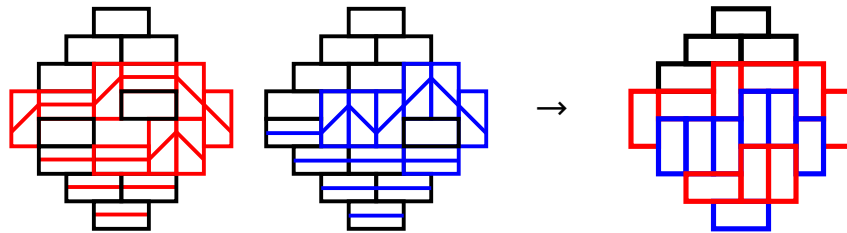


Figure 4.14: Example of the bijection at $t = 0$ for $k = 2$: the 2-tiling with the frozen dominos in black (left) and the corresponding 1-tiling (right)

An example of the bijection for two colors is given in Figure 4.13. The bijection can also be defined directly on the tilings (see Figure 4.14).

With this bijection, along with Theorem 4.1.2, we can compute the arctic curve for k -tilings of the Aztec diamond when $t = 0$ (see Figure 4.15). For each m , consider a uniformly random k -tiling of the Aztec diamond of rank m . We scale each tiling by a factor $1/m$ in each axis to fit into the limiting diamond $AD_\infty = \{|x| + |y| \leq 1\}$. In the case $k = 2$, we get the following result.

Theorem 4.4.6 ([20, Thm. 5.4]). *When $t = 0$, the arctic curves (for both colors) for 2-tilings of the Aztec diamond are given by*

$$\begin{cases} x^2 + y^2 = \frac{1}{2}, & x \in [-\frac{1}{2}, \frac{1}{2}], y > \frac{1}{2} \\ (x + y)^2 + (2y)^2 = \frac{1}{2}, & x \in [-\frac{1}{4}, \frac{3}{4}], y < -\frac{1}{4} \\ \left(\frac{3x+y-1}{2}\right)^2 + \left(\frac{3y+x-1}{2}\right)^2 = \frac{1}{2}, & y \in [-\frac{1}{4}, \frac{1}{2}], x > -\frac{1}{3}y + \frac{2}{3} \\ \left(\frac{3x+y-1}{4}\right)^2 + \left(\frac{5y-x-1}{4}\right)^2 = \frac{1}{2}, & y \in [-\frac{1}{4}, \frac{1}{2}], x < -\frac{1}{3}y - \frac{1}{3} \end{cases}$$

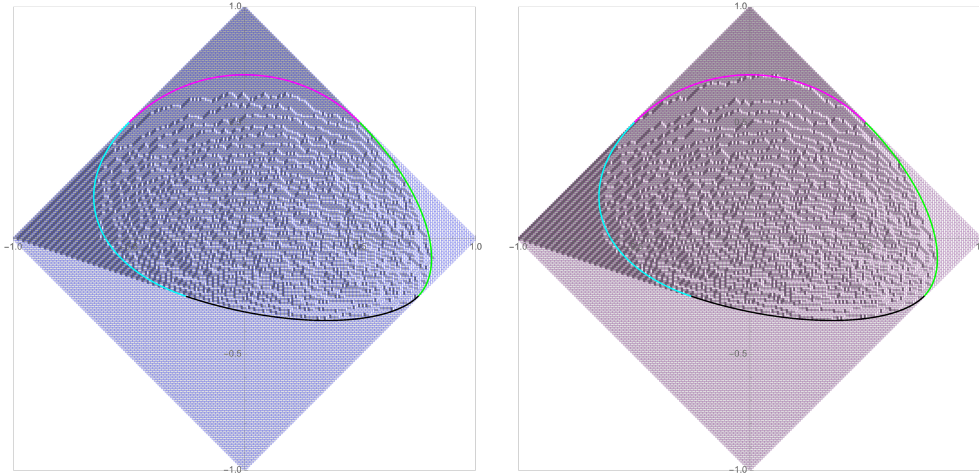


Figure 4.15: Simulation and computed arctic curve for a 2-tiling of the Aztec diamond of rank 128 for $t = 0$

Proof. From Theorem 4.1.2, we know that for the normal Aztec diamond the arctic curve is the circle $x^2 + y^2 = \frac{1}{2}$. Reversing the bijection in the previous proposition determines how one should deform the circle to get the arctic curve for the 2-tilings of the Aztec diamond of rank m when $m \rightarrow \infty$. (Each piece of the arctic circle becomes a piece of a different ellipse.)

For example, in terms of the Schröder paths, the upper portion of the arctic curve separates the region of no paths from the disordered region inside the arctic curve. This boundary is determined by the asymptotic trajectory of the upper most path. As this path doesn't shift under our bijection, the portion of the arctic curve remains the same. This gives us the first region of the theorem: $x^2 + y^2 = \frac{1}{2}$ for $x \in [-\frac{1}{2}, \frac{1}{2}]$, $y > \frac{1}{2}$.

Now consider the western portion of the arctic curve. For 1-tilings of the Aztec diamond, this section of the arctic curve separates the region of up-right paths from the disordered region. Recall that the $2i$ -th path of the 1-tiling of the Aztec diamond maps to the i -th blue path, and the $(2i - 1)$ -th path of the 1-tiling of the Aztec diamond maps to the i -th red path. Reversing the bijection means shifting these paths up and right i steps or $i - 1$ steps, respectively.

Suppose that our Aztec diamond has rank m and we rescale it by a factor of $\frac{1}{m}$ in each axis. Now each square of our checkerboard has size $\frac{1}{m} \times \frac{1}{m}$. Then the starting

location of the $2i$ -th path is at the coordinate

$$(x_{2i}, y_{2i}) = \left(-1 + \frac{2i-1}{m}, -\frac{2i-1}{m} - \frac{1}{2m} \right).$$

Reversing the bijection will shift the $2i$ -th path of the 1-tiling up and right by

$$\frac{i}{m} = \frac{1}{4}(x_{2i} - y_{2i} + 1) + O\left(\frac{1}{m}\right),$$

where it will become the i -th blue path in the 2-tiling. In fact, since we are considering the frozen region of up-right paths, any point (x, y) along the $2i$ -th path will also shift by $\frac{1}{4}(x - y + 1) + O(\frac{1}{m})$. The same holds for the $(2i - 1)$ -th path, except that it will become the i -th red path in the 2-tiling.

Now we take $m \rightarrow \infty$. With this choice of coordinates, any point (x, y) in this region of up-right paths in the 1-tiling of the Aztec diamond maps to a point in the blue or red Aztec diamond according to

$$(x, y) \mapsto \left(x + \frac{x - y + 1}{4}, y + \frac{x - y + 1}{4} \right) = \left(\frac{5x - y + 1}{4}, \frac{x + 3y + 1}{4} \right).$$

Since the arctic curve separating the region of up-right paths from the disordered region in the 1-tiling is given by $x^2 + y^2 = \frac{1}{2}$ with $x < -\frac{1}{2}$, $-\frac{1}{2} < y < \frac{1}{2}$, after inverting the above map, we see that the arctic curve in the 2-tiling is given by

$$\left(\frac{3x + y - 1}{4} \right)^2 + \left(\frac{5y - x - 1}{4} \right)^2 = \frac{1}{2} \text{ with } -1 < \frac{3x + y - 1}{4} < -\frac{1}{2} \text{ and } -\frac{1}{2} < \frac{5y - x - 1}{4} < \frac{1}{2}$$

for both colors. We can simplify the constraints to $y \in [-\frac{1}{4}, \frac{1}{2}]$, $x < -\frac{1}{3}y - \frac{1}{3}$, and we get the last region in the theorem.

The remaining two portions of the arctic curve can be worked out similarly. \square

It is straightforward to generalize our discussion for 2-tilings to k -tilings. We end up with the following bijection.

Proposition 4.4.7 ([20, Prop. 5.5]). *For any $k \geq 1$, there is a weight-preserving bijection between k -tilings of the rank m Aztec diamond at $t = 0$ and domino tilings of the rank m Aztec diamond, given by shifting the i -th path of color a down $i(k-1)-a+1$ steps and left $i(k-1) - a + 1$ steps.*

In other words, the new order of the paths is

path 1 color k , ..., path 1 color 1,
 path 2 color k , ..., path 2 color 1,
 path 3 color k , ..., path 3 color 1,
 ...

i.e. path i color a becomes path $(i - 1)k + (k - a + 1)$. Using this bijection, we can then compute the arctic curve for k -tilings when $t = 0$, which is Theorem 4.1.4.

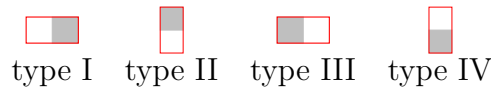
The case $t \rightarrow \infty$ and other values of t

In this section, we compute the arctic curve for the k -tilings of the Aztec diamond as $t \rightarrow \infty$. We do this by defining a bijection between k -tilings with no interactions (i.e. $t = 0$) and k -tilings with the maximum possible number of interactions (i.e. $t \rightarrow \infty$). Then we can apply the arctic curve computations in the $t = 0$ case given in the previous section.

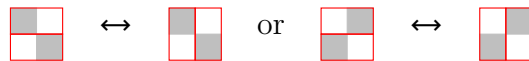
Let ϕ be the involution on the set of k -tilings of the Aztec diamond of rank m given by reflecting over the line $y = x$. This involution leads to the following lemma.

Lemma 4.4.8 ([20, Lemma 6.1]). *Let \mathbf{T} be a k -tiling of the Aztec diamond of rank m with j interactions. Then $\phi(\mathbf{T})$ is a k -tiling of the Aztec diamond of rank m with $\binom{k}{2} \binom{m+1}{2} - j$ interactions.*

Proof. The dominos are of four types, as shown below.



In the 1-tiling where all dominos are horizontal, there are $\binom{m+1}{2}$ dominos of type I or II. When we perform a flip



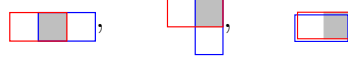
the number of dominos of type I or II is unchanged, and we can get all 1-tilings starting from the 1-tiling where all dominos are horizontal and performing flips. Therefore there are $\binom{m+1}{2}$ dominos of type I or II in every 1-tiling of the Aztec diamond of rank m .

When applying ϕ , the dominos of type I become dominos of type II (and vice versa), and the dominos of type III become dominos of type IV (and vice versa).

Fix a k -tiling \mathbf{T} . Suppose \mathbf{T} has j interactions and $\phi(\mathbf{T})$ has ℓ interactions. Fix two colors a (blue) $<$ b (red). When a red domino is of type I, we get a power of t for



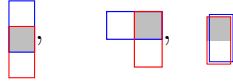
in which case we say the red domino is in case I-A with the color blue, and no power of t for



in which case we say the red domino is in case I-B with the color blue. When a red domino is of type II, we get no power of t for



in which case we say the red domino is in case II-A with the color blue, and a power of t for



in which case we say the red domino is in case II-B with the color blue. The red dominos of type III or IV never get a power of t . Therefore

$$\begin{aligned}
 j + \ell &= \sum_{1 \leq a < b \leq k} \sum_{\substack{\text{dominos } D \\ \text{of color } b}} \mathbf{1}_{D \text{ is in case I-A or II-B with } a} + \sum_{1 \leq a < b \leq k} \sum_{\substack{\text{dominos } D \\ \text{of color } b}} \mathbf{1}_{D \text{ is in case I-B or II-A with } a} \\
 &= \sum_{1 \leq a < b \leq k} \sum_{\substack{\text{dominos } D \\ \text{of color } b}} \mathbf{1}_{D \text{ is in case I-A, I-B, II-A, or II-B with } a} \\
 &= \sum_{1 \leq a < b \leq k} \sum_{\substack{\text{dominos } D \\ \text{of color } b}} \mathbf{1}_{D \text{ has type I or II}} \\
 &= \sum_{1 \leq b \leq k} (b - 1) \sum_{\substack{\text{dominos } D \\ \text{of color } b}} \mathbf{1}_{D \text{ has type I or II}} \\
 &= \sum_{1 \leq b \leq k} (b - 1) \binom{m + 1}{2} \\
 &= \binom{k}{2} \binom{m + 1}{2}.
 \end{aligned}$$

□

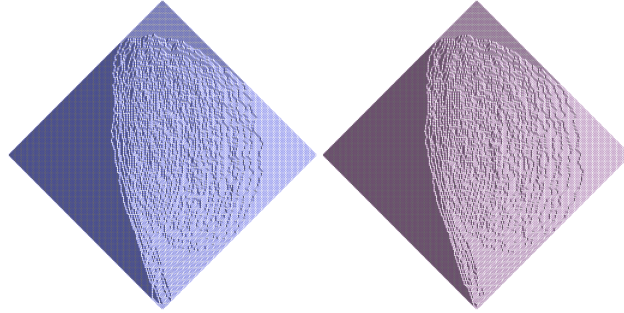


Figure 4.16: Simulation of a 2-tiling Aztec diamond of rank 128 for $t = 1000$

Thus ϕ is a bijection between k -tilings for $t = 0$ and k -tilings for $t \rightarrow \infty$. Thus ϕ relates the $t = 0$ arctic curve and the $t \rightarrow \infty$ arctic curve, and Cor. 4.1.5 follows. See Figure 4.16.

Moreover, ϕ relates the $t = t_0$ arctic curve and the $t = 1/t_0$ arctic curve, for fixed $t_0 > 0$:

Corollary 4.4.9. *Fix $t_0 > 0$. Then reflecting the arctic curve for k -tilings of the Aztec diamond when $t = t_0$ for color i over the line $y = x$ gives the arctic curve for k -tilings of the Aztec diamond when $t = 1/t_0$ for color i .*

Proof. Recall Definition 4.4.1. Using Lemma 4.4.8 and letting $c = \binom{k}{2} \binom{m+1}{2}$, we have

$$\begin{aligned}
 p(\mathbf{T}; t_0) &= t_0^{\# \text{ interactions in } \mathbf{T}} / \sum_{\mathbf{S}} t_0^{\# \text{ interactions in } \mathbf{S}} \\
 &= t_0^{c - \# \text{ interactions in } \phi(\mathbf{T})} / \sum_{\mathbf{S}} t_0^{c - \# \text{ interactions in } \phi(\mathbf{S})} \\
 &= t_0^{-\# \text{ interactions in } \phi(\mathbf{T})} / \sum_{\mathbf{S}} t_0^{-\# \text{ interactions in } \phi(\mathbf{S})} \\
 &= (1/t_0)^{\# \text{ interactions in } \phi(\mathbf{T})} / \sum_{\mathbf{S}} (1/t_0)^{\# \text{ interactions in } \phi(\mathbf{S})} \\
 &= (1/t_0)^{\# \text{ interactions in } \phi(\mathbf{T})} / \sum_{\mathbf{S}} (1/t_0)^{\# \text{ interactions in } \mathbf{S}} \\
 &= p(\phi(\mathbf{T}); 1/t_0).
 \end{aligned}$$

Let $f(x, y) = 0$ be the arctic curve when $t = t_0$ for color i , meaning that for all $\epsilon > 0$,

$$\lim_{m \rightarrow \infty} \sum_{\mathbf{T} \text{ s.t. } A(f, \mathbf{T})} p(\mathbf{T}; t_0) = 1$$

where $A(f, \mathbf{T})$ is the condition

$$\{(x, y) \in AD_\infty : f(x, y) > \epsilon\} \cap \left(\frac{1}{m}AD_m\right) \subset P_m(T_i) \subset \{(x, y) \in AD_\infty : f(x, y) > -\epsilon\}.$$

Let $g(x, y) = 0$ be the result of reflecting $f(x, y) = 0$ over $y = x$. Then $A(f, \mathbf{T})$ if and only if $A(g, \Phi(\mathbf{T}))$. Thus

$$\begin{aligned} \lim_{m \rightarrow \infty} \sum_{\mathbf{T} \text{ s.t. } A(g, \mathbf{T})} p(\mathbf{T}; 1/t_0) &= \lim_{m \rightarrow \infty} \sum_{\mathbf{T} \text{ s.t. } A(g, \Phi(\mathbf{T}))} p(\Phi(\mathbf{T}); 1/t_0) \\ &= \lim_{m \rightarrow \infty} \sum_{\mathbf{T} \text{ s.t. } A(f, \mathbf{T})} p(\mathbf{T}; t_0) = 1 \end{aligned}$$

so $g(x, y)$ is the arctic curve when $t = 1/t_0$ for color i . □

See Figure 4.17.

Remark 4.4.10. *In this chapter, we have computed the arctic curves for k -tilings of the Aztec diamond when $t = 0, 1$ and $t \rightarrow \infty$. Our current techniques do not generalize to any other values of t . We leave it as an open problem to compute the arctic curves for the k -tilings of the Aztec diamond for other values of t . See Figure 4.18 for an example with $t = 5$.*

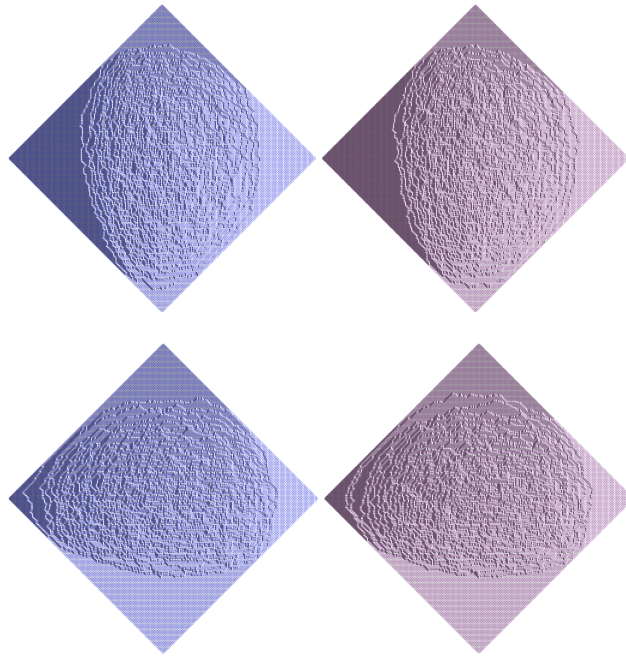


Figure 4.17: Top: Simulation of a rank 128 Aztec diamond for $t = 3$. Bottom: Simulation of a rank 128 Aztec diamond for $t = 1/3$.

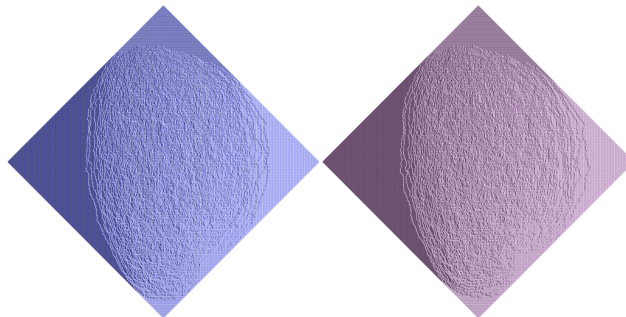


Figure 4.18: Simulation of a 2-tiling of a rank 256 Aztec diamond for $t = 5$. Note the formation of a cusp along the South-East boundary of the Aztec diamond.

Bibliography

- [1] Amol Aggarwal, Alexei Borodin, and Michael Wheeler. “Colored fermionic vertex models and symmetric functions”. In: *arXiv preprint arXiv:2101.01605* (2021).
- [2] Federico Ardila. “Algebraic and geometric methods in enumerative combinatorics”. English. In: *Handbook of enumerative combinatorics*. Boca Raton, FL: CRC Press, 2015, pp. 3–172. ISBN: 978-1-4822-2085-8.
- [3] Arvind Ayyer, Olya Mandelshtam, and James B Martin. “Stationary probabilities of the multispecies TAZRP and modified Macdonald polynomials: I”. In: *arXiv preprint arXiv:2011.06117* (2020).
- [4] Rodney J Baxter. *Exactly solved models in statistical mechanics*. Elsevier, 2016.
- [5] V Bazhanov and A Shadrnikov. “Trigonometric solutions of triangle equations. Simple lie superalgebras”. In: *Theor. Math. Phys.* 73.3 (1987), pp. 402–419.
- [6] Allan Berele and Amitai Regev. “Hook Young diagrams with applications to combinatorics and to representations of Lie superalgebras”. In: *Adv. in Math.* 64.2 (1987), pp. 118–175.
- [7] Jonah Blasiak et al. “A shuffle theorem for paths under any line”. In: *arXiv preprint arXiv:2102.07931* (2020).
- [8] Alexei Borodin and Michael Wheeler. “Coloured stochastic vertex models and their spectral theory”. In: *arXiv preprint arXiv:1808.01866* (2018).
- [9] Alexei Borodin and Michael Wheeler. “Nonsymmetric Macdonald polynomials via integrable vertex models”. In: *arXiv preprint arXiv:1904.06804* (2019).
- [10] Cédric Boutillier et al. “Dimers on rail yard graphs”. In: *Ann. Inst. Henri Poincaré D* 4.4 (2017), pp. 479–539. ISSN: 2308-5827. DOI: 10.4171/AIHPD/46.
- [11] Jérémie Bouttier, Guillaume Chapuy, and Sylvie Corteel. “From Aztec diamonds to pyramids: steep tilings”. In: *Trans. Amer. Math. Soc.* 369.8 (2017), pp. 5921–5959. ISSN: 0002-9947. DOI: 10.1090/tran/7169.

- [12] Ben Brubaker, Daniel Bump, and Solomon Friedberg. “Schur polynomials and the Yang-Baxter equation”. In: *Comm. Math. Phys.* 308.2 (2011), p. 281.
- [13] Ben Brubaker et al. “Colored five-vertex models and Demazure atoms”. In: *arXiv preprint arXiv:1902.01795* (2019).
- [14] Ben Brubaker et al. “Colored vertex models and Iwahori Whittaker functions”. In: *arXiv preprint arXiv:1906.04140* (2019).
- [15] Ben Brubaker et al. “Vertex operators, solvable lattice models and metaplectic Whittaker functions”. In: *Comm. Math. Phys.* 380.2 (2020), pp. 535–579.
- [16] Valentin Buciumas, Travis Scrimshaw, and Katherine Weber. “Colored five-vertex models and Lascoux polynomials and atoms”. In: *J. Lond. Math. Soc.* (2020).
- [17] Henry Cohn, Noam Elkies, and James Propp. “Local statistics for random domino tilings of the Aztec diamond”. In: *Duke Math. J.* 85.1 (1996), pp. 117–166. ISSN: 0012-7094. DOI: 10.1215/S0012-7094-96-08506-3.
- [18] Henry Cohn, Richard Kenyon, and James Propp. “A variational principle for domino tilings”. In: *J. Amer. Math. Soc.* 14 (2001), pp. 297–346.
- [19] Henry Cohn, Michael Larsen, and James Propp. “The shape of a typical boxed plane partition”. In: *New York J. Math.* 4 (1998), pp. 137–165.
- [20] Sylvie Corteel, Andrew Gitlin, and David Keating. “Colored vertex models and k-tilings of the Aztec diamond”. In: *arXiv preprint arXiv:2202.06020* (2022).
- [21] Sylvie Corteel, Olya Mandelshtam, and Lauren Williams. “From multiline queues to Macdonald polynomials via the exclusion process”. In: *arXiv preprint arXiv:1811.01024* (2018).
- [22] Sylvie Corteel et al. “A vertex model for LLT polynomials”. In: *Int. Math. Research Notices* (2021). rnab165. ISSN: 1073-7928. DOI: 10.1093/imrn/rnab165.
- [23] Michael Curran et al. “A lattice model for LLT polynomials”. In: (2019). URL: <https://www-users.cse.umn.edu/~reiner/REU/CurranYostWolffZhangZhang2019.pdf>.
- [24] Noam Elkies et al. “Alternating-sign matrices and domino tilings. I”. In: *J. Algebraic Combin.* 1.2 (1992), pp. 111–132. ISSN: 0925-9899. DOI: 10.1023/A:1022420103267.
- [25] Noam Elkies et al. “Alternating-sign matrices and domino tilings. II”. In: *J. Algebraic Combin.* 1.3 (1992), pp. 219–234. ISSN: 0925-9899. DOI: 10.1023/A:1022483817303.

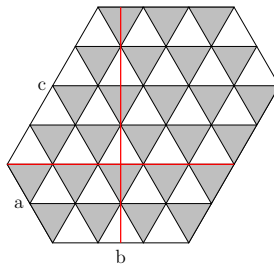
- [26] Sen-Peng Eu and Tung-Shan Fu. “A simple proof of the Aztec diamond theorem”. In: *Electron. J. Combin.* 12 (2005), Research Paper R18, 8. URL: http://www.combinatorics.org/Volume_12/Abstracts/v12i1r18.html.
- [27] Alexandr Garbali and Michael Wheeler. “Modified Macdonald polynomials and integrability”. In: *Comm. Math. Phys.* (2020), pp. 1–68.
- [28] Andrew Gitlin and David Keating. “A vertex model for supersymmetric LLT polynomials”. In: *arXiv preprint arXiv:2110.10273* (2021).
- [29] Ian Grojnowski and Mark Haiman. “Affine Hecke algebras and positivity of LLT and Macdonald polynomials”. In: *Unpublished manuscript* (2007).
- [30] James Haglund et al. “A combinatorial formula for the character of the diagonal coinvariants”. In: *Duke Math. J.* 126.2 (2005), pp. 195–232.
- [31] Jim Haglund, Mark Haiman, and Nick Loehr. “A combinatorial formula for Macdonald polynomials”. In: *J. Amer. Math. Soc.* 18.3 (2005), pp. 735–761.
- [32] Kazuto Iijima. “A q -multinomial expansion of LLT coefficients and plethysm multiplicities”. In: *European J. Combin.* 34.6 (2013), pp. 968–986.
- [33] William Jockusch, James Propp, and Peter Shor. “Random Domino Tilings and the Arctic Circle Theorem”. In: *arXiv preprint arXiv:9801068* (1998).
- [34] Kurt Johansson. “Edge fluctuations of limit shapes”. In: *Current developments in mathematics 2016*. Int. Press, Somerville, MA, 2018, pp. 47–110.
- [35] Kurt Johansson. “Non-intersecting paths, random tilings and random matrices.” In: *Probab. Theory Related Fields* 123.2 (2002), pp. 249–260.
- [36] Kurt Johansson. “The arctic circle boundary and the Airy process”. In: *Ann. Probab.* 33.1 (2005), pp. 1–30. ISSN: 0091-1798. DOI: 10.1214/009117904000000937.
- [37] Petr Petrovich Kulish, Nicolai Yuryevich Reshetikhin, and Evgeny Konstantinovich Sklyanin. “Yang-Baxter equations and representation theory. I.” In: *Lett. Math. Phys.* 5.5 (1981), pp. 393–403.
- [38] Thomas Lam. “Ribbon tableaux and the Heisenberg algebra”. In: *Mathematische Zeitschrift* 250.3 (2005), pp. 685–710.
- [39] Alain Lascoux, Bernard Leclerc, and Jean-Yves Thibon. “Ribbon tableaux, Hall–Littlewood functions, quantum affine algebras, and unipotent varieties”. In: *J. Math. Phys.* 38.2 (1997), pp. 1041–1068.
- [40] Bernard Leclerc and Jean-Yves Thibon. “Littlewood–Richardson Coefficients and Kazhdan–Lusztig Polynomials”. In: *Combinatorial Methods in Representation Theory*. Tokyo, Japan: Mathematical Society of Japan, 2000, pp. 155–220. DOI: 10.2969/aspm/02810155.

- [41] D. E. Littlewood. “Modular Representations of Symmetric Groups”. In: *Proceedings of the Royal Society of London. Series A, Mathematical and Physical Sciences* 209.1098 (1951), pp. 333–353. ISSN: 00804630. URL: <http://www.jstor.org/stable/98912>.
- [42] George Lusztig. “Green polynomials and singularities of unipotent classes”. In: *Adv. Math.* 42.2 (1981), pp. 169–178.
- [43] Ian Grant Macdonald. *Symmetric functions and Hall polynomials*. Oxford University Press, 1998.
- [44] Percy A. MacMahon. *Combinatory Analysis*. Vol. 2. Cambridge University Press, 1916.
- [45] Christopher Roman Miller. “On the k-Schur Positivity of k-Bandwidth LLT Polynomials”. PhD thesis. UC Berkeley, 2019.
- [46] Els Moens. “Supersymmetric Schur functions and Lie superalgebra representations”. PhD thesis. Ghent University, 2007.
- [47] Stephan Pfannerer. “A refinement of the Murnaghan-Nakayama rule by descents for border strip tableaux”. In: *arXiv preprint arXiv:2105.13750* (2021).
- [48] N Reshetikhin. “Lectures on the integrability of the six-vertex model”. In: *Exact Methods in Low-Dimensional Statistical Physics and Quantum Computing* (2010), pp. 197–266.
- [49] Dan Romik. “Arctic circles, domino tilings and square Young tableaux”. In: *Ann. Probab.* 40.2 (2012), pp. 611–647. ISSN: 0091-1798. DOI: 10.1214/10-AOP628.
- [50] Mark Shimozono and Jerzy Weyman. “Graded characters of modules supported in the closure of a nilpotent conjugacy class”. In: *European J. Combin.* 21.2 (2000), pp. 257–288.
- [51] Richard P Stanley. “Enumerative Combinatorics, vol. 2.” In: *Cambridge Stud. Adv. Math.* (1999).
- [52] Dennis W Stanton and Dennis E White. “A Schensted algorithm for rim hook tableaux”. In: *J. Combin. Theory Ser. A* 40.2 (1985), pp. 211–247.
- [53] Michael Wheeler and Paul Zinn-Justin. “Refined Cauchy/Littlewood identities and six-vertex model partition functions: III. Deformed bosons”. In: *Adv. Math.* 299 (2016), pp. 543–600. ISSN: 0001-8708. DOI: 10.1016/j.aim.2016.05.010. URL: <http://www.sciencedirect.com/science/article/pii/S0001870815301687>.

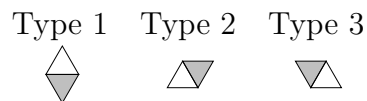
Appendix A

Lozenge tilings of the hexagon

We tile the plane with equilateral triangles with side length one, either pointing up \triangle or pointing down ∇ ; we shade the former white and the latter gray. The $a \times b \times c$ hexagon is the following region in \mathbb{R}^2 .



(The coordinate axes are in red. The y -axis goes through the midpoint of the bottom edge of length b , and the x -axis goes through the intersection of the leftmost edges of lengths a and c .) A lozenge is a pair of two triangles sharing an edge. There are three types of lozenges:



A lozenge tiling of a region is a partitioning of the region into non-overlapping lozenges, and a k -tiling is a k -tuple of lozenge tilings. We will consider k -tilings of the $a \times b \times c$ hexagon.

Much is already known in the case $k = 1$. The asymptotic behavior of lozenge tilings of the $sa \times sb \times sc$ hexagon (for fixed a, b, c) when $s \rightarrow \infty$ exhibits an arctic curve phenomenon, similar to that of domino tilings of the rank m Aztec diamond when $m \rightarrow \infty$ (Theorem 4.1.2).

Theorem A.0.1 ([19]). *For each a , consider a uniformly random lozenge tiling of the $a \times a \times a$ hexagon H_a scaled by a factor of $\frac{2}{a}$ in each axis to fit into the limiting $2 \times 2 \times 2$ hexagon H_∞ and let P_a be the image of the polar regions of the random tiling under this scaling transformation. Then, for all $\epsilon > 0$, as $a \rightarrow \infty$,*

$$\{(x, y) \in H_\infty : x^2 + y^2 > 3 + \epsilon\} \cap \left(\frac{2}{a}H_a\right) \subset P_a \subset \{(x, y) \in AD_\infty : x^2 + y^2 > 3 - \epsilon\}$$

holds with probability tending to 1.

See the tiling on the left of Figure A.2 for an example. In the rest of this section, we say that the arctic curve of the $a \times a \times a$ hexagon is the circle

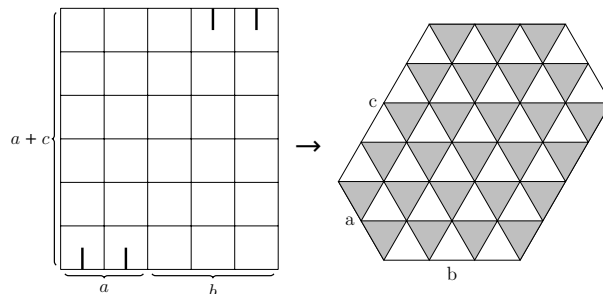
$$x^2 + y^2 = 3.$$

More generally, the arctic curve of the $a \times b \times c$ hexagon (where we take a uniformly random lozenge tiling of the $sa \times sb \times sc$ hexagon scaled by $\frac{2}{sa}$ in each axis and then take $s \rightarrow \infty$) is the largest inscribed ellipse (in the limiting $2 \times \frac{2b}{a} \times \frac{2c}{a}$ hexagon) [18].

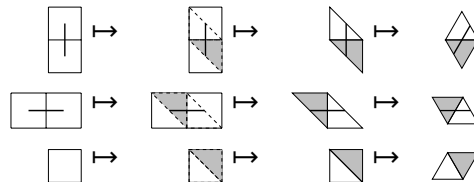
We define the weight of a tiling T of the $a \times b \times c$ hexagon by

$$w(T) = \prod_{i=1}^{a+c} x_i^{\#\text{ lozenges in } T \text{ of type } 2 \text{ in row } i}$$

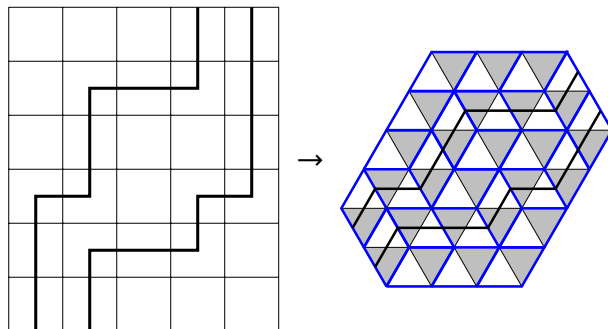
where we label the rows of triangles $1, \dots, a + c$ from bottom to top. There is a weight-preserving bijection between $LC(W_{a+c}(\boldsymbol{\lambda}))$, where λ is the partition (b^a) and $\boldsymbol{\lambda}$ is the 1-tuple (λ) , and lozenge tilings of the $a \times b \times c$ hexagon.



To construct this bijection, we map paths to lozenges via



and then remove all frozen sections of paths (that is, the first $i - 1$ steps of the i -th rightmost path, which must be vertical steps, for all $i \in [a]$). For example:



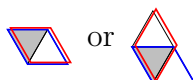
We define the generating function for lozenge tilings of the $a \times b \times c$ hexagon to be

$$Z_{a,b,c}(X_{a+c}) = \sum_{\mathbf{T}} w(\mathbf{T})$$

where the sum is over lozenge tilings of the $a \times b \times c$ hexagon. Using this weight-preserving bijection, we get

$$Z_{a,b,c}(X_{a+c}) = s_{(b^a)}(X_{a+c}).$$

Now fix the number of colors k . We can extend this bijection to a bijection between $LC(W_{a+c}(\boldsymbol{\lambda}))$, where $\boldsymbol{\lambda} = ((b^a)^k)$, and k -tilings of the $a \times b \times c$ hexagon as follows. Map paths of each color to colored lozenges as described above. Note that in terms of the lozenges, we get a power of t for every interaction, where an interaction is a pair of lozenges of the form



when blue is a smaller color than red. We define the weight of a k -tiling \mathbf{T} to be

$$w(\mathbf{T}) = w(T_1, \dots, T_k) = t^{\#\text{interactions in } \mathbf{T}} \prod_{i=1}^k w(T_i)$$

and we define the generating function for k -tilings of the $a \times b \times c$ hexagon to be

$$Z_{a,b,c}^{(k)}(X_{a+c}; t) = \sum_{\mathbf{T}} w(\mathbf{T})$$

where the sum is over k -tilings of the $a \times b \times c$ hexagon. Then this bijection is weight-preserving, so we get

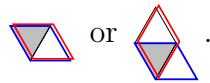
$$Z_{a,b,c}^{(k)}(X_{a+c}; t) = \mathcal{L}_{\boldsymbol{\lambda}}(X_{a+c}; t).$$

First, we consider a symmetry of the k -tilings.

Proposition A.0.2 ([20, Prop. A.2]). *Reflecting over the y -axis and reversing the order of the colors gives a bijection between k -tilings of the $a \times b \times c$ hexagon and k -tilings of the $c \times b \times a$ hexagon such that a configuration with $\binom{k}{2}(ab - bc) + j$ interactions maps to a configuration with j interactions.*

Proof. Let ϕ be the bijection described in the statement of the proposition. Note that every tiling of an $a \times b \times c$ hexagon has ac lozenges of type 1, bc lozenges of type 2, and ab lozenges of type 3. Under ϕ , lozenges of type 2 map to those of type 3 and vice versa, while those of type 1 stay the same.

Consider any pair of colors $\alpha < \beta$. We'll draw color α as blue and color β as red. Consider the 2-tiling (T_α, T_β) . Recall the lozenges that give an interaction are



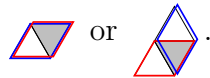
Note that

$$\# \left(\text{blue lozenge with red triangle} \right) + \# \left(\text{red lozenge with blue triangle} \right) + \# \left(\text{blue triangle with red lozenge} \right) = ab$$

since the number of blue lozenges of type 3 is ab . Rearranging we have

$$\# \left(\text{blue lozenge with red triangle} \right) + \# \left(\text{red lozenge with blue triangle} \right) = ab - \# \left(\text{blue triangle with red lozenge} \right) \tag{A.1}$$

The lozenges in (T_α, T_β) that will count as an interaction after applying ϕ are of the form



Similarly to the previous calculation, we have

$$\# \left(\text{blue lozenge with red triangle} \right) + \# \left(\text{red lozenge with blue triangle} \right) = bc - \# \left(\text{blue triangle with red lozenge} \right). \tag{A.2}$$

Subtracting (A.2) from (A.1), we see that the difference in the number of interactions is constant, and in particular, it is $ab - bc$. Doing this for every pair of colors $\alpha < \beta$ gives the result. \square

Similar to the Aztec diamond, for special values of t we have bijections with 1-tilings.

Proposition A.0.3 ([20, Prop. A.3]). *There is a bijection between 2-tilings of the $a \times b \times c$ hexagon at $t = 0$ and lozenge tilings of the $2a \times b \times (c - a)$ hexagon. (If $a > c$, then there are no 2-tilings of the $a \times b \times c$ hexagon at $t = 0$.)*

Proof. In terms of the vertex model, we need to exhibit a bijection between lattice configurations of $W_{a+c}((b^a)^2)$ at $t = 0$ and lattice configurations of $W_{a+c}((b^{2a})^1)$. A similar sliding argument as in Section 4.4 works again.

More precisely, let blue be color 1 and let red be color 2, and label the paths of each color $1, \dots, a$ by starting column from left to right. Shift red path i right i columns, and shift blue path i right by $i - 1$ columns. We claim that now the paths are non-intersecting.

We can see this by first noting that when $t = 0$, red path i must be weakly right of blue path i ; they start at the same place, and the blue path can never exit right in a vertex in which the red path is present, as this would give a factor of t . Furthermore, a blue path cannot exit right in a vertex in which the red path exits right. Therefore, after the shifting, red path i is strictly right of blue path i .

Next we see that red path i is also strictly left of blue path $i + 1$; the red path starts and ends strictly left of the blue path, so if the two paths ever share a face, the blue path must eventually exit right in a vertex in which the red path is present, resulting in a factor of t . Therefore, after the shifting, red path i is still strictly left of blue path $i + 1$.

Thus, after the shifting, red path i is strictly between blue paths i and $i + 1$. Clearly this process is reversible. \square

See Figure A.1 for an example. A similar result holds for k -tilings.

Proposition A.0.4 ([20, Prop. A.4]). *There is a bijection between k -tilings of the $a \times b \times c$ hexagon at $t = 0$ and lozenge tilings of the $ka \times b \times (c - (k - 1)a)$ hexagon. (If $(k - 1)a > c$, then there are no k -tilings of the $a \times b \times c$ hexagon at $t = 0$.)*

From this we can calculate the arctic curve when $t = 0$.

Theorem A.0.5 ([20, Thm. A.5]). *When $t = 0$, the arctic curves (for both colors)*

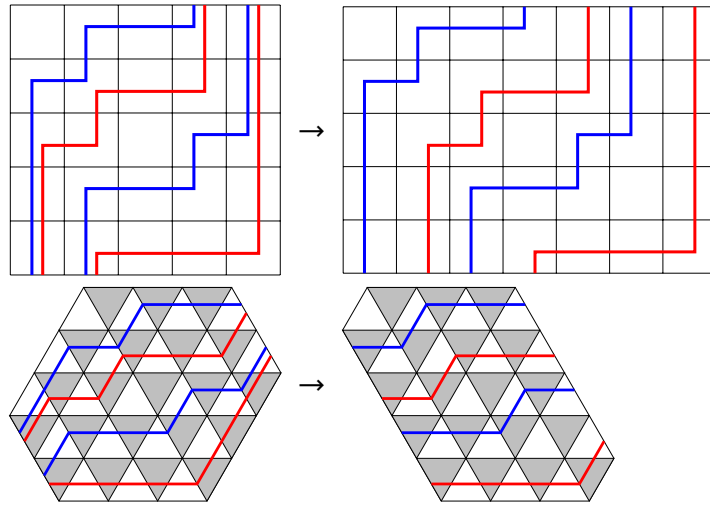


Figure A.1: Example of the bijection between the 2-tilings of the $2 \times 3 \times 3$ hexagon at $t = 0$ and tilings of the $4 \times 3 \times 1$ hexagon. The top gives the bijection in terms of lattice path, while the bottom gives the lozenge tilings.

of the 2-tilings of the $a \times 2a \times 3a$ hexagon are given by

$$\begin{cases} \left(\frac{6x-\sqrt{3}y+6}{3}\right)^2 + y^2 = 3, & x \leq -\frac{3}{2}, \quad -\frac{\sqrt{3}}{2} \leq y \leq \frac{\sqrt{3}}{2} \\ x^2 + y^2 = 3, & x \leq 0, \quad \frac{\sqrt{3}}{2} \leq y \leq \sqrt{3} \\ \left(\frac{3x-\sqrt{3}y+3}{3}\right)^2 + y^2 = 3, & x \geq 0, \quad \frac{\sqrt{3}}{2} \leq y \leq \sqrt{3} \\ \left(\frac{6x-\sqrt{3}y}{3}\right)^2 + y^2 = 3, & x \geq \frac{1}{2}, \quad -\frac{\sqrt{3}}{2} \leq y \leq \frac{\sqrt{3}}{2} \\ (x+1)^2 + y^2 = 3, & x \geq -1, \quad -\sqrt{3} \leq y \leq -\frac{\sqrt{3}}{2} \\ \left(\frac{3x-\sqrt{3}y}{3}\right)^2 + y^2 = 3, & x \leq -1, \quad -\sqrt{3} \leq y \leq -\frac{\sqrt{3}}{2} \end{cases}$$

(More generally, for k -tilings of an $a \times ka \times (2k-1)a$ hexagon, the arctic curve can be worked out similarly.)

Proof. The arctic curve for lozenge tilings of the $2a \times 2a \times 2a$ hexagon is the circle $x^2 + y^2 = 3$ (Theorem A.0.1). Using this arctic curve, we can derive the arctic curve for 2-tilings of the $a \times 2a \times 3a$ hexagon at $t = 0$, using the bijection from Prop. A.0.3 (as in Theorem 4.4.6). \square

See Figure A.2 for an example of the arctic curves for 2 colors and $t = 0$.

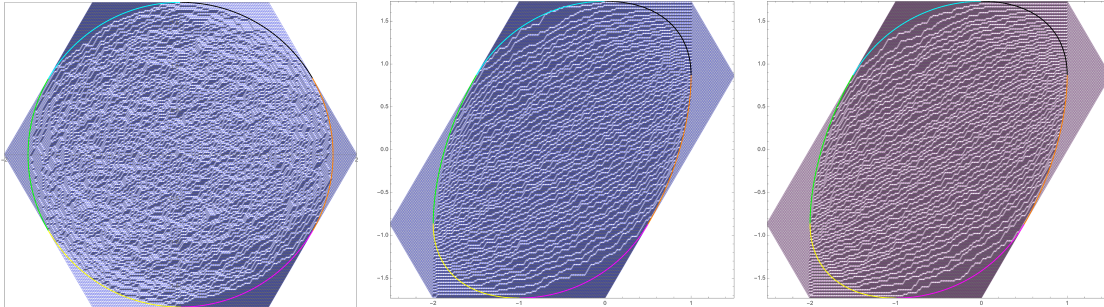


Figure A.2: A simulation and computed arctic curve of a 1-tiling of an $100 \times 100 \times 100$ hexagon (left) and a simulation and computed arctic curve for 2-tiling a $50 \times 100 \times 150$ hexagon with $t = 0$ (right). The colors of the arctic curve show which pieces map to each other under the bijection.

We can also work out the case when $t \rightarrow \infty$. Unlike the Aztec diamond (Lemma 4.4.8 and Cor. 4.1.5), the mapping in this case takes a different form than that of $t = 0$. First, we need a small lemma.

Lemma A.0.6 ([20, Lemma A.6]). *Consider a configuration of the lattice $W_{a+c}((b^a)^2)$ whose weight has the maximum power of t amongst all configurations of this lattice. For each color, label the paths of each color $1, \dots, a$ by starting column from left to right. Let $r_{i,j}^{(l)}$ be the row in which path i color l takes its j -th right step, for $i \in [a], j \in [b], l \in [2]$. Then*

$$r_{i,1}^{(1)} \leq r_{i,1}^{(2)} \leq r_{i,2}^{(1)} \leq r_{i,2}^{(2)} \leq \dots \leq r_{i,b}^{(1)} \leq r_{i,b}^{(2)}.$$

Proof. For 2 colors, a white face contributes a factor of t whenever a path of color 1 takes a right step and a path of color 2 is present. In any configuration of $W_{a+c}((b^a)^2)$, path i color 1 takes b right steps for all $i \in [a]$, hence the power of t in the weight of the configuration is at most ab . Moreover, the power of t in the weight of the

Proof. We express the bijection in terms of the appropriate lattices. Let $r_{i,j}$ be the row in which the i -th path of the 1-tiling goes right on its j -th step. Then the bijection is given by taking

$$r_{i,2j-1} = r_{i,j}^{(1)} \text{ and } r_{i,2j} = r_{i,j}^{(2)}.$$

The previous Lemma A.0.6 ensures this is a valid configuration of paths. \square

More generally, a similar argument holds for k -tilings.

Proposition A.0.8 ([20, Prop. A.8]). *There is a bijection between k -tilings of the $a \times b \times c$ hexagon when $t \rightarrow \infty$ and lozenge tilings of the $a \times kb \times c$ hexagon.*

By reversing this bijection, we can compute the arctic curves for k -tilings of a particular hexagon when $t \rightarrow \infty$.

Theorem A.0.9 ([20, Thm. A.9]). *The arctic curves (for both colors) for 2-tilings of the $2a \times a \times 2a$ hexagon when $t \rightarrow \infty$ are given by*

$$\begin{cases} x^2 + y^2 = 3, & x \leq -\frac{3}{2}, \quad -\frac{\sqrt{3}}{2} \leq y \leq \frac{\sqrt{3}}{2} \\ \left(\frac{6x-\sqrt{3}y+6}{3}\right)^2 + y^2 = 3, & x \leq -\frac{1}{2}, \quad \frac{\sqrt{3}}{2} \leq y \leq \sqrt{3} \\ \left(\frac{6x+\sqrt{3}y}{3}\right)^2 + y^2 = 3, & x \geq -\frac{1}{2}, \quad \frac{\sqrt{3}}{2} \leq y \leq \sqrt{3} \\ (x+1)^2 + y^2 = 3, & x \geq \frac{1}{2}, \quad -\frac{\sqrt{3}}{2} \leq y \leq \frac{\sqrt{3}}{2} \\ \left(\frac{6x-\sqrt{3}y}{3}\right)^2 + y^2 = 3, & x \geq -\frac{1}{2}, \quad -\sqrt{3} \leq y \leq -\frac{\sqrt{3}}{2} \\ \left(\frac{6x+\sqrt{3}y+6}{3}\right)^2 + y^2 = 3, & x \leq -\frac{1}{2}, \quad -\sqrt{3} \leq y \leq -\frac{\sqrt{3}}{2} \end{cases}$$

(More generally, the arctic curves for k -tilings of the $ka \times a \times ka$ hexagon when $t \rightarrow \infty$ can be worked out similarly.)

Proof. Prop. A.0.7 gives a bijection between 2-tilings of the $2a \times a \times 2a$ hexagon when $t \rightarrow \infty$ and 1-tilings of the $2a \times 2a \times 2a$ hexagon. Rescale both hexagons by a factor of $\frac{1}{a}$ in each axis. Now each lozenge has side length $\frac{1}{a}$; moreover, the $2a \times 2a \times 2a$ hexagon has sides of length 2 and is centered at $(x, y) = (0, 0)$.

Consider a 1-tiling of the $2a \times 2a \times 2a$ hexagon, which we will think of interchangeably as paths and lozenges. We label the paths $1, \dots, 2a$ by starting point from NW to SE. For all $i \in [2a]$, path i of each color starts on the SW side of the hexagon at

$$(x_i, y_i) = \left(-2 + \frac{2i-1}{4a}, -\frac{\sqrt{3}(2i-1)}{4a} \right).$$

Note that each path will take $2a$ horizontal steps, with each horizontal step moving the path $\frac{1}{a}$ to the right. For path i the center of the j -th horizontal step will occur along the line

$$y = \sqrt{3} \left(x + 2 - \frac{i + 2j - 2}{2a} \right).$$

Reversing the bijection from Prop. A.0.7, the $(2j - 1)$ -th horizontal step of path i in the 1-tiling will map to the j -th horizontal step of path i color 1 in the 2-tiling, while the $2j$ -th horizontal step of path i will map to the j -th horizontal step of path i color 2. Therefore, the bijection has the following geometric interpretation.

- The y -coordinates of the steps do not change.
- We shift the $(2j - 1)$ -th horizontal step of path i in the 1-tiling to the right by $\frac{j-1}{a}$ to get the j -th horizontal step of path i color 1 in the 2-tiling.
- We shift the $2j$ -th horizontal step of path i in the 1-tiling to the right by $\frac{j}{a}$ to get the j -th horizontal step of path i color 2 in the 2-tiling.

We can use this to see how to map different sections of the arctic curve.

For example, consider path 1 in the 1-tiling, which starts at (x_1, y_1) . The trajectory of this path gives the boundary between the upper frozen region of lozenges of type 2 and the disordered region. In the 1-tiling, this portion of the arctic curve is given by

$$x^2 + y^2 = 3, \quad x \leq 0, \quad \frac{\sqrt{3}}{2} \leq y \leq \sqrt{3}.$$

As stated above, to get path 1 color 1 we shift the $(2j - 1)$ -th horizontal step in the 1-tiling to the right by $\frac{j-1}{a}$. Since in the 1-tiling this horizontal step lies along the line $y = \sqrt{3} \left(x + 2 - \frac{4j-1}{2a} \right)$, we have $\frac{j-1}{a} = \frac{1}{6} (6 + 3x - \sqrt{3}y) + O(\frac{1}{a})$. Thus the map from path 1 of the 1-tiling to path 1 color 1 of the 2-tiling is given by

$$(x, y) \mapsto \left(x - \frac{1}{6} (6 + 3x - \sqrt{3}y), y \right) = \left(\frac{1}{6} (3x + \sqrt{3}y - 6), y \right)$$

up to terms that go to zero as $a \rightarrow \infty$. Inverting this we see that this portion of the arctic curve for color 1 is given by

$$\left(\frac{6x - \sqrt{3}y + 6}{3} \right)^2 + y^2 = 3.$$

The analysis for path 1 color 2 works the same. This gives the second case in the statement of the theorem.

The other portions of the arctic curve can be done similarly. □

See Figure A.3 for an example.

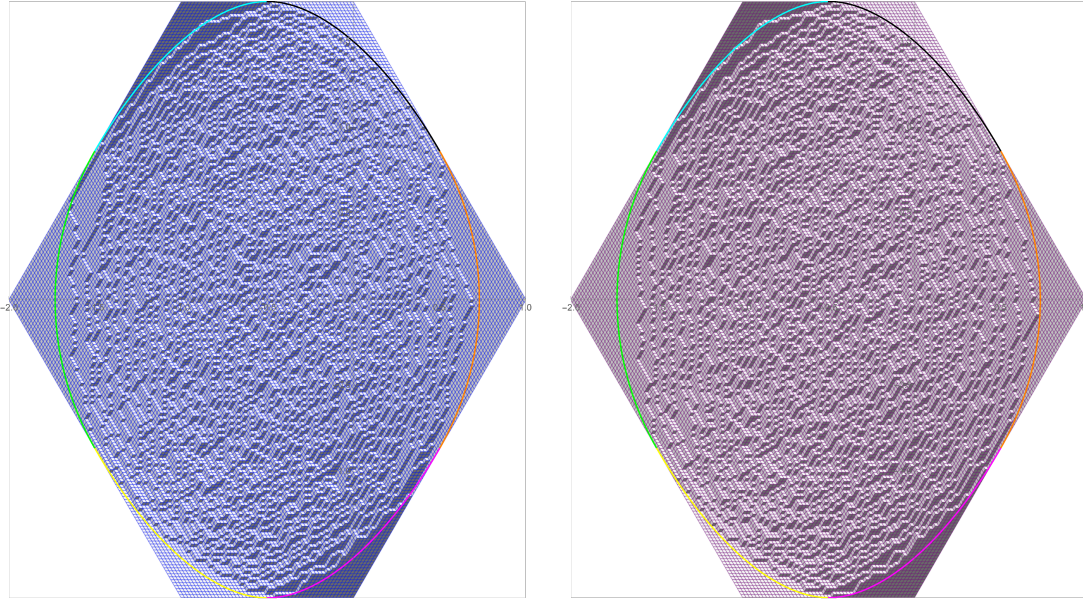


Figure A.3: A simulation and computed arctic curve for 2-tilings of the $100 \times 50 \times 100$ hexagon for large t ($t = 100$).

Prop. A.0.4 and Prop. A.0.8 can also be used to derive some properties of the generating function $Z_{a,b,c}^{(k)}(X_{a+c}; t)$ in the specialization $x_i = q^{i-1}$ for all $i \in [a+c]$. With this specialization, the weight of a lozenge tiling T is $q^{\text{vol}(T)}$, where vol is the “volume” of a lozenge tiling (which corresponds to the size of the associated plane partition). Thus

$$Z_{a,b,c}^{(k)}(1, q, \dots, q^{a+c-1}; t) = \sum_{\mathbf{T}} t^{\#\text{ interactions in } \mathbf{T}} q^{\sum_{i=1}^k \text{vol}(T_i)}.$$

In the case $k = 1$, a classical result of MacMahon [44] states that this equals

$$Z_{a,b,c}(1, q, \dots, q^{a+c-1}) = q^{\binom{a}{2}b} \prod_{i=1}^a \prod_{j=1}^b \frac{1 - q^{c+i+j-1}}{1 - q^{i+j-1}}.$$

Thus, in the case $t = 1$, we have

$$Z_{a,b,c}^{(k)}(1, q, \dots, q^{a+c-1}; 1) = \left(Z_{a,b,c}(1, q, \dots, q^{a+c-1}) \right)^k = q^{k \binom{a}{2}b} \left(\prod_{i=1}^a \prod_{j=1}^b \frac{1 - q^{c+i+j-1}}{1 - q^{i+j-1}} \right)^k.$$

When $t = 0$, we can use the bijection in Prop. A.0.4 to conclude

$$Z_{a,b,c}^{(k)}(1, q, \dots, q^{a+c-1}; 0) = Z_{ka,b,c-(k-1)a}(1, q, \dots, q^{a+c-1}) = q^{k\binom{a}{2}b} \prod_{i=1}^{ka} \prod_{j=1}^b \left(\frac{1 - q^{c-(k-1)a+i+j-1}}{1 - q^{i+j-1}} \right).$$

We leave the computation of $Z_{a,b,c}^{(k)}(1, q, \dots, q^{a+c-1}; t)$ as an open problem. This is a polynomial in t of degree $\binom{k}{2}ab$. Using the bijection in Prop. A.0.8, we know that its leading coefficient is

$$Z_{a,kb,c}(1, q, \dots, q^{a+c-1}) = q^{k\binom{a}{2}b} \prod_{i=1}^a \prod_{j=1}^{kb} \left(\frac{1 - q^{c+i+j-1}}{1 - q^{i+j-1}} \right).$$

Note that

$$Z_{a,b,c}^{(k)}(1, q, \dots, q^{a+c-1}; t) = \mathcal{L}_{((b^a)^k)}(1, q, \dots, q^{a+c-1}; t)$$

and in particular, setting $q = 1$,

$$Z_{a,b,c}^{(k)}(1^{a+c}; t) = \mathcal{L}_{((b^a)^k)}(1^{a+c}; t).$$

A table for small values of a, b, c and $q = 1, k = 2$ is presented in Table A.1.

a	b	c	Generating function
1	1	1	$3t + 1$
1	1	2	$6t + 3$
1	1	3	$10t + 6$
1	2	1	$5t^2 + 3t + 1$
1	2	2	$15t^2 + 15t + 6$
1	2	3	$35t^2 + 45t + 20$
2	1	1	$3t(2t + 1)$
2	1	2	$20t^2 + 15t + 1$
2	1	3	$50t^2 + 45t + 5$
2	2	1	$t^2(15t^2 + 15t + 6)$
2	2	2	$105t^4 + 175t^3 + 104t^2 + 15t + 1$
2	2	3	$490t^4 + 1050t^3 + 770t^2 + 175t + 15$
3	1	1	$t^2(10t + 6)$
3	1	2	$5t(10t^2 + 9t + 1)$
3	1	3	$175t^3 + 189t^2 + 35t + 1$
3	2	1	$t^4(35t^2 + 45t + 20)$
3	2	2	$t^2(490t^4 + 1050t^3 + 770t^2 + 175t + 15)$
3	2	3	$4116t^6 + 11340t^5 + 10689t^4 + 3850t^3 + 594t^2 + 35t + 1$

Table A.1: Generating functions of 2-tilings of the $a \times b \times c$ hexagon

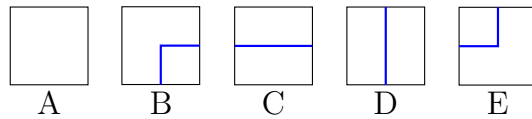
Appendix B

Equivalence of algebraic and graphical definitions for the L and M vertices

Recall the algebraic definition of the L matrix:

$$L_x^{(k)}(\mathbf{I}, \mathbf{J}, \mathbf{K}, \mathbf{L}) = \mathbf{1}_{\mathbf{I}+\mathbf{J}=\mathbf{K}+\mathbf{L}} \prod_{i=1}^k \mathbf{1}_{I_i+J_i \neq 2} \cdot x^{|\mathbf{L}|} t^{\varphi(\mathbf{L}, \mathbf{I}+\mathbf{J})}.$$

Due to the factor of $\mathbf{1}_{\mathbf{I}+\mathbf{J}=\mathbf{K}+\mathbf{L}} \prod_{i=1}^k \mathbf{1}_{I_i+J_i \neq 2}$, in order for the weight to be non-zero, we require $I_i + J_i = K_i + L_i$ and $I_i + J_i \neq 2$ for all $i \in [k]$. In terms of our graphical interpretation, this means that each color must have one of the following five forms.



Note that $L_i = 1$ if color i has form B or C (i.e. color i exits right) and 0 otherwise. Also note that $I_i + J_i = 1$ if color i has form B, C, D, or E (i.e. color i is present) and 0 otherwise. Assuming each color has one of these five forms, the weight is

$$x^{|\mathbf{L}|} t^{\varphi(\mathbf{L}, \mathbf{I}+\mathbf{J})} = x^{\sum_{i=1}^k L_i} t^{\sum_{i=1}^k (L_i \sum_{j=i+1}^k (I_j + J_j))} = \prod_{\substack{1 \leq i \leq k \\ L_i = 1}} x t^{\sum_{j=i+1}^k (I_j + J_j)} = \prod_{\substack{1 \leq i \leq k \\ \text{color } i \text{ exits right}}} x t^{\delta_i}$$

where δ_i is the number of colors greater than i that are present. It is easy to see that this matches the graphical definition of the L matrix.

Now recall the algebraic definition of the M matrix:

$$M_x^{(k)}(\mathbf{I}, \mathbf{J}, \mathbf{K}, \mathbf{L}) = x^k t^{\binom{k}{2}} L_{\bar{x}}^{(k)}(\mathbf{I}, \mathbf{J}, \mathbf{K}, \mathbf{L})$$

where $\bar{x} = \frac{1}{xt^{k-1}}$. In order for $M_x^{(k)}(\mathbf{I}, \mathbf{J}, \mathbf{K}, \mathbf{L})$ to be non-zero, we need $L_{\bar{x}}^{(k)}(\mathbf{I}, \mathbf{J}, \mathbf{K}, \mathbf{L})$ to be non-zero, which requires each color to have form A, B, C, D, or E. Assuming each color has one of these five forms, the weight is

$$x^k t^{\binom{k}{2}} \cdot L_{\bar{x}}^{(k)}(\mathbf{I}, \mathbf{J}, \mathbf{K}, \mathbf{L}) = x^k t^{\binom{k}{2}} \prod_{\substack{1 \leq i \leq k \\ \text{color } i \text{ exits right}}} \frac{1}{xt^{k-1}} t^{\delta_i}$$

which has the form $x^p t^q$ for some $p, q \in \mathbb{Z}$. We see that

$$p = k - \# \text{ colors that exit right} = \# \text{ colors that don't exit right}$$

and

$$\begin{aligned} q &= \binom{k}{2} + \sum_{\substack{1 \leq i \leq k \\ \text{color } i \text{ exits right}}} \delta_i - \sum_{\substack{1 \leq i \leq k \\ \text{color } i \text{ exits right}}} (k-1) \\ &= \sum_{1 \leq i < j \leq k} 1 + \sum_{\substack{1 \leq i < j \leq k \\ \text{color } i \text{ exits right} \\ \text{color } j \text{ is present}}} 1 - \left(\sum_{\substack{1 \leq i < j \leq k \\ \text{color } i \text{ exits right}}} 1 + \sum_{\substack{1 \leq h < i \leq k \\ \text{color } i \text{ exits right}}} 1 \right) \\ &= \sum_{1 \leq i < j \leq k} 1 + \sum_{\substack{1 \leq i < j \leq k \\ \text{color } i \text{ exits right} \\ \text{color } j \text{ is present}}} 1 - \left(\sum_{\substack{1 \leq i < j \leq k \\ \text{color } i \text{ exits right}}} 1 + \sum_{\substack{1 \leq i < j \leq k \\ \text{color } j \text{ exits right}}} 1 \right) \\ &= \sum_{1 \leq i < j \leq k} \begin{cases} 0 = 1 + 0 - (1 + 0) & i \text{ right, } j \text{ not present} \\ 1 = 1 + 1 - (1 + 0) & i \text{ right, } j \text{ present but not right} \\ 0 = 1 + 1 - (1 + 1) & i \text{ right, } j \text{ right} \\ 1 = 1 + 0 - (0 + 0) & i \text{ not right, } j \text{ not present} \\ 1 = 1 + 0 - (0 + 0) & i \text{ not right, } j \text{ present but not right} \\ 0 = 1 + 0 - (0 + 1) & i \text{ not right, } j \text{ right} \end{cases} \\ &= \sum_{\substack{1 \leq i < j \leq k \\ \text{color } i \text{ doesn't exit right}}} \alpha_i + \sum_{\substack{1 \leq i < j \leq k \\ \text{color } i \text{ exits right}}} \beta_i \end{aligned}$$

where

$\alpha_i = \# \text{ colors } j > i \text{ that don't exit right,}$

$\beta_i = \# \text{ colors } j > i \text{ that are present but don't exit right} = \# \text{ colors } j > i \text{ that exit top.}$

Thus the weight is

$$x^p t^q = \prod_{\substack{1 \leq i < j \leq k \\ \text{color } i \text{ doesn't exit right}}} x t^{\alpha_i} \cdot \prod_{\substack{1 \leq i < j \leq k \\ \text{color } i \text{ exits right}}} t^{\beta_i}.$$

It is easy to see that this matches the graphical definition of the M matrix.

Appendix C

Proof of Lemma 3.2.13

Throughout this section, whenever we consider a skew shape α/β , we assume α and β have the same number of parts $\ell(\alpha/\beta)$. Moreover, using Remark 3.2.3, we can take the Maya diagrams of α and β to have the same length. We let $f_k(\alpha/\beta)$ denote the k -quotient of α/β .

Let λ/μ be a skew shape and let $\boldsymbol{\lambda}/\boldsymbol{\mu} = f_k(\lambda/\mu) = (\lambda^{(0)}/\mu^{(0)}, \dots, \lambda^{(k-1)}/\mu^{(k-1)})$ be its k -quotient. Let

$$T \in \text{SSRT}_k(\lambda/\mu) \leftrightarrow \mathbf{T} = (T^{(0)}, \dots, T^{(k-1)}) \in \text{SSSYT}_k(\boldsymbol{\lambda}/\boldsymbol{\mu})$$

via the Littlewood k -quotient map. We want to prove the following two claims.

1. A ribbon in T labelled i corresponds to a cell labelled i in \mathbf{T} , so the number of ribbons in T labelled i equals the number of cells labelled i in \mathbf{T} .
2. Two ribbons R, R' in T whose tails u, u' have the same content modulo k correspond to two cells v, v' in the same shape in \mathbf{T} . Moreover, in this case,

$$\frac{c(u) - c(u')}{k} = c(v) - c(v').$$

We begin by discussing Maya diagrams and content lines. Let α/β be a skew shape, and let $(a_0, \dots, a_{s-1}), (b_0, \dots, b_{s-1})$ be the Maya diagrams of α, β respectively. Given a cell u in α/β , we define its **adjusted content** to be

$$ac(u) := c(u) + \ell(\alpha/\beta) - 1,$$

where $c(u)$ is its content. The following facts are straightforward to show.

- (A) The skew shape α/β consists of a single cell u iff $a_i = b_{i+1} = E$, $a_{i+1} = b_i = S$, and $a_j = b_j$ for $j \neq i, i+1$, for some i . In this case, if u is the single cell in α/β , we have $ac(u) = i$.
- (B) The skew shape α/β consists of a single ribbon iff $a_i = b_{i+k} = E$, $a_{i+k} = b_i = S$, and $a_j = b_j$ for $j \neq i, i+k$, for some i . In this case, if u is the tail of the single ribbon in α/β , we have $ac(u) = i$.

The claims will follow from the following lemma.

Lemma C.0.1. *If λ/μ is a k -ribbon, then $|\lambda/\mu| = 1$ i.e. λ/μ consists of a single cell v . Let u be the tail of the ribbon in λ/μ and write $ac(u) = qk+r$ where $0 \leq r < k$. Then v appears in $\lambda^{(r)}/\mu^{(r)}$ and has adjusted content $ac(v) = q$.*

Proof of Lemma C.0.1. Let u be the tail of the ribbon λ/μ . Let

$$(a_0, \dots, a_{s-1}), (b_0, \dots, b_{s-1})$$

be the Maya diagrams of λ, μ respectively. By Remark 3.2.3, we may assume $t = s/k$ is an integer. By Fact B, for some i , we have

$$ac(u) = i; a_i = b_{i+k} = E; a_{i+k} = b_i = S; \text{ and } a_j = b_j \text{ for } j \neq i, i+k.$$

Let $(a_0^{(j)}, \dots, a_{t-1}^{(j)}), (b_0^{(j)}, \dots, b_{t-1}^{(j)})$ be the Maya diagrams of $\lambda^{(j)}, \mu^{(j)}$ respectively for each j . By the definition of the k -quotient map, we have $a_l^{(j)} = a_{lk+j}$ and $b_l^{(j)} = b_{lk+j}$ for each j and l . Since $a_j = b_j$ for $j \neq i, i+k$,

$$(a_0^{(j)}, \dots, a_{t-1}^{(j)}) = (b_0^{(j)}, \dots, b_{t-1}^{(j)}) \text{ for } j \neq r$$

and thus $\lambda^{(j)} = \mu^{(j)}$ for $j \neq r$. Since $a_i = b_{i+k} = E$, $a_{i+k} = b_i = S$, and $a_j = b_j$ for $j \neq i, i+k$,

$$a_q^{(r)} = b_{q+1}^{(r)} = E; a_{q+1}^{(r)} = b_q^{(r)} = S; \text{ and } a_j^{(r)} = b_j^{(r)} \text{ for } j \neq q, q+1.$$

Thus, by Fact A, $\lambda^{(r)}/\mu^{(r)}$ has a single cell v with adjusted content $ac(v) = q$. \square

We now prove Claim 1, using Lemma C.0.1. Suppose there are m ribbons R_1, \dots, R_m labelled i in T . Then we can construct a series of partitions

$$\alpha^{(0)} = \lambda_{\leq i-1}, \dots, \alpha^{(m)} = \lambda_{\leq i}$$

such that $\alpha^{(j)}/\alpha^{(j-1)} = R_j$ for each $j \in [m]$. Using the lemma,

$$|f_k(\lambda_{\leq i}/\lambda_{\leq i-1})| = |f_k(\alpha^{(m)}/\alpha^{(0)})| = \sum_{j=1}^m |f_k(\alpha^{(j)}/\alpha^{(j-1)})| = \sum_{j=1}^m |f_k(R_j)| = \sum_{j=1}^m 1 = m.$$

However, by the definition of the Littlewood k -quotient map, $f_k(\lambda_{\leq i}/\lambda_{\leq i-1})$ (lying inside $\boldsymbol{\lambda}/\boldsymbol{\mu}$) consists of exactly the cells labelled i in \mathbf{T} , so there are m cells labelled i in \mathbf{T} .

We now prove Claim 2, again using Lemma C.0.1. Write $ac(u) = qk + r$ and $ac(u') = q'k + r'$, where $0 \leq r, r' < k$. Since u and u' have the same content modulo k , they have the same adjusted content modulo k , hence $r = r'$. Thus, by the lemma, both v and v' appear in the same shape in \mathbf{T} , namely $T^{(r)} = T^{(r')}$. Moreover, again using the lemma,

$$\frac{c(u) - c(u')}{k} = \frac{ac(u) - ac(u')}{k} = q - q' = ac(v) - ac(v') = c(v) - c(v').$$